HIGH PERFORMANCE ELECTRICALLY CONDUCTIVE ADHESIVES (ECAS) FOR LEADFREE INTERCONNECTS

A Thesis
Presented to
The Academic Faculty

by

Yi Li

In Partial Fulfillment
of the Requirements for the Degree
Doctor of Philosophy in the
School of Materials Science and Engineering

Georgia Institute of Technology
December 2007

HIGH PERFORMANCE ELECTRICALLY CONDUCTIVE ADHESIVES (ECAS) FOR LEADFREE INTERCONNECTS

Approved by:

Dr. C. P. Wong, Advisor
School of Materials Science and Engineering
Georgia Institute of Technology

Dr. Karl Jacob
School of Polymer, Textile and Fiber Engineering
Georgia Institute of Technology

Dr. Meilin Liu
School of Materials Science and Engineering
Georgia Institute of Technology

Dr. Valeria Milam
School of Materials Science and Engineering
Georgia Institute of Technology

Dr. Z. L. Wang
School of Materials Science and Engineering
Georgia Institute of Technology

Date Approved: October 29, 2007

ACKNOWLEDGEMENTS

This thesis is dedicated to my family for their love, support, and encouragement throughout my Ph.D study.

I would like to express my sincere gratitude to my advisor, Dr. C. P. Wong for his guidance, support, and encouragement throughout the course of this research. His dedication to work and expertise in electronics packaging area have been a great source of inspiration for me. I would like to extend my gratitude to Dr. Karl Jacob, Dr. Meilin Liu, Dr. Valeria Milam and Dr. Z. L. Wang for serving on my committee and providing invaluable suggestions and recommendations.

My special thanks go to several administrator and staff in the School of Materials Science and Engineering and Microelectronics Packaging Research Center for their guidance and support. They are Dr. Rao Tummala, Dr. Robert L. Snyder, Dr. Thomas H. Sanders, Dr. Brent Carter, Ms. Susan Bowman, Mr. Dean Sutter, Ms. Mechelle Kitchings, Mr. James Cagle, Ms. Karen H. Mayo, Ms. Yolande Berta, Ms. Nancy Pinion, Ms. Jyoti Ghosh, Mr. Tim Banks.

I would like to acknowledge the input and help I received from my fellow co-workers in Dr. Wong's group during this research work. They are Dr. Kyoung-sik Moon, Dr. Lianhua Fan, Dr. Dr. Haiying Li, Dr. Zhuqing Zhang, Dr. Jianwen Xu, Dr. Fei Xiao, Dr. Hai Dong, Dr. Myung Jin Yim, Dr. Brian Englert, Mr. Suresh Pothukuchi, Ms. Lara Martin, Mr. Hongjin Jiang, Mr. Lingbo Zhu, Ms. Jiongxin Lu, Mr. Yonghao Xiu, Mr. Brian Bertram, Ms. Jessica Burger, Ms. Gusuel Yun, Mr. Qizhen Liang, Mr. Rongwei

Zhang, and Mr. Wei Lin. I would also like to thank the undergraduate students and high school intern students who worked with me during the PhD study. They are Mr. Andrew Whitman, Ms. Elizabeth Owensby, Ms. Melody Lin, Ms. Qian Wan, Mr. Danny Nguyen, Mr. John Guthrie and Mr. Nick Knowles.

My Special appreciation is extended to National Science Foundation, Environmentally Protection Agency, Intel Corporation, Nokia Corporation, Indium Corporation of America, Hitachi Chemical and ASE Group for their interests and supports of this work, and to Ferro Corporation, nGmat Corporation, Emerson & Cumming, Hexion Specialty Chemicals and Lindau Chemicals for their supply of the materials. This work is also partially funded by Microelectronics Packaging Research Center of Georgia Tech. Special appreciation is extended to Nano Science and Technology Scholarship at Georgia Tech during 2004-2006 terms.

TABLE OF CONTENTS

LIST OF TABLES

LIST OF FIGURES

SUMMARY

Electrically conductive adhesives (ECAs) are one of the lead-free interconnect materials in microelectronics packaging with the advantages of environmental friendliness, mild processing conditions (enabling the use of heat-sensitive and low-cost components and substrates), fewer processing steps (reducing processing cost), low stress on the substrates, and fine pitch interconnect capability (enabling the miniaturization of electronic devices). However, some challenging issues still exist for the currently available ECAs, including lower electrical conductivity, conductivity fatigue in reliability tests, limited current-carrying capability, poor impact strength, etc. The interfacial properties is one of the major considerations when resolving these challenges and developing high performance conductive adhesives.

Surface functionalization and interface modification are the major approaches used in this thesis. Fundamental understanding and analysis of the interaction between various types of interface modifiers and ECA materials and substrates are the key for the development of high performance ECA for lead-free interconnects. The results of this thesis provide the guideline for the enhancement of interfacial properties of metal-metal and metal-polymer interactions. Systematic investigation of various types of ECAs contributes to a better understanding of materials requirements for different applications, such as surface mount technology (SMT), flip chip applications, flat panel display modules with high resolution, etc. Improvement of the electrical, thermal and reliability of different ECAs make them a potentially ideal candidate for high power and fine pitch microelectronics packaging option.

CHAPTER 1

INTRODUCTION

1.1 Electronics Packaging and Interconnects

Integrated Circuits (ICs) form the bases of all modern electronic products. Every IC has to be packaged before it can be used. “Electronic Packaging” is defined as the bridge that interconnects the integrated circuits (ICs) and other components into a system-level board to form electronic products [1]. The packaging has four main functions. 1) Signal distribution, involving mainly topological and electromagnetic consideration; 2) Power distribution, involving electromagnetic, structural, and materials aspects; 3) Heat dissipation (cooling), involving structural and materials consideration; 4) Protection (mechanical, chemical, electromagnetic) of components and interconnections. The challenge for the package is to provide all crucial functions required by the microelectronic part without limiting the performance of the part.

Figure 1.1 shows the hierarchy of electronics packaging [2]. From the bare chip fabricated from the silicon wafer, to the final product ready for use, the whole system can be divided into three levels of the packaging. The first level packaging provides the interconnection between an IC chip and a module. There are at least three popular methods for interconnecting the chips on the substrates (either to the module or the board): 1) face-up wire boding, 2) face up tape-automated bonding (TAB), 3) flip-chip technology. Figure 1.2 summarizes different types of chip to package interconnect techniques. Second level packaging provides the interconnection between the module to the printed wiring board (PWB) or a card, which could be realized by the pin through

hole (PTH) technology, or surface mount technology (SMT). Third-level packaging mainly is the process to put second-level packages onto a motherboard. With the requirements towards low-cost, miniaturization and high performance for the current semiconductor devices, the bare IC chips can also be connected to the integrated board using flip-chip technology directly [3], which is called flip-chip on board (FCOB) or direct chip attach (DCA).

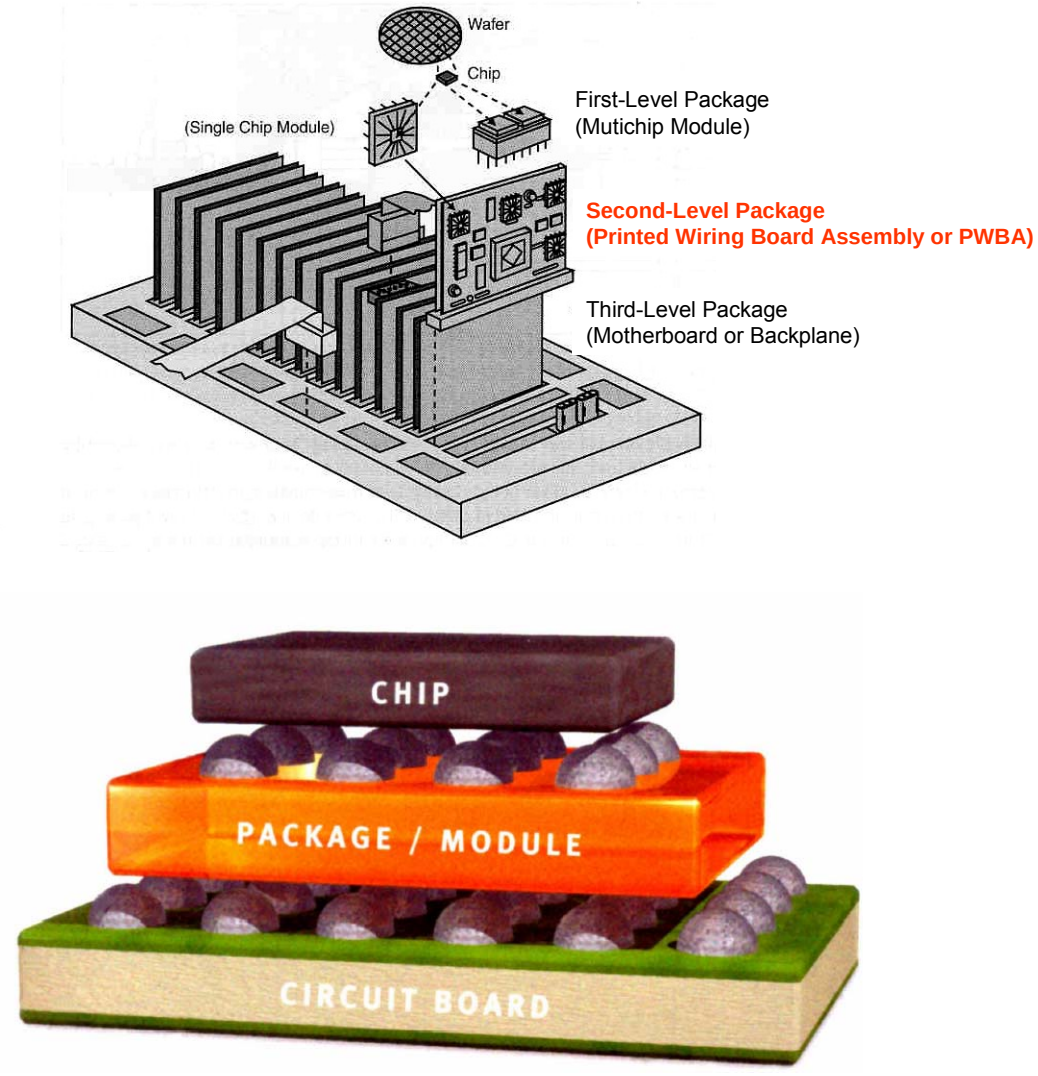

Figure 1.1 Electronic Packaging Hierarchy

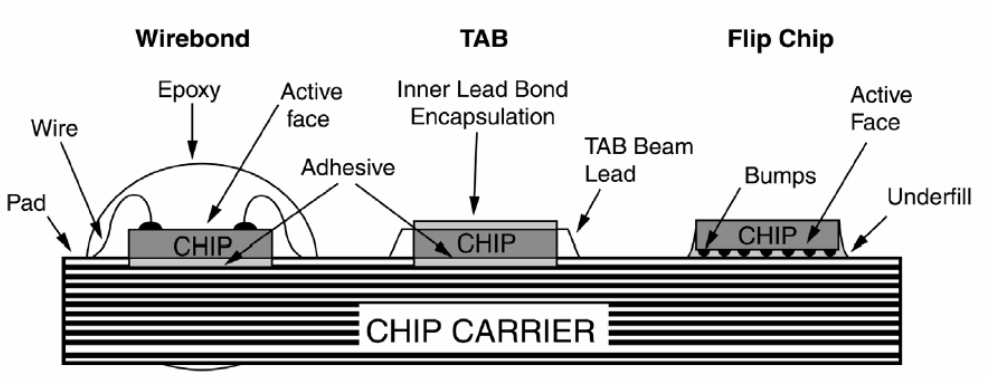

Figure 1.2 Chip to package interconnect techniques

Different levels of packaging are connected through interconnect materials. Although semiconductor electronics industry has made considerable advances over the past couple decades, the essential requirements of interconnects among all types of components in all electronic systems remain unchanged. The components need to be electrically connected for power, ground and signal transmissions, where lead-containing solder especially eutectic tin/lead (Sn/Pb) solder alloy has been the *de facto* interconnect material in most areas of electronic packaging. Such interconnection technologies include pin through hole (PTH), surface mount technology (SMT), ball grid array (BGA) package, chip scale package (CSP), and flip chip technology [4, 5]. Figure 1.3 shows an example of a functional component bonded to the substrate via interconnect materials.

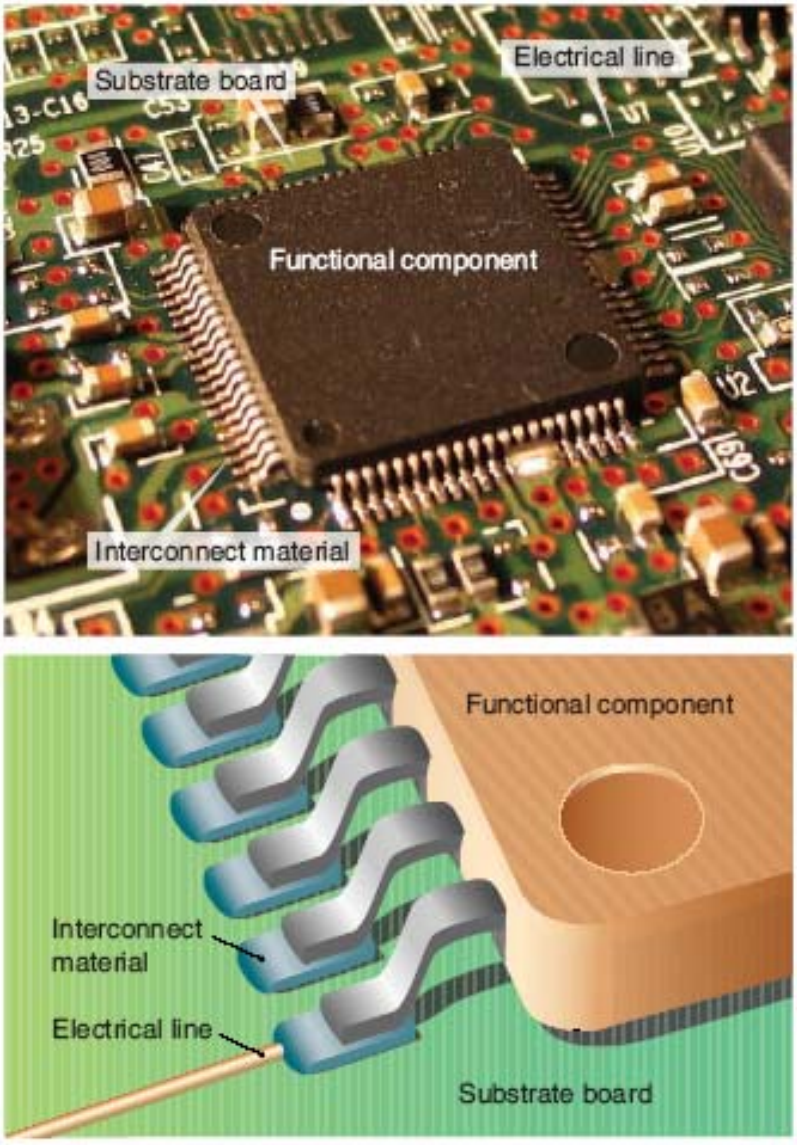

Figure 1.3 (top) Photo of a functional component that is assembled on the board substrate via interconnects. (bottom) Side view of the bonding between the component and the substrate via the interconnect material.

1.2 Electrically Conductive Adhesives

1.2.1 Lead-free interconnect materials

There are increasing concerns with the use of tin-lead alloy solders. First, tin-lead solders contain lead, a material hazardous to human and environment. Each year, thousands of tons of lead are manufactured into various products, especially consumer electronic products (e.g., cell phones, pagers, electronic toys, PDA (personal digital assistant),. etc.) which tend to have a short life cycle (2-3 years) and millions of such lead-containing products simply end up in landfills. According to 2001 U.S. Geological Survey, the total lead consumption by the U.S. industries in 2000 was 52,400 metric tons. More than 10% of the lead (5,430 metric tons) was used to produce alloy solders. Worst of all, most of the electronic products have a very short service life. Recycling of lead-containing consumer electronic products has proven to be very difficult. In Japan, the legislation prohibiting lead from being sent to land fills and other waste disposal sites is already in place. The European Union has officially designated 1 July 2006 as the date when the Directive on the Restriction of Hazardous Substances in Electrical and Electronic Equipment requires ‘‘the use of lead, mercury, cadmium, hexavalent chromium, and halogenated flame retardants’’ be phased out [6, 7]. This requirement applies to the manufacturing of both domestic and export products. In the US, legislations in limiting the use of lead have been introduced in both the Senate and the House of Representatives [8]. In response to the new legislations, most major electronic manufacturers have stepped up their search for alternatives to lead-containing solders.

To date, these efforts have been focused on two alternatives: lead-free solders and polymer-based electrically conductive adhesives (ECAs) [9-11]. The most promising

lead-free alloys contain tin as the primary element, because it melts at a relatively low temperature (232^{o}C), inexpensive and easily wets other metals. Depending on the applications, a number of lead-free solder alloys have found their way in commercial products [9, 12-14]. However, most currently commercial lead-free solders, such as tin/silver (Sn/Ag), tin/silver/copper (Sn/Ag/Cu), have higher melting temperatures (Tm of Sn/Ag and Sn/Ag/Cu are 217^{o}C and 221^{o}C, respectively) than of the conventional tin-lead eutectic solder (183^{o}C). Therefore, the reflow temperature during electronic assembly must be raised by 30^{o}C to 40^{o}C. This increased temperature reduces the integrity, reliability and functionality of printed wiring boards, components and other attachment. As such, the applicability of these metal alloys to organic/polymer packaged components and low-cost organic printed circuit boards are severely limited. Although some low melting point alloys are available such as tin/indium (Sn/In, Tm=120^{o}C), tin/bismuth (Sn/Bi, Tm=138 ^{o}C), tin/zinc/silver/aluminum/gallium (Sn/Zn/Ag/Al/Ga, Tm=189 ^{o}C) [15], their material properties and processibility in assembly are still of concern.

On the other hand, electrically conductive adhesives (ECAs) mainly consist of an organic/polymeric binder matrices and metal fillers. The conductive fillers provide the electrical properties and the polymeric matrices provide the physical and mechanical properties. Electrical and mechanical properties of ECAs are provided by different components, which is different from the case for metallic solders that provide both electrical and mechanical properties. Compared to the solder technology, ECAs offer numerous advantages, such as environmental friendliness (elimination of lead usage and flux cleaning), mild processing conditions, fewer processing steps (reducing processing

cost), and especially, the fine pitch capability due to the availability of small-sized conductive fillers. Figure 1.4 compares chip-to-substrate interconnects with solder joints or different ECA joints. However, like all lead-free materials, currently commercialized ECAs still have some limitations and challenging properties, such as a lower electrical and thermal conductivity compared to solder interconnects materials, conductivity fatigue in reliability tests, limited current carrying capability, metal migration fatigue in reliability and high voltage tests, and poor impact strength [16-20]. Table 1.1 gives a general comparison between tin-lead solder and generic commercialized ECAs [21].

Table 1.1 Conductive Adhesives Compared with Solder

Characteristic	**Sn/Pb solder**	**ECA**
Volume resistivity	10^{-4} Ohm-cm	10^{-3} ~10^{-4} Ohm-cm
Typical Junction R	10-15 mW	< 25 mW
Thermal conductivity	30W/m-deg.K	3.5 W/m-deg.K
Shear strength	2200 psi	2000 psi
Finest pitch	300 μm	< 150 -200 μm
Minimum Processing temperature	215^{o}C	150-170^{o}C
Environmental impact	Negative	Very minor
Thermal fatigue	yes	minimal

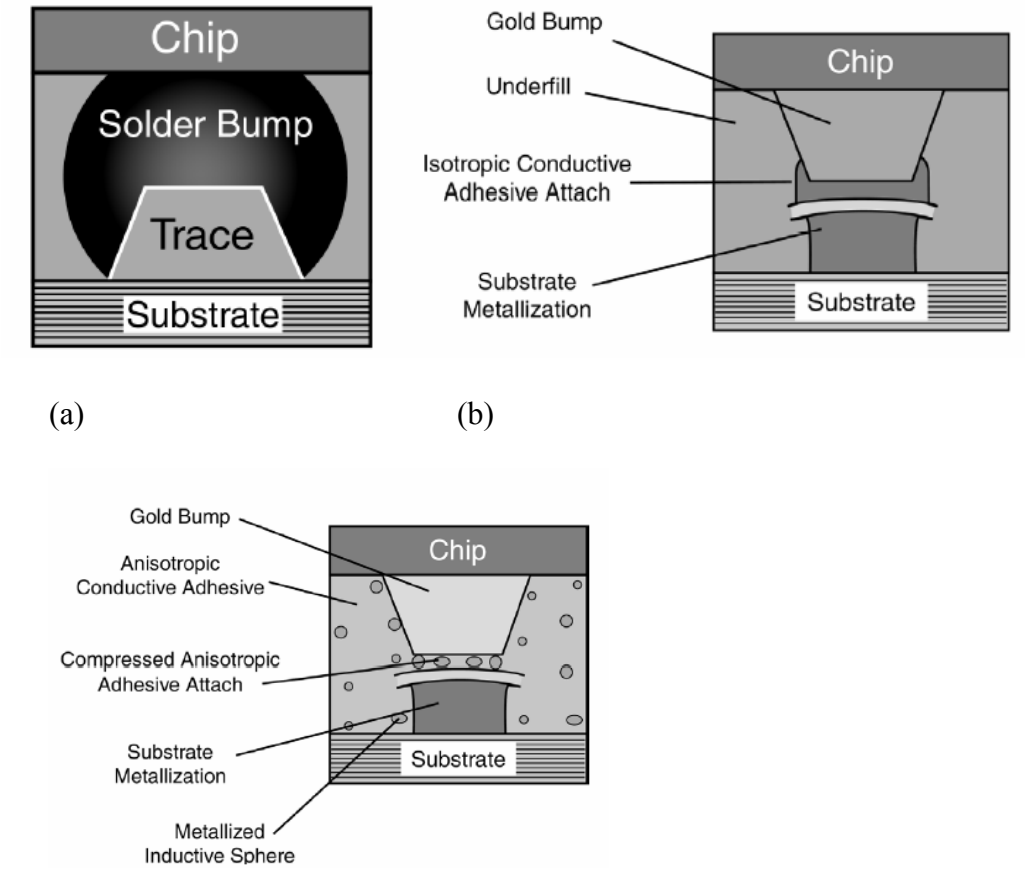

Figure 1.4 Comparison of various types of interconnect approaches. (a) solder interconnect; (b) isotropically conductive adhesive (ICA) interconnect; (c) anisotropically conductive adhesive (ACA) interconnect.

1.2.2 Electrically Conductive Adhesives (ECA) categories

Depending on the conductive filler loading level, ECAs are divided into isotropically conductive adhesives (ICAs, with typically 1-10 μm sized Ag flakes fillers), anisotropically conductive adhesives (ACAs, with typical 3-5 μm sized conductive fillers) and nonconductive adhesives (NCAs, typically without conductive fillers). The

difference between ICA and ACA/NCA is based on the percolation theory as shown in Figure 1.5. The percolation threshold depends on the shape and size of the fillers, but typically in the order of 15 ~ 25% volume fraction. For ICA, the loading level of conductive fillers exceeds the percolation threshold, providing electrical conductivity in all x, y and z directions. For ACAs or NCAs, the electrical conductivity is provided only in z-direction between the electrodes of the assembly. Figure 1.6 shows the schematics of the interconnect structures and typical cross-sectional images of flip chip joints by ICA, ACA and NCA materials illustrating the bonding mechanism for all three adhesives.

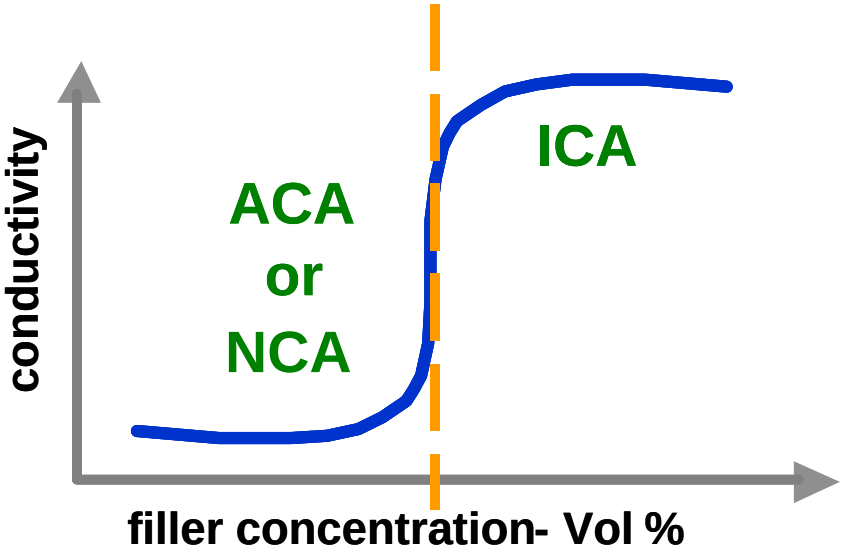

Figure 1.5 Typical percolation curve of conductive adhesives.

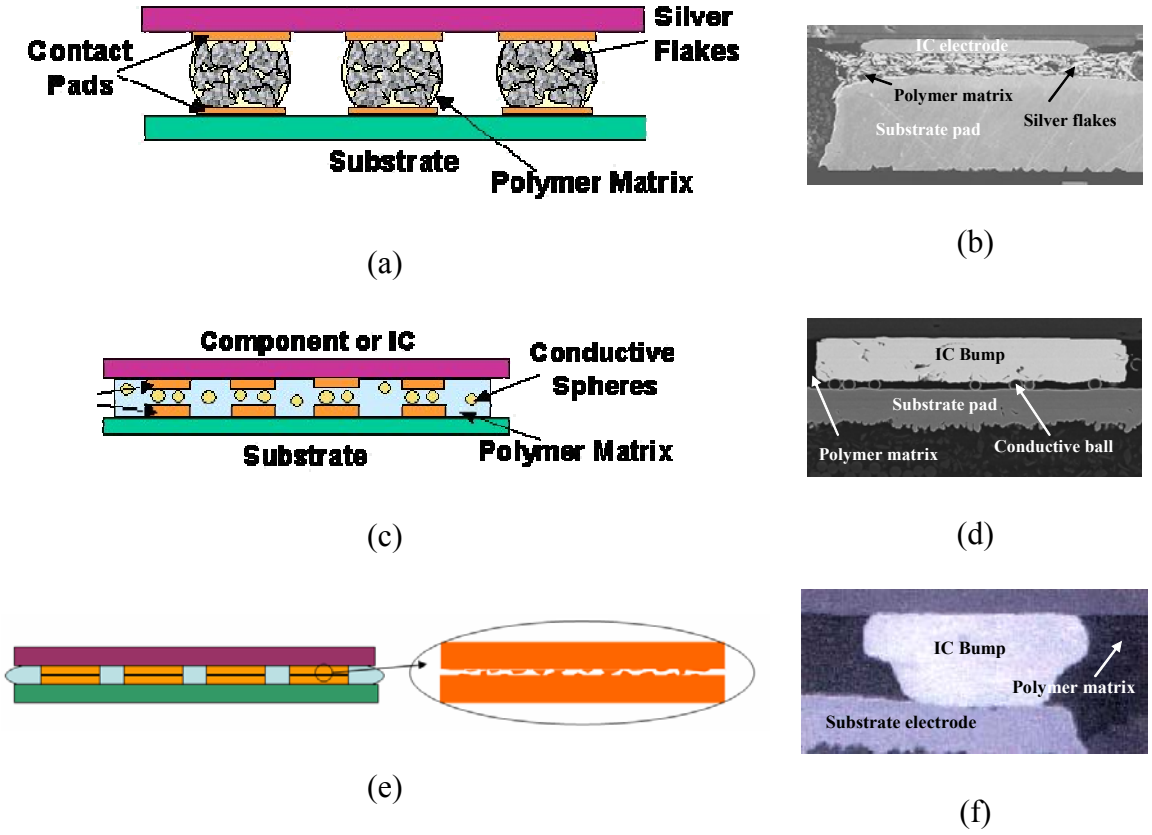

Figure 1.6 Schematic illustrations and cross sectional views of (a)(b) ICA, (c)(d) ACA and (e)(f) NCA flip chip bonding.

1.2.3 Isotropically Conductive Adhesives (ICAs)

Isotropic conductive adhesives, also called as “polymer solder”, are composites of polymer resin and conductive fillers. The adhesive matrix is used to form an electrical and mechanical bond at the interconnects. An ideal matrix for ICAs should have the following properties: long shelf life (good room temperature latency), fast cure, relatively high glass transition temperature (Tg), low moisture absorption, and good adhesion. Both thermosetting and thermoplastic materials are used as the polymer matrix. Epoxy, cyanate ester, silicone, polyurethane, etc. are widely used thermosets, while maleimide acrylic preimidized polyimide, etc. are the common used thermoplastics. An attractive

advantage of thermoplastic ICAs is that they are reworkable, i.e., can be easily repaired. A major drawback of thermoplastic ICAs, however, is the degradation of adhesion at high temperature. Another drawback of polyimide-based ICAs is that they generally contain solvents. During heating, voids are formed when the solvent evaporates. Most of commercial ICAs are based on thermosetting resins. Thermoset epoxies are by far the most common binders due to the superior balanced properties, such as excellent adhesive strength, good chemical and corrosion resistances and low cost, while thermoplastics are usually added to allow softening and rework under moderate heat. The conductive fillers provide the composites with electrical conductivity through contact between the conductive particles. The possible conductive fillers include silver (Ag), gold (Au), nickel (Ni), copper (Cu) and carbon in various sizes and shapes. Among different metal particles, silver flakes are the most commonly used conductive fillers for current ICAs because of the high conductivity, simple process and the maximum contact with flakes. In addition, silver is unique among all the cost-effective metals by nature of its conductive oxide. Oxides of most common metals are good electrical insulators, and copper powder, for example, becomes a poor conductor after aging. Nickel and copper-based conductive adhesives generally do not have good resistance stability, because both nickel and copper are easily oxidized. Even with antioxidants, copper-based conductive adhesives show an increase in bulk resistivity after aging, especially under high -temperature and -humidity conditions. ICAs have been used in the electronic packaging industry primarily as die attach adhesives [22-24]. Recently, ICAs have been proposed as an alternative to tin/lead solders in surface mount technology (SMT) [25, 26], flip chip

[27] and other applications. Figure 1.7 shows the schematics of SMT components and flip chip devices interconnected by ICAs instead of solder alloy.

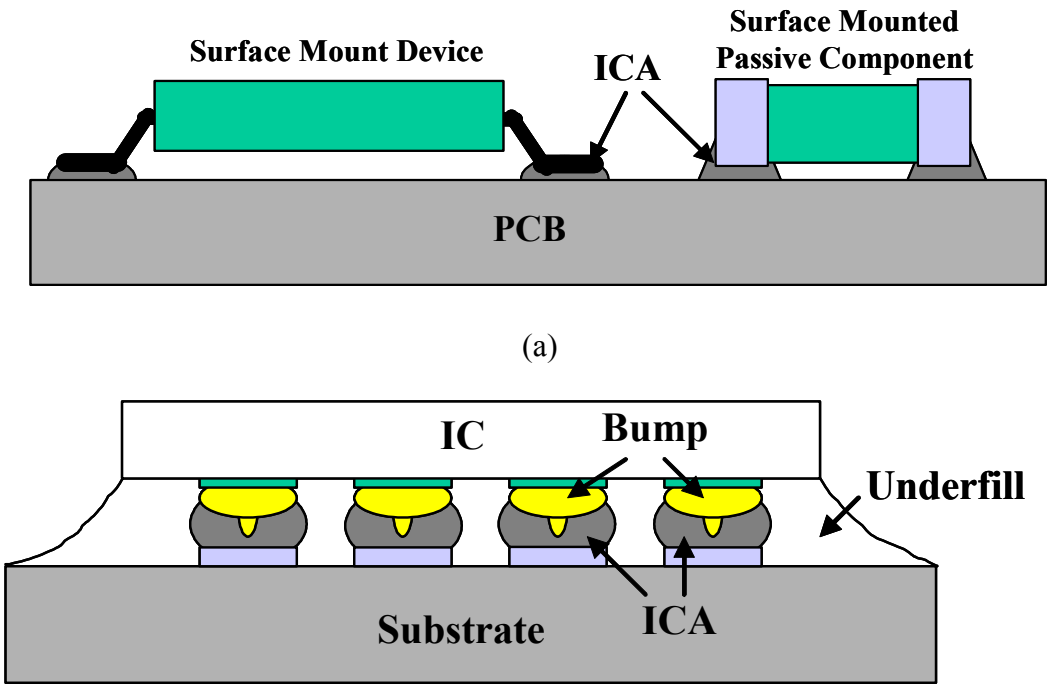

Figure 1.7 Schematic structures of (a) surface mount interconnection using ICA, and (b) flip chip interconnection using ICA.

1.2.3.1 ICAs for Die (chip) attach adhesives

The principal function of die attach adhesives is to mechanically attach the integrated chip (IC) to the substrates in a highly reliable manner. Die attach can be accomplished using one of several materials. A good die attach material must have attributes fitted to the desired functionality which is often governed by mechanical, thermal, and electrical properties. Sufficient adhesion is required to ensure that the die

remains fixed in place when it is subjected to assembly processing or during actual device service. Thermally, it shall impart the least stress during expansion and effectively accommodate transfer of heat generated in the die to the package. Until recently, hermetic die attach was accomplished using inorganic adhesives such as silver filled glass, gold/tin or gold/silicon eutectic. Eutectic die attach is a low throughput, manual method that cannot be easily adapted for high speed automation. Although silver/glass die attach has provided some processability improvements over the eutectic process, it still requires a lengthy and precise temperature profile in order to remove the organic vehicle at a controlled rate. As die sizes become larger, silver glass firing process becomes difficult to control. In hermetic packages, the high temperature eutectic and silver filled glass die attach raise concern on mechanical, thermal, and diffusional stresses that greatly affect device performance, thereby prompting the use of a polymeric substitute processed at low temperatures. Good dispensibility is certainly a process concern, which is necessary to minimize non-uniform die attach especially in large die. Non-uniform die attach can enhance die stresses (causing the die cracks), thus becoming a reliability issue. Polymer adhesives are used extensively in the attachment of IC to a variety of electronic packages. The polymer based adhesives offer many advantages such as lower stresses on IC die due to low material moduli (both the storage and loss moduli) and curing temperature, ease of use in a manufacturing environment, and low cost compared to inorganic adhesives [28-30]. For certain cases, the attachment of some bare IC die also requires electrical contact to the backside of the die. In these applications, a conductive die attach adhesive is used. The electrical reliability of polymer adhesive is crucial to the operation of certain IC devices and is related to the thermal treatments that

the adhesive is subjected to during the fabrication of the electronic package. For example, wirebonding and lid sealing (brazing) are two steps which expose the die attach adhesive to temperatures on the order of 300^{o}C.

Another factor that affects not only die attach process but also device functioning is outgassing. Evolution of solvents in solvent-based die attach material in the succeeding steps, e.g. curing, sealing, which produces voids exceeding 15% of the die attach area is rejected. Voids are considered stress raisers and can bring some degree of inhomogeneity in the die attach, altering some operational properties. In some hermetic packages, outgassing of dissolved moisture increases moisture content in the package headspace, consequently hasten a number of physi-chemical mechanisms that eventually lead to device failures. Thus, control of moisture in electronic packages is very important [31].

Most conventional epoxy-based die attach adhesives currently in use for plastic packaging have reached their limits due to trends toward larger die sizes, thinner packages in a wide diversity of configurations including Thin Small Outline Package (TSOP), Thin Quad Flat Package (TQFP), Ball Grid Array (BGA), Power Quad Packages (PQP), etc. Die attach delamination and "popcorn" cracking (the absorbed moisture within the polymer becomes vaporized rapidly during the surface mounting reflow process of the components, as such, it cracks the plastic package or the silicon die) are among the most troublesome problems with these types of packages. To date, attempts to prevent problems have been focused on improvement of epoxy compounds, reduction of moisture absorption, dimpling of leadframes, dry pack bags and have achieved some success. The die attach adhesive still remains the weak link and epoxy die attach is inadequate for the most difficult package configurations. Cyanate-ester-based die attach

adhesives have found increased popularity for many applications including hermetic as well as plastic molded IC packages. Principal advantages of cyanate thermosets are high heat resistance, low outgassing of volatiles, and easily modified to satisfy various application requirements. The unmodified cyanate/silver material has gained rapid acceptance in the industry for solder seal hermetic applications because if offers both ease of processing and high reliability. New product development includes formulations with multi-modal silver size and silver loading as high as > 90 weight % to enhance electrical and thermal performance. With its high modulus, this adhesive is not suitable for most plastic package applications. Copolymerization of polycyanate thermoset and a thermoplastic elastomer yields a toughened and flexible composite suitable for use in the formulations with low stress die attach adhesive for plastic packages. With increasing chip sizes, "popcorn cracking" is among the most of the reliability problems. Modified cyanate-ester-based adhesives with low moisture absorption can offer a unique combination of properties such as lower modulus, good heat strength and less moisture outgassing at reflow temperature (>260^{o}C), and provides a solution to the persistence popcorn problem.

1.2.3.2 ICAs for Surface Mount Technologies

Surface-mount technology (SMT) is the main technique for interconnecting chip components to substrate by packing and placing the components on the printed circuit board and using the reflow furnace to melt the solder alloy for the electronic system interconnection. Tin-lead (Sn-Pb) solder has been exclusively used as the interconnection material in surface-mount technology, because current commercial ECAs, in spite of the numerous advantages, cannot be used as drop-in replacements for solder in all

applications due to some challenging issues. Due to the extreme toxicity of lead and legislations for lead-free electronics, world-wide efforts have been put in the study of ICAs. Significant progress has been made to address different materials properties and reliability issues for the development of high performance ICAs as a potential replacement of lead-containing solders in SMT application as well.

1.2.3.3 ICAs for Flip Chip Interconnects

Isotropic conductive adhesive materials use much higher loading than ACAs to give electrical conduction isotropically or in all directions throughout the material. In order for these materials to be used for flip-chip applications, it is necessary to apply them selectively onto those areas which are to be electrically interconnected, and to ensure that spreading of the materials does not occur during placement or curing which would cause electrical shorts between the separate pathways. ICAs are generally supplied in paste form. To precisely deposit the ICA paste, screen or stencil printing is most commonly used. However, to do this to the scale and accuracy required for flip-chip bonding would require very accurate pattern alignment. To overcome this requirement, the transfer method may be used. For this technique, raised studs or pillars are required on either the die or the substrate. The ICA is then selectively transferred to the raised area by contacting the face of the die or the substrate to a flat thin film of the ICA paste which adheres to the prominent surfaces. This thin film may be produced by screen printing and the transfer thickness may be controlled by changing the printed film thickness. This method confines the paste to the area of the contact surfaces and the quantity may be adequately controlled so as to prevent spreading between pathways when the die is

placed. Pressure during bonding is not required for this technique which gives the option of oven curing the assembly.

In a high volume environment, the high precision screen printing techniques to print the ICA paste directly onto the I/O pads of the substrate can be used. This would remove the requirement for stud pillars on the substrate track terminations and quite possibly the need for bumping of the flip-chip pads. Once such a process is in place, the ICA technique could then compete with the ACA method on the basis of speed and ease of processing, however, substantial improvements in bond strength will need to be made before the technique can be realistically considered. Unlike ACA flip-chip bonding, however, a separate underfilling step would be required with ICA flip-chip bonding to improve long-term reliability of the bond. It shows that reliability is quite good with ICA flip-chip joining on rigid substrate [32]. The difficulties with the ICA flip-chip joining technology are the poor processibility and small process window in handling of the flip-chip module directly after assembly.

1.2.4 Anisotropically Conductive Adhesives/Films (ACAs/ACFs)

Anisotropic conductive adhesives (ACAs) or anisotropic conductive films (ACFs) provide uni-directional electrical conductivity in the vertical or Z-axis. This directional conductivity is achieved by using a relatively low volume loading of conductive filler (5 to 20 volume percent) [33-35]. The low volume loading is insufficient for inter-particle contact and prevents conductivity in the X-Y plane of the adhesive. The Z-axis adhesive, in film or paste form, is interposed between the surfaces to be connected. Heat and pressure are applied simultaneously to this stack-up until the particles bridge the two conductor surfaces. Because of the anisotropy, ACA/ACF may be deposited over the

entire contact region, greatly facilitating materials application. Also, an ultra fine pitch interconnection (<0.04 mm) could be achieved easily. The fine pitch capability of ACA/ACF would be limited by the particle size of the conductive filler, which can be a few microns or a few nanometers in diameter.

1.2.4.1 ACAs Materials and Processing

When designing materials to achieve fine pitch interconnections, several important variables must be considered and are application dependent. These variables include adhesive characteristics as well as particle types.

Two basic types of adhesives are available: thermosetting and thermoplastic materials. Thermoplastic adhesives are rigid materials at temperatures below the glass transition temperature (Tg) of a polymer. Above Tg, polymers exhibit flow characteristics. When using this type of material, assembly temperatures must exceed the Tg to achieve good adhesion. The principal advantage of the thermoplastic adhesives is the relative ease with which the interconnection can be disassembled for repair operations. Thermosetting adhesives, such as epoxies and silicones, form a three-dimensional cross-linked structure when cured under specific conditions. Curing techniques include: heat, UV light, and added catalyst. As a result of this irreversible cure reaction, the initial uncross-linked material is transformed into a rigid solid. The curing reaction is not reversible. This fact may hinder disassembly and interconnection repair. The ability to maintain strength at high temperature and the deformation of robust adhesive bonds are the principal advantages of these materials. For the selection of the adhesive, the robust bonds should be formed to all surfaces involved in the interconnection. Numerous materials surfaces can be found in the interconnection region

including: SiO_2, Si_3N_4, SiON, polyester, polyimide, FR-4, glass, gold, copper, and aluminum. Adhesion to these surfaces must be preserved after standard tests such as temperature-humidity-bias aging and temperature cycling. Some surfaces may require chemical treatment to achieve good adhesion. In addition, the adhesive must not contain ionic impurities that would degrade electrical performance of the interconnections.

The materials used as conductive particles must also be carefully selected. Silver (Ag) offers moderate cost, high electrical conductivity, high current carrying ability- even its oxide is still electrical conductive, and low chemical reactivity. Therefore, silver is the most commonly used conductive fillers for ICAs. However, problems with electromigration, especially under high bias condition may occur. Besides silver, gold (Au) is also widely used conductive filler due to its high conductive and inertness nature. However, it is a noble metal and costs may be prohibitive for large-volume applications. Copper (Cu) due to its high conductivity and low cost appears to be another logical choice, but the challenge of easy oxidation under heat and humidity conditions somewhat limits the widely applications in conductive adhesives unless plating or complexing approaches are used. Nickel (Ni) is a lower cost alternative, but corrosion and oxidation of nickel surfaces has been found during accelerated aging tests. Metal (Ni and Au) plated polymeric particles may offer the best combination of properties at moderate cost and therefore are commonly used in fine pitch interconnection. Some ACA/ACF materials used solder (Sn/Pb) particles to ensure electrical contacts with high reliability by creating a metallurgical bond.

ACF assembly process requires the application of pressure during adhesive cure. Curing of adhesive needs standard method to supply the energy and initiate the chemical

reaction. Heat is the typical used method while sometimes ultra-violet (UV) radiation is also used to initiate the reaction. These energy sources are easily incorporated into the process. Special equipment is needed to apply pressure during cure. Typically, heat is supplied from the thermode used for component pick-up, whereas UV is usually brought through the substrate by optical fiber bundles. The chip would be aligned to the contact pads on the substrate prior to being heated and pressed during assembly process. Therefore, an ultra fine pitch interconnection can be achieved easily using ACF.

Important process parameters for ACA/ACF assembly are temperature, pressure load, tacking time (time needed for the adhesive to soften and flow), and bonding time (final cure time) [36]. For typical ACA/ACF processes, one of the interconnecting parts is preheated to a temperature below the ACA/ACF bonding temperature, but high enough to partially soften the film so that it has the ability to flow and fill void areas. The bonding load should be high enough to allow the conductive spheres to make good physical contact between conductors but not high enough to damage any of the parts. Finally, the tacking time should be sufficient to give adequate time for the film to flow before cure begins so that it seals the contact area during the final bonding process. Many parameters can affect the bonding quality during the ACA/ACF bonding process, including [37]:

- Curing temperature and time
- Bonding temperature and time
- Temperature ramp rate
- Alignment accuracy
- Pressure value, pressure distribution and pressure application rate

- Bump height and uniformity
- Board planarity and stiffness of the contact interfaces.

1.2.4.2 ACAs/ACFs for Flat Panel Displays

Interconnection technologies using ACFs are major packaging methods for flat panel display modules to be high resolution, light weight, thin profile and low consumption power [38], and already successfully implemented in the forms of Out Lead Bonding (OLB), flex to PCB bonding (PCB), reliable direct chip attach such as Chip-On-Glass (COG), Chip-On-Film (COF) for flat panel display modules [39-42], including liquid crystal display (LCD), plasma display panel (PDP) and organic light emitting diode display (OLED). As for the small and fine pitched bump of driver ICs to be packaged, fine pitch capability of ACF interconnection is much more desired for COG, COF and even OLB assemblies. There have been advances in development works for improved material system and design rule for ACF materials to meet fine pitch capability and better adhesion characteristics of ACF interconnection for flat panel displays.

In addition to the LCD industry, ACA/ACF is now finding applications in flex circuits and surface mount technology (SMT) for chip-scale package (CSP), application specific integrated circuit (ASIC), and flip chip attachment for cell phones, radios, personal digital assistants (PDAs), sensor chip in digital cameras, and memory chip in lap-top computers. Figure 1.8 shows various packaging technologies using ACF for LCD modules; tape-carrier packages (TCP), COG and COF bonding. Since connection pitch of driver IC electrode has been decreased and the number of output electrodes per IC increased for the progress of high resolution LCD modules, ACF materials and packaging technologies have also been developed to meet high density interconnection capability.

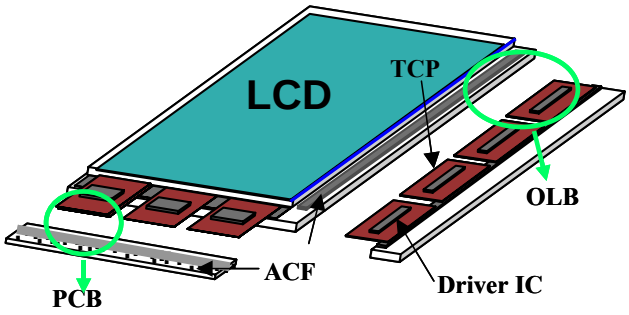

(a)

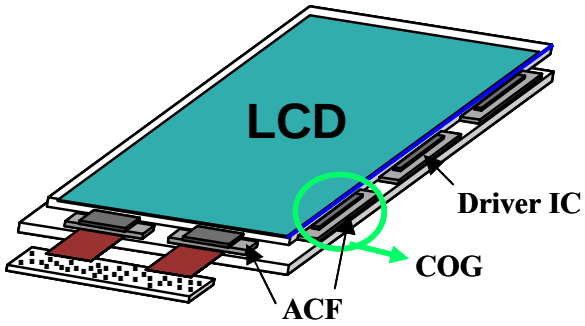

(b)

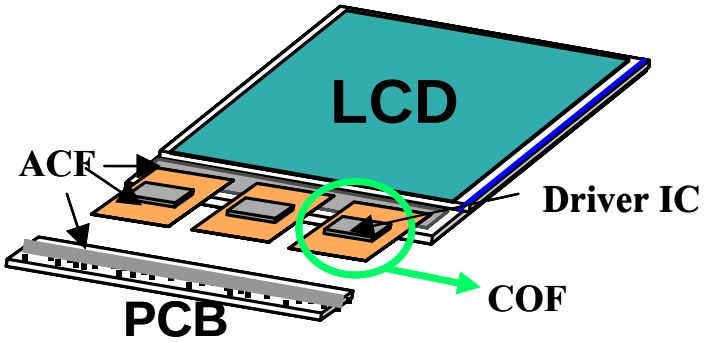

(c)

Figure 1.8 Various packaging technologies using ACF in LCD modules (a) TCP; Outer Lead Bonding (OLB) and PCB bonding, (b) COG bonding and (c) COF bonding.

ACF bonding process is thermo-compression bonding as shown in Figure 1.9. In case of TCP bonding, ACF material is attached on glass substrate after release film removal and TCP with driver IC is pre-attached. Then final bonding is established by

thermal cure of ACF resin, typically at 180 ^{o}C, 20 seconds and 30 kgf/cm^{2} and conductive particle deformation between the electrodes of TCP and glass substrate by applied bonding pressure.

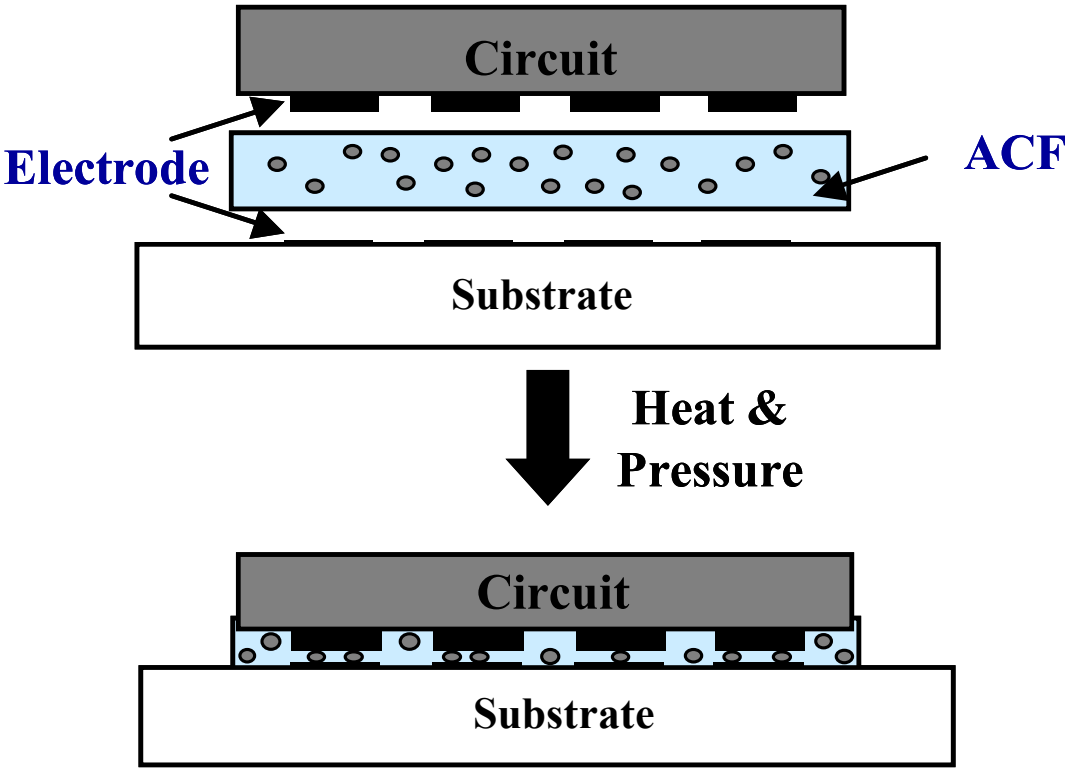

Figure 1.9 Thermo-compression bonding using ACF

The kind, size, density of conductive fillers and adhesive resin systems are different according to packaging technologies for LCD module. When TCP is mounted using ACF on LCD glass substrate, the CTE mismatch between TCP and the panel should be considered for thermal bonding, and this is more serious for finer pitch TCP bonding below 50 μm. For flex to glass bonding below 50 μm pitch, COF using ACF

become more popular due to several advantages like fine pitch capability, design flexibility and low CTE base material. ACF are also used in attaching fine-pitched driver IC on COF substrates. The geometry of COF is very similar to that of TCP. However the substrate is different, that is two-layer structure, normally Cu and polyimide (PI) which is thinner, higher density, better flexible and more durable in high temperature than TCP with three-layer structure (Cu, adhesive and PI). COF's two-layer structure without adhesive layer is normally weak adhesion property with ACF materials. Therefore, there has been development in ACF adhesion improvement to two-layer COF substrate.

In COG technology, the bare driver ICs are flip chip bonded on glass substrate using ACF, and it is most advantageous technology for low cost and compact size LCD module production [43]. The CTE difference between driver IC and glass substrate is relatively small compared with that in TCP applications and it provides more reliable COG connections.

1.2.4.3 ACAs/ACFs for Fine Pitch Interconnections

As the function of driver IC for high-resolution LCD module increases, the bump density on IC also becomes increased and this mean bump size and pitch are reduced. For fine pitch COG connection using ACF, the number of conductive particles trapped between the bump and substrate pad should be enough. Therefore, conductive particle density of ACF for COG is much higher than that of ACF for TCP OLB. But due to high density of conductive particles, there is high possibility of electrical short between adjacent bumps, mainly due to conductive particle accumulation by being flowed into the bump gap during COG bonding process. Therefore double-layer ACF, which composed of ACF layer and NCF layer without conductive filler, was developed to have high

electrical conductivity between bump and ITO electrode and electrical insulation between adjacent bumps [44]. As bump size and pitch of driver IC decreased, insulating layer coated conductive particle was introduced instead of conventional conductive particles in ACF layer, and non-conductive fillers were incorporated together with conductive particles to ensure electrical insulation [45].

1.2.5 Nonconductive Adhesives/Films (NCAs/NCFs)

Electrically conductive adhesive joints can be formed using non-filled organic adhesives, i.e. without any conductive filler particles. The electrical connection of NCA is achieved by sealing the two contact partners under pressure and heat. Thus, the small gap contact is created, approaching the two surfaces to the distance of the surface asperities. The formation of contact spots depends on the surface roughness of the contact partners [46-51]. Approaching the two surfaces enables a small number of contact spots to form which allows the electric current to flow. When the parts are pressed together during the sealing process, the number and area of the single contact spots are increased according to the macroscopic elasticity or flexibility of the parts and the micro-hardness and plasticity of the surfaces, respectively.

Conductive joints with non-conductive adhesives provide a number of advantages compared to other adhesive bonding techniques. NCA joints avoid short-circuiting and are not limited, in terms of particle size or percolation phenomena, to a reduction of connector pitches. Further advantages include cost-effectiveness, ease of processing regarding the possibility of non-structured adhesive application, good compatibility with a wide range of contact materials, and low temperature cure. In fact, the pitch size of the NCA joint can be limited only by the pitch pattern of the bond pad, rather than the

adhesive materials. This NCA has showed higher current carrying capability than the ACA joints. In addition, the contact resistance was found to be the same order of magnitude as the copper foils. Figure 1.10 shows the schematic illustration of flip chip CSP using NCF as first level interconnection and its cross-section view of Au stud bump joint.

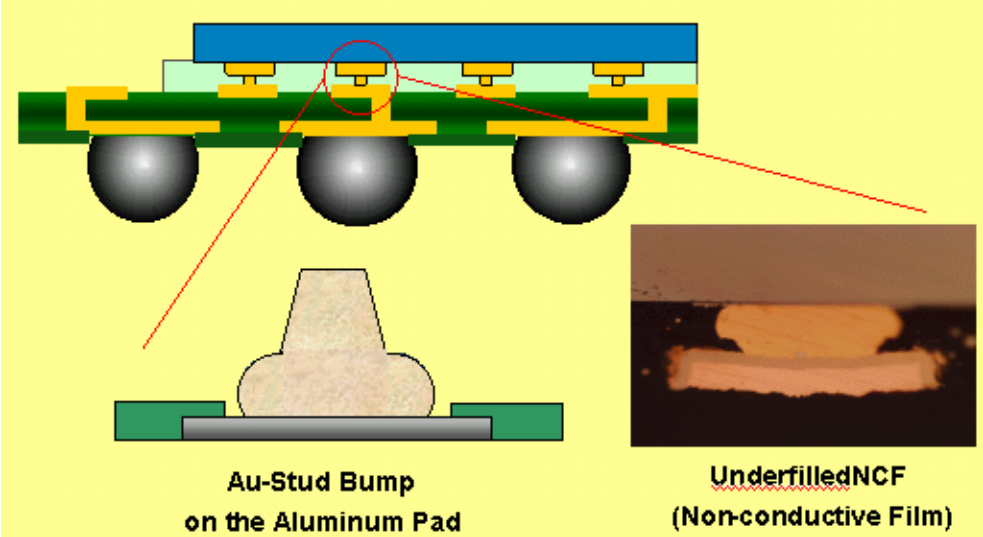

Figure 1.10 Schematic illustration of flip chip CSP using NCF and cross-section of NCF interconnection.

For NCA the electrical conductivity is also achieved through physical contact (although formed under high pressure), and no metallurgical joints were formed. Therefore, it has the unstable contact resistance problem. Finite element method (FEM) was applied by researchers to investigate the shear stress distribution induced by coefficient of thermal expansion (CTE) mismatch. Effect of temperature variation and failure mechanism of the adhesive material were also studied by means of FEM [52]. It

shows that failures occurring in NCA joints are caused by moisture induced hygroscopic swelling and stress relaxation. These factors affect the degradation of the compressive force that maintains the mechanical contact in NCA flip chip structure. The common failure modes include interfacial delamination, bump/pad opening as well as cracking. In order to improve the CTE mismatch problem, non conducting silica fillers were incorporated to enhance the reliability of NCA interconnects by providing a stronger anchoring force which minimizing the shear stress deformation of joining structure [53]. It was reported that the content of nonconducting filler is a key factor that controls the basic properties of NCA materials. Addition of nonconducting fillers could noticeably affect CTE of NCA and adhesion on flip chip assemblies. By optimizing the non-conducting filler content, a significantly improved NCA flip chip assembly reliability was achieved.

1.3 Electrically Conductive Adhesives Challenges

Although ECAs have exhibited numerous advantages over the traditional solder joints as environmentally friendly lead-free interconnect materials, current ECAs materials still have some limitations and challenging properties, such as a lower electrical and thermal conductivity compared to solder interconnects, conductivity fatigue in reliability tests, limited current carrying capability, metal migration fatigue in reliability and high voltage tests, and poor impact strength, etc. The mechanism behind the challenges is mainly the limited interfacial properties. Therefore, fundamental understanding and the enhancement of the interfacial properties of ECAs are important for the development of high performance ECAs as solder replacement in various applications.

Furthermore, according to the National Electronic Manufacturing Initiative (NEMI), a North American Consortium and the International Technology Roadmap for Semiconductor Technology (ITRS) (2004), project fine pitch (<150 μm) and large I/O (>5,000) devices are needed. In addition, the roadmap in NEMI Chip Interconnect Needs shows 25~50 μm for wire bonding, Tape Automatic Bonding (TAB) and area arrayed flip-chip by 2012. 10 μm pitch is required for opto-electronics by 2012. For the IC feature, 65 nm technologies are being used from 2006 and 45 nm technologies are on the way for next generation microarchitecture from major industry such as Intel. Table 1.2 shows some trends in the microelectronic manufacturing [54]. The most frequently cited trend is so-called scaling down, e.g. the ability for industry to exponentially decrease the minimum feature size used to fabricate integrated circuits. As such, the requirements for the pitch size reduction become very stringent which result in the nano interconnect and manufacturing technologies. In addition, the requirements for high frequency and high power delivery capability in the microelectronics manufacturing are pushing the acceleration of innovation in design concepts, packaging architectures, materials, manufacturing processes and systems integration technologies.

Table 1.2 Trends in the microelectronic manufacturing

Year	2005	2007	2010	2013	2017
DRAM ½ pitch (nm)	80	65	45	32	22
Chip Size DRAM (mm^2)	568	662	563	560	464
Max Substrate Diameter (mm)	300	300	450	450	450
Max No. of I/O MPU	3072	3072	3840	4224	4416
Flip-chip Pitch (micron) Area Array	130	120	100	90	80
On-chip Frequency (MHz)	5204	9285	15079	22980	39683
Allowable Max Power (W) MPU	167	189	218	251	288

1.4 Research Objectives/Methodology

Electrically conductive adhesives (ECAs) are composite of polymeric matrix and conductive fillers. Recently, ECA materials have been identified as one of the major alternatives for lead-containing solders for microelectronics packaging applications. ECAs offer numerous advantages over conventional solder technology, such as environmental friendliness, mild processing conditions (enabling the use of heat-sensitive and low-cost components and substrates), fewer processing steps (reducing processing cost), low stress on the substrates, and fine pitch interconnect capability (enabling the miniaturization of electronic devices). However, the limited interfacial properties of ECAs have restricted their application in some high power/high reliability devices. The objectives of this work are to conduct fundamental study on the interfacial properties of different types of conductive adhesives and enhance their electrical and thermal

properties with surface functionalization or interfacial modification. The detailed goals and methodology of this research are highlighted as following:

1.4.1 Investigation of interfacial properties of ICAs and improvement of electrical conductivity and reliability of ICAs interconnect materials

In order to enhance the electrical properties and reliability of ICAs as a potential solder replacement in microelectronics interconnects, interfacial properties of the ICA composites will be investigated and modified with various types of acids. Interactions between dicarboxylic acids and silver flakes will be investigated and incorporated into the ICA formulation to partially replace or remove to insulation layer on silver flakes. The effects of dicarboxylic acids on the electrical and mechanical properties of ICAs will be studied and the mechanism on the conductivity change will be elucidated

Ag flake-filled ECAs generally show dramatically increased contact resistance on non-noble metal finishes at elevated temperature and humidity environment due to the galvanic corrosion. In order to stabilize the contact resistance on low cost metal finishes, such as Sn surface, various types of corrosion inhibitors will be introduced. The interaction of the corrosion inhibitors and their effects on the reliability of ECAs on Sn surface will be conducted. The goal is to develop a highly reliable ICA formulation as a potential solder replacement in SMT applications.

1.4.2 Understanding of interfacial properties of ACA/ACF joints and enhancement of their electrical and thermal performance with nanotechnology

In order to enhance the electrical and thermal performance of ACA/ACF, interfacial properties between conductive fillers and electrodes should be improved. Two approaches will be employed to enhance the interface bonding of ACA/ACF joints. One

is the introduction of nano conductive fillers with low temperature sintering behavior, while the other one is the application of self-assembled monolayers (SAMs) with various functional groups and structures. Effects of nano-sized conductive fillers and SAMs on the interfacial properties, joint resistance, current carrying capability, reliability of ACA/ACF joints will be evaluated.

In addition, the silver migration behavior, insulation properties in the x-y plane as well as the high frequency characteristics of nano-ACF will be investigated. Various approaches such as monolayer protection and processing control will be applied to control the silver migration and improve the insulation properties in the nano-ECAs. The objective is to develop a novel high performance nano-ACF to be potentially used for high power and fine pitch microelectronics packaging applications.

1.4.3 Investigation of contact resistance of NCF joints with experimental and modeling and development of high performance NCF for ultra-fine pitch interconnect applications

To understand the contact resistance of NCF joints, a micromechanical model will be established. Based on the analytical expressions, effects of various processing conditions and materials properties, such as dielectric constant, thickness, metal work function, will be predicted and compared.

To verify the model and reduce the joint resistance, conjugated molecular wires will be introduced at the interface of NCF joints. Bonding of conjugated molecular wires on the Au electrodes and their thermal stability will be established. Their effects on the tunneling resistivity associated with metal work function will be investigated. The

objective is to provide guidance for the improvement of NCF joints and develop a high performance, low cost NCF joint in ultra-fine pitch interconnects.

1.4.4 Design of eco-friendly ECA with biocompatible curing agents

In order to further reduce the toxicity of ECAs, amino acids will be employed as a novel curing agent in the epoxy crosslinking reaction. The curing reaction of different ratios of amino acid (e.g. tryptophan) and epoxy and the effect of imidazole catalyst on the reaction will be evaluated. Optimum reaction conditions and ratio of epoxy/tryptophan will be determined. The reaction mechanism of imidazole-initiated reaction will be established. Some of the materials properties such as glass transition temperature and thermal stability will be characterized and compared with typical ECA resins. The goal is to develop an environmentally friendly interconnect materials toward next-generation green electronics industry.

CHAPTER 2
IMPROVEMENT OF INTERFACIAL PROPERTIES OF ISOTROPICALLY CONDUCTIVE ADHESIVES (ICAS)

2.1 Improvement of electrical conductivity of ICAs

2.1.1 Introduction

ICAs are mainly composed of polymeric matrix and conductive fillers. ICAs typically have lower electrical conductivity than solders. To enhance the electrical conductivity of ICAs, various methods have been conducted and reported in literatures.

In general, ICA pastes exhibit insulative property before cure, but the conductivity increases dramatically after cure. ICAs achieve electrical conductivity during the polymer curing process caused by the shrinkage of polymer binder. Accordingly, ICAs with high cure shrinkage generally exhibit higher conductivity [55]. With increasing cross-linking density of ICAs, the shrinkage of the polymer matrix increases, and subsequently, the resistivity of ICAs decreases. For epoxy-based ICAs, a small amount of a multi-functional epoxy resin can be added into an ICA formulation to increase cross-linking density, shrinkage, and thus increase electrical conductivity.

Another approach for improving electrical conductivity is to incorporate transient liquid-phase metallic fillers in ICA formulations. The filler used is a mixture of a high-melting-point metal powder (such as Cu) and a low-melting-point alloy powder (such as Sn-Pb or Sn-In). The low-melting-alloy filler melts when its melting point is achieved during the cure of the polymer matrix. The liquid phase dissolves the high melting point particles. The liquid exists only for a short period of time and then forms an alloy and solidifies. The electrical conduction is established through a plurality of metallurgical

connections *in-situ* formed from these two powders in a polymer binder. (Figure 2.1) The polymer binder with acid functional ingredient fluxes both the metal powders and the metals to be joined and facilitates the transient liquid bonding of the powders to form a stable metallurgical network for electrical conduction, and also forms an interpenetrating polymer network providing adhesion. High electrical conductivity can be achieved using this method [56, 57]. One critical limitation of this technology is that the numbers of combinations of low melting and high melting fillers are limited. Only certain combinations of two metallic fillers which are mutually soluble exist to form this type of metallurgical interconnections.

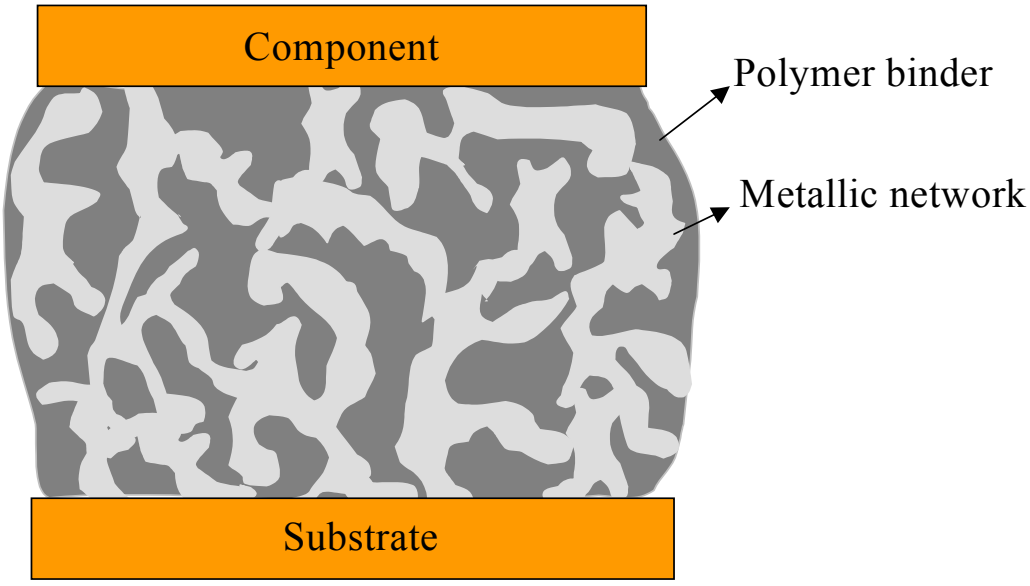

Figure 2.1 Diagram of transient liquid phase sintering conductive adhesives

For ICAs, silver flakes are the most commonly used conductive fillers because of the high conductivity, simple process and the maximum contact with flakes. In addition, silver is unique among all the cost-effective metals by nature of its conductive oxide.

Flaking of silver powder must be done in the presence of a thin layer of organic lubricant. The conventional lubricants on the surface of silver flakes are saturated or unsaturated fatty acids such as stearic, oleic, linoleic, and palmitic acid. After production of silver flakes, a thin layer of lubricant remains on the silver flake surface. The presence of such organic lubricants can reduce the viscosity of conductive adhesive paste and prevent agglomeration of silver flakes [58-61]. However, the lubricants also decrease the conductivity of the ICAs due to the insulative property of the long chain fatty acids. A possible solution to this problem is the introduction of short chain carboxylic acids into the ICA formulations. By *in-situ* replacing the stearic acid with such short chain acids, it is much easier for the electrons to tunnel/transport between silver flakes, provided that the added acids can attach to the silver flakes. An important consideration for the selection of short chain acid is the affinity of functional groups to the silver. Since carboxylic functional group (-COOH) has a strong affinity to self-assemble into a silver surface, the *in-situ* replacement of lubricant layer by short chain dicarboxylic acids should have potential for the improvement of conductivity in the ICA.

2.1.2 Experimental

2.1.2.1 Materials

The epoxy in use was a diglycidyl ether of bisphenol-F (DGEBF) EPON 862 from Shell Chemical Company. The hardener was methylhexa-hydrophthalic anhydride (MHHPA) from Lindau Chemicals, Inc. The ratio of epoxy to hardener was 1:0.85 based on the epoxide equivalent weight (EEW) of the epoxy resin and the hydroxyl equivalent weight (HEW) of the hardener. 1-cyanoethyl-2-ethyl-4-methylimidazole (2E4MZCN), from Shikoku Chemicals Corporation was employed as the catalyst and the concentration

of the catalyst was 1 part per hundred resin (phr). Two types of silver flakes (Ag FL 26LV and Ag FL52) , with particle sizes of 2–10 and 1–5 μm were donated by Ferro and incorporated at 80 wt% with 1 : 1 ratio in the ICA formulations. (SEM images of the silver flakes are shown in Figure 2.2). Malonic acid (acid M) and adipic acid (acid A) were purchased from Aldrich Chemical Company (The structure of all the acids are shown in Table 2.1). 0.5 wt% of those dicarboxylic acids were *in-situ* incorporated into the ICA formulations, respectively. All the chemicals were used as received.

Table 2.1 Chemical structures of the carboxylic acids

Acid name	**Chemical structure**	**Molecular weight**	**Molecular length (Å)**
Stearic acid	$CH_3(CH_2)_{16}COOH$	284.48	27
Adipic acid	$HOOC(CH_2)_4COOH$	146.14	9
Malonic acid	$HOOC\text{-}CH_2\text{-}COOH$	104.06	4.5

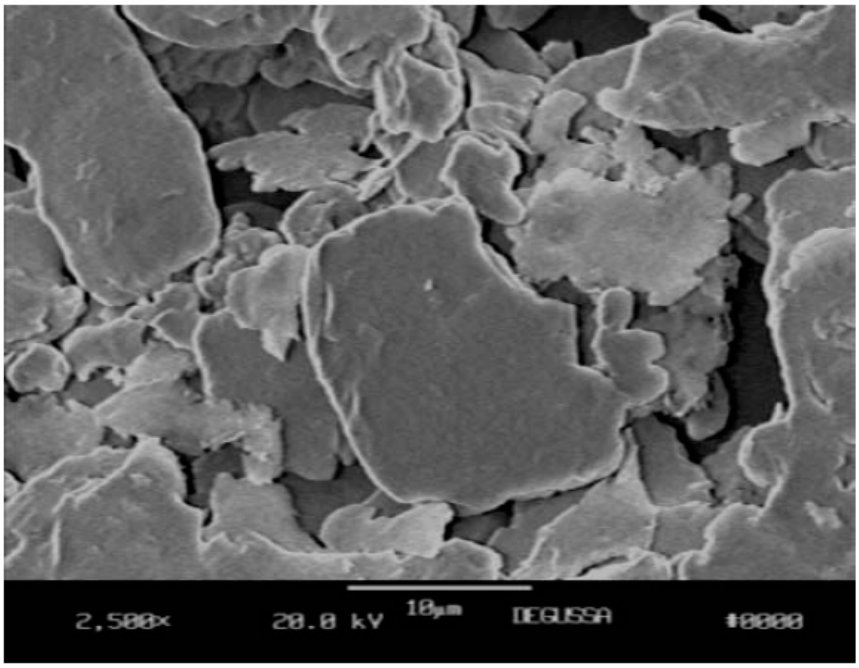

(a)

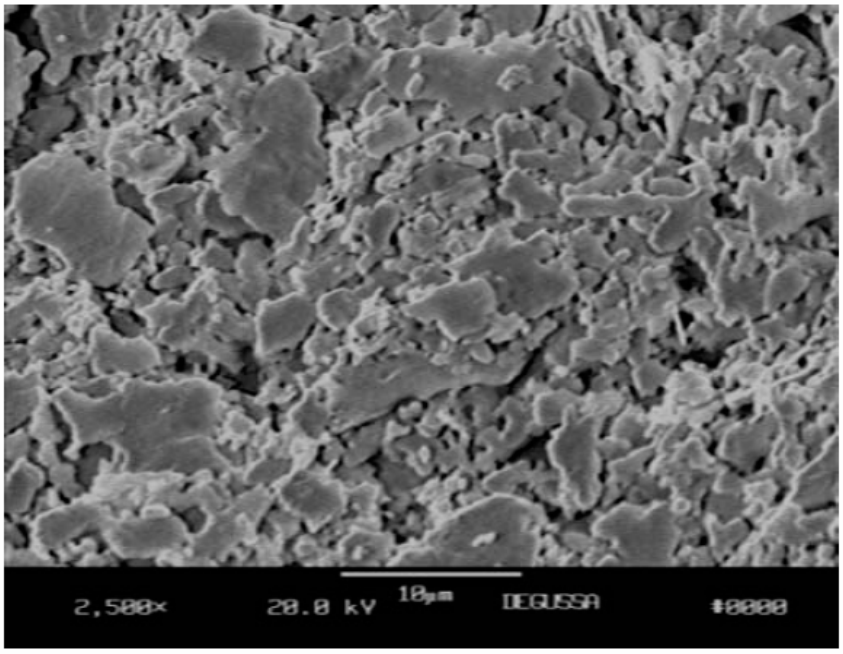

(b)

Figure 2.2 SEM pictures of commercial Ag flakes used in ICA formulations. (a) Ag flake 26LV; (b) Ag flake 52

2.1.2.2 Characterizations

The curing behavior of the ECAs was determined using a modulated differential scanning calorimeter (MDSC from TA Instruments, model 2970). A sample of about 10 mg was placed into a hermetically sealed DSC sample pan and placed in the DSC cell under a 40ml/min nitrogen purge. A dynamic scanning mode was used at a heating rate of 5°C/minute, usually from 25°C to 250°C.

Dicarboxylic acid solutions were prepared by dissolving the acids in ethanol. 15 ml of each solution was used to treat the pre-cleaned silver surfaces and silver flakes. After treatment for one hour, the samples were removed from the solutions and rinsed with ethanol in order to remove un-adhered/excess acids. The silver surfaces were dried off with argon and then the contact angle of a deionized (DI) water drpolet on the silver surfaces was measured by a goniometer.

To characterize the treatment with short chain acids, the weight loss of silver flakes before and after treatments with short chain acids was studied using a thermogravimetry analyzer (TGA) from TA Instruments, model 2050. The temperature was raised from 25°C to 600°C at a heating rate of 10°C/minute.

Resistivity of the ICAs was calculated from the bulk resistance of the specimen with specific dimensions. Two strips of an adhesive tape were applied onto a pre-cleaned glass slide with a gap between these two strips. The conductive adhesive paste was then coated within the gap space by means of a doctor blade, and then the tapes were removed. After cure, the bulk resistance (R) of this ICA strip was measured as well as the size of the specimen. A schematic of the bulk resistivity coupons is shown in Figure 2.3. The bulk resistivity, ρ, was calculated using Equation 2-1:

$$\rho = \frac{t \times w}{l} \times R \tag{2-1}$$

where l, w, t are the length, width and thickness of sample, respectively.

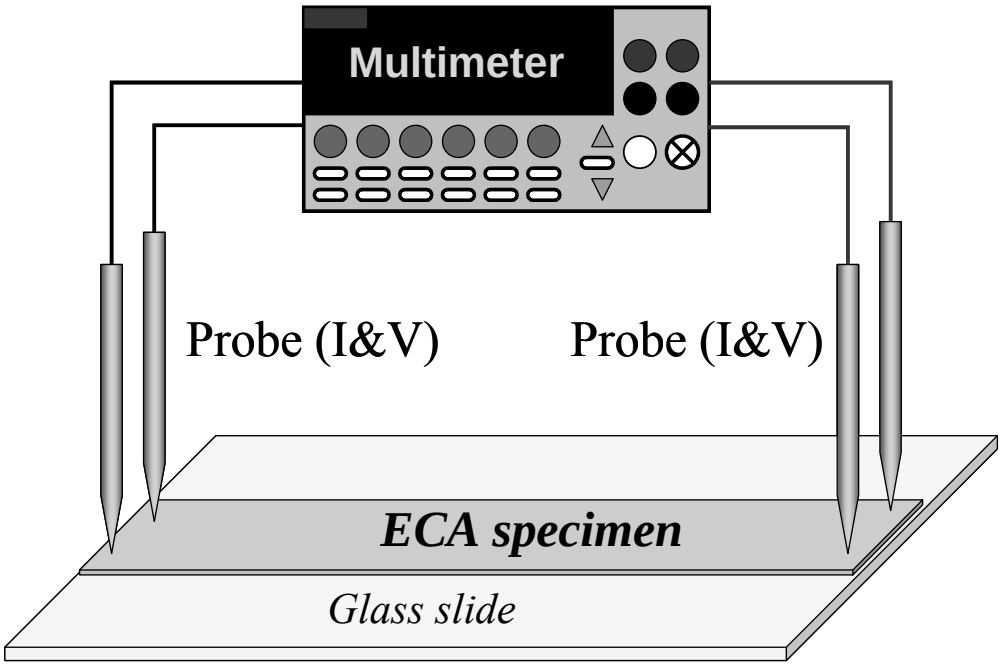

Figure 2.3 Schematic illustration of a bulk resistivity measurement

The rheology study of the adhesive formulations was conducted with a stress-controlled rheometer, model AR1000-N, from TA Instruments. A 4-cm steel parallel plate fixture was used in the study. The gap between two plates was set at 300 μm. The viscosity of the adhesive formulations was measured at room temperature under oscillation mode.

Dynamic mechanical properties of cured conductive adhesives were investigated using a dynamic mechanical analyzer (DMA) from TA Instruments, model 2980, with a

film tension clamp. After a sample was mounted on the clamp, the temperature was raised from 25°C to 200°C at a heating rate of 3°C/minute. The sample was studied under an oscillation mode with a frequency of 1 Hz. Tan delta versus temperature was recorded.

Coefficients of thermal expansions (CTEs) and glass transistion temperatures(Tgs) of ICA samples were measured with a thermomechnical analyzer (TMA) from TA Instruments, model 2940. An expansion probe was used and a static force applied on this probe was set to 0.050 Newton. Temperature was ramped from 25°C to 250°C at a heating rate of 5°C/min. The dimension change with temperature was recorded. The slope of the straight line before the Tg was the CTE, α_1, of the sample.

2.1.3 Results and Discussion

2.1.3.1 Characterization of Ag flakes

The presence and amount of surfactant (fatty acid) on silver flakes can be achieved by studying the weight change of Ag flakes with various temperatures. Two commercial Ag flakes used in ICA formulations (Ag flake 52 and Ag flake 26LV) were heated from room temperature to 500^{o}C under air atmosphere. The weight loss results of these Ag flakes were studied by TGA and shown in Figure 2.4. Both Ag flakes showed weight loss at the temperature range from 150 to 250°C and the weight loss percentages of the Ag FL 26LV and Ag FL 52 are 0.1 % and 0.2 %, respectively. Weight loss during heating indicates the presence of organic lubricants and the corresponding de-bonding/decomposition of these organic lubricants on the Ag flakes.

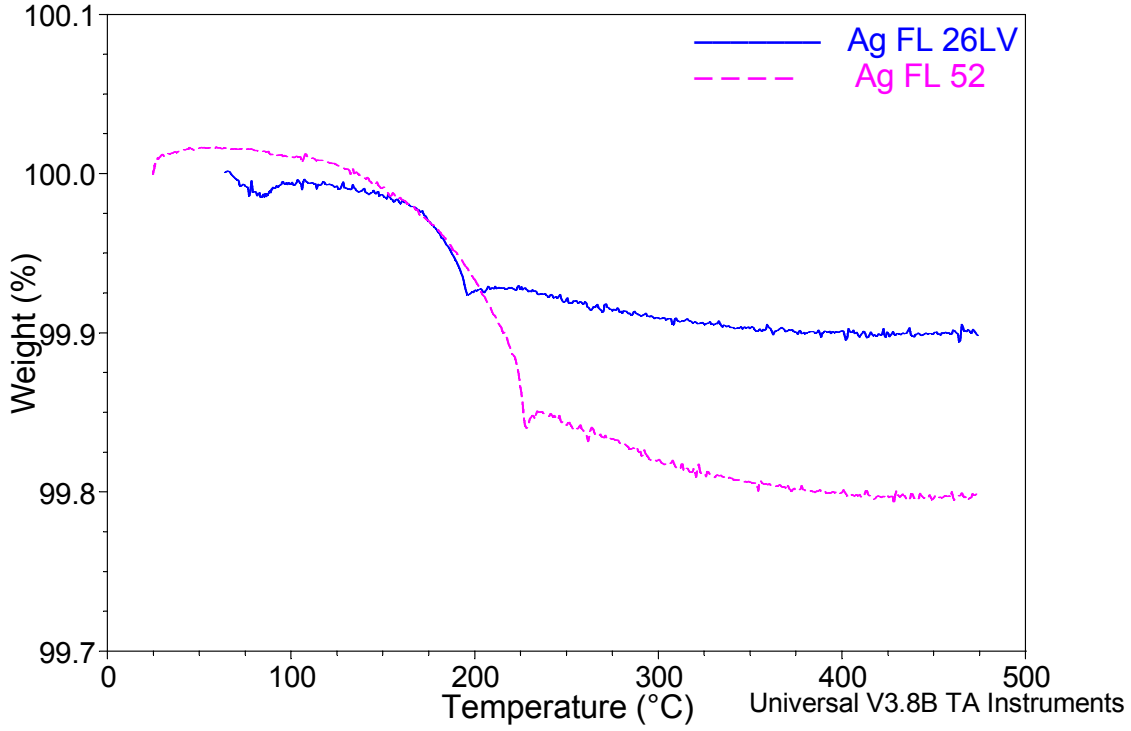

Figure 2.4 TGA analyses of Ag Flakes

2.1.3.2 Replacement of lubricants on Ag flakes with short-chain dicarboxylic acids

To investigate whether the short chain dicarboxylic acids can remove or replace the lubricant on silver flakes, the weight loss of silver flake 52 before and after di-acids treatment was measured by TGA and the results are shown in Figure 2.5. Before the treatment, silver flake (Ag FL52) showed weight loss of around 0.2 % at the temperature ranging from 200 to 250^{o}C. After treating with malonic acid (acid M) and adipic acid (acid A), there was very little weight loss in the temperature range. This indicated the lubricant on silver flakes has been partially removed or replaced by the short chain

dicarboxylic acids, due to the higher reactivity and the stronger interaction with Ag flakes.

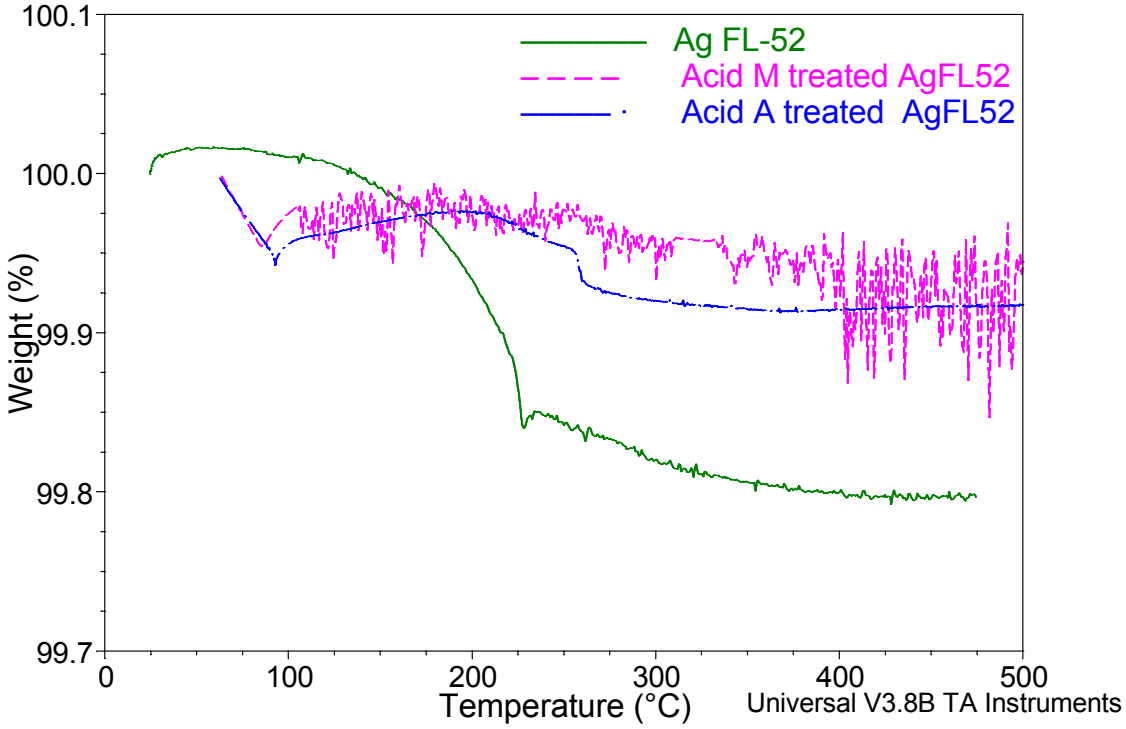

Figure 2.5 TGA curves of silver flake 52 before and after treatment with short chain dicarboxylic acids

2.1.3.3 Curing profile of ICAs

The conductivity of ICAs is established after the curing of the polymer matrix. Before curing, the composite is electrically insulating. Therefore, it is important to obtain the curing conditions of ICAs. The curing profiles of the formulated ICAs with different dicarboxylic acids are shown in Figure 2.6. From the figure, all the formulations showed similar curing behaviors and had a curing peak in the temperature range from 100 to

165°C. These DSC results suggested that addition of small amount of di-acid did not affect the curing profile of the ICAs.

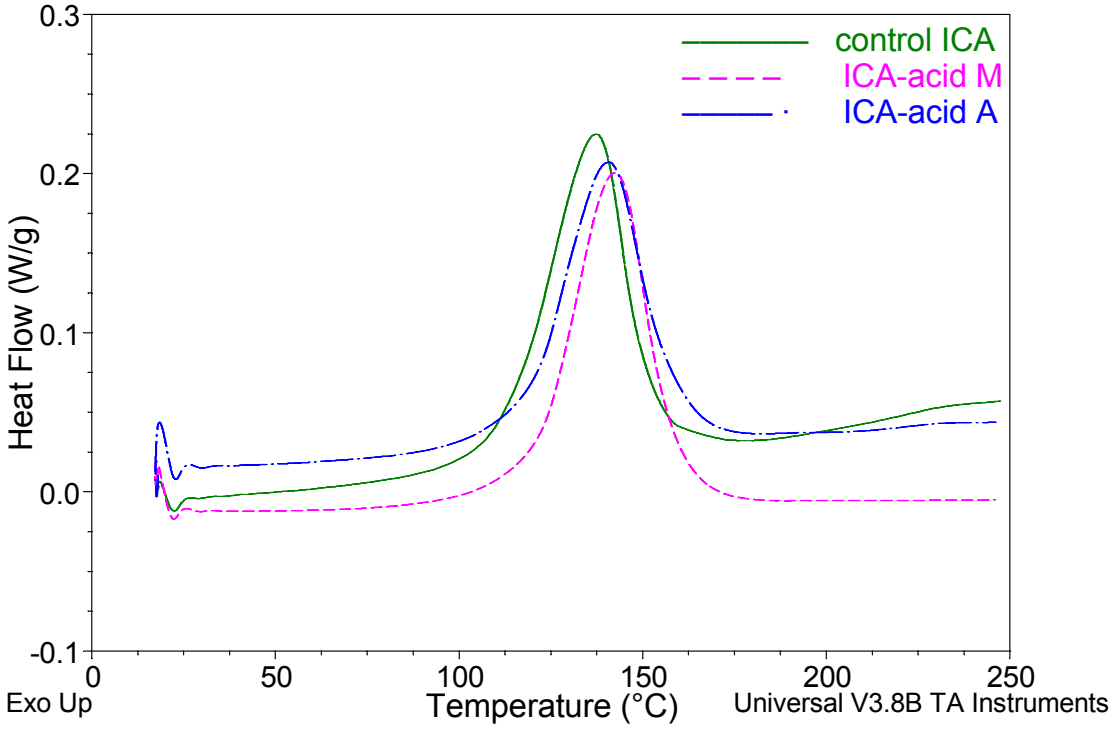

Figure 2.6 Curing profile of the ICAs with different acids measured by DSC

2.1.3.4 Effects of di-carboxylic acids on the electrical resistivity of ICAs

Effects of these short chain di-acids on the electrical conductivity of ICAs were studied. The bulk resistivity of ICA without short chain acids, the ICA with malonic acid, andthe ICA with adipic acid was measured and compared in Figure 2.7. The addition of only small amount (0.5 wt%) of malonic acid and adipic acid increased the conductivity of ICA and malonic acid performed better for the improvement of electrical conductivity

of ICA. For malonic acid and adipic acid, the molecular distance is much shorter than the stearic acid. In replacing the stearic acid in ICAs, the carboxylic groups on both ends of the added acid may form carboxylic ions (COO^-), which delocalize the charge of the anion and coordinate themselves with the Ag flakes. As such, it facilitates the electronic tunneling in the ICA, resulting a lower resistivity. The strong attraction between Ag flakes and the added acid is because the carboboxlyic anion has a strong affinity to Ag. The connection of silver flake with short-chain dicarboxylic acid helps electrons to transport along the chain and thereby improves the electrical conductivity. For malonic acid, there is only one alkyl between the dicarboxlylic groups, therefore, the transportation of electrons is much easier and showed a better result. The possible mechanism for the conductivity improvement with short-chain dicarboxylic acids can be illustrated in Figure 2.8.

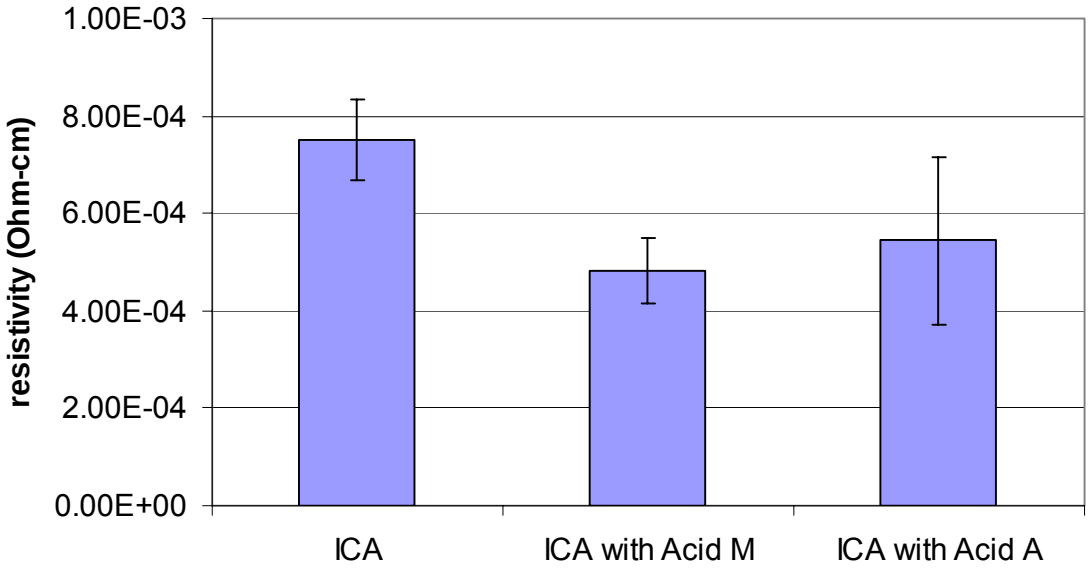

Figure 2.7 Effects of different dicarboxylic acids on the conductivity of ICAs

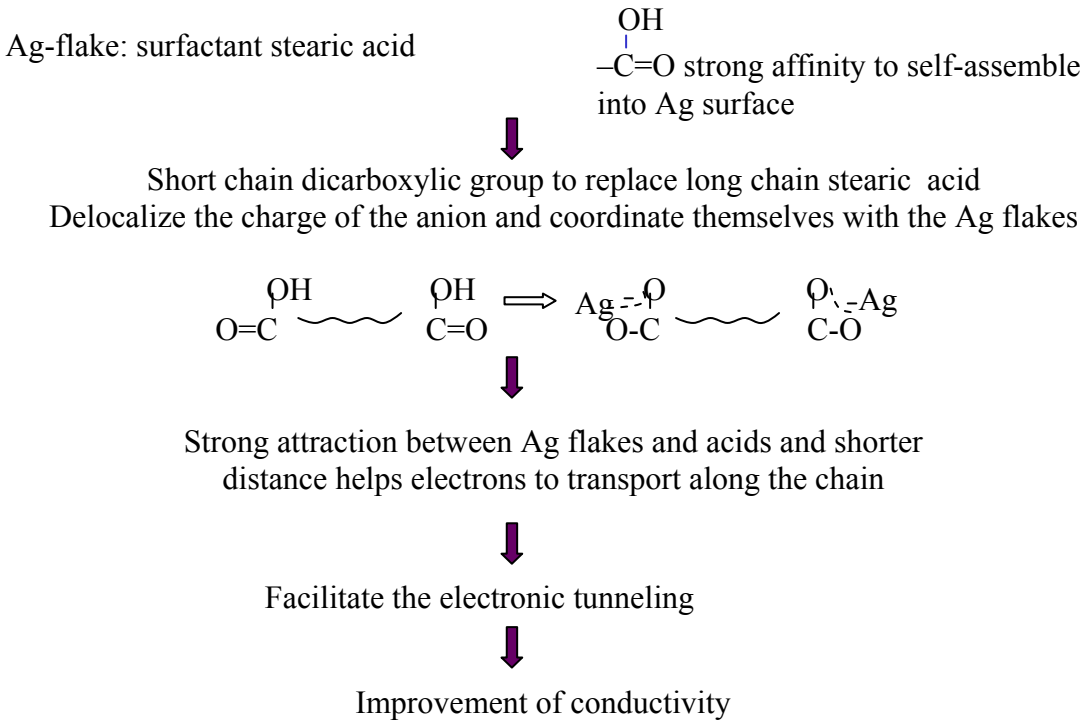

Figure 2.8 Mechanism of conductivity improvement of ICA with short chain di-acids

2.1.3.5 Effects of di-carboxylic acids on the viscosity of ICAs

Viscosity of ECAs reflects the interaction between ingredients in the formulation and also affects the processibility of the composite materials. In particular for ICAs, the higher loading of conductive fillers results in a higher viscosity. Therefore, rheology study of the ICAs is necessary. Viscosity changes of the ECA formulation after addition of a small amount (0.5% wt.) of dicarboxylic acids are shown in Figure 2.9. As can be seen from the figure, viscosity of the ICA formulation increased slightly with the addition of small amount of dicarboxylic acids. This phenomenon again suggested that these acids substituted the lubricant on Ag flakes and consequently affected the interaction between the Ag flakes and the resin and the interaction among Ag flakes. Another possible reason

is that the short chain dicarboxylic acids can work as a catalyst for crosslinking of the epoxy resin at room temperature, therefore lead to the slightly increased viscosity.

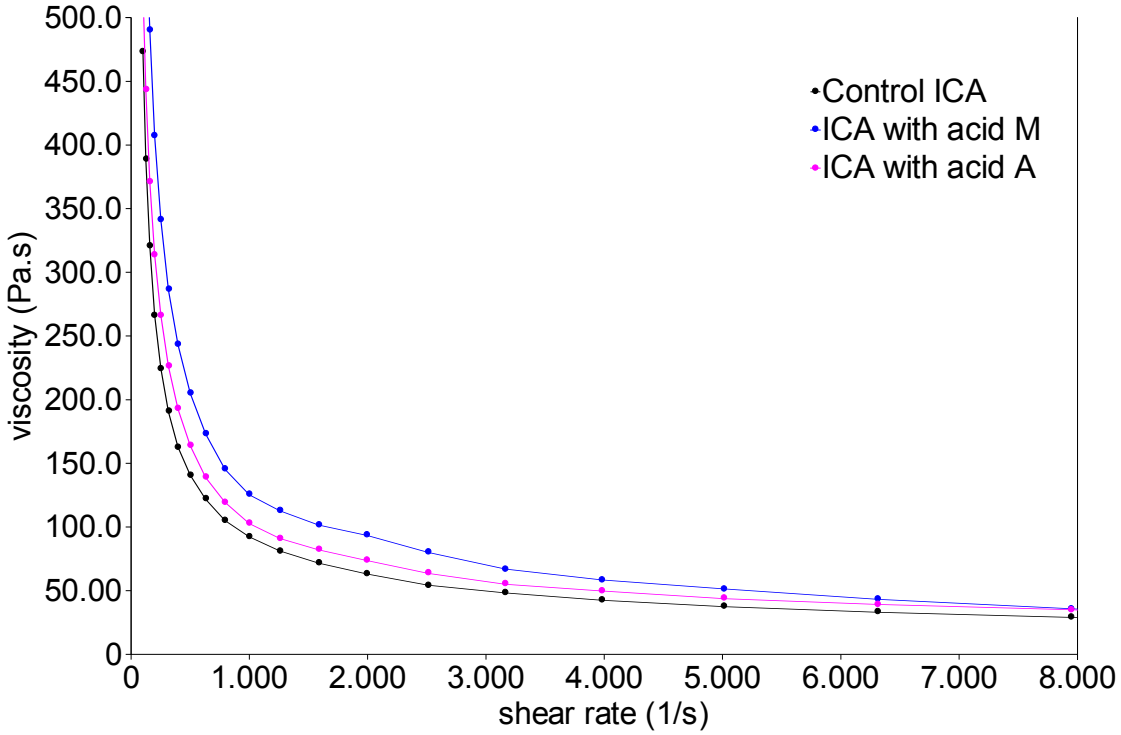

Figure 2.9 Effect of acids on viscosity of the ICA formulation

2.1.3.6 Effects of di-carboxylic acids on the modulus and coefficient of thermal expansion (CTE) of ICAs

For the interconnect materials, such as solder and conductive adhesives, not only a high electrical conductivity is required, but also a reliable mechanical strength and reasonable CTE is needed. The loss modulus of ICA is related to the damping properties

of the materials and therefore affects the impact performance of the composites. Figure 2.10 shows the loss modulus value changes with different temperatures at the temperature range from 25°C to 200°C. It can be seen that the addition of acid didn't show big difference for loss modulus. Therefore, the addition of short chain dicarboxylic acid, did not adversely affect the mechanical property.

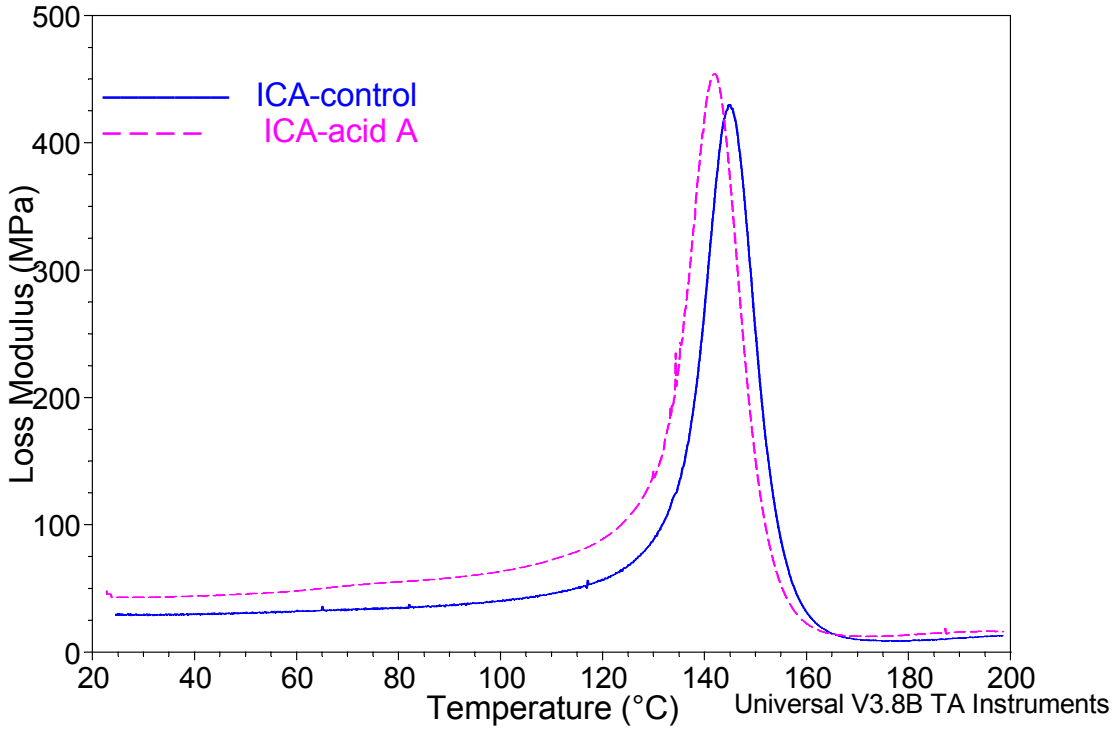

Figure 2.10 Loss Moduli of Cured ICAs without and with the carboxylic acid

Coefficient of thermal expansion (CTE) is another important parameter for the packaging materials because of the great concerns of the thermo-mechanical fatigue after exposed to various temperatures. Figure 2.11 shows the thermomechanical analyzer

(TMA) data for the ICA formulations. CTE before glass transition temperature (Tg) of the ICAs was calculated based on the slope of dimension expansion versus temperature before Tg. The CTE before Tg of ICAs with and without adipic acid are 19.5ppm/K and 22.3ppm/K, respectively. Both Tg and CTE did not show much difference after acid incorporation.

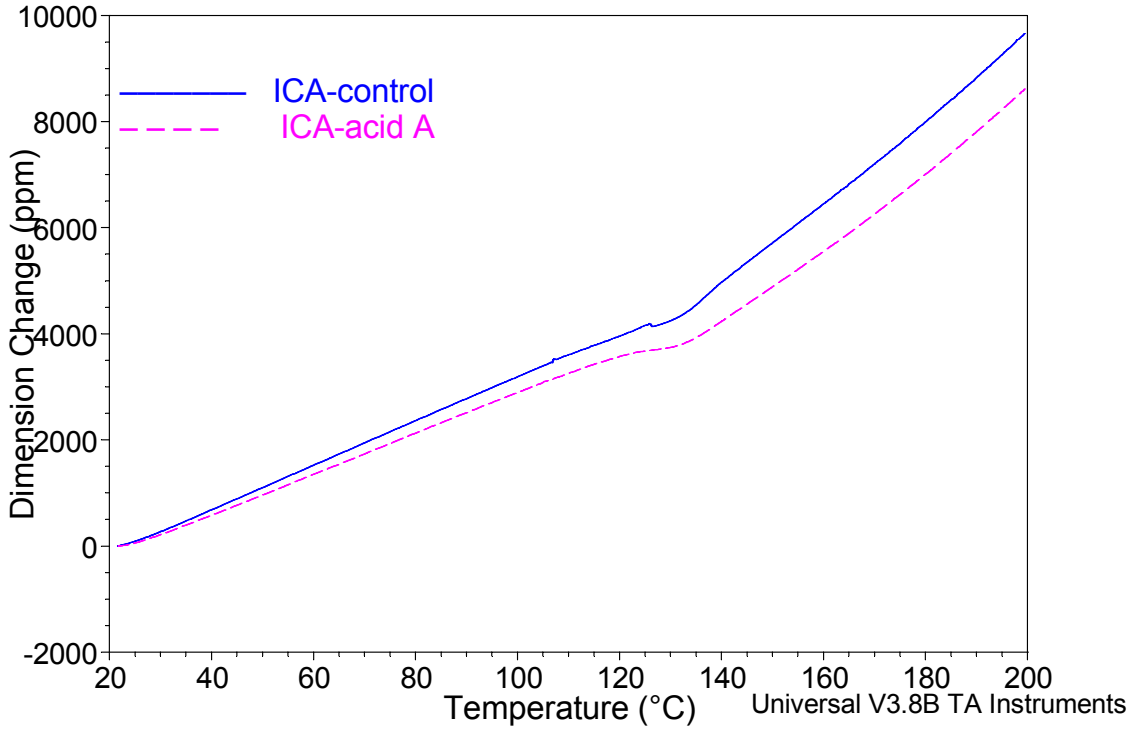

Figure 2.11 Dimension changes of Cured ICAs without and with the carboxylic acid

2.1.4 Summary

Long chain fatty acid is present on the commercial silver flakes. Short-chain dicarboxylic acids can *in-situ* remove or replace the stearic acid on Ag flakes in ICA formulations. Such replacement can improve the electrical properties of ICAs. Both

malonic acid and adipic acid, which have single-bond short chain in between the dicarboxylic groups, increase the conductivity of conductive adhesives. However, the viscosity of the ICA formulation also increases even with 0.5 wt% short chain di-acid incorporation. The increased viscosity may affect the ICA processibility.

2.2 Contact Resistance Stabilization of ICAs on Low cost Non-noble Metal Substrates

2.2.1 Introduction

Recently, polymer-based electrically-conductive adhesives (ECAs) have been identified as a potential alternative electronic interconnects for lead-containing solders in surface mount technology (SMT) applications due to their numerous advantages such as environmental friendliness, mild processing conditions, low stress on the substrates and good thermomechanical performance. However, some technical barriers concerning the ECAs still restrict their use only to the low-end products (e.g., low power device interconnects). One critical limitation of ECAs that prevents their use for high end products is their unstable contact resistance on non-noble metals, such as Sn, Ni and Sn/Pb [62, 63]. The National Center of Manufacturing Science (NCMS) defined the stability criterion for solder replacement conductive adhesives as a contact resistance shift of less than 20% after aging at 85^{o}C/85% RH for 500 hours [64], while most conductive adhesives do not satisfy on non-noble metal finishes.

Simple oxidation and galvanic corrosion of the non-noble metal surfaces are the two possible mechanisms for unstable contact resistance of ICAs. Studies have shown that galvanic corrosion at the interface between an ICA and non-noble metal is the dominant mechanism for the unstable contact resistance [65, 66]. (Figure 2.12)

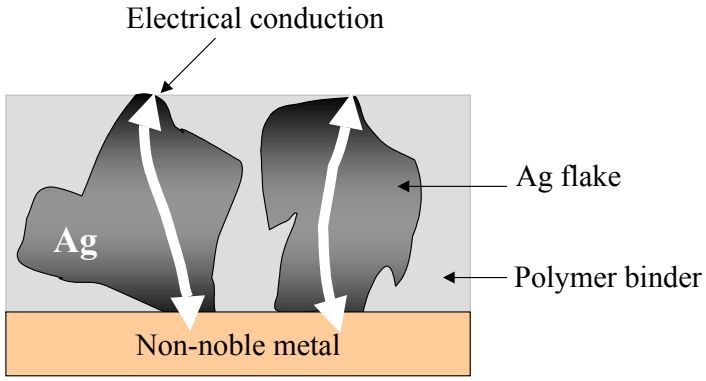

(Before corrosion)

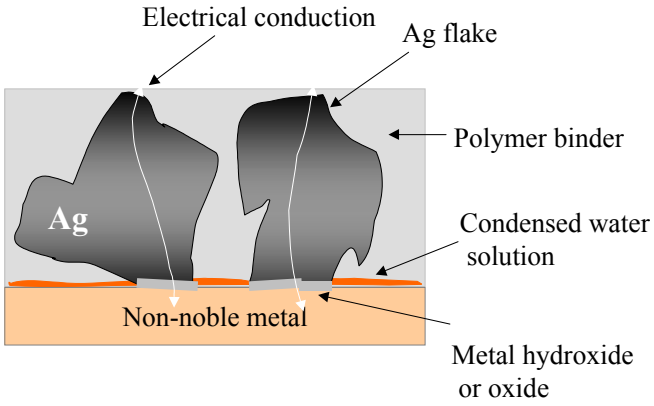

(After corrosion)

Figure 2.12 Metal hydroxide or oxide formation after galvanic corrosion

Under the aging conditions (for example, 85°C/85%RH), the non-noble metal (i.e., a metal with a lower electrochemical potential) acts as an anode, and is oxidized to a metal ion ($M - ne^- = M^{n+}$) by losing electrons. The noble metal acts as a cathode, and its reaction generally is $2H_2O + O_2 + 4e^- = 4OH^-$. Then M^{n+} combines with OH^- to form a metal hydroxide then further decomposes to metal oxide. After corrosion, a layer of metal hydroxide or metal oxide is formed at the interface. Because this layer is electrically

insulating, the contact resistance increases dramatically. A galvanic corrosion process has several characteristics: (1) occurs only under wet conditions, (2) an electrolyte must be present, and (3) oxygen generally accelerates the process and (4) dissimilar metals should be present. Based on the mechanism of unstable contact resistance of ICAs, several methods can be applied to stabilize the contact resistance and improve the reliability.

Based on the mechanism of unstable contact resistance of ECAs, three methods can be applied to prevent the metal finishes from galvanic corrosion. One method is by using oxygen scavengers [67]. Oxygen scavengers are chemicals which are added to water solutions to inhibit oxygen corrosion. Since oxygen accelerates galvanic corrosion, oxygen scavengers could be added into ECAs to slow down the corrosion rate [65]. When ambient oxygen molecules diffuse through the polymer binder, they react with the oxygen scavenger and are consumed. The main mechanism for oxygen scavengers to inhibit the corrosion is the cathodic mechanism which is based on the lowering of oxygen concentrations. In the system consisting of metal, water, oxygen, and oxygen scavenger, the cathodic reaction of O_2 competes with its chemical reduction. If the overall corrosion process is cathodically controlled, the reduction in corrosion rate depends on the relative magnitudes of the rates of the electrochemical cathodic process R_{el} and the chemical process R_{ch}. The overall rate of oxygen reduction R_{ox} is given by the sum of the rates of the two processes indicated in Equation 2-2:

$$R_{ox} = R_{el} + R_{ch} \qquad (2\text{-}2)$$

Since the rate of corrosion, Rcorr, is equal the rate of the electrochemical cathode process Rel, the corrosion rate is given by Equation 2-3:

$$R_{corr} = R_{ox} - R_{ch} \qquad (2\text{-}3)$$

It can be seen from Equation 2-2 that the smaller the corrosion rate, the greater the rate of the chemical reduction of oxygen. Therefore, the reactivity of an oxygen scavenger with oxygen is an important consideration of its properties. Some commonly used oxygen scavengers include sulfites (such as, sodium sulfates (Na_2SO_4), hydrazine ($H_2N\text{-}NH_2$), carbohydrazide ($H_2N\text{-}NH\text{-}CO\text{-}NH\text{-}NH_2$), diethylhydroxylamine ($(C_2H_5)_2N\text{-}OH$), and hydroquinone ($HO\text{-}C_6H_4\text{-}OH$) [68-71]. The application of oxygen scavengers could reduce the contact resistance increase obviously. However, with continuing aging test when the oxygen scavenger within the ECA is depleted, oxygen can again diffuse onto the interface and accelerate the corrosion process. Therefore, oxygen scavengers can only delay the galvanic corrosion process, but do not solve the corrosion problem completely.

Another method is to incorporate sacrificial materials with lower electrochemical potential than those of electrode-metal pads into the ECA [72]. For galvanic corrosion of ECAs during aging, the larger the difference in electrochemical potential, the faster the corrosion develops. Also, the self-corrosion rates of both metals will change; the comparably active metal (the anode) corrodes faster while the other (the cathode) corrodes slower. Table 2.2 shows the electrode potential values of some common metals. Generally, metals with a low potential tend to corrode faster and show increased contact resistance than those with a high potential value. Therefore, when applying sacrificial materials with lower electrochemical potential than those of electrode-metal pads into ECAs, the sacrificial materials are preferably corroded and, thus, can protect the metal finishes. This corrosion control is very important in reliability issues of the conductive adhesive joints. The addition of low corrosion potential individual metals, metal mixtures

or metal alloys greatly reduces the electrode potential of ECAs, or in other words, narrows down the potential gap between the ECA and the metal finishes. Thus, these sacrificial anode materials act as an anode in this configuration and they are corroded first instead of the metal finishes, resulting in protecting the surfaces at the cathode [72-74]. But the relatively high cost of the sacrificial anode materials and difficulty in handling the oxide-free metal particles somewhat limits their wide applications.

Table 2.2 Electrode Potentials of Selected Metal-ion Pairs

Electrode Reaction	Standard Potential (eV)
$Au - 3e^- = Au^{3+}$	1.50
$Pt - 2e^- = Pt^{2+}$	1.20
$Ag - e^- = Ag^-$	0.80
$2H_2O + O_2 + 4e^- = 4OH^-$	0.40
$Cu - 1e^- = Cu^+$	0.34
$Cu - 2e^- = Cu^{2+}$	0.52
$2H^+ + 2e^- = H_2$	0.00
$Pb - 2e^- = Pb^{2+}$	-0.13
$Sn - 2e^- = Sn^{2+}$	-0.14
$Ni - 2e^- = Ni^{2+}$	-0.25

Another approach to stabilize contact resistance of an ECA is the use of corrosion inhibitors in ECA formulations. In general, organic corrosion inhibitors are chemicals that adsorb on metal surfaces, and act as a barrier layer between the metal and the environment by forming a film over the metal surfaces [75-79]. Efficient corrosion inhibitors can reduce the corrosion rate by virtue of interacting with metal surface and, therefore, reducing its corrosion tendency. Some chelating compounds are especially

effective in preventing metal corrosion [77]. Chelating compounds are organic molecules with at least two polar functional groups capable of ring closure with a metal cation. The functional groups may either be basic groups, such as $–NH_2$, which can form bonds by electron donation, or acidic groups, such as –COOH, which can coordinate after the loss of the proton. Some effective corrosion inhibitors in ECAs have been developed for Sn/Pb, Cu and Al surfaces [65, 79]. However, the effectiveness of the corrosion inhibitors is highly dependent on the type of contact surfaces. Particular corrosion inhibitors are typically only effective in the specific metal finishes. Recently, tin (Sn) has been widely accepted as a potential surface finish for substrate bond pads in lead-free solder joints due to its low cost and a simple process for the Sn surface fabrication. However, conventional ECAs/Sn joints exhibited considerably unstable contact resistance at early stages under aging environment. Therefore, the research and development of effective corrosion inhibitors on Sn surface is of great significance and interest.

In this section, various organic compounds were introduced into a typical ECA formulation and the contact resistance of the ECAs on Sn surfaces under 85^{o}C/85%RH aging is presented. In addition, the roles of these additives were investigated by contact angle, grazing angle Fourier Transfer Infrared (FTIR) spectroscopy, X-ray Photoelectron Spectroscopy (XPS) and X-ray diffraction (XRD) techniques. The mechanism for the contact resistance stabilization on Sn surfaces was discussed.

2.2.2 Experimental

2.2.2.1 Materials

The base ICA formulations were prepared with the same diglycidyl ether of bisphenol-F (DGEBF) epoxy EPON 862, methylhexa-hydrophthalic anhydride

(MHHPA) hardener and 1-cyanoethyl-2-ethyl-4-methylimidazole (2E4MZCN) catalyst with 80wt% bimodal Ag flakes (Ag FL52 and Ag FL26LV with 1 : 1 ratio). Four different types of additives, glycine (aa1), lysine (aa2), aspartic acid (aa3), and dodecanedioic acid (aa4), with either -NH_2 or -COOH functional groups were purchased from Aldrich Chemical Company. The additives were incorporated in the ECA formulations and then mixed uniformly. All the chemicals were used as received.

2.2.2.2 Electrical characterizations of ICAs

Resistivity of the ICAs was calculated from the bulk resistance of the specimen with specific dimensions. Two strips of an adhesive tape were applied onto a pre-cleaned glass slide with a gap of 6.62 mm between these two strips. The conductive adhesive paste was then coated within the gap space by means of a doctor blade, and then the tapes were removed. After cure, the bulk resistance (R) of this ICA strip was measured as well as the size of the specimen. The bulk resistivity, ρ, was calculated using Equation 2-1.

Contact resistance of an ECA on Sn surface was measured using the test device in Figure 2.13. The device consists of metal patterns (e. g. Sn finish) printed on a printed circuit board (PCB). Conductive adhesives were dispensed on the gaps between every two metal patterns. After the adhesive was cured, the resistance of a circuit was measured from two ends of the pattern using a multimeter with a four-point probe. The specimens are exposed to 85°C/85% relative humidity (RH) in a temperature and humidity chamber chamber from Lunaire Environmental, model CEO932W-4). Contact resistance of each specimen was measured periodically and reported.

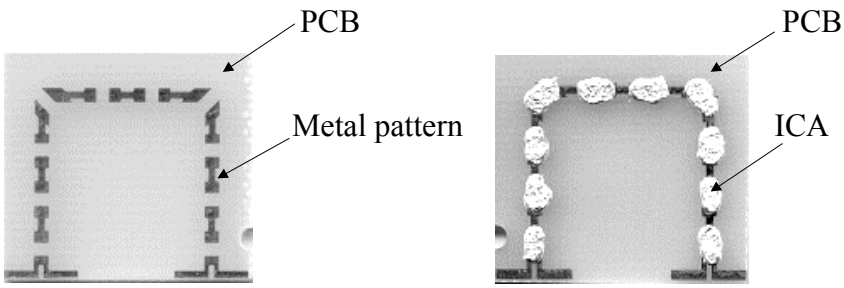

(a) (b)

Figure 2.13 Contact Resistance Test Device (a) before ICA Deposition and (b) after ICA Deposition

2.2.2.3 Characterization of adsorption and passivation effects of corrosion inhibitors on Sn surface

The corrosion inhibitor solutions were prepared at 10.0 mM by dissolving the additives in suitable solvents. The Sn surfaces were prepared by sputtering the metal on glass slides and cleaned by rinsing these surfaces with isopropyl alcohol and dried under a hood. 15 ml of each solution was used to treat the pre-cleaned Sn surfaces. After treatment for 24 h, the samples were removed from the solutions and rinsed with the solvent in order to remove un-adhered additives. The Sn surfaces were then dried under argon environment. The contact angle of a deionized (DI) water droplet on the Sn surfaces was measured by a goniometer.

Grazing angle FT-IR (Thermo, Woburn, MA, USA) spectroscopy was used for characterizing additive coatings on Sn surfaces. Grazing angle FT-IR spectra were acquired on a Nexus 870 (Thermo Electron) with a PM-IRRAS attachment including a photoelectric modulator (Hinds) and a nitrogen cooled MCT detector, at near grazing

angle. An average of 1000 scans per analysis was collected, with a resolution of 4 cm^{-1}. A clean reference Sn finished slide was used as control to collect the background spectrum.

Surface Science Model SSX-100 Small Spot ESCA spectrometer equipped with an Al Kα source was used to characterize and record the spectra of untreated and treated Sn surfaces. The fitting of the spectra was done by a non-linear least squares procedure provided by XPS International, Inc. X-ray diffraction was used for phase characterization of untreated and treated Sn surfaces before and after aging.

2.2.3 Results and Discussion

2.2.3.1 Bulk resistivity of ICAs with different corrosion inhibitors

The bulk resistivity data on ICAs without and with different additives are shown in Figure 2.14a. The resistivity of the typical ICA was 7.5×10^{-4} Ohm·cm. With the addition of 1wt% of acid additives, decreased resistivity values were achieved. For aa1, aa2 and aa4 added ECAs, the average values of resistivity were 5×10^{-4}, 6.5×10^{-4} and 6×10^{-4} Ohm·cm, respectively. With the addition of the same amount of aa3, however, the resistivity increased.

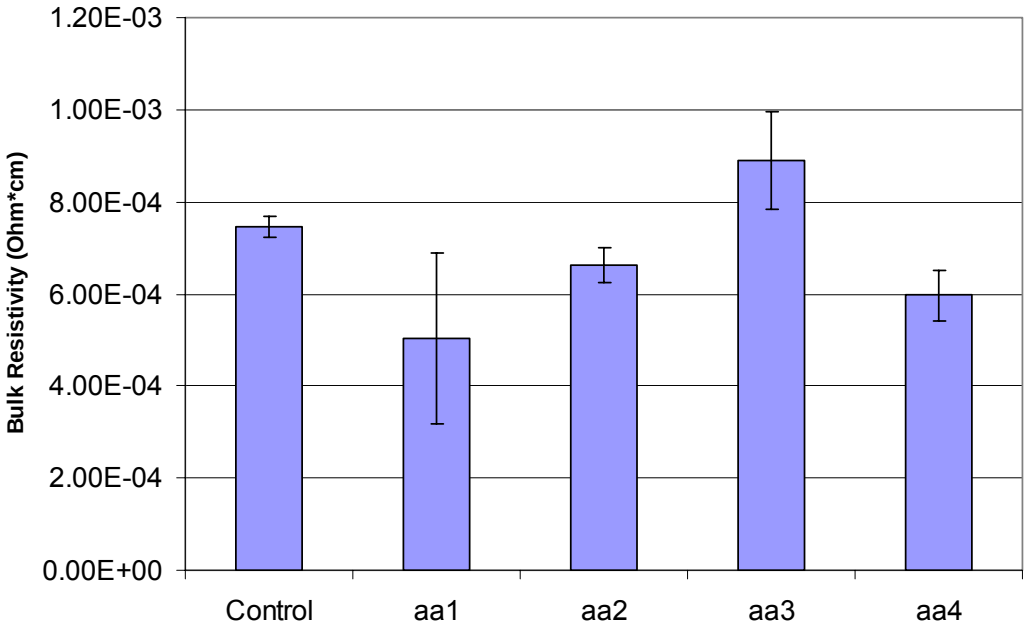

(a)

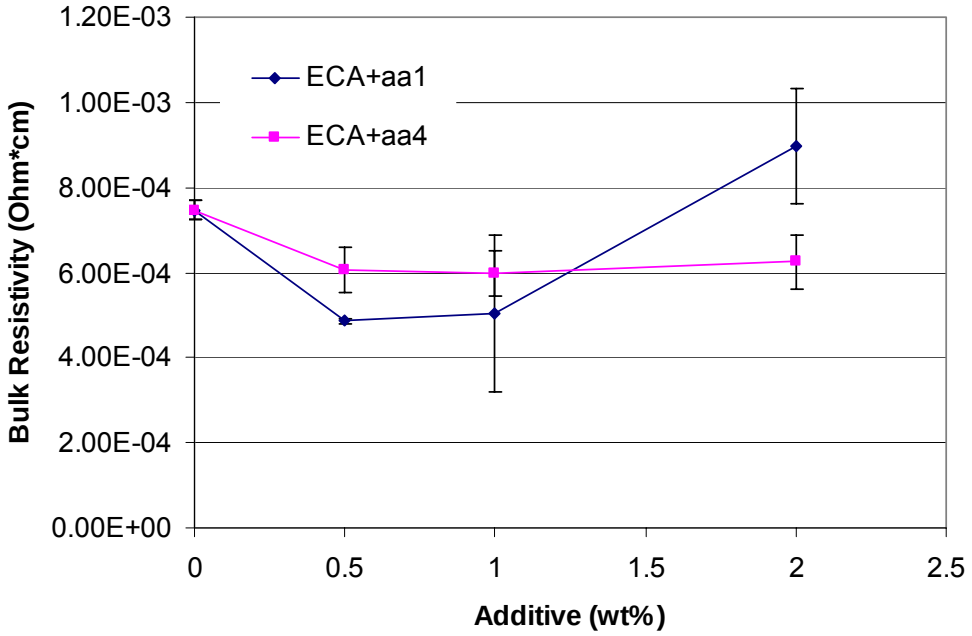

(b)

Figure 2.14 Bulk Resistivity of ECAs with 1wt% corrosion inhibitors (a) and with different amounts of aa1 and aa4 (b).

Since aa1 and aa4 performed best for the improvement of electrical conductivity of ECA, the effect of different loading levels of these additives on the resistivity was studied (Figure 2.14b). With the addition of 0.5wt% aa1 and aa4, the resistivity decreased by 30-40%. Increasing the loading level to 1 wt% did not change the resistivity. However, on further increasing the additives to 2 wt%, the resistivity started to increase. The improved conductivity with small amounts of additives may be due to the reaction between the additive and silver flakes. The acid additives, which served as surfactant removers, could help maintain good metallic contact and, therefore, led to a lower resistivity. However, because of the insulative properties of the organic compounds, excess additive in the ICA formulation could deteriorate the conductivity of ECAs.

2.2.3.2 Contact Resistance shift on Sn surfaces during 85°C/85%RH Aging

The effects of the additives on the contact resistance of the formulated ECAs were investigated and the contact resistance shifts of ECAs on Sn surfaces during 85°C/85%RH aging are shown in Figure 2.15a. The Sn surface has been known to be readily oxidized and corroded with aging, and, therefore, a dramatically increased contact resistance for ECA without any additives was observed. Within 24 hours, the contact resistance increased more than 200%. For aa2 and aa3 incorporated ECAs, slightly slower increase of contact resistance was observed in the initial stage of aging, however, considerably higher contact resistance was recorded with aging time. With the addition of aa1 and aa4, on the other hand, significantly stable contact resistance on Sn surfaces was achieved. The contact resistance increase was less than 40% over 600 hours with aa1 addition while the aa4 added samples showed even a slightly decreased contact resistance

on Sn surfaces after 600 hours' aging. Therefore, aa1 and aa4 acted as effective corrosion inhibitors for ECA on Sn surfaces.

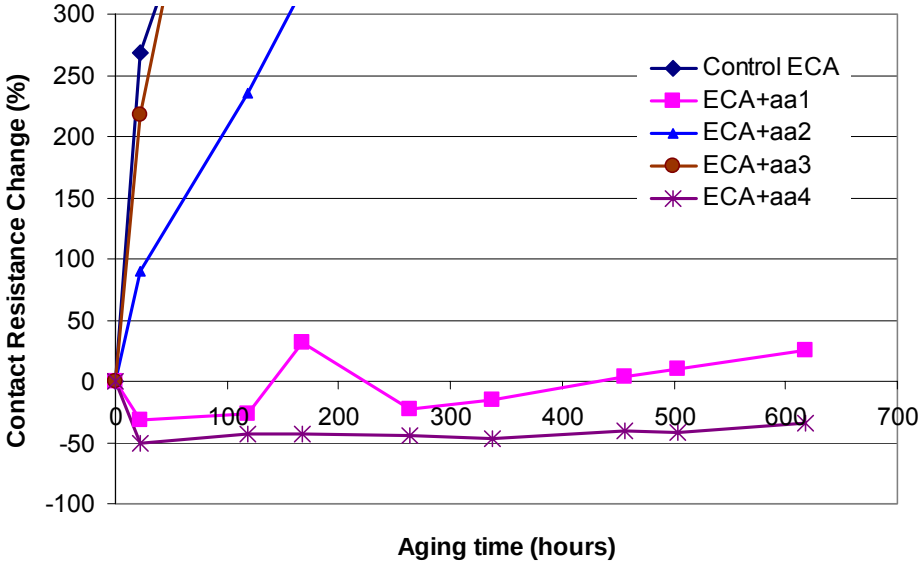

(a)

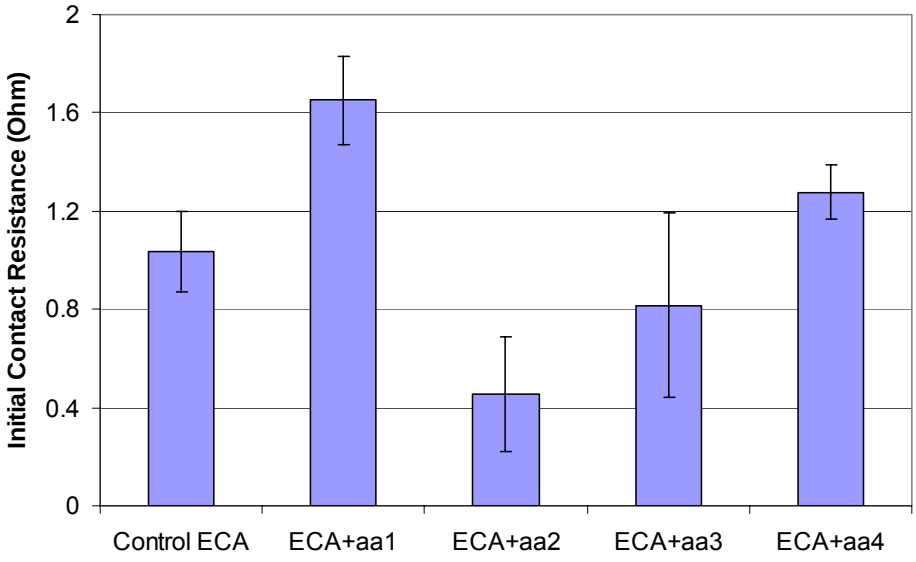

(b)

Figure 2.15 Contact resistance of ECAs on Sn surfaces with different additives. (a) contact resistance shift under 85°C/85%RH; (b) initial contact resistance values.

To study the possible mechanism for the contact resistance stabilization with these effective corrosion inhibitors, the initial contact resistance values were compared and the results are shown in Figure 2.15b. For aa1 and aa4 incorporated ECAs, even slightly higher initial contact resistance values than for control were observed. It is considered that the organic corrosion inhibitors formed a thin passivation layer on the Sn surfaces. The passivation layer could prevent the diffusion of oxygen and moisture during the aging and therefore protected the surfaces from oxidation and corrosion. However, the insulative properties of the organic corrosion inhibitors also led to the slightly higher initial contact resistance values.

2.2.3.3 Surface characterizations of Sn with corrosion inhibitors

To characterize the interaction between corrosion inhibitors and Sn finishes, contact angle values of DI water on Sn surfaces before and after treatment in aa1 and aa4 solutions were measured and the results are shown in Figure 2.16. The contact angles decreased on the treated Sn surfaces. The decreased contact angle indicated that both types of additives, with hydrophilic functional groups (-COOH or $–NH_2$), had strong affinity to Sn and were well coated on the Sn surfaces.

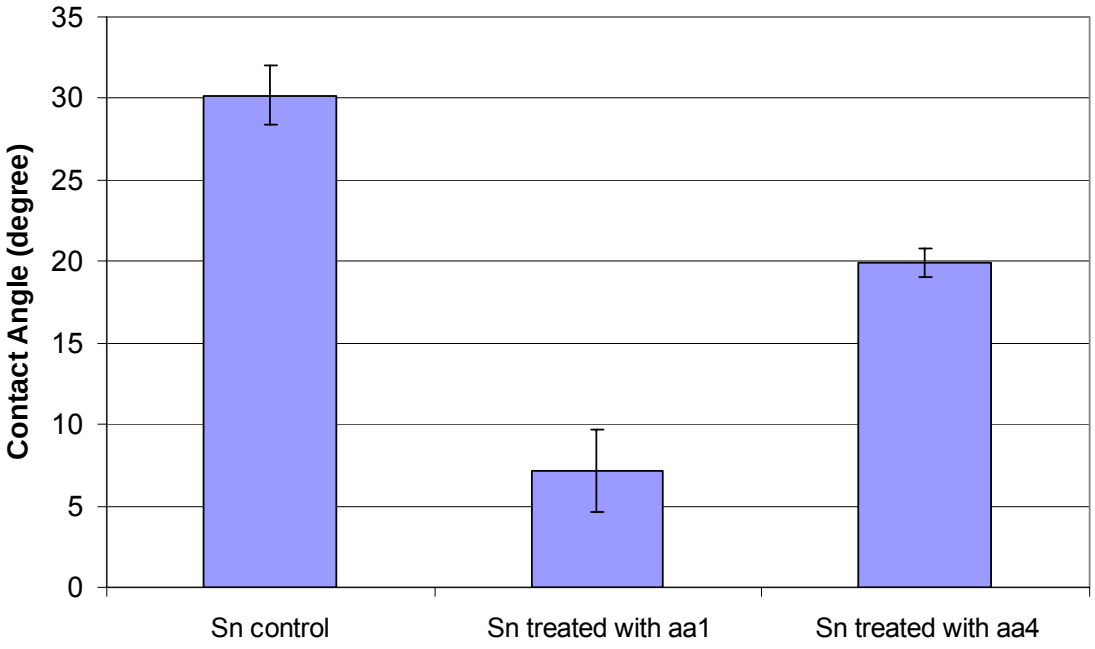

Figure 2.16 Contact Angles of DI H_2O on Sn surfaces

Grazing angle FTIR spectra of the treated Sn surfaces were also recorded. For aa1 treated Sn surface, typical -CH_2 stretching peaks, C=O stretching peaks and COO^- peaks were detected at around 2900 cm^{-1}, 1700cm^{-1} and 1400cm^{-1}, respectively (Figure 2.17a). Therefore, aa1 was confirmed to be well coated on the Sn surface. For aa4 treated surface, however, no obvious peaks were observed. (Figure 2.17b) The different behaviors of aa1 and aa4 from FTIR spectra could be due to their different structures and, consequently, different alignment modes on Sn surfaces. For aa4, a longer chain di-functional compound, both functional groups could anchor on the Sn surface and the resultant more flexible molecular structure may prefer to lie flat on the Sn surface rather than standing up. Therefore, no obvious functional groups were detected by FTIR.

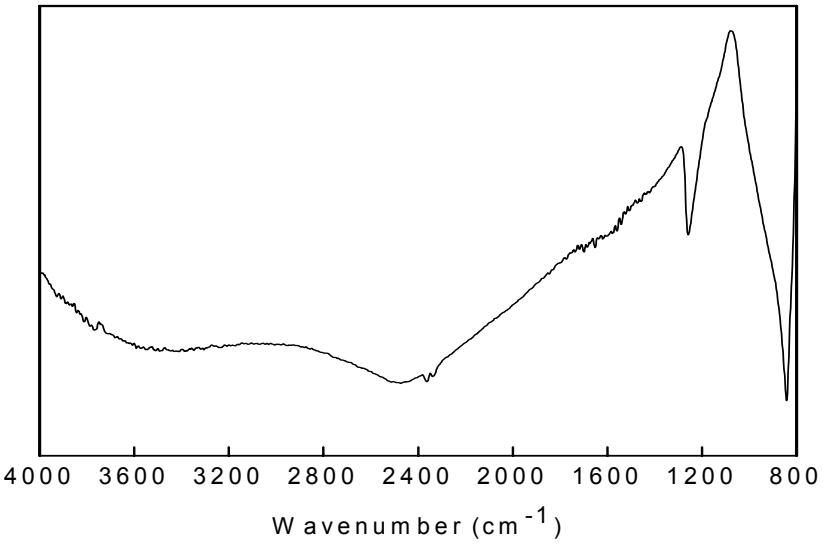

(a)

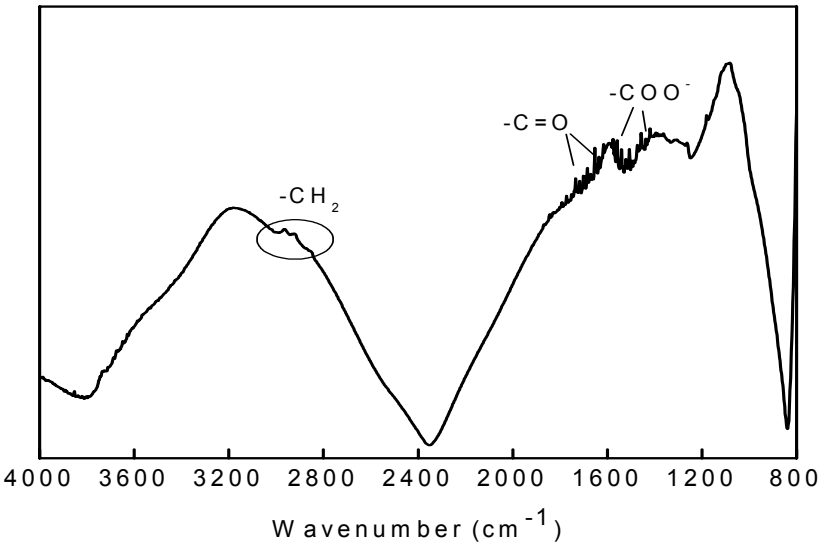

(b)

Figure 2.17 FTIR spectra of Sn surfaces a) untreated Sn surface; b) aa1 treated Sn surface; c) aa4 treated Sn surface

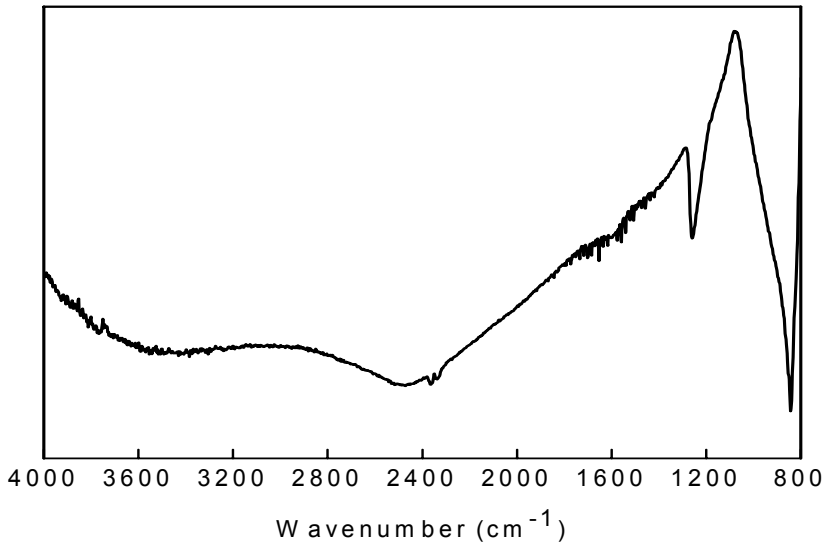

(c)

Figure 2.17 continued

The XPS spectra provided further information on the surface chemical changes induced by coatings of organic additives on Sn. Figure 2.18 and Table 2.3 show the general scan results of untreated and treated Sn surfaces. From XPS measurements, peaks of $Sn3d_{2/5}$ (~488eV) and $Sn3d_{2/3}$ (~496eV), C1s (~285eV), O1s (~532eV) were found for all Sn surfaces, while small N1s (~401eV) peaks were also detected for untreated and aa1 treated Sn surfaces.

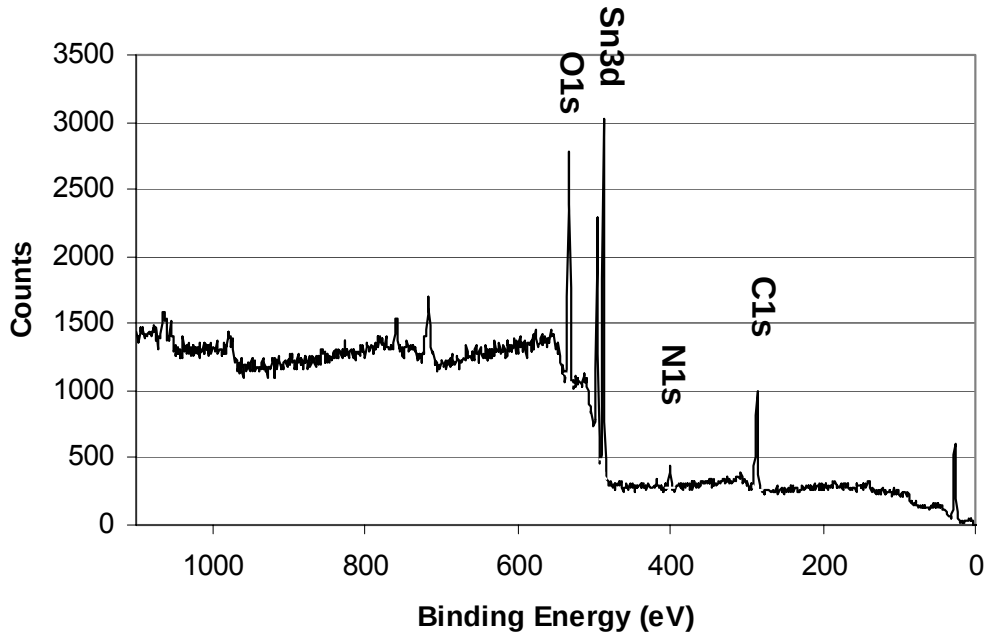

(a)

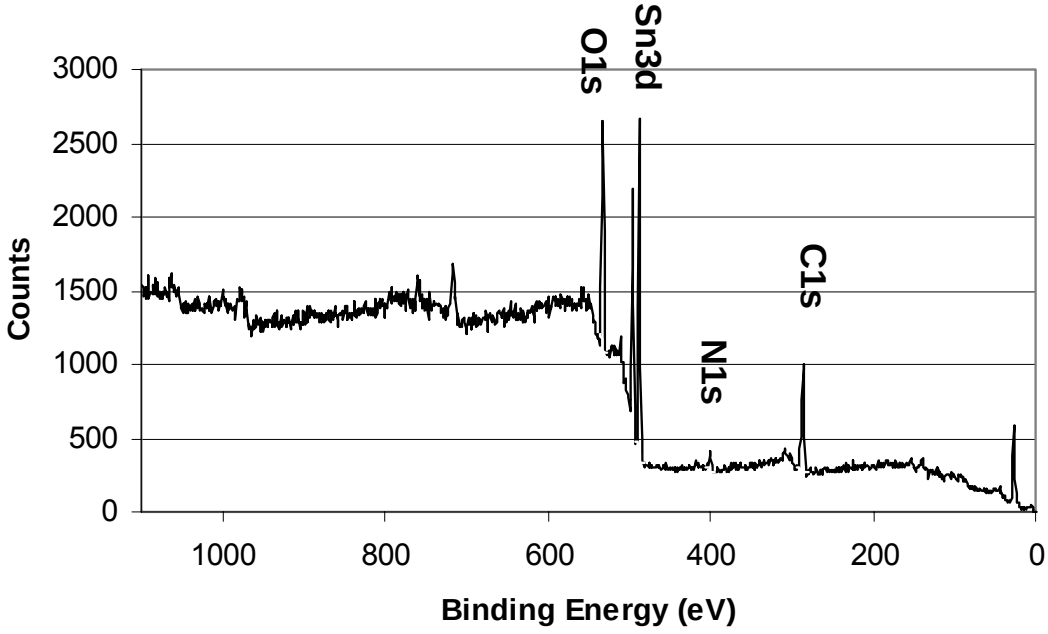

(b)

Figure 2.18 XPS general scans of Sn surfaces a) untreated Sn surface; b) aa1 treated Sn surface; c) aa4 treated Sn surface.

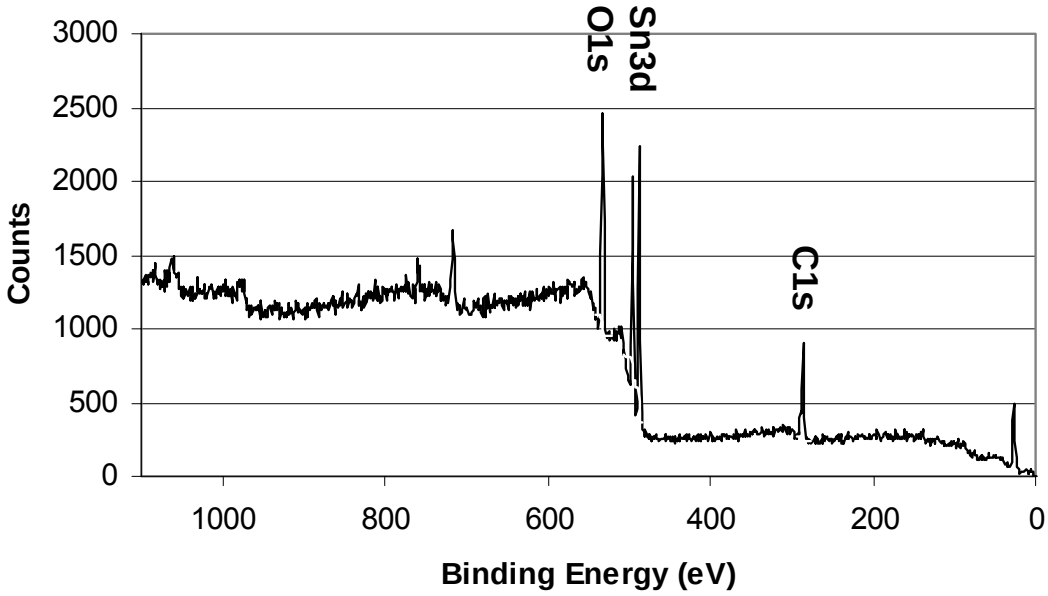

(c)

Figure 2.18 continued.

Table 2.3 XPS Elemental Composition (at %) of Sn Surfaces

Samples	Sn3d	C1s	O1s	N1s
Untreated Sn surface	9	46	40	5
aa1 treated Sn surface	8	50	38	4
aa 4 treated Sn surface	7	49	44	0

High resolution spectra of $Sn3d_{2/5}$ and $Sn3d_{2/3}$ peaks showed that the binding energy shifted to slightly lower values after treatment (Figure 2.19a and Table 2.4), suggesting that some reaction on the Sn surface had occurred during the treatment. Three

C1s peaks were observed for untreated surfaces at 285.8, 287.4 and 289.3eV which corresponded to the C-H, C-N and C-O chemical groups, respectively. (Figure 2.19b and Table 2.4) After treatment in aa1 solution, the bonding energy slightly shifted and the percentage of C-H bonding increased. After aa4 treatment, C-H bonding became more dominant and C-N bonding disappeared. The longer molecular chain which contains more $-CH_2$ functional groups for aa4 contributed to the higher C-H bonding, while the disappearance of C-N bonding is probably due to the reaction between aa4 and N-containing basic group. From N1s spectra, the N1s peak (401.2eV) for untreated surface shifted and split into two peaks at 400.7 and 402.0 eV after aa1 treatment, which corresponded to the C-N and N-H bondings, respectively. (Figure 2.19c and Table 2.4) This change is attributed to the $-NH_2$ functional group in aa1. Corresponding to the disappearance of C-N bonding at 287.4 eV after aa4 treatment, the N1s peak disappeared due to the strong acidity of aa4 and subsequently the neutralization reaction with N-containing basic group. Figure 2.19d depicts O1s spectra of the same samples. The two peaks for the untreated surface corresponded to C-O and O-O bondings. After treatment, significant change in O1s spectrum was observed. The shifted peaks at ~532eV and 533eV with 43:57 ratio were considered to be related to –OH and –O-C=O bondings, respectively, since both aa1 and aa4 have –COOH functional groups.

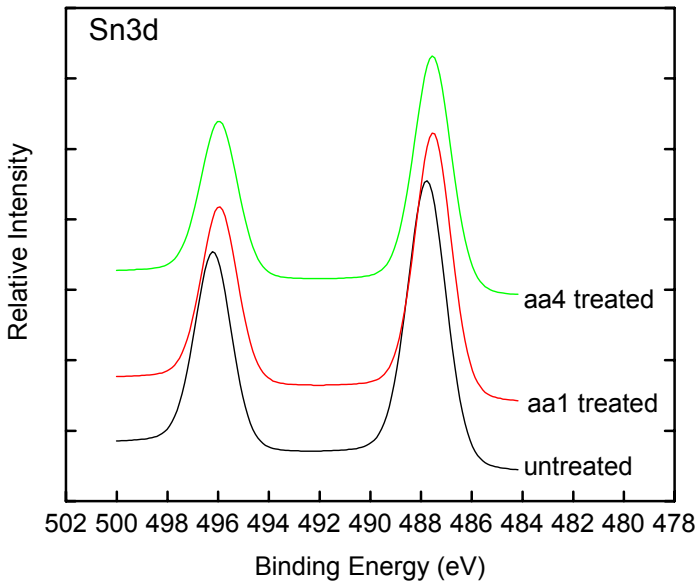

(a)

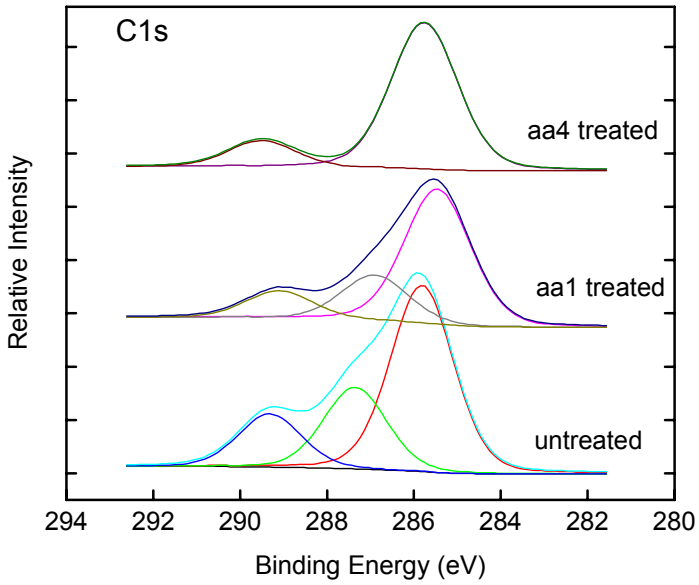

(b)

Figure 2.19 High resolution XPS spectra of a) Sn3d, b) C1s, c) N1s and d) O1s peaks for Sn surfaces

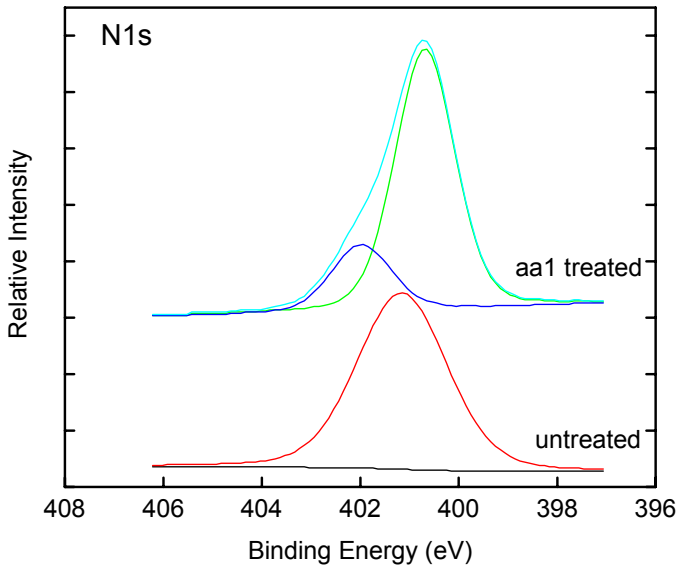

(c)

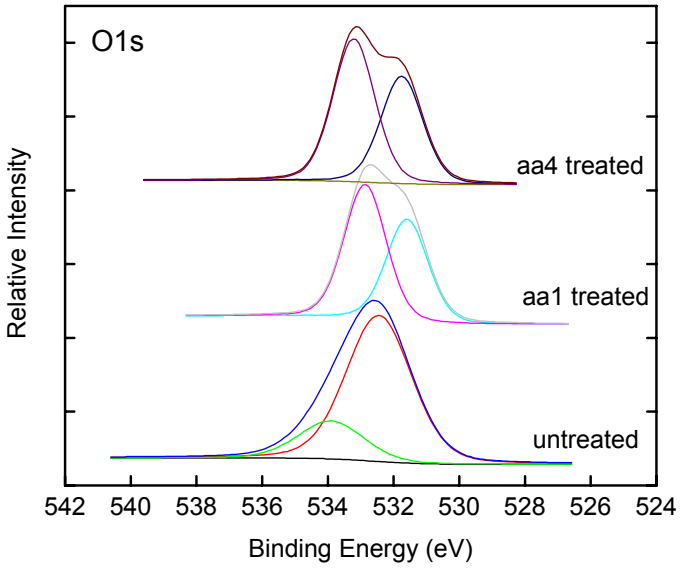

(d)

Figure 2.19 Continued

Table 2.4 High Resolution XPS for results for different Sn surfaces

Samples	***C 1s***		***N1s***		***O1s***		***Sn3d***	
	binding energy (eV)	amount (%)	binding energy (eV)	amount (%)	binding energy (eV)	amount (%)	binding energy (eV)	amount (%)
untreated Sn surface	285.8	58	401.2		532.5	79	487.8	60
	287.4	25			533.9	21	496.2	40
	289.3	17						
aa1 treated Sn surface	285.5	65	400.7	80	531.6	43	487.5	60
	286.9	22	402.0	20	532.9	57	496.2	40
	289.1	13						
aa4 treated Sn surface	285.8	85			531.8	43	487.5	60
	289.5	15			533.2	57	495.9	40

Comparing contact angle, FTIR and XPS results with the contact resistance data, the aa1 and aa4 coatings on Sn surfaces formed a thin passivation layer on the Sn substrate, which resulted in isolation of the Sn surface from the environment. Therefore, the Sn surfaces were protected. The slightly higher initial contact resistance values (Figure 2.15b) also indicated the formation of the organic layer since both types of

organic corrosion inhibitors are non-conductive and thus could increase the initial contact resistance.

2.2.3.4 X-ray diffraction of Sn surfaces under accelerated temperature and humidity conditions

Figure 2.20 shows the XRD results for Sn surfaces before and after aging test. For all the samples, only Sn (JCPDS card no. 04-0673.) was detected before aging. To accelerate the oxidation process at elevated temperature and humidity, the Sn surfaces were placed in a Highly Accelerated Stress Testing (HAST, 121^{o}C, 2 atm, 100%RH) chamber for 72 hours. After the HAST test, obvious extra peaks corresponding to SnO (JCPDS afd no. 01-0902) were detected for untreated, aa2 and aa3 treated Sn surfaces due to the oxidation of these Sn surfaces. For the aa1 and aa4 treated surfaces, however, no SnO peaks were observed. Similar results were also obtained for the 85^{o}C/85%RH aged Sn surfaces. Therefore, the addition of aa1 and aa4 was confirmed to be able to protect the Sn-finished test boards and prevent the formation of oxides during the aging test.

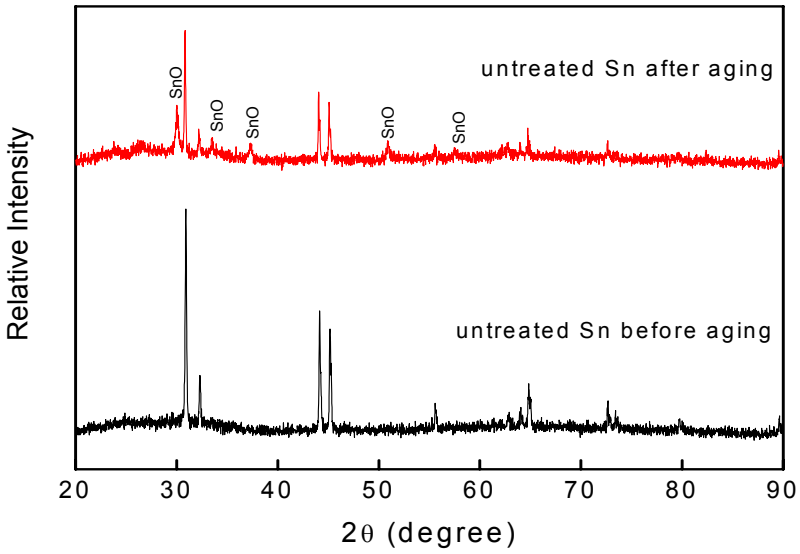

(a)

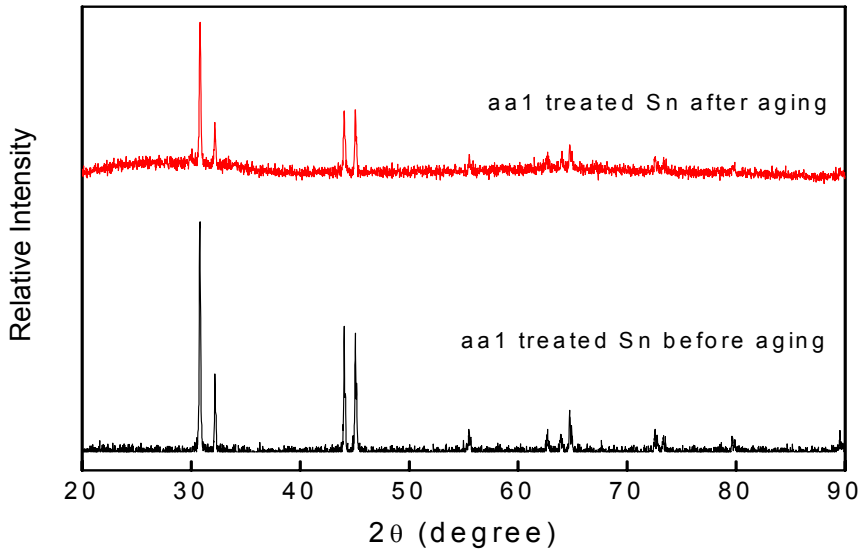

(b)

Figure 2.20 XRD patterns of Sn surfaces before and after aging. a) untreated Sn surface; b) aa1 treated Sn surface; c) aa2 treated Sn surface; d) aa3 treated Sn surface; e) aa4 treated Sn surface.

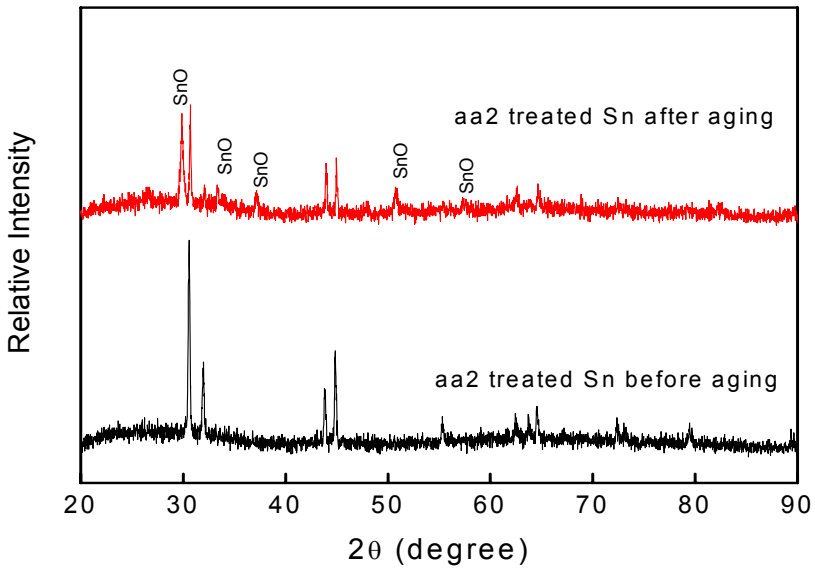

(c)

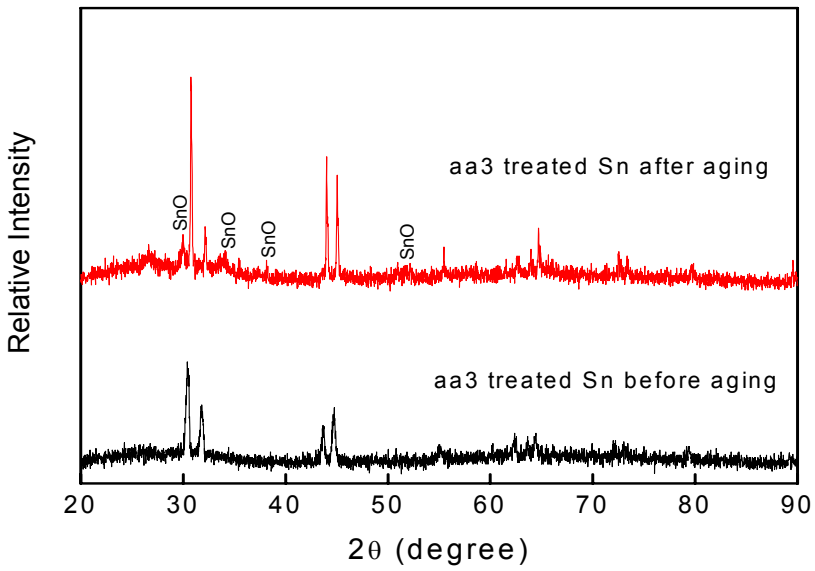

(d)

Figure 2.20 continued.

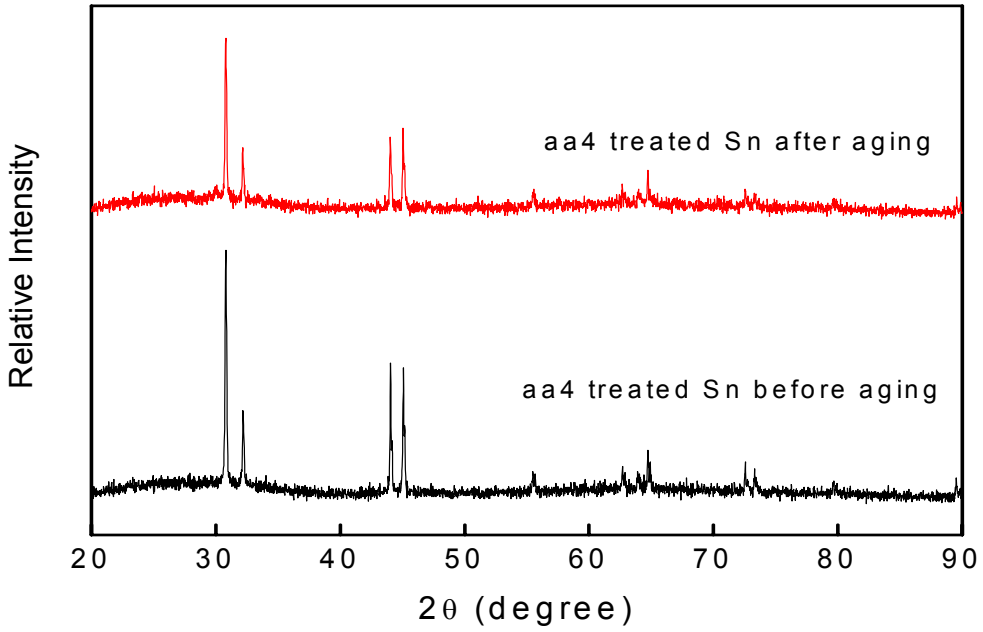

(e)

Figure 2.20 continued.

2.2.4 Summary

Effects of different corrosion inhibitors on the electrical properties of ECA/Sn joints were investigated. These acidic corrosion inhibitors have strong affinity to Sn finishes and form a passivation layer on the Sn surfaces. The passivation layer that acted as a barrier between the Sn surface and environment prevented the Sn pad surface from oxidation and corrosion during the elevated temperature and humidity environment. This protection capability of the additives led to stable contact resistance and, consequently, a significantly improved reliability in the aging test. The bulk resistance was also slightly decreased by using these additives.

2.3 Conclusions

In order to enhance the electrical properties and reliability of ICAs as a potential solder replacement in microelectronics interconnects, interfacial properties of the ICA composites were modified with various types of acids. Short-chain dicarboxylic acids, which could *in-situ* remove or replace the long chain fatty acids on Ag flakes, were used in a typical ICA formulation to improve the electrical conductivity by reducing the tunneling resistance between Ag flakes. Although the viscosity also increased with acid addition, other materials properties of ICA, such as the curing profile, glass transition temperatures, dynamic properties, etc. did not change.

Various types of corrosion inhibitors were introduced into the typical ICA formulations on Sn surfaces. Glycine and dodecanedioic acid significantly stabilized contact resistance on Sn surface after 85^{o}C/85%RH aging, due to the formation of a passivation layer on the Sn surfaces. A highly reliable ICA formulation was developed as a potential solder replacement in SMT applications.

CHAPTER 3
ENHANCEMENT OF ELECTRICAL AND THERMAL PROPERTIES OF ANISOTROPICALLY CONDUCTIVE ADHESIVES/FILMS (ACAS/ACFS) WITH NANOTECHNOLOGY

3.1 Nano-scale Anisotropically Conductive Adhesives (nano-ACAs)

3.1.1 Introduction

Microelectronics are driven toward smaller, higher density, and lower cost solutions. Polymer-based conductive adhesives have drawn much attention as an environmentally friendly solution for lead-free interconnects. Anisotropic conductive adhesives (ACAs) are becoming popular as one of promising candidates for lead-free interconnection solutions due to their technical advantages such as fine pitch capability (<40 μm pitch), low temperature processing ability, low cost and environmentally friendly materials and process, etc. ACAs consist of conducting particles (typically 5~10 μm in diameter) and adhesives which provide both attachment and electrical interconnection between electrodes. In particular, ACFs are widely used for high-density interconnection between liquid-crystal display (LCD) panels and tape carrier packages (TCPs) to replace the traditional soldering or rubber connectors. In LCD applications, traditional soldering may not be as effective as ACFs in interconnecting materials between indium tin oxide (ITO) electrodes and TCP. Recently, ACFs have also been used as an alternative to soldering for interconnecting TCP input lead bonding to printed-circuit boards (PCBs).

Despite of these promising characteristics of ACAs/ACFs, there are some key issues that hinder their implementation as interconnect materials for high performance devices such as microprocessor and Application Specific Integrated Circuit (ASIC) applications. The ACA/ACF joints have lower electrical conductivity and poor current

carrying capability because there is only mechanical/physical contact of the joints and no metallurgical contact of interconnects. To ensure low contact resistance and high current density, interface between conductive fillers and electrode should be improved.

One of the approaches to minimize the joint resistance is to make the conductive fillers fuse each other and form metallic joints such as metal solder joints. However, to fuse metal fillers in polymers does not appear feasible, since a typical organic printed circuit board, on which the metal filled polymer is applied, cannot withstand such a high temperature; the melting temperature (Tm) of Ag, the most commonly used filler, is around 960^{o}C. It has been found that the Tm or the sintering temperatures of materials could be dramatically reduced by decreasing the size of the materials [80-83]. It was also reported that the surface premelting and sintering processes are a primary mechanism of the Tm depression of the fine nano particles. For nano-sized particles, sintering behavior could occur at much lower temperatures, as such, the use of the fine metal particles in ACA/ACF would be promising for fabricating high electrical performance ACA/ACF joints through eliminating the interface between metal fillers. The application of nano-sized particles can also increase the number of conductive fillers on each bond pad and result in more contact area between fillers and bond pads. Therefore, application of nano-sized particles has potentials to improve the current density of the ACA joints by distributing current into more conductive paths (Figure 3.1).

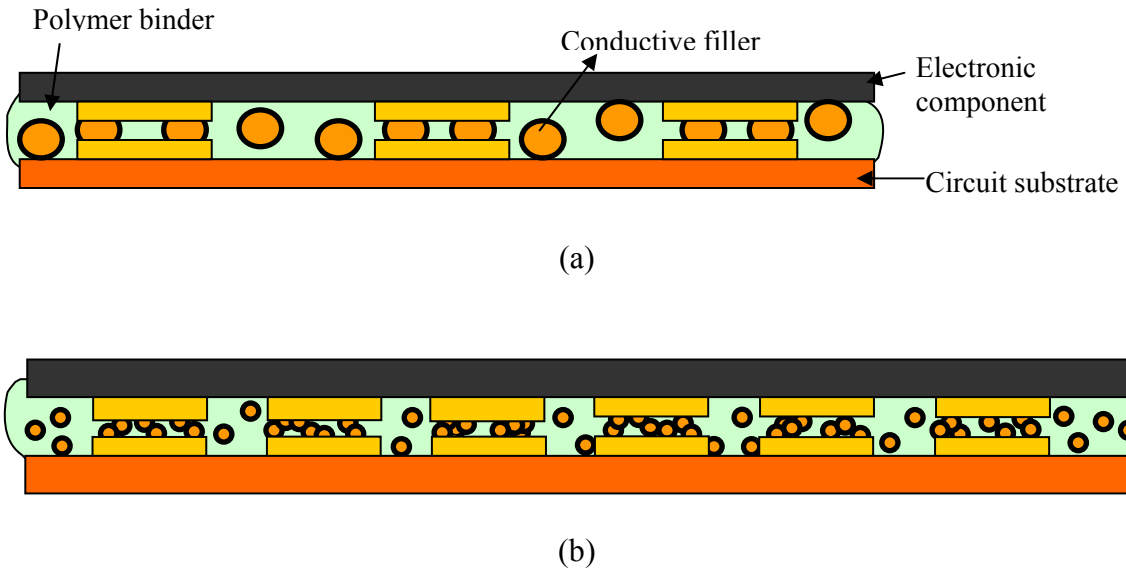

Figure 3.1 Illustration of a chip and substrate assembled by ACA. (a) Traditional ACA with micron-sized fillers and (b) novel ACA with nano-fillers.

In this section, in order to resolve the technical issues (high bonding pressure and lower electrical performance) of traditional ACA/NCA while maintaining the advantages of ultra fine pitch and low cost, a novel nano-scale conductive film incorporated with very low loading of nano-Ag fillers were studied for next generation high performance fine-pitch packaging applications. This novel nano-Ag ACA (as illustrated in Figure 3.2) combines the electrical conduction along the z-direction (ACA-like) and the ultra fine pitch (< 100 nm) capability (NCA-like).

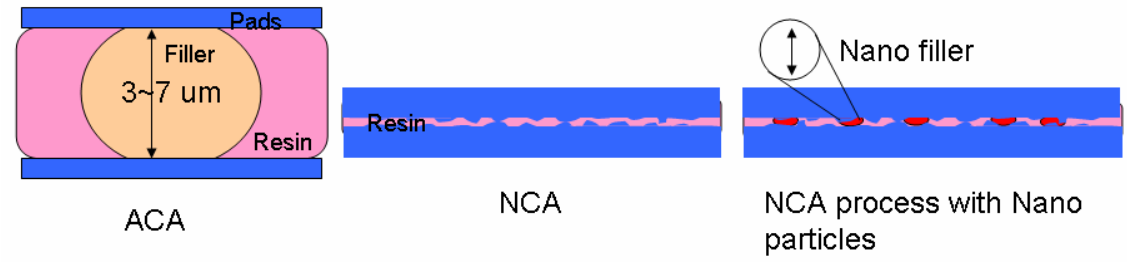

Figure 3.2 Comparison of ACA, NCA, and novel nano-ACA

3.1.2 Experimental

3.1.2.1 Materials

The nano silver particles synthesized by combustion chemical-vapor condensation (CCVC) method were obtained from nGmat Corp and the TEM picture of the nano silver particles is shown in Figure 3.3. The Ag particles were annealed at different temperatures (from 100^{o}C to 250^{o}C). The morphology of the annealed Ag particles was observed by scanning electron microscopy (SEM, Hitach S-800).

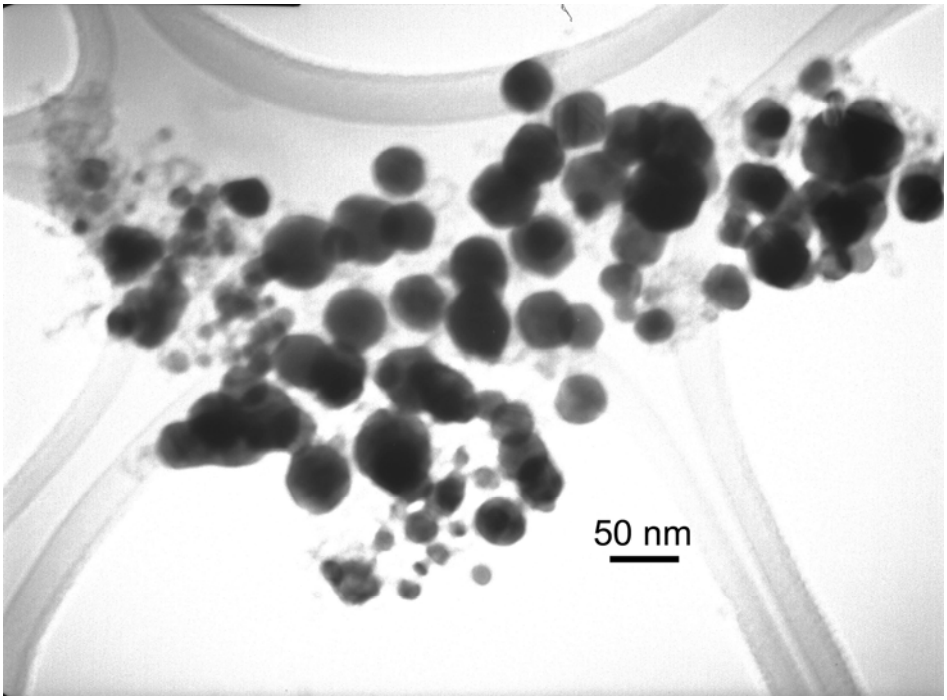

Figure 3.3 TEM picture of the nano-silver fillers used in this study

For the ACA formulations, diglycidyl ether of bisphenol-F (DGEBF) EPON 862 (from Shell Chemical Company) was used as epoxy resin. The hardener was methylhexa-

hydrophthalic anhydride (MHHPA) from Lindau Chemicals, Inc. The ratio of epoxy to hardener was 1:0.85 based on the epoxide equivalent weight (EEW) of the epoxy resin and the hydroxyl equivalent weight (HEW) of the hardener. 1-cyanoethyl-2-ethyl-4-methylimidazole (2E4MZCN) and cobalt (II) acetylacetonate (Co(II)AcAc) were employed as the catalyst for low temperature and high temperature curable formulations, respectively.

3.1.2.2 Characterizations

The curing profiles of the ACA resins were determined using a modulated differential scanning calorimeter (MDSC) from TA Instruments, model 2970. Dynamic MDSC scans were made on the samples at a heating rate of 5°C/minute, from 25°C to 300°C.

The electrical resistance of the joints (contact area: 100x100 μm^2) on Au-finished PI flex/PI flex test vehicle (Figure 3.4) was measured by a four-point probe method, where the current carrying capability was determined as the current at which the voltage shows non-linear behavior in the I-V or the resistance abruptly increases in the I-R curve. The applied currents were varied from 0.5 ~ 4.0 A by a power supply (HP model 6553A, HP Hewlett Packard, Palo Alto, CA) and the voltage of the interconnect joints was measured by a Keithley 2000 multimeter (Cleveland, Ohio).

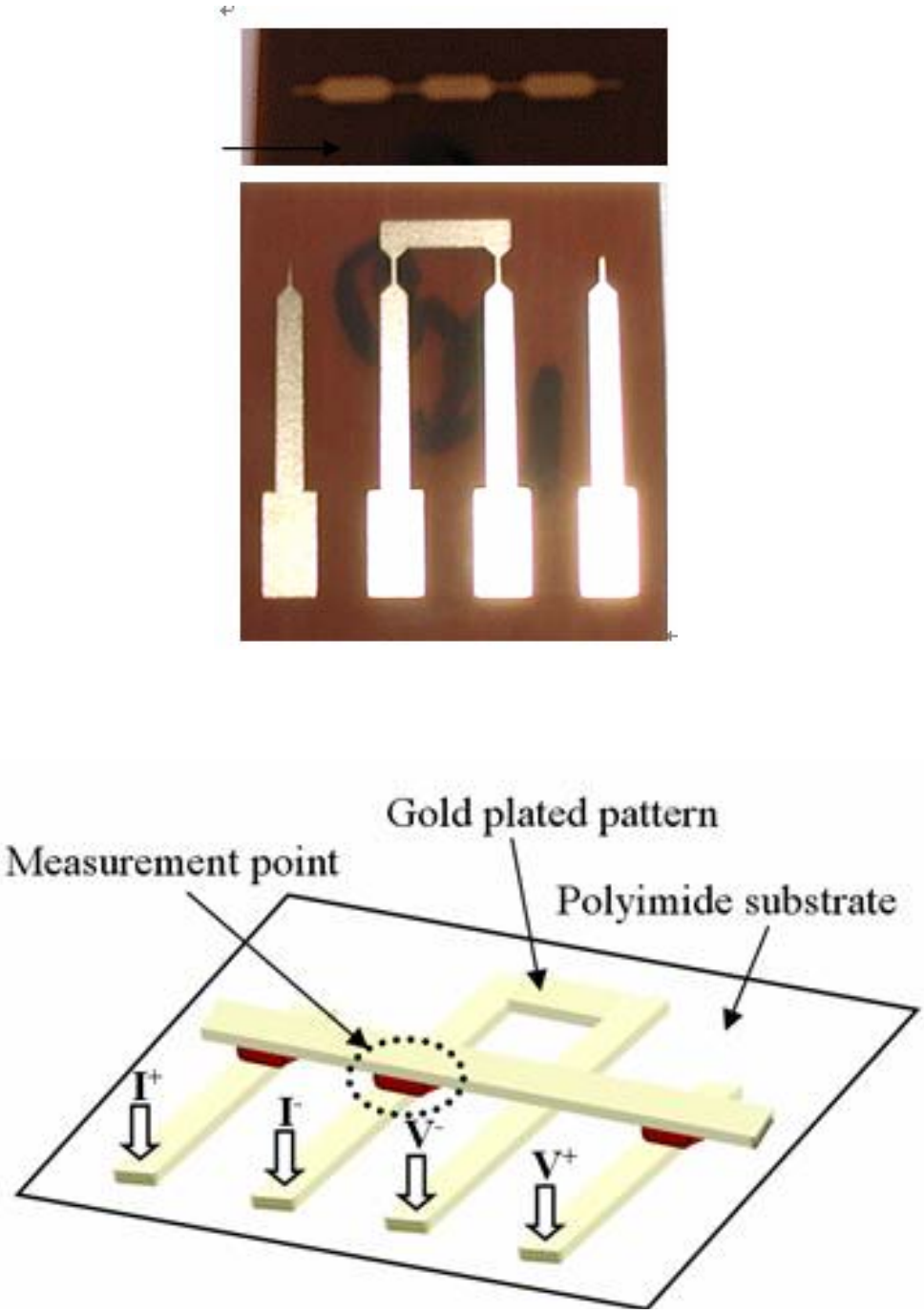

Figure 3.4 Test coupons for ACA/ACF assembly and the schematics of four-point probe method for electrical contact resistance and current carrying capability measurement

3.1.3 Results and Discussion

3.1.3.1 Sintering of nano Ag particles

In order to study sintering behavior of nano Ag particles, the nano Ag particles were annealed at different temperatures (100, 150, 200 and 250^{o}C). From Scanning Electron Micrograph (SEM) photographs as shown in Figure 3.5, sintered nano particles were observed at 150^{o}C and higher temperatures. Although very fine particles were found in the as-received (in Figure 3.5a) and the 100^{o}C treated particles (in Figure 3.5b), dramatically larger particles were observed after heat treatment at 150^{o}C and above. With increasing temperatures, the particles became larger and appeared as a solid matter rather than porous particles or agglomerates. The particles shown in Figures 3-5 c-e were fused through their surface and many of dumbbell type particles could be found. The morphology was similar to a typical morphology of an initial stage in the typical sintering process of ceramic, metal and polymer powders. This low temperature sintering behavior of the nano particles is attributed to the extremely high inter-diffusivity of the nano particle surface atoms, due to the significantly energetically unstable surface status of the nano particles, in particular, nano-sized particles with large proportion of the surface area to the entire particle volume.

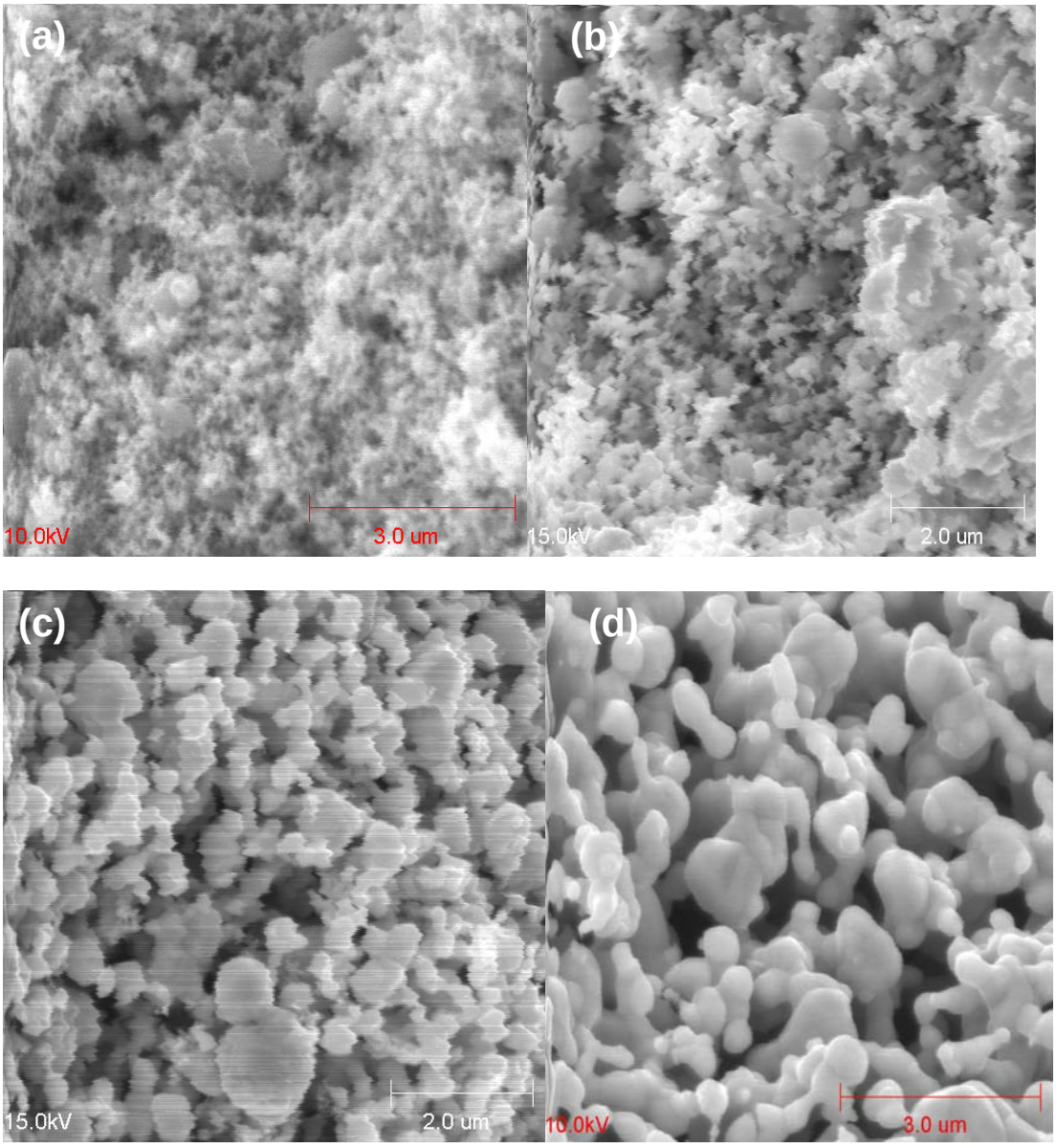

Figure 3.5 SEM photographs of nano Ag particles annealed at different temperatures for 30 minutes: (a) room temperature (no annealing); (b) annealed at 100^{o}C; (c) annealed at 150^{o}C; (d) annealed at 200^{o}C and (e) annealed at 250^{o}C.

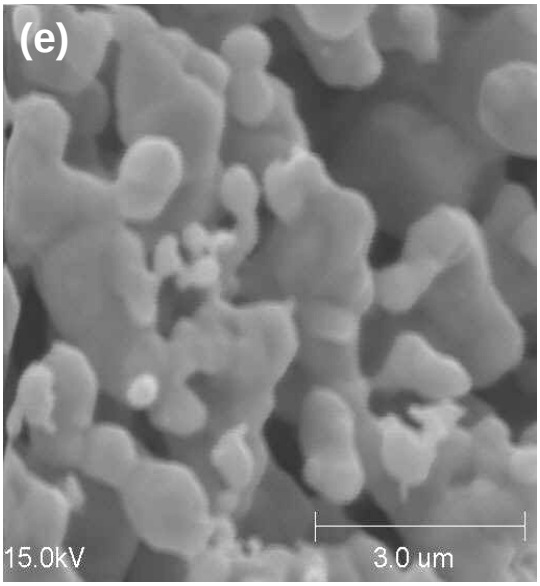

Figure 3.5 continued.

3.1.3.2 Electrical properties of nano-Ag ACAs with sintering effect

The nano particle sintering behavior may help improve the interfaces of the conductive adhesives/metal bond pads of the substrate and the components. For the sintering reaction in a certain material system, temperature and duration are the most important parameters, in particular, the sintering temperature. To study the sintering behavior of nano Ag particles in the ACA formulations, the two resin systems with two different curing temperatures were selected. 2E4MZCN and Co(II)AcAc were used as catalysts for low and high curing temperature catalysts, respectively. The curing profile of the resins is shown in Figure 3.6. The resin 1 with 2E4MZCN had a curing peak at 156^{o}C, while resin 2 with latent catalyst Co (II)AcAc started curing at 190^{o}C and the curing peak occurred at 239^{o}C, both at a scan rate of 5^{o}C/min.

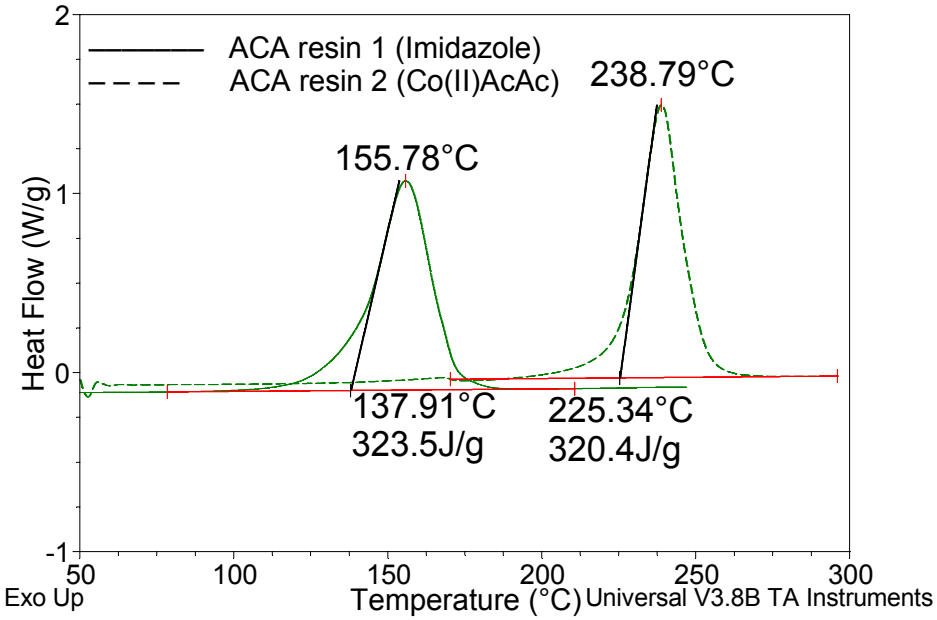

(a)

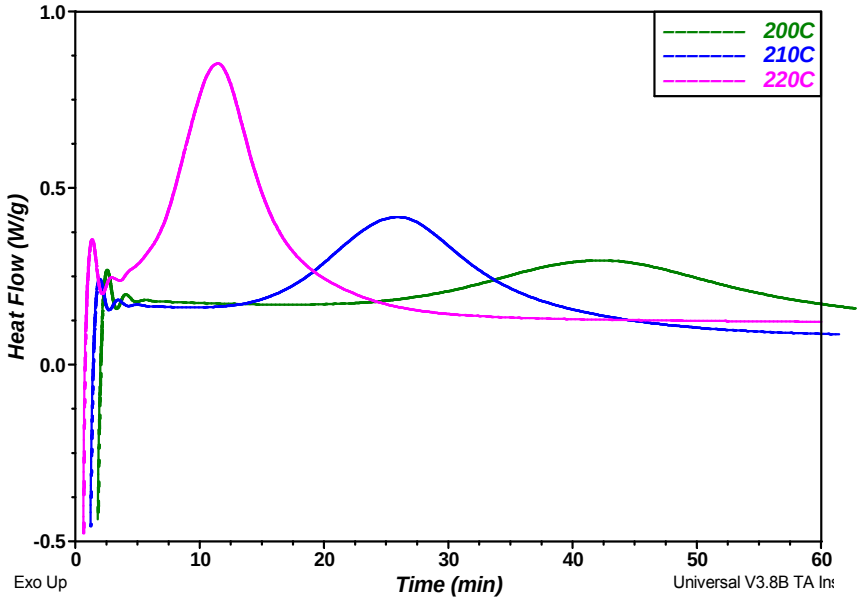

(b)

Figure 3.6 Curing profile of ACA resins: a) dynamic DSC for resins with different catalysts; b) isothermal DSC for resin with high curing latency

Three different curing temperatures, 200°C, 210°C and 220°C were selected for resin 2 and the total reaction heats from the isothermal DSC are shown in Figure 3.6 (b) and Table 3.1. With increasing temperatures, the total reaction heats increased due to the higher degree of curing. Compared with the reaction heat from dynamic DSC result, 210°C is required for the curing of resin 2. Therefore, 150°C (resin 1), 210°C and 220°C (resin 2) were used and the curing times were 60min, 45min and 30min, respectively.

Table 3.1 Curing profiles of ACA resins with high curing latency

Isothermal temperature (°C)	Reaction time (min)	Total reaction heat (J/g)
200	60	169.3
210	45	254.7
220	30	324.6

The current-voltage relationship of the nano-Ag filled ACAs is shown in Figure 3.7. As can be seen from these figures, with increasing curing temperatures, the resistance of the ACA joints decreased and the current carrying capability increased. The joint resistance decreased dramatically from 7×10^{-4} Ohm to 5×10^{-5} Ohm when increasing the processing temperature from 150°C to 220°C by using different catalysts. Also, the ACAs with higher curing temperature exhibited higher current carrying capability of 3.0 A than the low temperature curable samples (2.5 A). This phenomenon suggested that further sintering of nano Ag particles at higher temperature contributed to the superior electrical properties at the interface between fillers and metal bond pads. From the illustration shown in Figure 3.8, after the nano Ag-filled ACAs were cured under the

application of pressure, there was better contact between Ag fillers and metal bond pad, and a reduced contact resistance could be achieved. For typical ACAs, the physical contact between fillers and bond pad gave a relatively higher joint resistance. With the sintering behavior, the nano Ag particles in the ACA formulations could fuse each other through their surfaces, which decreased the number of interfaces between particles. Therefore, the significantly improved joint resistance and current carrying capability were achieved at higher temperatures.

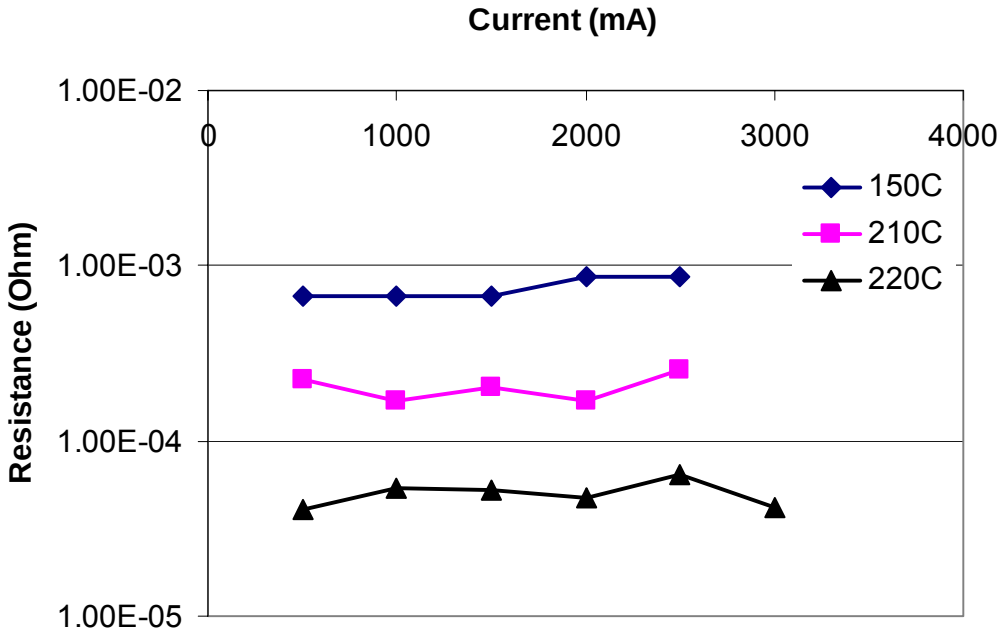

Figure 3.7 Current-voltage relationship of the nano Ag filled ACA with different curing conditions

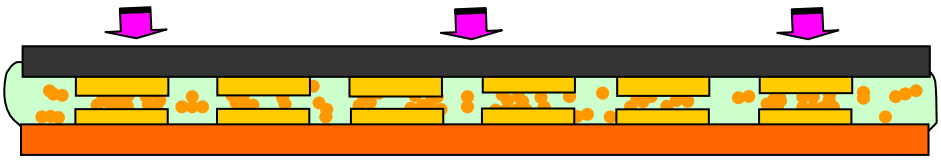

Figure 3.8 Schematic illustration of nano-ACA with sintering

3.1.4 Summary

A nano-Ag conductive adhesive (nano-ACA) which combines the advantages of both traditional anisotropic conductive adhesives and nonconductive adhesives was introduced for next generation high performance fine-pitch packaging applications. This nano-ACA combines the electrical conduction along the z-direction with a relatively low bonding pressure (ACA-like) and the ultra fine pitch (<30 μm) capability (NCA-like). With the low temperature sintering of nano-silver fillers, the joint resistance of the nano-ACA could be significantly reduced. The enhanced electrical properties of the nano-ACA joints were attributed to the reduced number of particle interfaces and improved interfacial contact between nano Ag fillers and bond pads by sintering and compressing processes of the ACA.

3.2 Improvement of electrical and thermal properties of ACAs with Self-assembled Monolayer (SAM)

3.2.1 Introduction

Although ACAs/ACFs exhibit promising characteristics such as fine pitch capability (<40 μm pitch), low temperature processing capability, low cost and environmentally friendliness, there are some key issues that hinder their implementation as interconnect materials for high performance devices microprocessor and Application

Specific Integrated Circuit (ASIC) applications. The ACA/ACF joints have lower electrical conductivity and poor current carrying capability. In addition to the low temperature sintering of nano-ACA/ACF, another possible approach to enhance the electrical and thermal properties of ACA/ACF joints is the introduction of self-assembled monolayer (SAM).

Self-assembled monolayers (SAMs) of small molecules, polymers, and proteins have attracted much attention in both experimental and theoretical fields for about two decades, and they offer the means to alter and control the chemical nature of surfaces. Self-assembled monolayers (SAMs) provide a convenient, flexible, and simple system with which to tailor the interfacial properties of metals, metal oxides, and semiconductors. SAMs are organic assemblies formed by the adsorption of molecular constituents from solution or the gas phase onto the surface of solids or in regular arrays on the surface of liquids (in the case of mercury and probably other liquid metals and alloys); the adsorbates organize spontaneously (and sometimes epitaxially) into crystalline (or semicrystalline) structures. The molecules or ligands that form SAMs have a chemical functionality, or "head-group", with a specific affinity for a substrate; in many cases, the head-group also has a high affinity for the surface and displaces adsorbed adventitious organic materials from the surface [84, 85]. There are a number of head-groups that bind to specific metals, metal oxides, and semiconductors. The most well studied SAMs are those prepared by the adsorption of alkanethiols ($CH_3(CH_2)_nSH$) on gold [86-93]. When adsorbed from the solution onto the Au (111) surface, alkanethiols form well-ordered monolayers possessing a ($\sqrt{3} \times \sqrt{3}$) $R30^o$ structure, wherein the sulfur atoms are bound to the 3-fold hollow sites of the Au (111) surface [94, 95]. On silver, the

hydrocarbon chain is tilted much less, at about 13^{o} from the surface normal. The adsorption of carboxylic acids ($CH_3(CH_2)_nCOOH$) has also been studied on silver surface and some experimental results suggested an epitaxial film with an in-plane structure of p (2×2) overlayer structure on Ag (111) surface. The bonding between carboxylic acids and Ag is considered as an acid-base reaction, and the driving force is the formation of a surface salt between the carboxylate anion and a surface metal cation [96-100]. As an example, Figure 3.9 is a schematic diagram of an ideal, single-crystalline SAM of alkanethiolates supported on a gold surface with a (111) texture [85]. The thickness of a SAM is typically 1-3 nm; they are the most elementary form of a nanometer-scale organic thin-film material. The composition of the molecular components of the SAM determines the atomic composition of the SAM perpendicular to the surface; this characteristic makes it possible to use organic synthesis to tailor organic and organometallic structures at the surface with positional control approaching 0.1 nm.

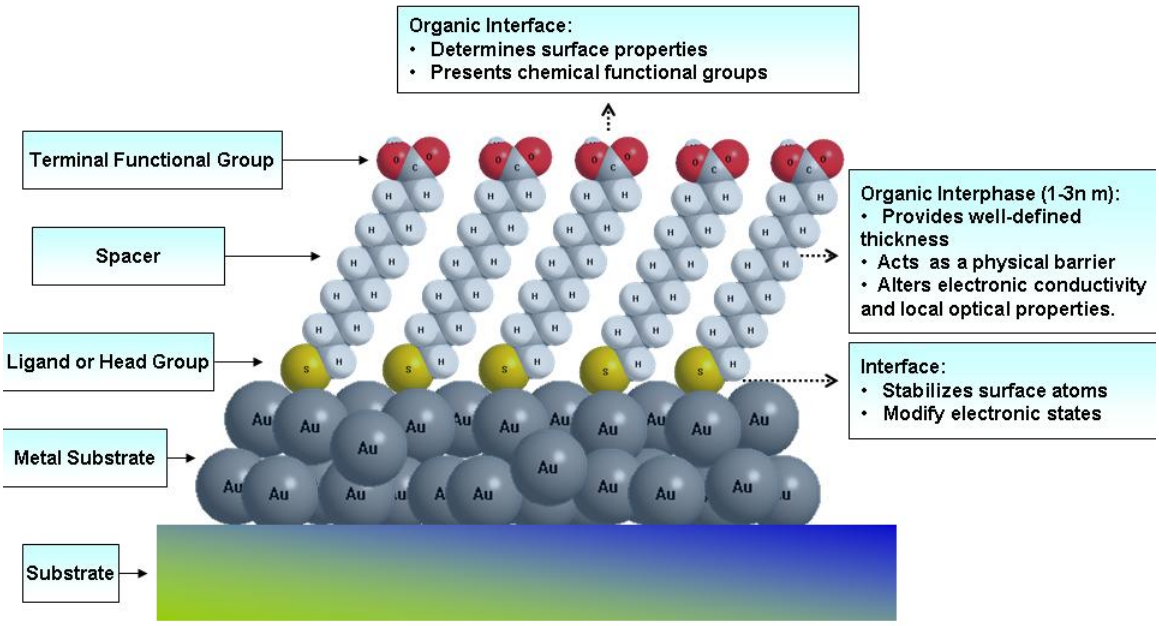

Figure 3.9 Schematic diagram of an ideal, single-crystalline SAM of alkanethiolates supported on a gold surface with a (111) texture. The anatomy and characteristics of the SAM are highlighted.

Self-assembled monolayers (SAMs) offer unique opportunities to increase fundamental understanding of self-organization, structure-property relationships, and interfacial phenomena. The ability to tailor both head and tail groups of the constituent molecules makes SAMs excellent systems for a more fundamental understanding of phenomena affected by competing intermolecular, molecular-substrates and molecule-solvent interactions like ordering and growth, wetting, adhesion, lubrication, and corrosion. The thermal stability and structural properties of SAMs are governed by both the substrate-acid interactions and chain-chain interactions in the adsorbed layer. The structural features of these SAMs have been studied in detail by several experimental

techniques such as IR spectroscopy [96, 97], X-ray diffraction [99], Surface-enhanced Raman spectroscopy (SERS) [100, 101], X-ray photoemission spectroscopy (XPS) [102]. These experimental studies reveal that the ordered or crystalline nature of the SAMs is a function of the temperature and chain length. At room temperature, SAMs with longer chain lengths prefer a more ordered structure as compared to shorter chains, which show no preferred tilt direction. At higher temperatures, the melting point can be reached which is chain-length-dependent.

In ACA interconnections, if SAM molecules can be introduced and monitored as electrical junctions or molecular wires, the interface properties between the conductive fillers and contact pad should be enhanced (Figure 3.10). In particular, some preliminary data has shown that the current density of some SAM molecular wires can be up to $1X10^{9}Å/cm^{2}$, therefore the potential of using SAMs for the improvement of electrical and thermal performance of ACA is significant.

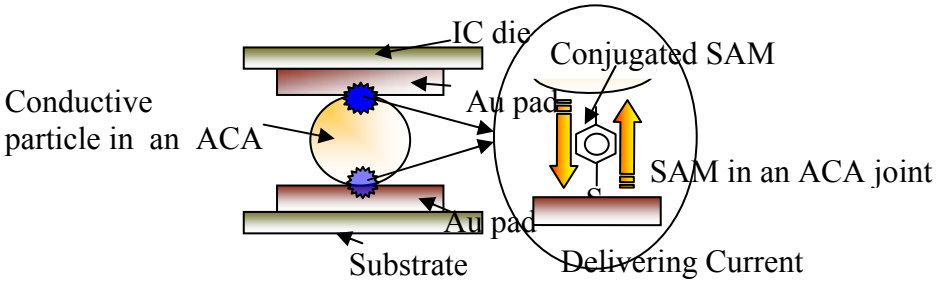

Figure 3.10 Schematic illustration of SAM molecule formed in an ACA joint

An important consideration when examining the advantages of organic monolayers pertains to the affinity and thermal stability of organic compounds to specific

metal surfaces. Table 3.2 gives the examples of molecules preferred for maximum interactions with specific metal finishes.

Table 3.2 Potential organic interfacial modifiers for different metal finishes

Formula	**Compound**	**Metal finishes**
R-S-H	Thiols	Au, Ag, Cu, Pt, Zn
R-COOH	Carboxylates	Fe/Fe_xO_y, Ti/TiO_2, Ni, Al, Ag
R-C≡N	Cyanides	Au, Ag, Pt
R-N=C=O	Isocyanates	Pt, Pd, Rh, Ru
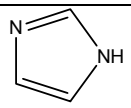	Imidazole & derivatives	Cu
R-SiOH	Organosilicone derivatives	SiO_2, Al_2O_3, quartz, glass, mica, ZnSe, GeO_2, Au

In this section, various types of SAM molecules such as thiols, carboxylic acids with different chain structures and chain lengths are evaluated on specific metal substrates or particles. Their coating capability, thermal stability as well as their effects on the electrical and thermal properties of ACA joints are investigated. Appropriate selection and incorporation of SAM is proposed as an efficient way to enhance the performance of ACA interconnects.

3.2.2 Experimental

The structures of SAM molecules used in this session are shown in Table 3.3.

Table 3.3 Chemical structures of the SAM compounds used in this section

Name	Chemical Structure
Octadecanethiol (ODT)	$HS(CH_2)_{17}CH_3$
Mercaptoacetic acid (MAA)	$HSCH_2COOH$
1, 4-benzene dithiol (Dithiol)	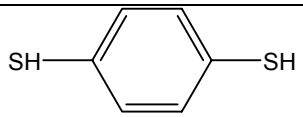
Malonic acid (acid M)	$HOOC\text{-}CH_2\text{-}COOH$

The Au, Ag and Cu surfaces were prepared by sputtering the corresponding metals on glass and wafer substrates, and the Sn/Pb surface was prepared on a copper/FR-4 board. All the surfaces were cleaned by rinsing these substrates with the isopropyl alcohol and dried under the hood. These specimens were then treated with a UV/ozone at 0.75 L/min flow rate of the oxygen for 3 minutes. The substrates were dipped into the SAM solution, and allowed to incubate for different time under a controlled nitrogen environment. The SAM solutions were prepared at 0.1-10.0 mM by dissolving the SAMs in ethanol. After each treatment time, the various surface samples were removed from the solution and rinsed with ethanol in order to remove excess un-adhered SAM molecules. The solvent surfaces were then dried off with argon.

The contact angles of deionized (DI) water on those surfaces were obtained by a goniometer (Rame-Hart Co.). To investigate the thermal treatment effect, the contact angle of water droplets was measured after holding the samples at room temperature, 100 °C and 150 °C for 30 min, 1 hr, and 2 hrs. To characterize the coating and bonding of SAM on particles, the weight loss of Au coated polymer particles (Au/EH) and naon-

silver particles before and after treatment with SAM compounds was measured by a thermogravimetric analyzer (TGA).

In order to study the effect of SAM on the electrical and thermal properties of ACA interconnects at various temperatures, two different types of ACA formulations were used. Polymer matrix of formulation 1 with a lower curing temperature was a bisphenol-A epoxy with 14 phr tetraetylenepentamine (TEPA). Formulation 2 was a typical ACA resin in which diglycidyl ether of bisphenol-F (DGEBF) EPON 862, methylhexa-hydrophthalic anhydride (MHHPA) and 1-cyanoethyl-2-ethyl-4-methylimidazole (2E4MZCN) were employed as epoxy resin, curing agent and catalyst, respectively. The electrical resistance of the ACA joints (contact area: 100x100 μm^2) was measured by four-point probe method.

The thermal conductivity of ACAs was determined by using an LFA 447 NanoFlash apparatus manufactured by NETZSCH. The cured ACA samples were cut into a square of 10x10 mm with a thickness of ~1.0 mm. A Xenon flash lamp fired a pulse at the sample's lower surface, while the infrared detector measured the temperature rise of the sample's top surface. A computer software then determined the sample's thermal diffusivity (α). Thermal conductivity (k) of the sample was obtained from Equation 3-1, where Cp was specific heat measured by DSC, and ρ was the sample density.

$$k = \alpha \rho C_p \tag{3-1}$$

3.2.3 Results and Discussion

3.2.3.1 Coating of thiol compounds on various metal surfaces

Figure 3.11 shows contact angle values of DI water on gold, copper and tin/lead surfaces as a function of treatment time with different concentrations (0.1, 1 and 10 mM) of octadecanethiol (ODT). The contact angles increased obviously on ODT-coated metals, indicating that the ODT molecules were coated on the Au surface, because the SH functional group anchored on the metal surface and the hydrophobic terminal material groups (CH_3) contacted the water droplets. The contact angles on the gold surfaces increased greatly with a longer treatment time and higher concentrations of the ODT. On the contrary, the angles on copper surface increased by more than half almost immediately, and the different concentrations of ODT did not appear to create significant changes in contact angles. The angles of the tin-lead surfaces also leveled off rather fast, around two hours. The difference should be due to the various reactivity of different metals with the ODT treatment.

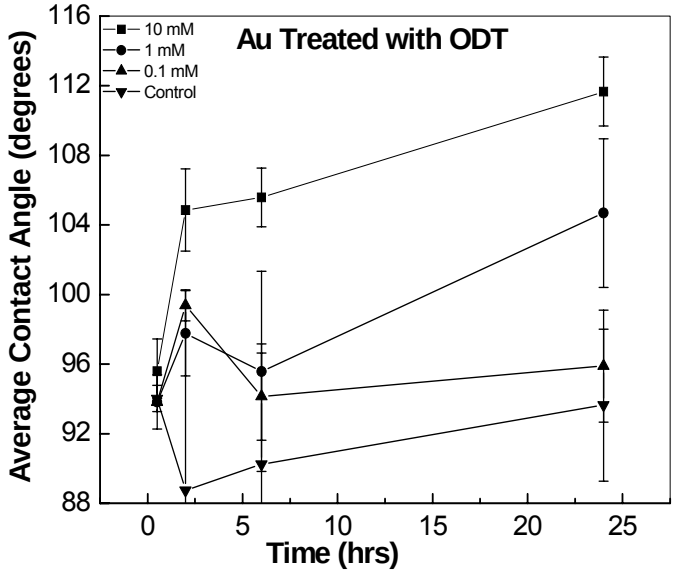

(a)

Figure 3.11 Contact angles of DI water droplet on (a) Au (b) Cu and(c) SnPb surfaces as a function of treatment time with difference concentrations (0.1, 1 and 10 mM) of octadecanethiol (ODT).

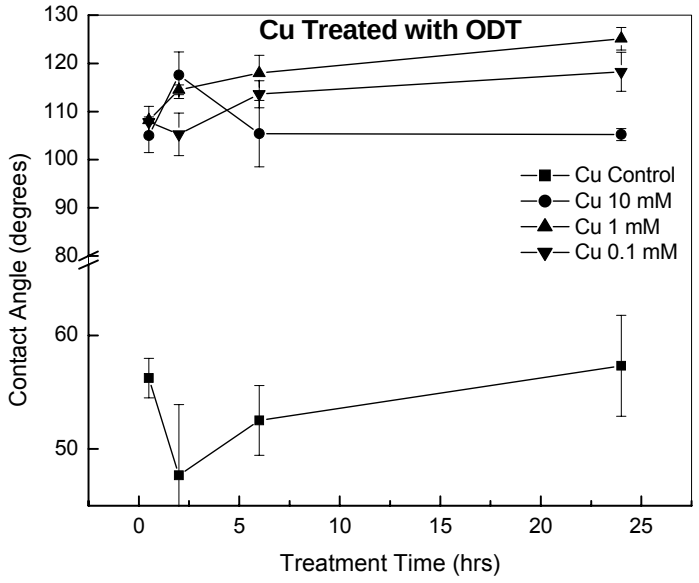

(b)

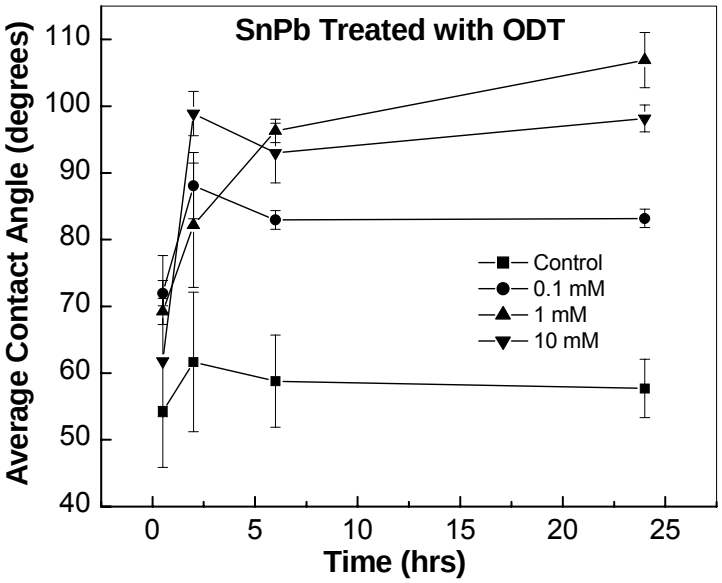

(c)

Figure 3.11 continued.

MAA, with a hydrophilic tail group (carboxylate), exhibited more obvious trend (as shown in Figure 3.12). All the metal surfaces showed decreased contact angles after treatment. Especially, the contact angles on the gold plated surfaces decreased dramatically. As evidenced by the plateaus in the graph, MAA adhered to the metal surfaces quickly and there was no big difference for the contact angles with different treating time.

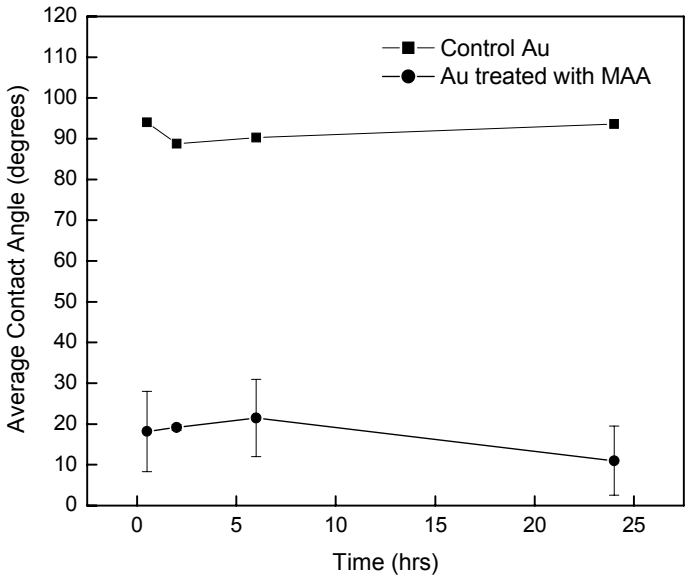

(a)

Figure 3.12 Contact angle values of DI water droplets on (a) Au (b) Cu and(c) SnPb surfaces as a function of treatment time with MAA

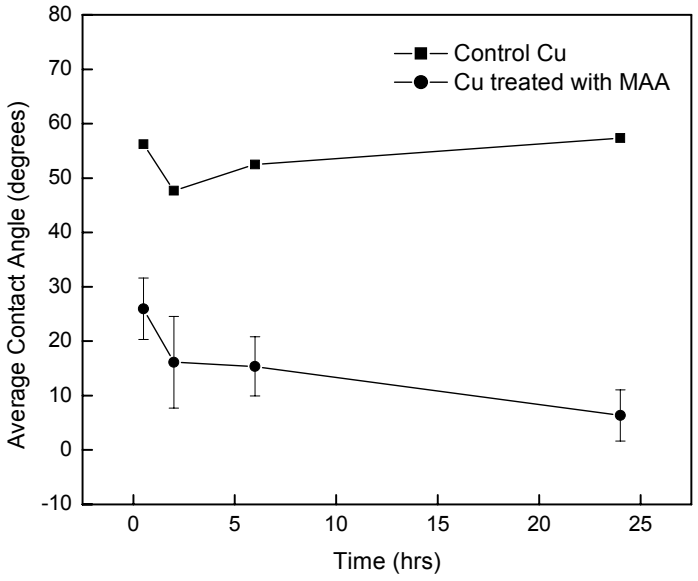

(b)

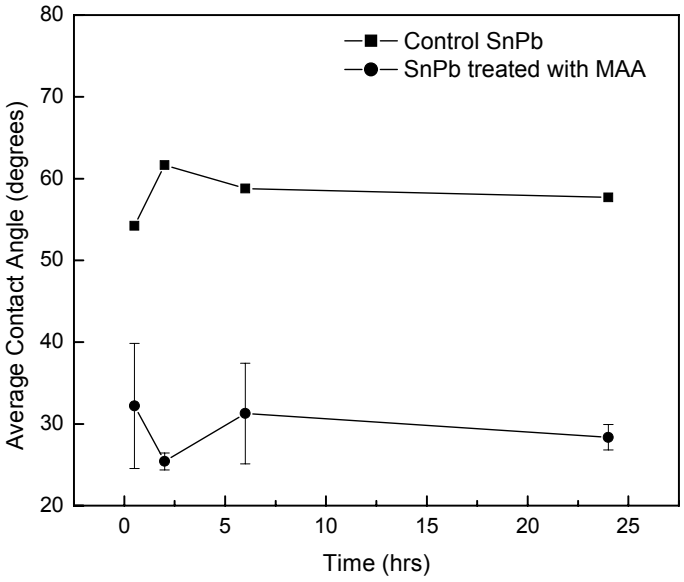

(c)

Figure 3.12 continued

As for another hydrophilic di-functional SAM, 1,4-benzendithiol, the contact angles value also showed an obvious decrease on Au after treatment (Figure 3.13) The contact angles continued to decrease after two hours since the aromatic moiety may have a slower coating rate than the aliphatic group. Therefore, the length of deposition time is important for coating of the SAM on the gold surfaces.

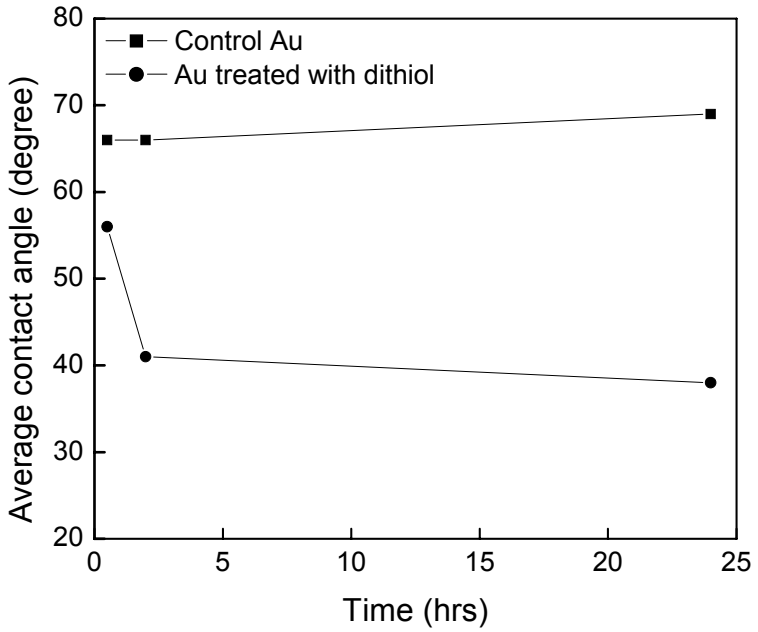

Figure 3.13 Contact angle values of DI water droplets on the Au surfaces treated with dithiol solution.

3.2.3.2 Thermal Stability of thoil coating on Au surface

Temperature is an important factor for SAM molecules to survive on metal finishes, as such, the thermal stability of SAM coating on metal surface needs to be evaluated. Since Au-coated polymer ball is the most widely used conductive fillers for

ACA/ACF and Au-finished substrate is also currently the accepted metal finishes for the interconnects, the thermal stability of thiols on Au was studied by measuring the contact angle changes after annealing the coated Au surfaces at various temperatures.

Figure 3.14 shows contact angle values of DI water droplet on gold surfaces as a function of treatment time at room temperature, 100°C and 150°C, respectively. The contact angles for all SAM treated surfaces remained relatively the same for 2 hrs at room temperature and 100°C. However, when heat-treated at 150 °C, the contact angles decreased slightly for ODT treated gold surface, indicating that the coating of ODT suffered degradation at 150°C. The contact angles of the hydrophilic MAA coatings on the heat-treated (at 150°C) surfaces showed gradual increases with time. These increases indicated that MAA also decomposed at 150^{o}C. For the dithiol treated surface, on the other hand, no obvious difference of the contact angles could be observed even after heat-treated (at 150°C) for 2 hours. Therefore, 1,4-benzeneditihol was more thermally stable at 150^{o}C than ODT and MAA. A possible explanation for the relatively stable coating is due to the rigid benzene ring existing in the chemical structure which enhanced the thermal stability of the SAM coating.

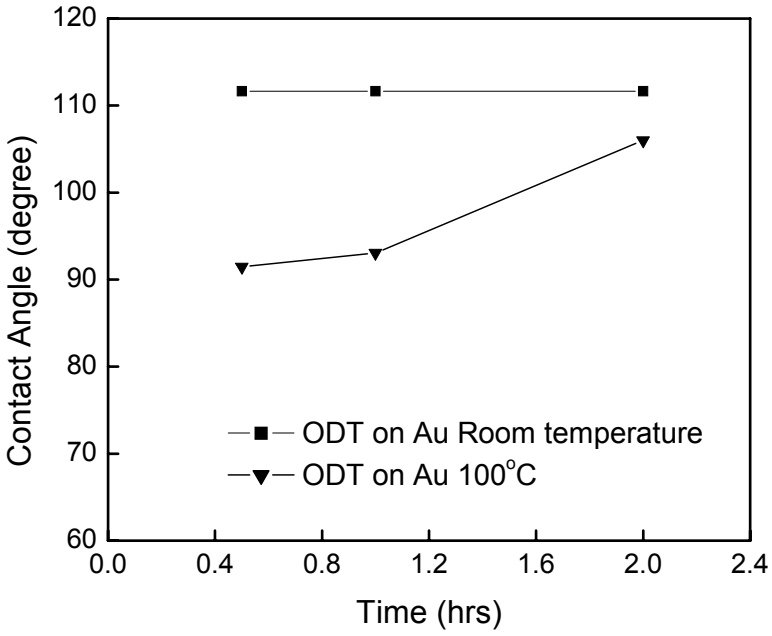

(a)

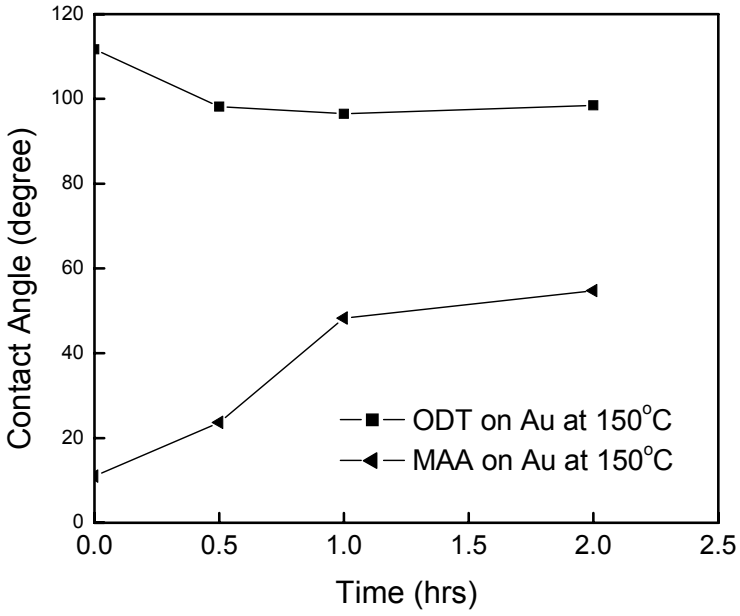

(b)

Figure 3.14 Contact angle values of SAMs on gold surfaces at different temperatures. a) ODT treated Au at room temperature and 100°C; b) ODT and MAA treated Au at 150°C; c) Dithiol treated Au at room temperature, 100°C and 150°C.

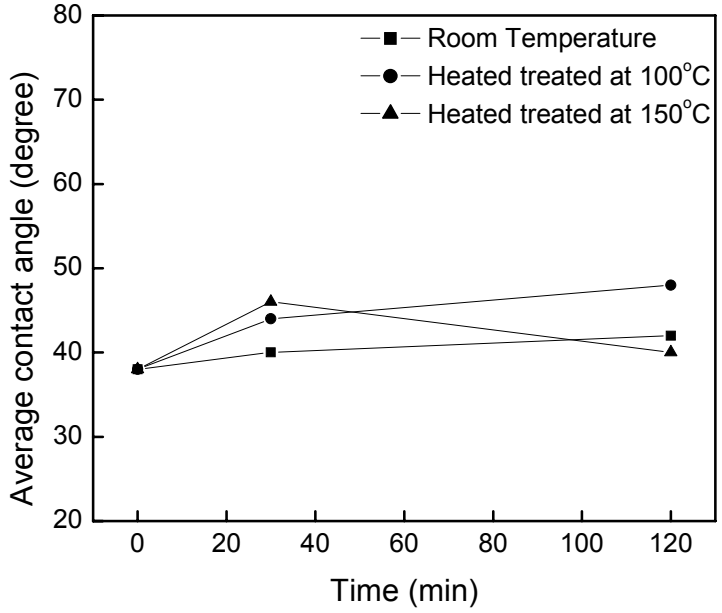

(c)

Figure 3.14 continued.

3.2.3.3 Coating of thiol compounds on Au-coated polymer conductive fillers

Au-coated polymer particles (Au/EH) are usually used as conductive fillers in ACA/ACF. In order to get a clear profile whether thiol SAM compounds can be well coated on gold and consequently improve the electrical properties of ACAs, the weight losses of Au/polymer particles before and after treatment in ODT and dithiol solutions was measured and the results are shown in Figure 3.15. For both treated and untreated samples, they showed obvious weight loss over 30% at 300-400°C. This corresponds to the decomposition of the core polymer at the temperature.

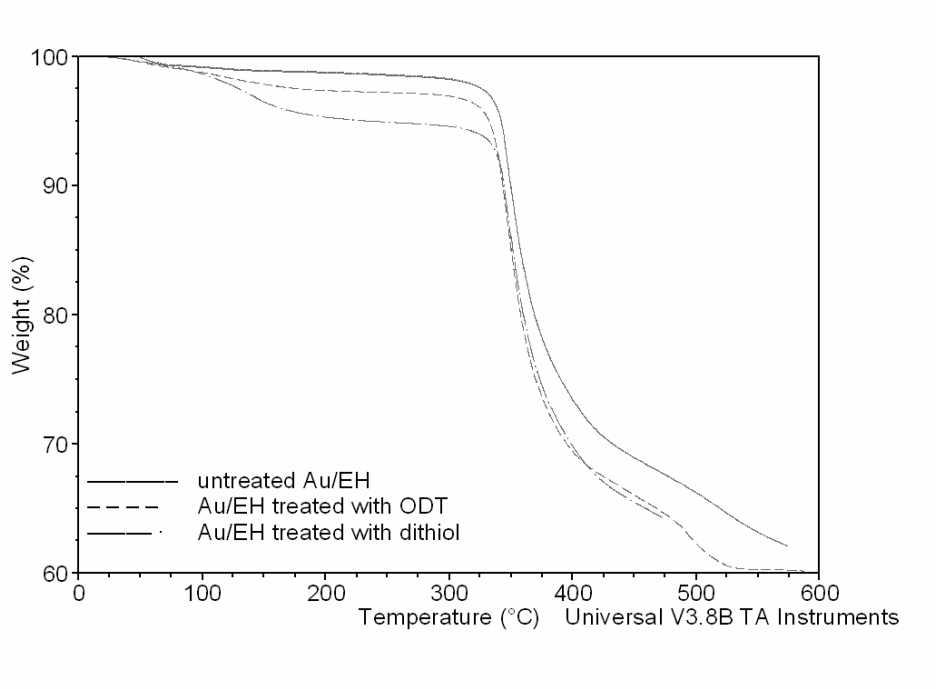

(a)

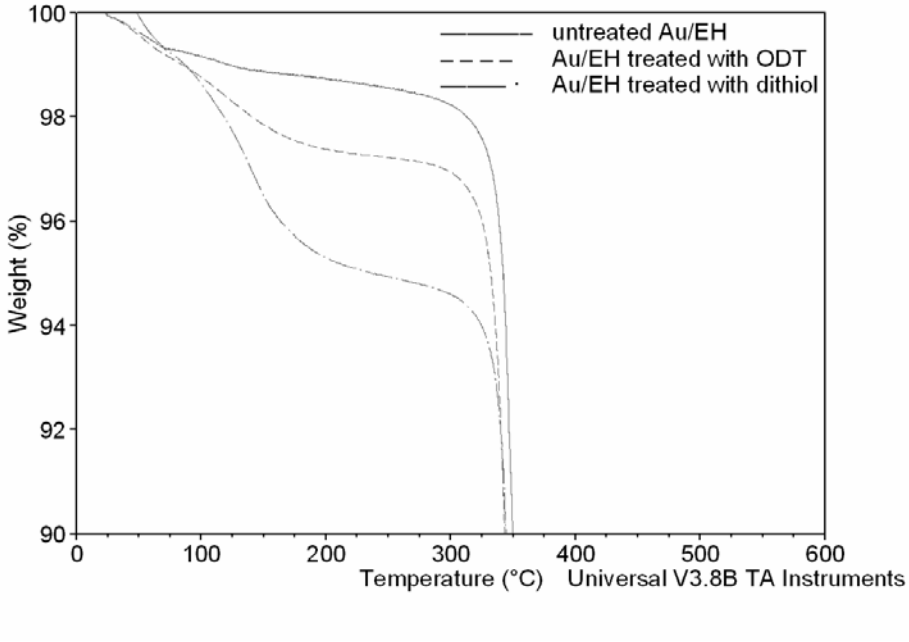

(b)

Figure 3.15 TGA Curves of Au/EH particles before and after treating with different SAM compounds. a) Full range for the weight loss b) Enlarged image for the weight loss.

The weight of the untreated Au/polymer was constant below 300^{o}C, indicating the polymer in the particle itself was stable at relatively lower temperatures. For the ODT treated particles, weight loss of 2% was observed at 100-150^{o}C, suggesting the ODT has been well coated on the particles during the treating process due to the strong affinity of thiol functional group toward gold. However, the weight loss may correspond to de-bonding of the SAM molecules from the particle and their thermal decomposition at those temperatures. Compared to the thermal stability results of SAM coating, the weight loss is also due to the degradation of SAM at the temperature. As for the dithiol treated particles, they exhibited more definitive results with the weight loss around 5%. Also, the temperature for the weight loss was slightly higher than those for ODT treated particles. Therefore, the dithiol has stronger coating capability on Au and the thermal stability is better than the mono-thiol compound (ODT). The result of the thermal stability is in accordance with the contact angle results for the thiol-treated Au surfaces (Figure 3.14).

3.2.3.4 Curing profile of the ACAs resins

Temperature was an important factor for SAM molecules to survive on metal substrates. As such, when the SAM molecules are incorporated into an epoxy resin, the epoxy curing temperature may influence the SAM survival.

In order to study the effect of the curing temperature, two different types of epoxy resins were employed for the present study. As shown in Figure 3.16, the low (formulation 1) and high (formulation 2) temperature curing epoxy formulations were selected. It can be seen that the curing peaks of the formulation 1 and 2 were found at

93°C and 145°C, respectively. The two formulations were cured at 75°C for 30 minutes and 150°C for 1 hour, respectively.

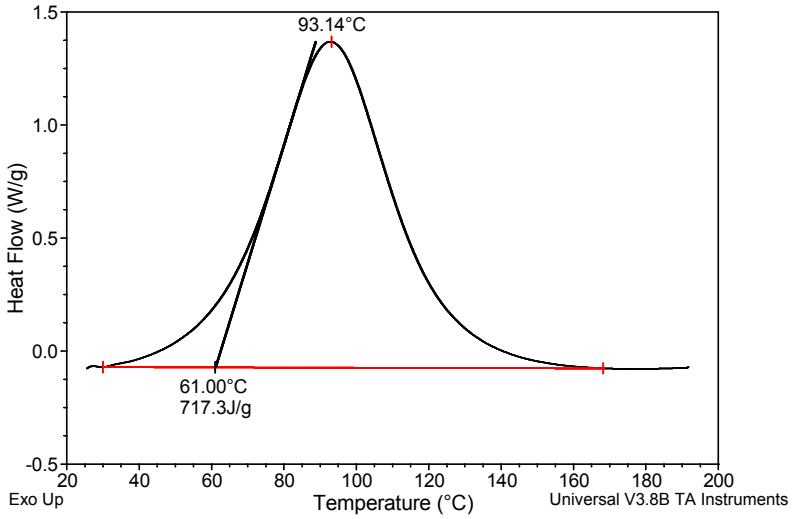

(a)

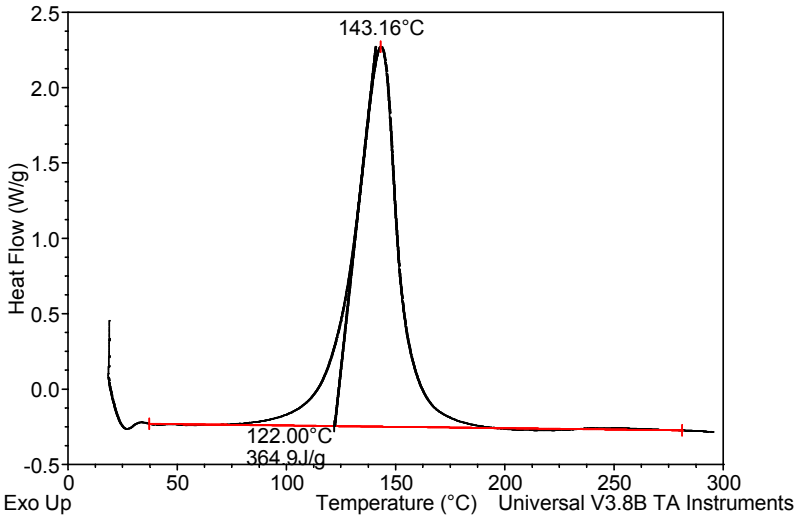

(b)

Figure 3.16 DSC Dynamic Scan of (a) low curing temperature (formulation 1) and (b) high curing temperature (formulation 2) ACA resins.

3.2.3.5 I-V (Current-Voltage) measurement of ACAs with 1,4-benzenedithiol

Since 1,4-benzenedithiol has the best coating capability and thermal stability on Au, it was introduced into the ACA formulations to treat the conductive fillers and gold-finished bond pads. The current-voltage (I-V) curve of the low curing temperature ACA (formulation 1) joint is shown in Figure 3.17. It can be seen that with the introduction of SAM treated conductive fillers and/or substrates, the slope of I-V curve decreased significantly and consequently a dramatically decreased resistance could be obtained. The resistance was achieved as low as 10^{-5}Ohm for the ACA with both treated bond pads and treated conductive fillers. It is believed this is because the dithiol compounds can adhere to the conductive fillers and substrate, forming physi-chemical bonds and allowing electrons to flow through, as such, it reduces electrical resistance and can also carry high current flow through ACA joints.

For the high curing temperature ACA (formulation 2) joints, although a lower slope in the of I-V curve and subsequently lower resistance could also been observed at lower current (less than 2A) with dithiol-treated fillers and substrates,the resistance was dramatically increased above 2A. (Figure 3.18) Compared to the low temperature curable ACA, the SAM in the formulation 2 was less effective in improving the electrical property. This may be due to the partial degradation of SAM compounds at the high curing temperature. Although contact angle results did not show obvious degradation at 150^{o}C for the dithiol treated Au surface, the application of pressure together with heat during the bonding and curing process for ACAs may accelerate the degradation of SAM compounds.

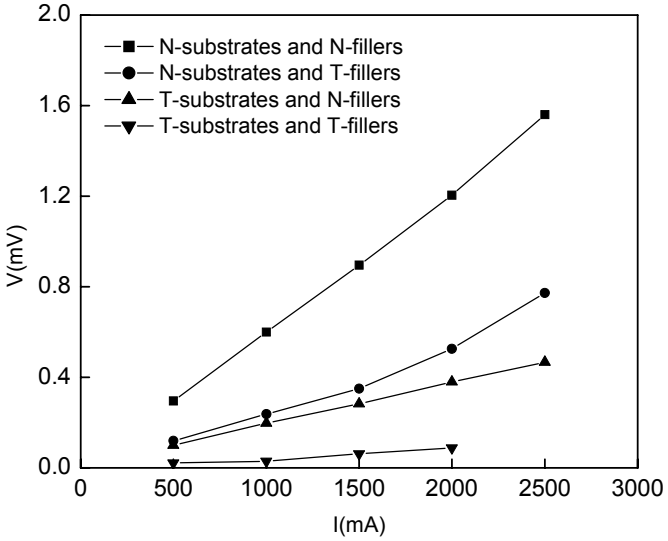

(a)

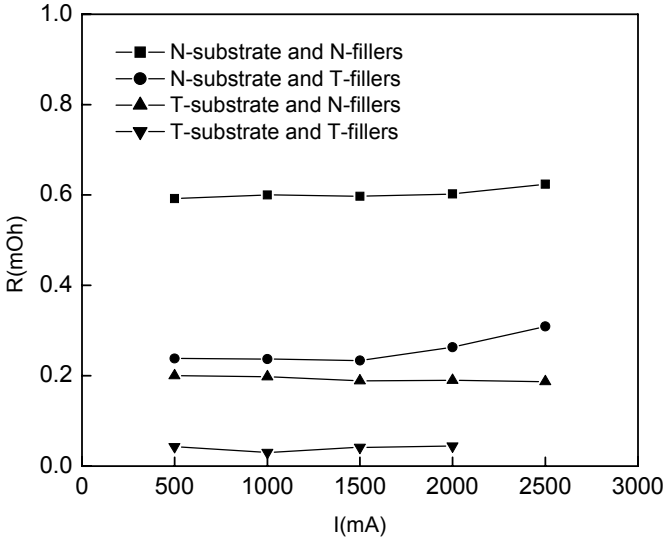

(b)

Figure 3.17 Electrical properteis of low temperature curable ACA (Formulation 1) with untreated (N) and treated (T) conductive fillers and substrates

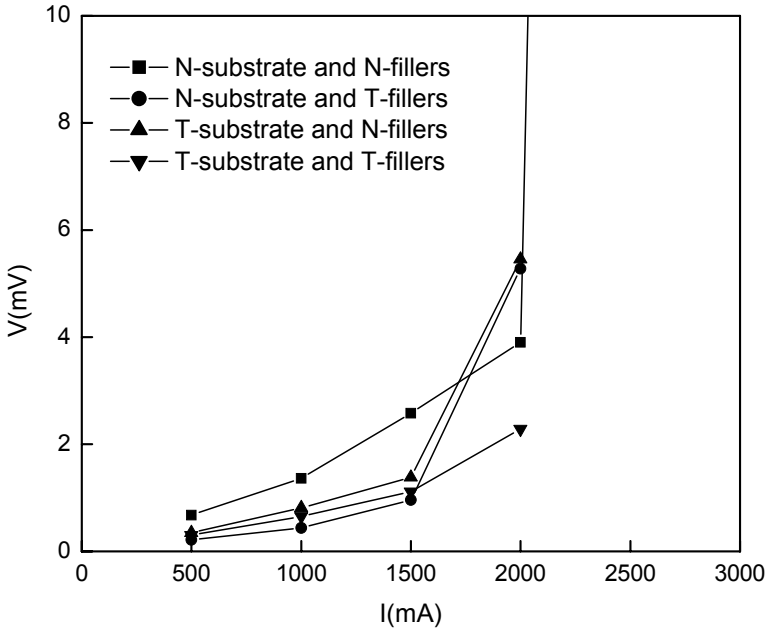

(a)

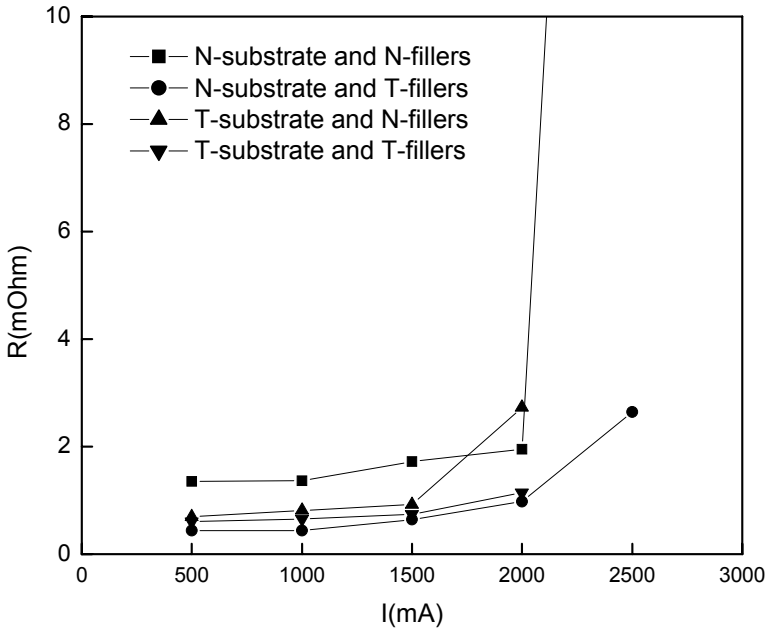

(b)

Figure 3.18 Electrical properteis of high temperature curable ACA (Formulation 2) with untreated (N) and treated (T) conductive fillers and substrates

3.2.3.6 Coating of SAMs on Ag

Other than gold, silver is the potential conductive fillers in next generation ACA/ACF because of the balanced properties and relatively low cost. Silver has highest room temperature electrical and thermal conductivity among all the metals. Silver is also unique among all the cost-effective metals by nature of its conductive oxide (Ag_2O). In addition, silver nano-particles are relatively easy to form into different sizes (a few nanometers to 100nm) and shapes (such as spheres, rods, wires, disks, flakes, etc.) andcan be sintered at the curing temperautre of ACA/ACF. Therefore, the interaction between SAM molecules with Ag was investigated and their effects on the electrical and thermal properties of nano-Ag ACA joints were also evaluated.

Figure 3.19 shows contact angle values of deionized (DI) water droplet on flat Ag surfaces with and without SAM treatments. For the untreated Ag surfaces, the contact angle was ~70 degrees. After treated in SAM solutions, lower contact angles were observed. A lower contact angle of the water droplet indicates a more hydrophilic surface, suggesting that both acid M and dithiol have been coated on the silver surfaces, since these SAM compounds have hydrophilic functional groups (-COOH and -SH) as the terminal groups.

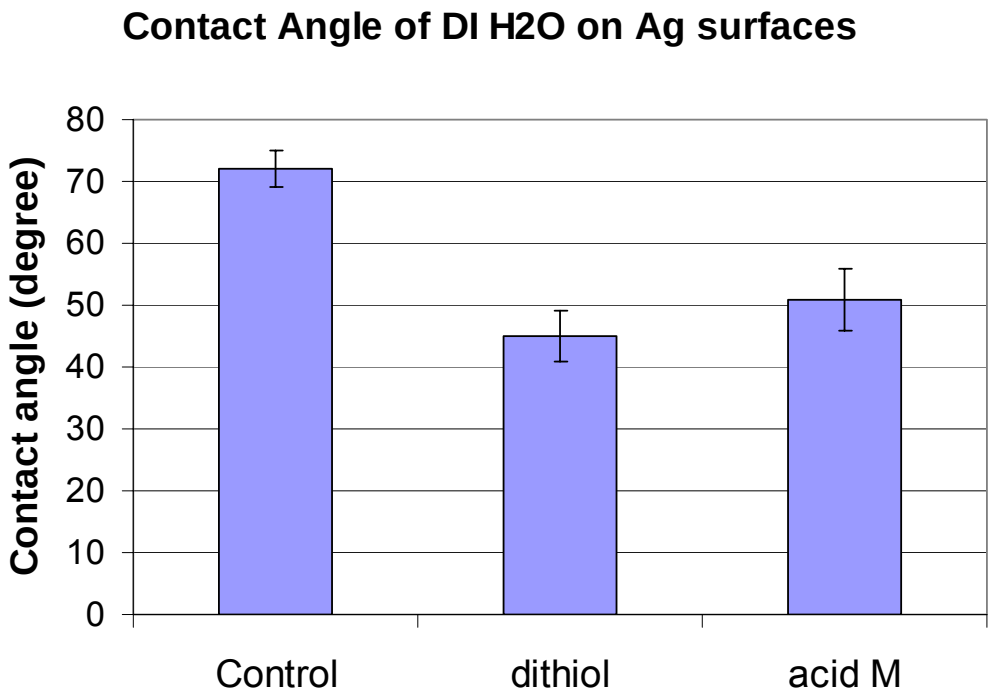

Figure 3.19 Contact angle of DI H_2O on Ag surfaces

From the lower contact angle value, some possible alignment modes of the di-functional SAMs compounds on Ag finishes could be proposed assuming a similar alignment configuration on silver nanoparticles and silver surfaces (in Figure 3.20). One end of the hydrophilic functional groups (carboxylic or thiol) anchored on the Ag finish and the other group might face upward with a tilted angle, ready to attach to another silver particle. This configuration may attribute to the short molecular length of acid M (Figure 3.20a) and the rigidity and planarity of the benzene ring sandwiched between the two thiol functional groups (in Figure 3.20b). The lower contact angle after treatment suggested the tilted and aligned configuration. The adherence and alignment modes of SAM on silver surfaces shown in Figure 3.20 could help protect the silver surfaces and enhance the connection between silver nanoparticles and metal bond pads. These

configurations are expected to be beneficial to the electrical properties of the monolayer protected nano silver-filled ACAs, as the current can flow freely between these interfaces.

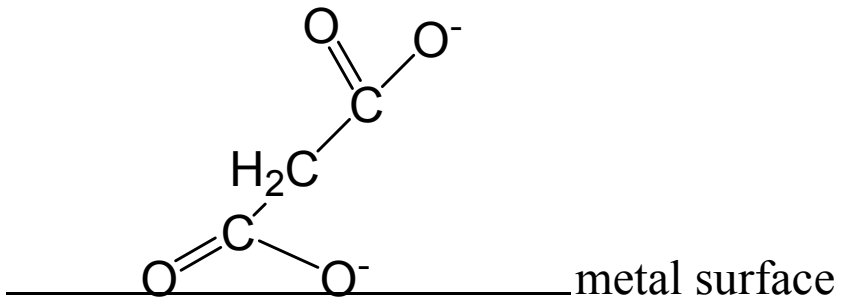

(a)

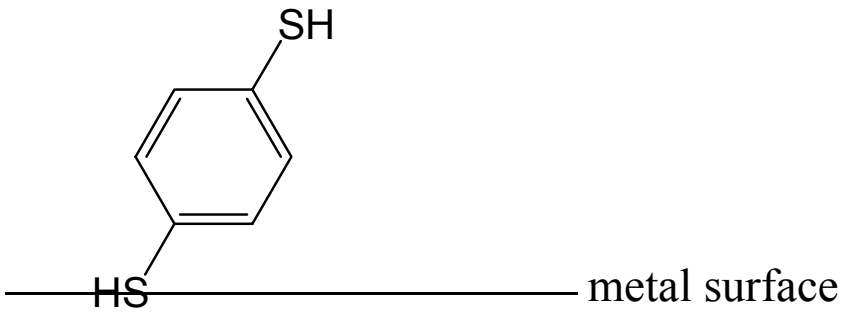

(b)

Figure 3.20 Possible alignment modes for different SAMs on silver finishes a) malonic acid on silver surface; b) 1,4 benzene dithiol on silver surface

To characterize coating of organic molecules on the silver nanoparticles, the weight changes of untreated and treated silver nanoparticles were recorded by TGA and the result is shown in Figure 3.21.

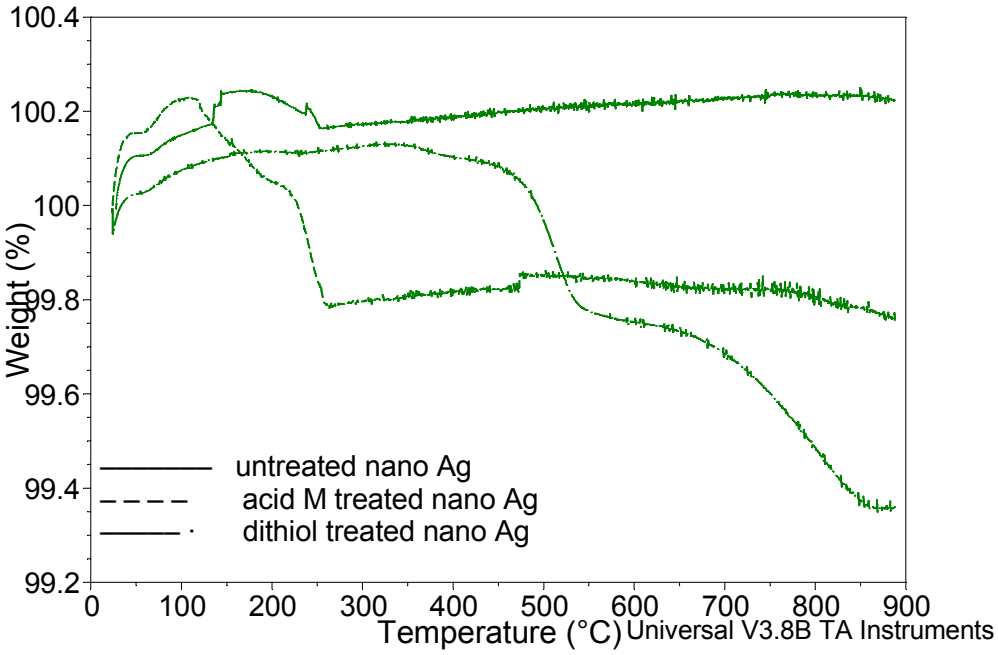

Figure 3.21 Weight change of untreated and SAM treated silver nano particles

For untreated silver nanoparticles, there was no obvious weight change during heating, indicating no organic compounds or SAMs were present on the untreated nano Ag particles. However, obvious weight loss was observed for both acid M and dithiol treated silver nanoparticles. For the acid M treated particles, approximately 0.4wt% weight loss occurred at 200-250^{o}C. The weight loss may correspond to the decomposition of the de-bonded acid M in the temperature range since the typical decomposition temperature of malonic acid is ~140^{o}C. For dithiol treated samples, there were two stages of weight loss, one around 0.3 wt% at 500^{o}C and the other 0.5 wt% at 700^{o}C. The weight loss of SAM treated silver nanoparticles suggested the SAM organic molecules were well coated on the silver nanoparticles due to the strong affinity of carboxylic and thiol

functional groups of the organic molecule toward the Ag surface. The two stages of weight loss for thiol treated particles may be due to the loss of thiol compound and the decomposition of Ag_2S complex, respectively. Compared to the degradation temperatures of 100-150^oC for SAM treated micro-sized Au particles (Figure 3.14), the thermal stability of SAM treated silver nanoparticles was superior and the decomposition temperature was much higher. The improved thermal stability may be due to the higher surface energy of nano particles than that of the micron-sized particles as well as the high affinity of the SAM to the nano-metal, thus, the stronger bonding and complexing between SAM compounds and Ag particles.

3.2.3.7 I-V (Current-Voltage) measurement of ACAs with SAM-coated nano Ag fillers

The silver nano fillers and metal bond pads were treated with acid M and dithiol solutions, respectively, and then these monolayer coated silver nanoparticles were incorporated into ACAs. The current-voltage (I-V) curve of ACA joints is shown in Figure 3.22 and compared with varoius types of lead-free interconenct materials. For the untreated nano Ag-filled ACAs, the electrical resistance of the ACA joints was around 10^{-3} Ohm and the highest current applied without inducing joint failure (maximum allowable current) was 2.5 A. Over 2.5 A, the adhesive joints could not survive and the adhesive joints was burned and damaged. With the introduction of monolayer protected silver nano fillers, the slope of I-V curve decreased dramatically, indicating a significantly improved conductivity of the joint. For the dithiol treated nano Ag filled ACAs, the joint resistance decreased to 10^{-4} Ohm, but the current carrying capability was the same as untreated samples. Increasing current over 2.5 A led to the failure of adhesive joints. For the acid M-treated ACA samples, dramatically decreased joint resistance was

achieved as low as 10^{-5} Ohm. The resistance value was comparable or even lower than some of the metallic solder joints. (10^{-4}~10^{-5} Ohm) Moreover, the maximum allowable current of acid M-treated samples also increased significantly, from 2.5 A to 3.5 A. Interestingly, at current higher than 4 A when failure occurred, the failure location was between the probe tip and the substrate rather than the adhesive joints. This observation suggested that acid M-treated nano Ag ACA joints had the potential to carry even higher current, provided a suitable or optimized test vehicle could be designed and used in this study. The improved electrical properties for SAM-coated nano Ag ACA may be due to higher thermal stability of the SAM compounds on the silver nanoparticles. Those SAM compounds can also help the dispersion of silver nanoparticles in the epoxy resin and protect the metal fillers. The SAM compounds adhere to the conductive fillers, forming physi-chemical bondings and allowing electrons to freely flow/tunnel through the interfaces, as such, it reduces electrical resistance and can also carry a high current flow for ACA joints. Unlike the SAMs on micro-sized metal fillers which suffered degradation at temperatures higher than 100^{o}C, the larger surface area and higher surface energy of nano particles enabled the SAMs to be more readily coated and relatively thermally stable on the metal surfaces. The stronger bonding between SAM and silver nanoparticles and the superior thermal stability made it more effectively improve the electrical properties of ACA cured at relatively higher temperature (e.g. 150^{o}C).

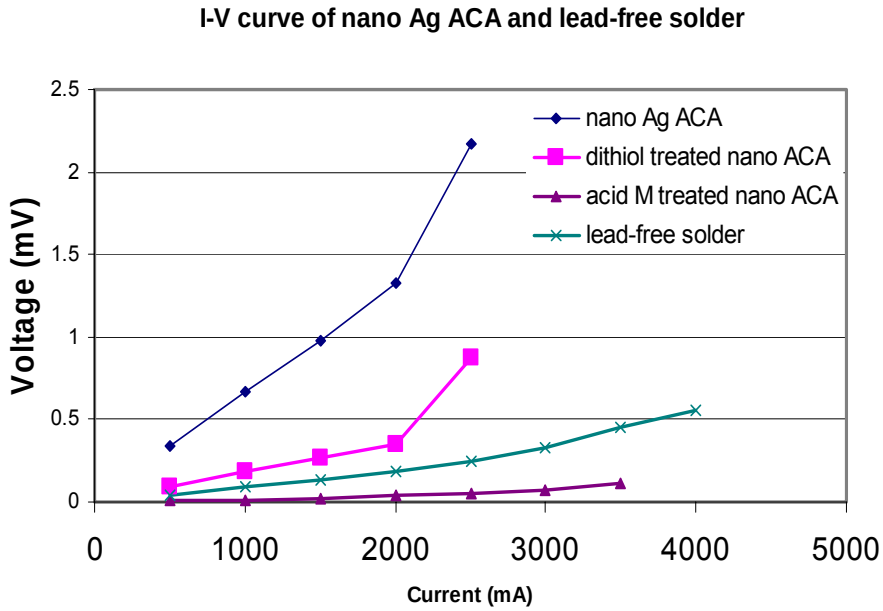

(a)

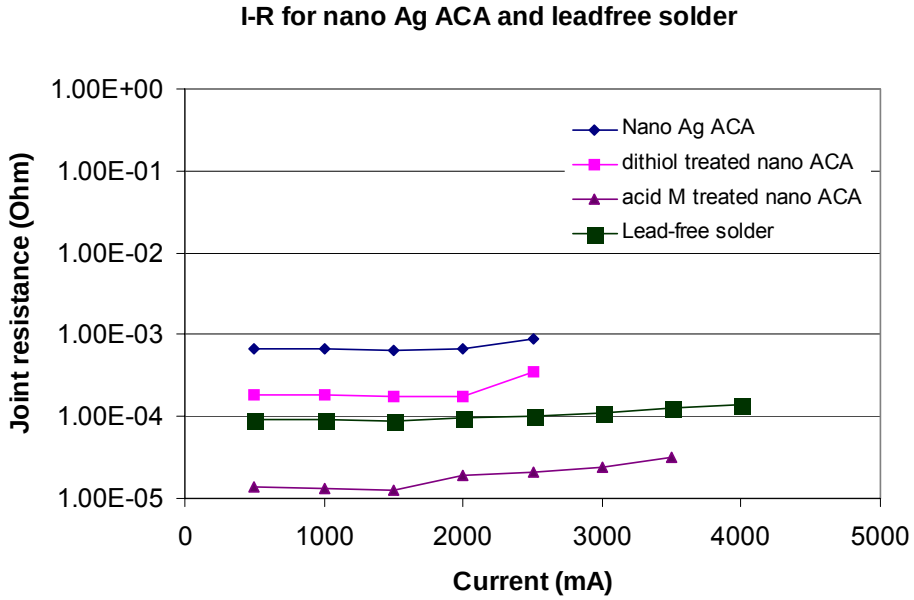

(b)

Figure 3.22 Electrical properties of nano Ag filled ACA with SAM and lead-free solder (tin-silver-copper) a) I-V curve of nano Ag ACA and leadfree solder; b) corresponding I-R curve

3.2.3.8 Thermal conductivity of nano Ag-filled ACA with SAMs

For the ACA interconnect joints to deliver high current, not only a low electrical resistance, but also a high thermal conductivity of the interconnect materials is required. It was reported that the addition of high thermal conductivity fillers into the ACA formulation rendered high current carrying capability. Therefore, the effects of the SAM-treatment on the thermal conductivity of the ACA were also investigated. Thermal conductivity variation with response to temperature is important information, because the ACA joint material is heated up during the applying current. Therefore, the thermal conductivity as a function of temperature was measured. The heat capacity and thermal conductivity of cured nano Ag ACA with SAM are shown in Figures 3-23 and 3-24, respectively. For the untreated nano Ag ACA, the thermal conductivity changed from 0.2 to 0.24 W/g•m. With SAM-treated nano Ag ACA, the thermal conductivity was significantly increased. Especially for acid M-treated samples, the thermal conductivity increased over 35% at room temperatures. The significantly improved thermal conductivity could attribute to the improved interface properties between metal fillers and the epoxy matrix with SAM treatment. The higher thermal conductivity could help dissipate heat more effectively from adhesive joints generated at high current by the high frequency devices, such as the high performance microprocessors. Therefore, higher thermal conductivity nano Ag ACA also contributed to the improved current carrying capability. With increasing temperatures, the thermal conductivity improvement of monolayer incorporated nano-Ag ACA was less significant, especially at temperatures higher than 170^{o}C, probably due to the thermal degradation of the coated monolayer molecules. Therefore, to further improve the electrical and thermal behaviors of ACA

with monolayer protected nano particle fillers, both the strong interaction between monolayer and metal finishes and the high thermal stability are preferred.

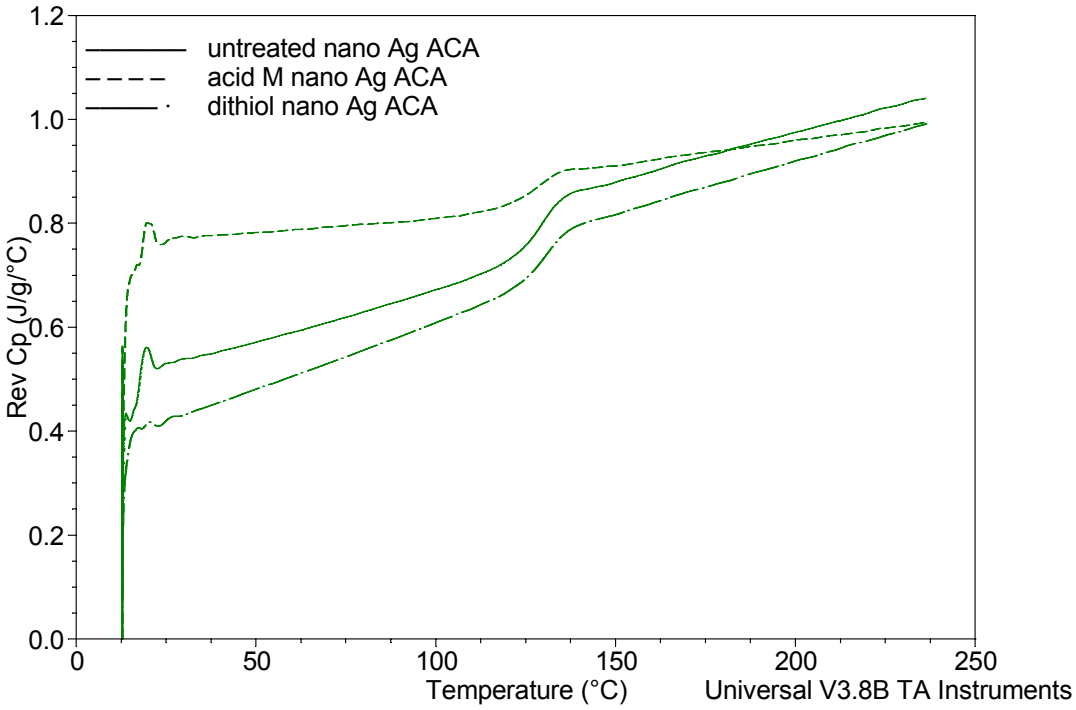

Figure 3.23 Heat capacity of nano Ag filled ACA with SAM

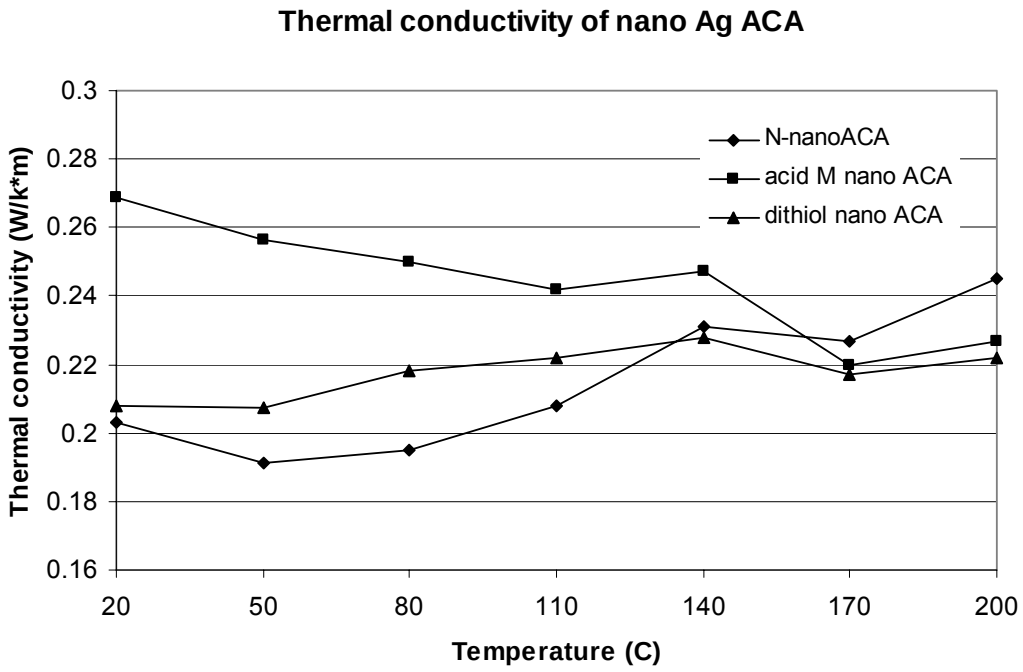

Figure 3.24 Thermal conductivity of nano Ag-filled ACAs with SAM

3.2.4 Summary

Different types of thiol and carboxylic acid SAM molecules, mono-thiol compound ODT, difunctional thiol-carboxylate compound MAA, 1,4-benzenedithiol and dicarboxylic acid malonic acid, all adhered to specific metal surfaces. The electrical property of ACAs with micron-sized Au/polymer filler improved obviously for low curing temperature curable formulation with treated conductive fillers and treated bond pad. However, the improvement was not obvious for high curing temperature ACAs.

With the introduction of SAM-treated nano Ag fillers and metal bond pads in the nano-Ag ACAs, on the other hand, the electrical conductivity and current carrying capability of ACAs were enhanced significantly even at relatively high curing temperature. The better thermal stability on for nano-Ag ACA should be due to the high

surface area and surface energy of the nano conductive fillers and therefore the stronger bonding. The improved interfacial properties of nano Ag ACA with SAM through the metal-polymer and metal-metal filler interactions also contributed to the increased thermal conductivities of the ACAs.

3.3 Silver migration control in the nano-Ag conductive adhesives

3.3.1 Introduction

Silver is the most widely used conductive fillers in ICAs, and currently also considered as a potential candidate for ACA/ACF fillers because of the many unique properties of silver particles, in particular, the silver nano-particles. Silver has highest room temperature electrical and thermal conductivity among all the metals. Furthermore, silver is also unique among all the cost-effective metals by nature of its conductive oxide (Ag_2O). In addition, silver nano-particles are relatively easy to form into different sizes (a few nanometers to 100nm) and shapes (such as spheres, rods, wires, disks, flakes, etc.) and well dispersed in a variety of matrices materials. Therefore, silver nano-composites are considered as a promising material in electronic industry, such as nano-Ag ACA/ACF as a fine pitch lead-free interconnects and high dielectric constant composites in embedded passives. However, a major problem that impedes the use of silver-containing materials in electronics is the electrochemical migration of silver in the presence of moisture and applied bias. In microelectronic devices, silver migration usually occurs between adjacent conductors, which leads to the formation of dendrites, growing from the cathode to the anode, and finally accumulating with an electrical short-circuit failure [103]. To avoid short-circuit, self-passivated aluminum (Al) has long been used in semiconductor devices, while copper (Cu) are being used in most electronic devices in

recent years due to the better electrical conductance. However, copper is easily oxidized and a lot of efforts are needed to prevent the oxidation problem. Silver is the most promising metal for next-generation semiconductor devices because of the excellent electrical and thermal properties. By solving the migration issue for silver, it will have great potential to be used for next-generation high performance advanced semiconductor devices.

Metal migration is an electrochemical process, which requires chemical interaction between the surroundings and the metal (generating metal ions); a polar transport electrolyte in aqueous conditions through which ionic migration occurs; and under an electric field. In fact, this situation prevails in most electronic packages where three conditions are present. When a potential is applied across the electrodes, a chemical reaction takes place at the positively biased electrode where positive metal ions are formed. ($Ag \rightarrow Ag^{+} + e^{-}$) These ions, through ionic conduction, migrate toward the negatively charged cathode, where over time, they accumulate to form metallic dendrites ($Ag^{+} + e^{-} \rightarrow Ag$). As the dendrite growth increases, a reduction of electrical spacing occurs. Eventually, the silver growth reaches the anode and creates a metal bridge between the electrodes, resulting in an electrical short circuit [104]. In particular in metal-polymer nano-composites, polymers tend to absorb water and other ionic pollutants from the environment, i.e. H_2S, HNO_3, CO_2, and tend to migrate between electrodes under the driving force of an electric field. Therefore, the insulation resistance of the polymer is curtailed. Water not only can act as the solvent and vehicle for ionic transport, but also participate pervasively in the conduction through electrolysis, especially at the higher voltages.

Although other metals may also migrate under specific environment, silver has been the most prominent on the metal migration species, mainly due to the high solubility of silver ion in water, low activation energy for silver migration, high tendency to form dendrite and low propensity/possibility to form stable passivation oxide layer like aluminum [105-107]. The rate of metal migration is increased by: 1) an increase in the applied potential;) an increase in the time of the applied potentials; 3) an increase in the level of relative humidity; 4) an increase in the presence of ionic and hydroscopic contaminants on the surface of the substrate; and 5) a decrease in the distance between electrodes of the opposite polarity. Metal migration can be considered as a two-step process involving ionization and diffusion of the migrating species. DiGiacomo [105, 107] proposed a semi-empirical model of metal migration based on the electrochemistry of solutions, theory of adsorption and condensation, and transport through water films and polymers characterized by the products of four functions. Since migration can be characterized by the current density, the model relates the current density to various functions in Equation 3-2.

$$J = B(M, P)\, F(T)\, G(RH, T)\, H(E, T) \tag{3-2}$$

where B (M, P) is a function of materials (M) and process parameters (P), F (T) is the integrated form of the Arrhenius equation as a function of activation energy and temperature (T), G (RH, T) is the relative humidity (RH) function (which also depends on temperature T), and H (E, T) is the electric filed (E) or voltage (V) function, which also depends on temperature. By considering different factors contributing to migration, an approximation relates these factors to the current density as Equation 3-3.

$$J = ZFDC_0(1-\exp(-\frac{ZFDE}{RT}t)) \\ = ZFC_0D_0\exp(-\Delta H_D/kT)(1-\exp(-\frac{ZFD_0\exp(-\Delta H_D/kT)E}{RT}t)) \quad (3\text{-}3)$$

In the equation, Z=valence, F=Faraday's electrochemical equivalent, D is the diffusitivity of migration component, $D=D_0\exp(-\Delta H_D/kT)$, where ΔH_D is activation energy of diffusion component, C_0 is the ionic concentration of migration component, E=V/d is the electric field, where V is the applied voltage, d is the distance between electrodes, t is time, k and R are Boltzmann constant and molar gas constant, respectively.

In order to reduce silver migration and improve the reliability, several methods have been reported. The methods include: 1) alloying the silver with an anodically stable metal such as palladium [104] or platinum [108] or even tin [109]; 2) using hydrophobic coating over the PWB to shield its surface from humidity and ionic contamination [110], since water and contaminates can act as a transport medium and increase the rate of migration; 3) plating of silver with metals such as tin, nickel or gold, to protect the silver fillers and reduce migration; 4) coating the substrate with polymer [111]; 5) applying benzotriazole (BTA) and its derivatives in the environment [112]; 6) employing siloxane epoxy polymers as diffusion barriers due to the excellent adhesion of siloxane epoxy polymers to conductive metals [113]. Although these approaches can more or less reduce the silver migration, they may need to compromise electrical properties of silver, or increase the cost and processing complexity.

In order to control the silver migration in the nano-silver conductive adhesives while maintaining the high electrical performance, various types of carboxylic acids are introduced due to the strong interaction between carboxylic group and silver. Effects of monolayer protection of nano-silver particles on the leakage current and electrical

properties of nano-Ag conductive adhesives are investigated. Mechanism of silver migration control with the monolayer protection is illuminated by studying the current-voltage relationships of the nano-ECAs.

3.3.2 Experimental

A diglycidyl ether of bisphenol-F (DGEBF) EPON 862 epoxy resin (Shell Chemical Co.) and an anhydride type hardener of methylhexa-hydrophthalic anhydride (MHHPA) (Lindau Chemicals, Inc.) were employed as matrix resin and crosslinker, respectively. The ratio of epoxy to hardener was 1:0.85 based on the epoxide equivalent weight (EEW) of the epoxy resin and the hydroxyl equivalent weight (HEW) of the hardener. 1-cyanoethyl-2-ethyl-4-methylimidazole (2E4MZCN), from Shikoku Chemicals Corporation, was employed as the catalyst and the concentration of the catalyst was 1 part per hundred resin (phr). The silver nanoparticles synthesized by the combustion chemical vapor condensation (CCVC) were used as fillers. Glutaric acid (di-carboxylic acid, HOOC-$(CH_2)_3$-COOH)) and heptonioc acid (mono-carboxylic acid, CH_3-$(CH_2)_5$-COOH) were purchased from Aldrich Chemical Company. 2wt% of carboxylic acids was incorporated in the nano- conductive adhesives by dissolving the acid in 1ml ethanol first and then mixing with the nano-composites.

The formulated nano-conductive adhesives were sonicated by Sonicator 3000 (from Misonix) for 2 hours and stencil printed on the patterned FR-4 boards with a spacing of 1.5mm between electrodes (Figure 3.25). The nano-conductive adhesives were dried in the oven at 80^{o}C for 30min to eliminate the solvent and then cured at 150^{o}C for 1 hour. The leakage current –voltage (I-V) relationship was measured by applying various voltages and testing the leakage current using a multimeter (Keithley 6517A).

The test was conducted under an accelerated condition of applying a drop of de-ionized water in between the electrodes, and thus, the time variation of the ion migration was very rapid, and the characteristics shown were established within seconds of application of the field.

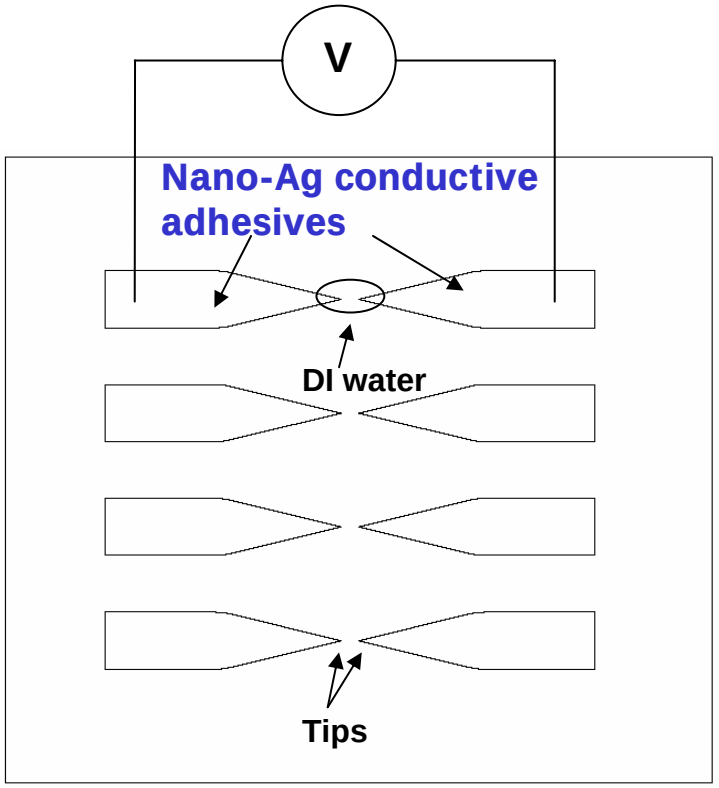

Figure 3.25 Schematic illustration of migration test vehicle for nano-Ag conductive adhesives

3.3.3 Results and Discussion

3.3.3.1 Leakage current – voltage (I-V) relationship of nano-Ag ECAs at low voltages

Figure 3.26 (dots) shows the relationship between leakage current and applied voltage for nano-Ag conductive adhesives at low voltages (0-5 V). An obvious threshold

voltage of migration was observed at 0.5 V for all the formulations. Below the threshold voltage, the leakage currents were stabilized at a near-zero value, while increasing the voltage over 0.5 V increased the leakage current. Although the untreated Ag nano-conductive adhesive showed a dramatic increase with increasing voltage, the adhesievs incorporated with carboxylic acids showed much slower increase in leakage current. This observation indicated that carboxylic acids could mitigate the silver migration in the conductive adhesives. In comparison of two types of carboxylic acids, di-carboxylic acid showed a more significant improvement than mono-carboxylic acid.

The obvious stabilized current leakage and subsequently the well controlled electrochemical migration is due to the protection of silver ions with carboxylic acids by forming the chelating compounds. The adsorption of carboxylic acids on silver has been widely studied. The reaction is considered as an acid-base reaction, and the driving force is the formation of chelating bond/complex between the carboxylate anion and a surface silver ion. (Equation 3-4)

$$Ag - e^- \rightarrow Ag^+ \quad ; \quad Ag^+ + COO^- \rightarrow Ag^+ \ldots COO^- \tag{3-4}$$

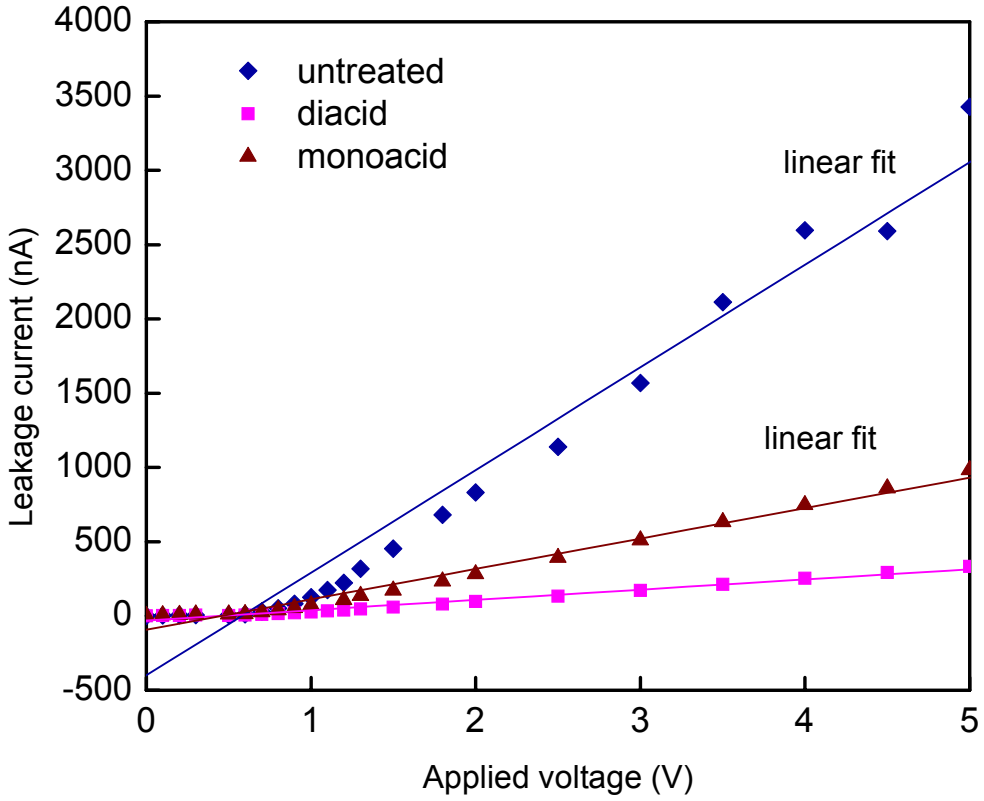

Figure 3.26 I-V relationship of Ag nano-ECA at low voltages.

It was also reported that on Ag surfaces, the two oxygen atoms in carboxylate tend to delocalize and bind to the surface nearly symmetrically. The bonding can change the surface properties of silver and control the properties of the metal-organic interfaces. Although the adsorption and alignment configurations of molecular monolayers on metal surfaces have been studied for over a decade, there were no reports on the applications of those organic monolayers until recently. The researchers use molecular monolayers such as thiolates to tune the chemistry as well as electrical and adhesion properties [114-118]. Studies have been conducted by surface analyses such as contact angle, x-ray

photoelectron spectroscopy (XPS), infrared (IR) characterization, surface-enhanced Raman scattering (SERS) for the understanding of bonding energy and alignment configurations between various carboxylic acid and silver. The accepted conformations of mono- and di-carboxylic acids adsorption on silver surfaces are shown in Figure 3.27. To reduce the energy, the molecules of mono-carboxylic acids tend to have an all-trans conformation on bonding to silver surface (Figure 3.27a). By adopting the all-trans forms the molecule may lie close to the surface with a hydrophobic tail ($-CH_3$), protecting the silver clusters. For di-carboxylic acid, it was found that both carboxylate groups were chelating to silver surface sites. The molecule gains sufficient stability by bonding two carboxylate groups to the surface that it is able to adopt less favorable chain conformation. The polymethylene chain was therefore arranged in a way best to accomplish both carboxylate groups chelating. The gauche or gauche-like conformations were most possible in order to stand on the surface of its two carboxylic groups due to the repulsion between methylene groups and the particle surfaces (Figure 3.27b). With the incorporation of carboxylic acid and the subsequently interaction between carboxylic acids and silver nano fillers, the interface properties of the nano-composites are changed. Unlike typical nano Ag composite in which Ag^+ is the major migration species, for carboxylic acid incorporated nano-Ag composite, the major diffusion component becomes complex $Ag^+ \ldots COO^-$. $Ag^+ \ldots COO^-$ has much lower solubility in water and higher activation energy for migration towards cathode than that of free Ag^+ , due to the neutral charge of the complex. The lower solubility decreased C_0 value, while the higher activation energy decreased D value in Equation 3-3. Therefore, migration became a

kinetically unfavorable reaction and the leakage current of carboxylic acid incorporated nano-composites were much lower than that of untreated composites.

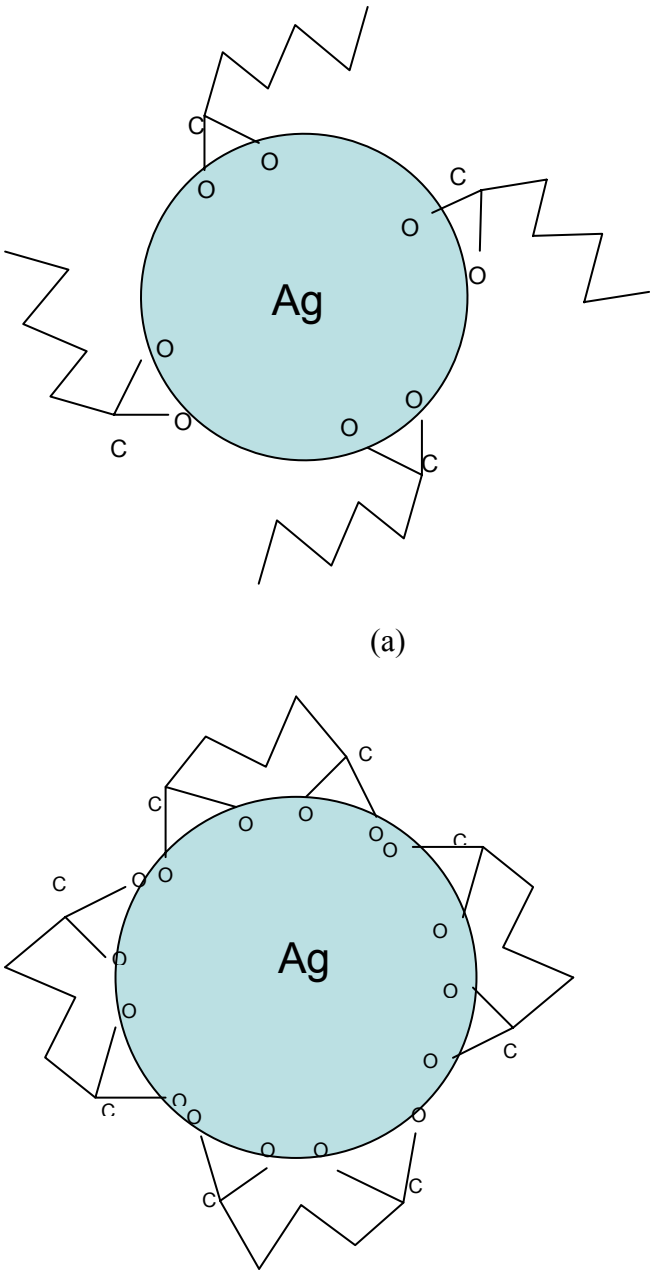

(a)

(b)

Figure 3.27 Schematic illustrations of surface bonding conformation between mono-carboxylic acid-Ag (a) and di-carboxylic acid-Ag (b).

Comparing mono- and di-carboxylic acids, di-carboxylic acid performed better in terms of migration control, due to the more coverage on Ag surfaces (Figure 3.27) and consequently the better protection of silver from migration.

It is interesting to notice that the curves of leakage current – voltage relationship can be well fitted into a linear relationship (Figure 3.26, lines) by the polynomial fitting of the curves. The linear relationship can be explained by extracting Equation 3-3. At low voltage, ZFDE/(RT)t <<1, then Equation 3-3 can be rewritten as Equation 3-5:

$$J = ZFDC_0(1-\exp(-\frac{ZFDE}{RT}t)) \approx ZFDC_0(\frac{ZFDE}{RT}t) = ZFDC_0(\frac{ZFDV}{RTd}t) \propto \mathrm{V} \qquad (3\text{-}5)$$

Therefore, there is a near-linear relationship between leakage current and applied voltage.

3.3.3.2 Leakage current – voltage (I-V) relationship of nano-Ag ECAs at high voltages

When the nano-Ag ECAs were tested at higher voltage (5-500 V), the difference of leakage current before and after carboxylic acid incorporation was more obvious (Figure 3.28, dots). The carboxylic acids incorporated nano-Ag ECAs showed a more stable leakage current value than the untreated sampels, which had a dramatically increased leakage current, in particular, at voltages higher than 200 V. By using the polynomial fitting of the curves of leakage current – voltage relationship, it was found that at high voltage test, the leakage current-voltage curve of untreated nano-Ag ECA did not follow the linear relationship, instead, a three-order polynomial fits the curve very well. On the other hand, the carboxylic acid, both mono- and di- carboxylic acid, incorporated nano-composites still follow a linear relationship (Figure 3.28, lines). The different phenomena can also be explained by analyzing Equation 3-3. For untreated nano-Ag composite at high voltage V, ZFDE/(RT)t is not a near-zero value, and thus,

Equation 3-3 cannot be simplified as Equation 3-5. According to Taylor expansion, Equation 3-3 can be expanded as Equation 3-6:

$$J = ZFDC_0(1-\exp(-\frac{ZFDE}{RT}t)) = ZFDC_0((\frac{ZFDE}{RT}t) - \frac{1}{2}(\frac{ZFDE}{RT}t)^2 + \frac{1}{6}(\frac{ZFDE}{RT}t)^3 + ...) \quad (3\text{-}6)$$

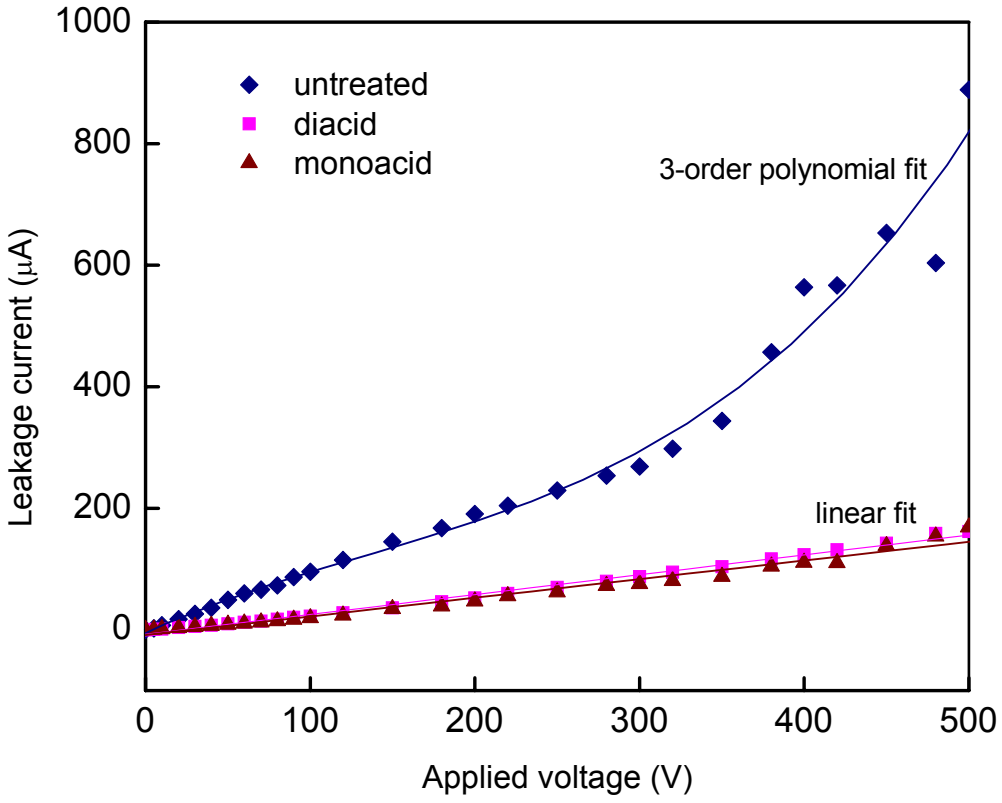

Figure 3.28 I-V relationship of Ag nano-Ag ECAs at high voltages.

For the carboxylic acid incorporated nano-Ag composite, however, due to the much higher activation energy ΔH_D and subsequently the much lower D ($D=D_0\exp(-\Delta H_D/kT)$) value, $ZFDE/(RT)t << 1$, and thus, Equation 3-3 can also be simplified as a linear relationship as Equation 3-5. Although di-acid showed better protection of nano-silver fillers at low voltages than mono-acid protection, the difference at high voltages

was not obvious. The difference is because at low voltage, most Ag^+ are in the vicinity of nano Ag particles, and the better coverage of di-acid than mono-acid shown in Figure 3.27 contributed to the better protection of silver from migration. At high voltages, however, some Ag^+ could be separated from the particles and exist in the water droplet. The interaction between acid and Ag^+ will not be limited by the coverage or configuration shown in Figure 3.27. Therefore, same amount of acids have similar effect on the migration control.

3.3.3.3 Morphology study after high voltages test

Figure 3.29 shows the photographs of test boards in the vicinity of nano-Ag ECAs after current-voltage tests up to 500 V. Obvious silver dendrites with several branches were observed for untreated nano-Ag ECAs, indicating the severe Ag migration. For the di-carboxylic acid incorporated nano-Ag ECA, however, no obvious dendrites were detected. The dark area around the edge of nano-Ag ECAs is considered to be from the typical inter-diffusion between different materials (nano-ECA and test board) rather than the ionic migration. The monoacid incorporated nano-Ag ECA also shows a dendrite formation, but with a shorter dendrite length and less dendrite branches.

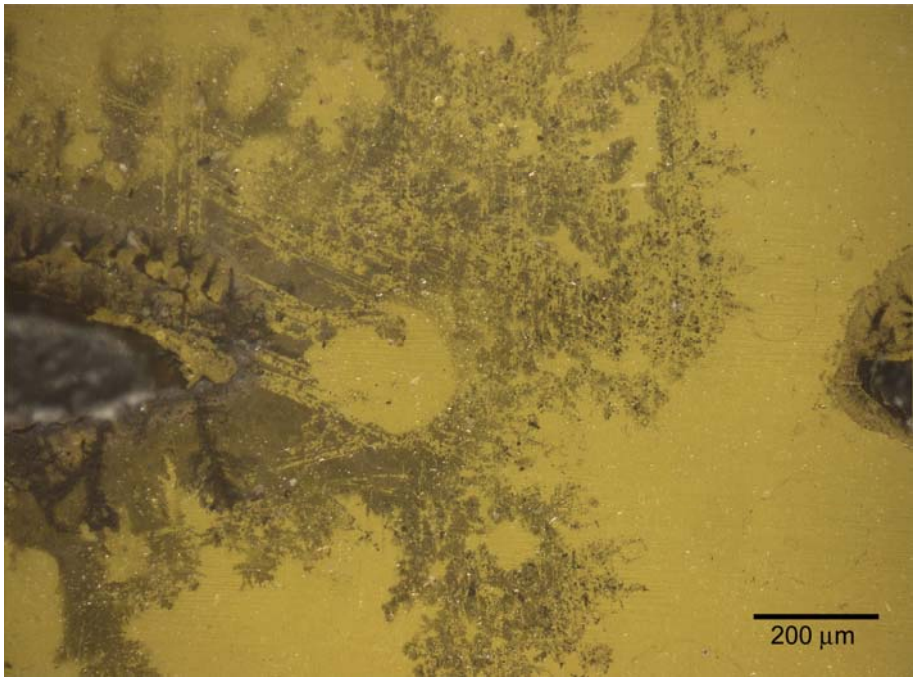

(a)

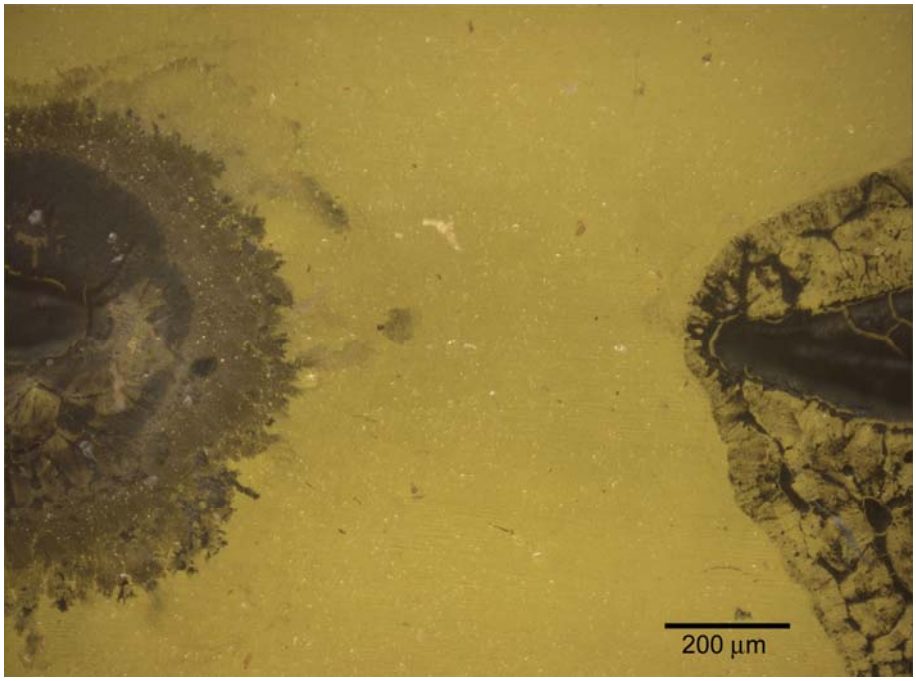

(b)

Figure 3.29 Morphology in the vicinity of silver nano-Ag ECA after high voltage migration tests. (a) untreated nano-Ag ECA (b) dicarboxylic acid incorporated nano-Ag ECA and (c) monocarboxylic acid incorporated nano-Ag ECA.

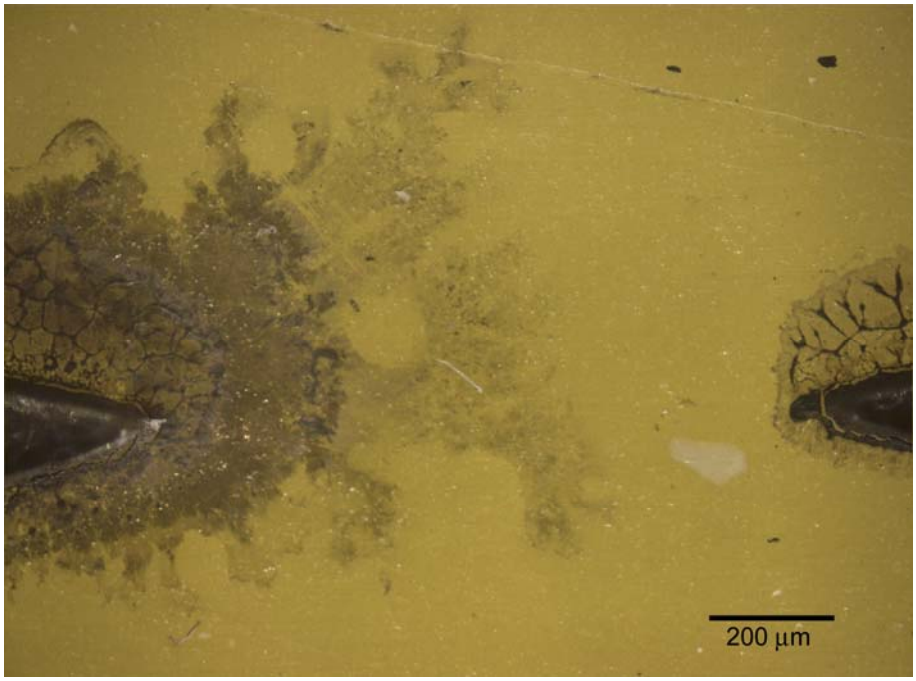

(c)

Figure 3.29 continued.

3.3.4 Summary

Monolayer protection of nano silver particles with carboxylic acids is discovered to protect the filler and control the silver migration in the nano-Ag ECAs. Formation of surface salt between the carboxylate anion and a surface silver ion reduces the solubility and diffusitivity significantly of migration components and therefore leads to effective migration control. A better understanding of the mechanism of migration control is conducted by studying the current-voltage relationships of the nano-Ag ECAs. Di-carboxylic acid performs better in controlling silver migration in the composite at relatively low voltage due to the more coverage and better protection of silver. The control of migration of nano-Ag ECA enables the application of the composite in fine pitch and high performance electronic devices.

3.4 Development of Nano-scale Anisotropically Conductive Films (nano- ACF) for High Performance Fine Pitch Interconnects

3.4.1 Introduction

ACFs have the similar structure and conduction mechanism as ACAs, except that the resin has been modified to form film and realize the fast cure condition (from a few seconds to a few minutes). Due to the easy handling and fast cure capability, ACFs are more widely used in industry than ACAs. Interconnection technologies using ACFs are major packaging methods for flat panel display modules to be high resolution, light weight, thin profile and low consumption power, and already successfully implemented in the forms of Out Lead Bonding (OLB), flex to PCB bonding (PCB), reliable direct chip attach such as Chip-On-Glass (COG), Chip-On-Film (COF) for flat panel display modules, including LCD, Plasma display panel (PDP) and organic light emitting diode display (OLED). As for the small and fine pitched bump of driver ICs to be packaged, fine pitch capability of ACF interconnection is much more desired for COG, COF and even OLB assemblies. Therefore, evaluation and development of high performance fine pitch ACF interconnect materials and processing is very important.

3.4.2 Experimental

The base formulation of ACF was prepared with bisphenol-A epoxy, bisphenol-F epoxy, phenoxy, amine-type curing agent and silane coupling agent.

The procedure for assembly nano-ACF is as following:

1) preparation nano-ACF;

2) pre-bonding of ACF on substrate;

3) heat and pressure applying on pre-bonded ACF at 80^{o}C for 5 second;

4) removal of separator film;

5) alignment;

6) final bonding of ACF with bonding condition of 180^{o}C at determined bonding pressure and time.

The electrical resistance of the joints (contact area: 100x100 μm^2) on Au-finished PI flex/PI flex test vehicle (Figure 3.4) was measured by a four-point probe method, where the current carrying capability was determined as the current at which the voltage shows non-linear behavior in the I-V or the resistance abruptly increases in the I-R curve. The applied currents were varied from 0.5 ~ 4.0 A by a power supply (HP model 6553A, HP Hewlett Packard, Palo Alto, CA) and the voltage of the interconnect joints was measured by a Keithley 2000 multimeter (Cleveland, Ohio). The reliability of joints was conducted under the environment of 85°C/85%RH (using an accelerated temperature and humidity chamber, Lunaire Environmental, model CEO932W-4) by measuring the joint resistance periodically during aging.

To characterize the insulation/dielectric properties, the conductive adhesives or films were coated on a Cu substrate (as a bottom electrode) with 20~30 μm thickness on which the top electrodes were created by a DC sputter with a 3 mm diameter. Then two voltage probes were put on the top and bottom electrodes, respectively, as illustrated Figure 3.30. Voltage was applied between top and bottom electrodes where the adhesive was located and a curve tracer was used to measure the breakdown voltages of the films.

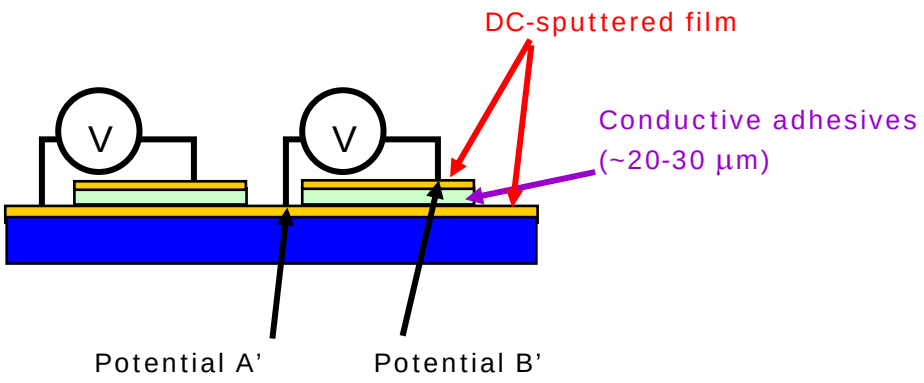

Figure 3.30 Schematic illustration of dielectric property measurement of conductive adhesives

The high frequency measurements were conducted by using a vector network analyzer (VNA; HP Model 8720 ES) up to 10 GHz. For simple characterization and comparison among three adhesive materials, the S-parameter, S_{21}, of flip chip joints using NACF, NCF and micron sized particle-filled ACF were measured. S_{21} indicates insertion loss of DUT (device under test). The test vehicle for the high frequency electrical characterization consists of two-port GSG 500 μm transmission lines method used in the literature [119]. A 500 μm pitch GSG probe was used for the two-port measurements. For simple characterization and comparison among three adhesive materials, the S-parameters were measured.

3.4.3 Results and Discussion

3.4.3.1 Effects of bonding pressure on the electrical property of nano-ACF

For the ACF interconnection, the bonding pressure is an important parameter in addition to the curing temperature and time. Therefore, it is important to study the required bonding pressure for the novel nano-ACF joints.

In order to study the required bonding pressure to achieve low resistance, the bonding pressure during thermo-compression bonding of nano-Ag-ACF and NCF joints was varied and the contact resistance was measured. Figure 3.31 shows the relationship between the various bonding pressures (50 to 200 MPa) and the contact resistance of the joints.

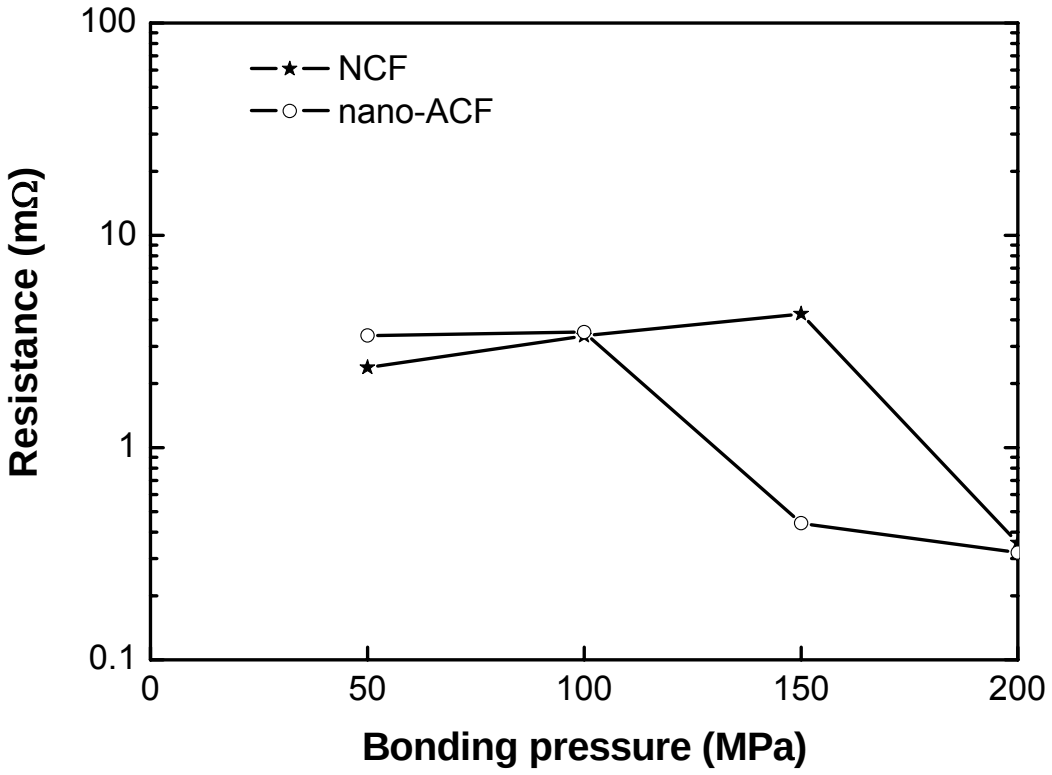

Figure 3.31 Bonding pressure effects on the joint resistance of NCF and nano-ACF

As the bonding pressure increases, the contact resistance of ACF/NCF joint generally decreases due to the contact area increment. For adhesives joints, there was a critical (minimum) pressure below which the contact resistance remained high. The result

shows that the minimum bonding pressure for the nano-ACF was 150 MPa, while the bonding pressure for NCF was 200 MPa. Therefore, the required bonding pressure can be decreased for nano-ACF joints.

3.4.3.2 Electrical properties of nano-ACF with sintering

The current-resistance (I-R) relationship of the nano-ACF joints are shown in Figure 3.32 with various curing time. As can be seen from the figure, for the nano-ACF joints cured at 180^{o}C for 2 minutes, a joint resistance of ~ 0.08 mΩ and current carrying capability of ~ 2.4 A were observed. The joint resistance was two orders of magnitude lower than a typical ACF (0.6 mΩ with micron-sized Au-coated polymer fillers as compared in Figure 3.33), while the current carrying capability was similar. The reduced joint resistance for the nano-ACF was attributed to the superior electrical conductivity of silver fillers. When increasing the curing time from 2 minutes to 120 minutes, the joint resistance was further reduced by over one order of magnitude (0.005 mΩ). In addition, the current carrying capability could also be enhanced from 2.4 to 3.4 A by prolonging the curing time. The further improved electrical performance (lower contact resistance and higher current density) is due to the further sintering with longer time. The more sintering of nano-sized fillers could enhance the interfacial properties of the joints. As such, the joint resistance, which is a sum of bulk resistance and interfacial resistance (as indicated in Figure 3.8, would be significantly reduced. In addition, the thermal properties could also be enhanced by improving the interfacial properties. The higher thermal performance could help dissipate the heat more efficiently at the adhesive joints. Therefore, with further sintering of nano-Ag fillers, the current carrying capability was also improved.

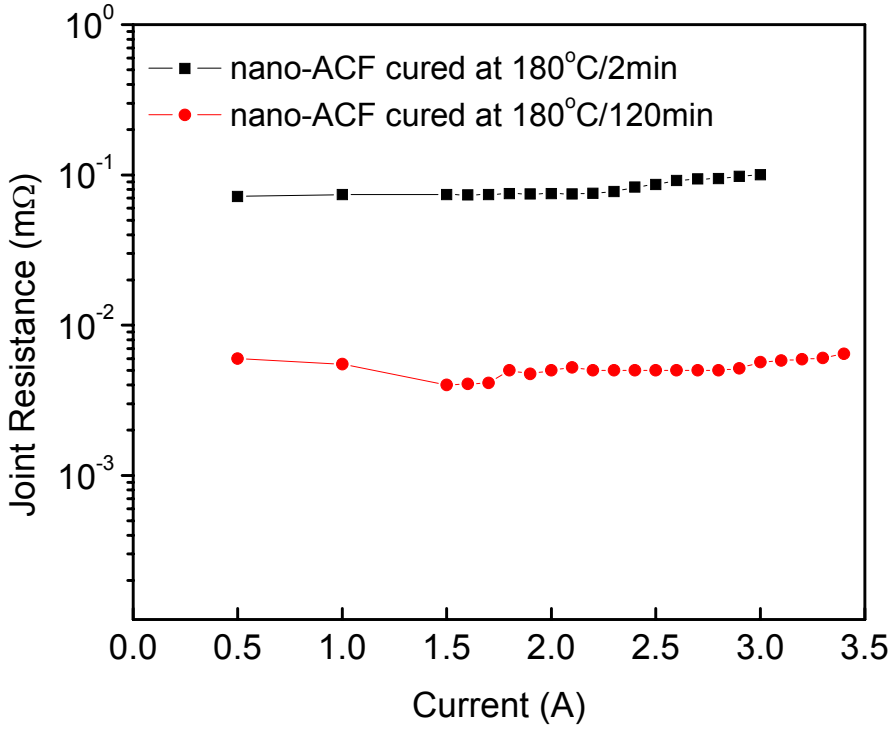

Figure 3.32 Current-Resistance (I-R) relationships of nano-ACF joints with different curing time

The I-R relationship of nano-ACF was compared with that of the NCF and a conventional ACF filled with micron-sized Au-coated polymer balls as shown in Figure 3.33. With the sufficient sintering, the joint resistance of the nano-ACF was much lower than that of the conventional ACF. In addition, the current carrying capability was also dramatically enhanced due to the superior interfacial properties and the more efficient thermal transport. The joint resistance was even lower than those of the NCF and lead-free solder joints, due to the intrinsic lower resistance of Ag fillers compared to the lead-free solders.

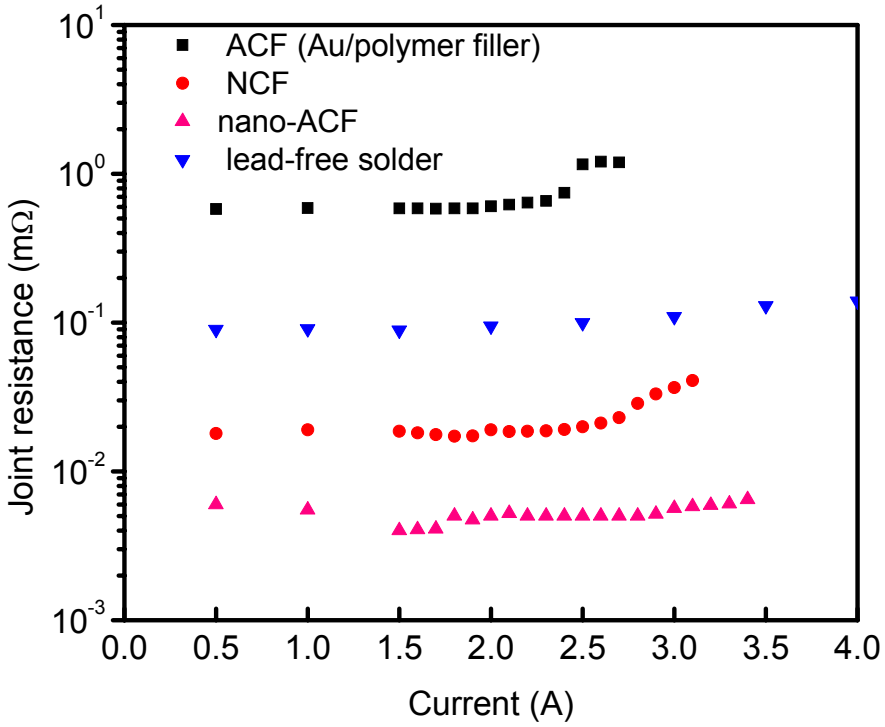

Figure 3.33 Comparison of I-R relationships of typical ACF, NCF, lead-free solder and nano-Ag ACF.

3.4.3.3 Reliability of nano-ACF and NCF

The electrical reliability of nano-ACF joint was evaluated at the elevated temperature and humid environment (85°C /85%RH). Figure 3.34 shows the contact resistance behaviors of nano-ACF and NCF joints under 85°C/85%RH condition for over 500 hours. The graph clearly shows that the nano-ACF joint had more stable joint resistance than NCF joints with aging at 85°C /85%RH, indicating a better reliability. This reliability improvement should be attributed to the stable electrical contact between two Au electrodes by sintering effect of nano-Ag fillers even under the moisture

absorption and hygrothermal expansion due to high temperature and humid test condition.

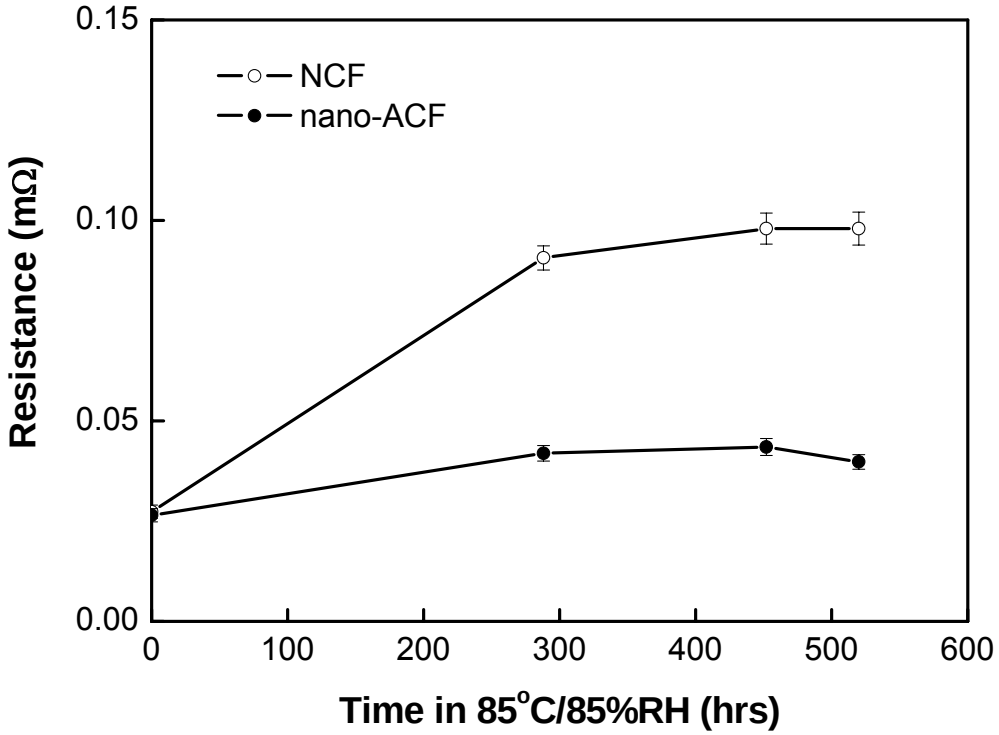

Figure 3.34 Reliability of NCF and nano-ACF under 85°C/85%RH

3.4.3.4 Insulation properties of nano-Ag ACF

For NCF and/or ACF joints, not only a high electrical property in the z-direction is important, but also the good insulation property in the x-y plane is required. Voltage was applied in between top and bottom electrodes where the adhesive was located and a curve tracer was used to measure the breakdown voltages of the films. As shown in Table 3.4, the typical ACF with 1wt% micron-seized Au/polymer fillers showed a breakdown voltage of 400 V and the NCF joint had a much higher breakdown voltage. However, the

nano-ACF with 1wt% nano-Ag fillers showed a very low breakdown, indicating the poor insulation property, probably due to the high surface area, high conductivity and lower percolation threshold with nano Ag fillers.

Table 3.4 Insulation properties of conductive films

Sample name	Filler type	Breakdown voltage (V)
Typical ACF	Au/polymer (1wt%)	400 ~ 450
Nano-ACF-1	Nano-Ag (1wt%)	Short
NCF	No filler	1200 ~1400

In order to improve the insulation property of the nano-ACF, there are two possible approaches. One is to reduce the filler loading of conductive fillers. For the nano-sized fillers, the percolation threshold for conductivity would be much lower than the micron-sized fillers, mainly due to the high surface area of the nano conductive fillers. Therefore, low resistance can be achieved at a much lower filler loading. As shown in Table 3.5, by lowering the filler loading from 1wt% to 0.1wt%, the breakdown voltage of the nano-ACF can be significantly enhanced, indicating a good insulation property. Alternatively, the nano Ag fillers can be protected by organic monolayers which can mitigate the Ag bridging or the migration. It has been demonstrated that carboxylic acids have strong affinity to Ag surfaces and tend to form the chelating compounds and protect the nano Ag fillers. Therefore, difunctional carboxylic acid was used in the nano-Ag ACF formulations and the insulation properties were compared in

Table 3.4. Obviously, the monolayer protection of Ag nano-fillers was quite efficient in improving the insulation properties as well.

Table 3.5 Comparison of insulation properties of nano-scale ACF and NCF

Sample name	Filler type	Breakdown voltage (V)
NACF-1	Nano-Ag (1wt%)	Short
NACF-2	Nano-Ag (0.1wt%)	1000-1400 V
NACF-3	Nano-Ag (with acid protection)	1000-1400 V
NCF	No filler	1200 V-1400 V

3.4.3.5 High frequency characteristics of nano-ACF joints

The high frequency characteristic for the nano-ACF joint is one of important properties for maintaining signal integrity in high speed flip-chip device interconnection. Therefore, it is necessary to characterize the high frequency behaviors of the developed nano-ACF in comparison with NCF and conventional micron-sized conductive filled ACF in the flip chip structure. Figure 3.35 shows the high frequency characteristics of ACF/NCF joints up to 10 GHz. The insertion loss of different ACF/NCF flip chip joints was almost the same, which indicated an acceptable high frequency behavior of nano-ACF compared with conventional ACF and NCF.

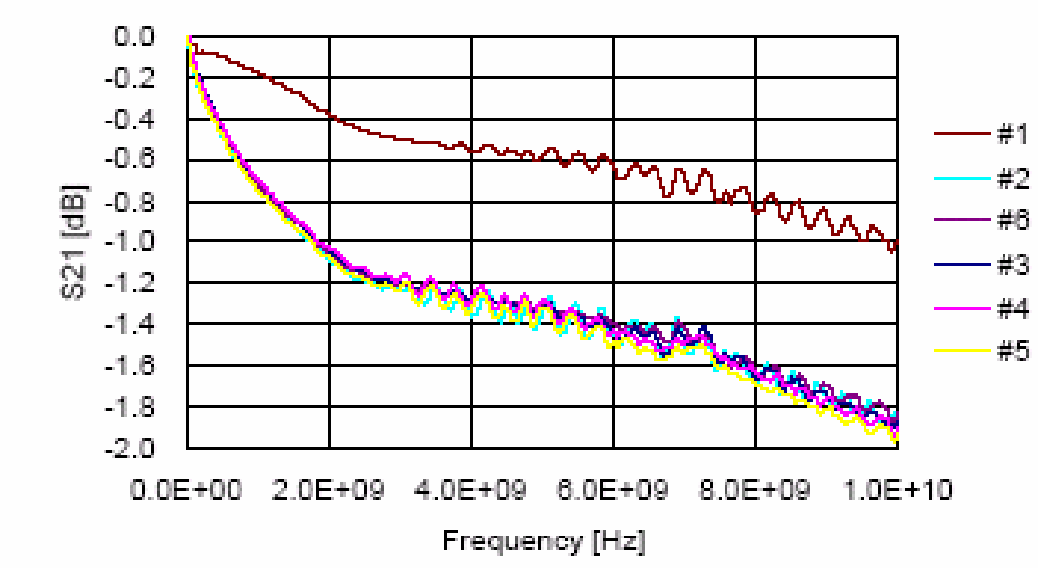

(a)

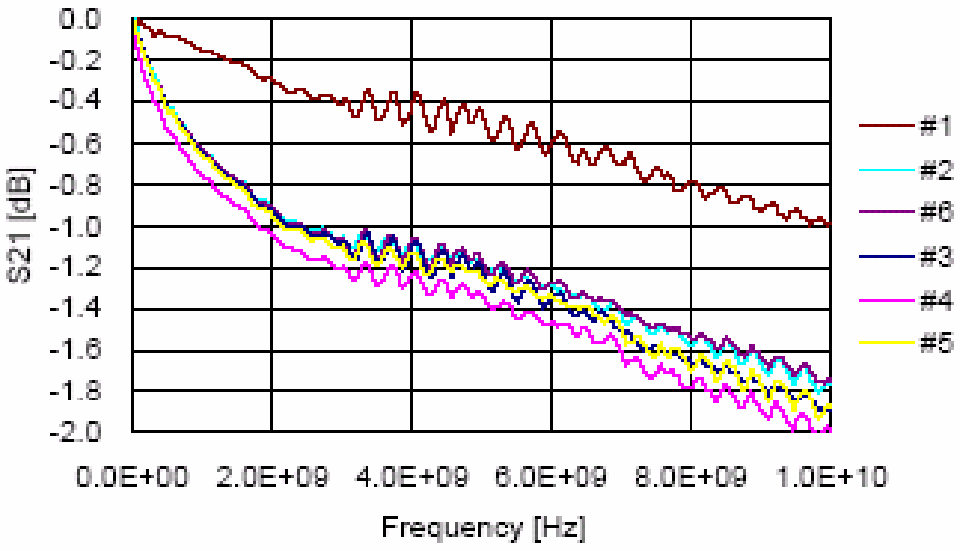

(b)

Figure 3.35 VNA measurement results of (a) typical ACF joints with micron-sized fillers, (b) NCF joints and (c) nano-ACF joints

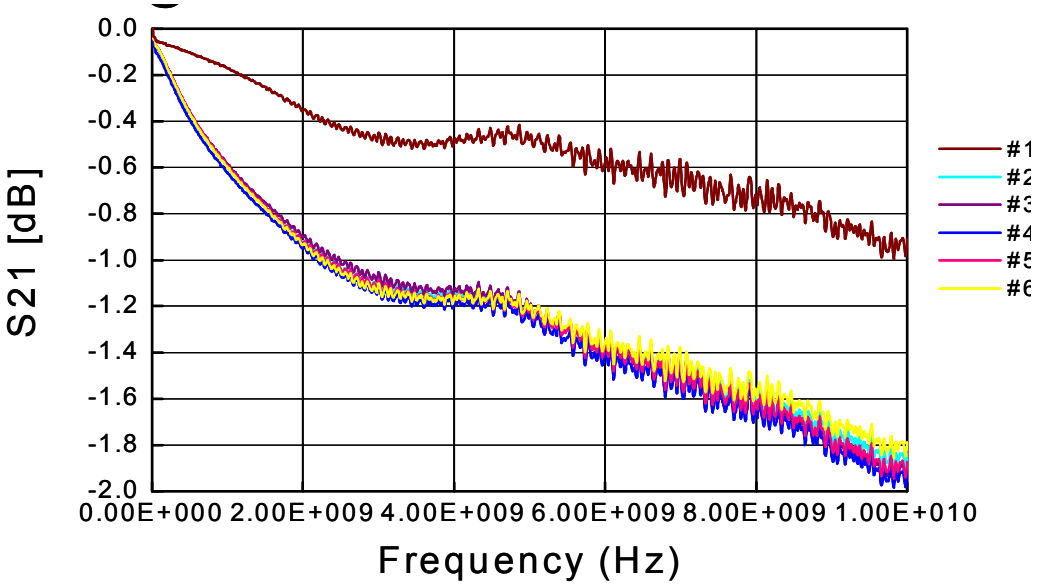

(c)

Figure 3.35 continued

3.4.4 Summary

A high performance nano-scale ACF was developed for next generation fine pitch interconnects. The nano-scale conductive film also allows a lower bonding pressure than NCF to achieve a much lower joint resistance (over two orders of magnitude lower than typical ACF joints) and higher current carrying capability. With low temperature sintering of nano-silver fillers, the joint resistance of the nano-scale conductive film was as low as 10^{-5} Ohm. The reliability of the nano-scale conductive film after high temperature and humidity test (85^{o}C /85%RH) was also improved compared to the NCF joints. Lowering the nano-Ag filler loading level or applying the monolayer protection on Ag particle surfaces could significantly improve the insulation/dielectric property of the x-y direction. The insertion loss of nano-scale conductive film joints up to 10 GHz was almost the same as that of the standard ACF or NCF joints, suggesting that the nano-scale

conductive film is suitable for reliable high frequency adhesive joints in microelectronics packaging.

3.5 Conclusions

In order to enhance the electrical and thermal performance of ACA/ACF, interfacial properties between conductive fillers and electrode should be improved. Two approaches have been developed in this chapter to improve the interface bonding. One is the introduction of nano conductive fillers. With the low temperature sintering of nano-silver fillers, the joint resistance of the nano-ACA could be significantly reduced. The enhanced electrical properties of the nano-ACA joints were attributed to the reduced number of particle interfaces and improved interfacial contact between nano Ag fillers and bond pads.

Another approach to improve the interfacial properties of ACA/ACF is the application of self-assembled monolayers (SAMs) on the interface between the metal particles and between the ECA/metal bond pads. Self-assembled monolayer (SAM) molecules can adhere to the metal surface and act as electrical junctions or molecular wires between the conductive filler of the ACA/ACF and the contact pad of the substrate. As such, the molecules can reduce electrical resistance and achieve a high current density for the interconnects. Different organic monolayers, dicarboxylic acid and dithiol have been introduced into ACA joints for silver-filled and gold-filled ACAs, respectively. For dithol incorporated ACA with micron-sized gold fillers, significantly lower joint resistance and higher maximum allowable current (highest current applied without inducing joint failure) was achieved for low temperature curable ACA ($<100^{o}$C). For high curing temperature ACA (150^{o}C), the improvement is not as significant as low

curing temperature ACAs, due to the partial degradation of organic monolayer coating at the relatively high temperature. However, when dicarboxylic acid or dithiol was introduced into the interface of nano-silver filled ACAs, significantly improved electrical properties could be achieved at high temperature curable ACA, suggesting the coated organic monolayers did not suffer degradation on silver nanoparticles at the curing temperature (150^{o}C). The enhanced bonding could attribute to the larger surface area and higher surface energy of nano particles, which enabled the monolayers to be more readily coated and relatively thermally stable on the metal surfaces.

In the Ag-filled conductive adhesives, an effective approach of using monolayer-protected silver nanoparticles was introduced to reduce silver migration for electronic device interconnect applications. Formation of surface complex between the carboxylate anion and surface silver ion reduces the solubility and diffusitivity significantly of migration components and therefore contributes to effective migration control. A fundamental understanding of the mechanism of silver migration control was conducted by studying the current-voltage relationships of the nano-Ag ECAs with a migration model. The control of silver migration enables the application of the silver composites in fine pitch and high performance electronic device interconnects.

With the application of nanotechnology, a high performance nano-ACF which combined the advantages of both ACF and NCF was developed. The nano-ACF exhibited much lower joint resistance, higher current carrying capability, stabilized contact resistance in high temperature/high humidity test, well-controlled silver migration and accepted insulation properties and high frequency performance. The nano-ACF could be

potentially used as high performance ultra-fine pitch lead-free interconnects in electronic packaging applications.

CHAPTER 4
HIGH PERFORMANCE NON-CONDUCTIVE FILM FUNCTIONALIZED WITH π-CONJUGATED SELF-ASSEMBLED MOLECULAR WIRES FOR ULTRA-FINE PITCH INTERCONNECT APPLICATIONS

4.1 Introduction

Recently, non-conductive adhesives/films (NCAs/NCFs) are considered as a low-cost option for flip chip assemblies. Conductive joints with NCF provide a number of advantages compared to other adhesive bonding techniques. NCF joints avoid short-circuiting and are not limited, in terms of particle size or percolation phenomena, to a reduction of connector pitches. The size reduction of electronic devices can be realized by the shrinkage of the package and the chip. Further advantages include cost-effectiveness, ease of processing regarding the possibility of non-structured adhesive application, good compatibility with a wide range of contact materials, and low temperature cure. In fact, the pitch size of the NCF joints can be limited only by the pitch pattern of the bond pad, rather than the adhesive materials. Contacts between the nanoscale rough structures of the bottom and top surfaces lead to the electrical conduction between the two pads. NCA/NCF requires no conductive fillers, but needs a relatively high pressure for bonding between the IC chip and the substrate coupled with heat. During bonding, the heat and pressure are applied and the direct physical contacts between the two surfaces of the IC bump and the substrate bond pad can be achieved. The electrical contact resistance of an NCA/NCF joint is controlled by the processing pressure, surface roughness and NCA/NCF material properties. An accurate prediction of contact resistance can help guide experiment setup towards improving the electrical

performance of NCA/NCF joint for the full realization of this fine pitch assembly approach.

In spite of the advantages of NCF joints, there are still some challenging properties of NCF. Since the electrical conductivity of NCF is achieved through physical/mechanical contact and no metallurgical joints are formed, it has limited electrical conductance and current carrying capability. Low contact resistance and high current carrying capability of NCF joints are demanding properties for lead-free solder alternatives and high current density application. To ensure low contact resistance and high current density, interface between electrodes plays important role. The interfaces between electrodes for NCF joints must be defect free and occupy the stable contact area even under high electrical current and harsh environments. This interface control in NCF joints contributes to performance and reliability of their joints in electronic packaging. In most NCF joints, electrical conductance between contacts is dependent upon the constriction resistance and tunneling resistance due to the presence of ultra-thin insulating film between contacts. The control of the tunneling resistance is important in reducing the contact resistance for NCF joints [120-122].

Self-assembled monolayer (SAM) has been extensively studied in the last decade, and recent discoveries on the capability of SAM to functionalize the materials and tailor their physical and chemical properties have attracted more interests in the research area. In particular, conjugated molecules which have a smaller band gaps between the highest occupied molecular orbital (HOMO) and the lowest unoccupied molecular orbital (LUMO) and possess delocalized conjugated π-electrons that can contribute to conduction. In semiconductors, self-assembled molecular wires have seen importance in

tuning the metal work function (Φ) and electrical conduction of metal-molecule contact [118, 123-129].

In this chapter, analytical expression of contact resistance of NCA/NCF is obtained. The effects of NCA/NCF material properties on electrical contact resistance are investigated. A series of π-conjugated molecular wires are introduced into the NCF joints and their effects on the contact resistance and reliability of NCF joints are evaluated and correlated with the analytical expression.

4.2 Experimental

4.2.1 Preparation and characterization of NCF

The NCF base formulation was prepared with epoxies and curing agent. Two types of self-assembled molecular wires, 1, 4-benzenedithiol (BDT) and biphenyldithiol (BPD) are mixed with NCF base formulation (the structures of π-conjugated molecules are shown in Table 4.1). The NCF was pre-bonded on the substrate at 80^{o}C for 5 seconds. After removal of separator film, the substrate was aligned and the final bonding of NCF was conducted at 150^{o}C for 40 min with the application of different bonding pressure. The electrical resistance and current carrying capability of the NCF joints (contact area: 100x100 μm^2) on Au-finished test vehicle was measured by a four-point probe method. The applied currents were varied from 0.5-4.0 A by a power supply (HP model 6553A, HP Hewlett Packard, Palo Alto, CA) and the voltage of the interconnect joints were measured by a Keithley 2000 multimeter (Cleveland, Ohio). The reliability of NCF joints was conducted under the environment of 85°C/85%RH (using an accelerated temperature and humidity chamber from Lunaire Environmental, model CEO932W-4). The joint

resistance of NCF was achieved periodically using the power supply and multimeter during aging.

Table 4.1 Chemical structures of the π-conjugated thiol molecules

Name	Chemical Structure
1, 4-benzene dithiol (BDT)	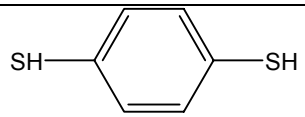
biphenyldithiol (BPD)	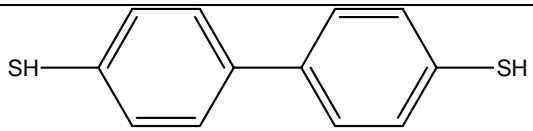

4.2.2 Characterizations of Au substrate with self-assembled molecular wires

The Au surfaces were prepared by sputtering gold on wafer substrate. The surfaces were first cleaned by acetone with sonication and then dipped into SAM solutions, respectively and allowed to incubate under a controlled nitrogen environment for 6 hours and 24 hours, respectively. After treatment, the surfaces were removed from the solution and rinsed in order to remove excess un-adhered molecules. The contact angles of deionized (DI) water on those surfaces were obtained by a goniometer (Rame-Hart Co. Netcong, NJ).

A surface science model SSX-100 small spot ESCA spectrometer equipped with Al K_α source was used to characterize and record the x-ray photoelectron spectra (XPS) of Au surfaces. The fitting of the spectra was done by a non-linear least squares procedure provided by Service Physics (Bend, OR).

4.3 Investigation of Electrical Contact Resistance of NCA/NCF

4.3.1 Contact formation between rough surfaces

Experimental investigation of Williamson et al. established that many of the manufacturing processes produce surfaces with an isotopic Gaussian distribution of heights of the surface asperities [130]. In most analyses of the micro-contact involving two rough Gaussian surfaces, the analysis can be simplified by considering the contact between a single surface (with effective surface roughness characteristics) and a perfectly flat surface. The equivalent root mean square (RMS) roughness, σ, and the equivalent mean absolute surface slope, m, are defined as Equation 4-1 and 4-2, respectively:

$$\sigma = \sqrt{\sigma_1^2 + \sigma_2^2} \tag{4-1}$$

$$m = \sqrt{m_1^2 + m_2^2} \tag{4-2}$$

where subscripts 1 and 2 are used to denote the two contacting bodies.

The number of contacts between two surfaces can be express as Equation 4-3 from the approach of Cooper et al [131].

$$n_s = \frac{1}{16}\left(\frac{m}{\sigma}\right)^2 \frac{\exp(-Y^2/\sigma^2)}{erf(Y/\sqrt{2}\sigma)} A_a \tag{4-3}$$

where A_a is the area of apparent contact of an NCA/NCF joint and Y is mean-planes separation of the contacting surfaces. For conforming rough surfaces at which the asperities undergo plastic deformation, Cooper et al. showed that the mean-planes separation, Y, can be written as Equation 4-4.

$$Y = \sqrt{2}\sigma \cdot erfc^{-1}\left(\frac{2P}{H_{mic}}\right) \tag{4-4}$$

where $P=F/A_n$, which is the applied pressure (A_n is the area normal to the applied force, in our case A_n equals to A_a), and H_{min} is the micro-hardness of the softer surface in contact.

The average radius of an elasto-plastic physical contact can be expressed as Equation 4-5:

$$a = \sqrt{8/\pi}(\sigma/m)\exp(\lambda^2)erfc(\lambda) \tag{4-5}$$

where $\lambda = Y/\sqrt{2}\sigma$.

From these equations, one can calculate the contact area and number of contacts based on the surface roughness, material hardness and applied external pressure.

4.3.2 Electrical resistance of an NCA/NCF joint

In order to obtain the electrical resistance of an NCA/NCF joint, one needs to determine the resistance of a physical contact first. For a micro-contact, the contact resistance is composed of constriction and tunnel resistance [132]. Constriction resistance occurs as the electrical current must squeeze through the asperities to cross the interface. Tunnel resistance is due to the intermediate layer between the metal surfaces. The total resistance of a physical contact can be written as Equation 4-6:

$$R = R_c + R_t = (\rho_1/4a + \rho_2/4a) + \xi/\pi a^2 \tag{4-6}$$

where R_c is the constriction resistance, R_t is the tunnel resistance, ρ_1 and ρ_2 are the bulk electrical resistivity of the two contacting bodies, a is the radius of contact area, and ξ is the tunnel resistivity of the interface.

Tunnel resistance is due to the intermediate layer between the metal surfaces. The intermediate layer may consist of a thin film of NCA/NCF material. Tunnel resistivity is a function of the film thickness *s*, the work function Φ for electron emission from metal into film (electron-injection barrier), and the relative permittivity ε_r of the material of the film. It can be expressed as Equation 4-7

$$\xi = 0.5 \times 10^{-12} \frac{A^2 \exp(AB)}{1 + AB} \left(\Omega \cdot cm^2\right) \tag{4-7}$$

where A=7.32(s-7.2/ø), $\mathrm{B} = 0.1265\sqrt{\phi - \frac{10}{s\varepsilon_r}}$ with ø in eV and s in Å.

Based on Equation 4-6, the electrical resistance of an NCA/NCF joint can be written as Equation 4-8 by assuming all physical contacts have average contact area.

$$R_{joint} = R / n_s = [(\rho_1 / 4a + \rho_2 / 4a) + \xi / \pi a^2] / n_s \tag{4-8}$$

where n_s is the number of physical contacts of an NCA/NCF joint, as in Equation 4-3. Based on the above derivation, one can tell that the contact resistance of a NCA/NCF joint is dependent on surface morphology, processing pressure and material properties. Among these parameters, the intermediate film thickness is the most difficult to identify. Therefore, experiments were conducted to obtain the film thickness, and then the effect of material properties can be investigated.

Atomic Force Microscopy (AFM) was applied to study the surface roughness of gold pad used in our experiment (Figure 4.1). Based on the measurement, the root mean square (RMS) roughness σ equaled to 820 nm, and the mean absolute surface slope m equaled to 0.27. From the literature, the micro hardness of gold was identified as 1386 MPa [133]. The bulk electrical resistivity for gold is 0.0452 Ω•nm, and the applied

pressure is 300 MPa. By substituting these values to Equations 4-3 and 4-5, one can obtain n_s as 36, and a as 2850 nm. Therefore, the constriction resistance of a micro contact is equal to 0.0452/(2×2850), which is 7.93×10^{-6} Ω. The total constriction resistance of all micro contacts on the NCF joint is equal to 7.93×10^{-6} /n_s, which is 2.20×10^{-7} Ω.

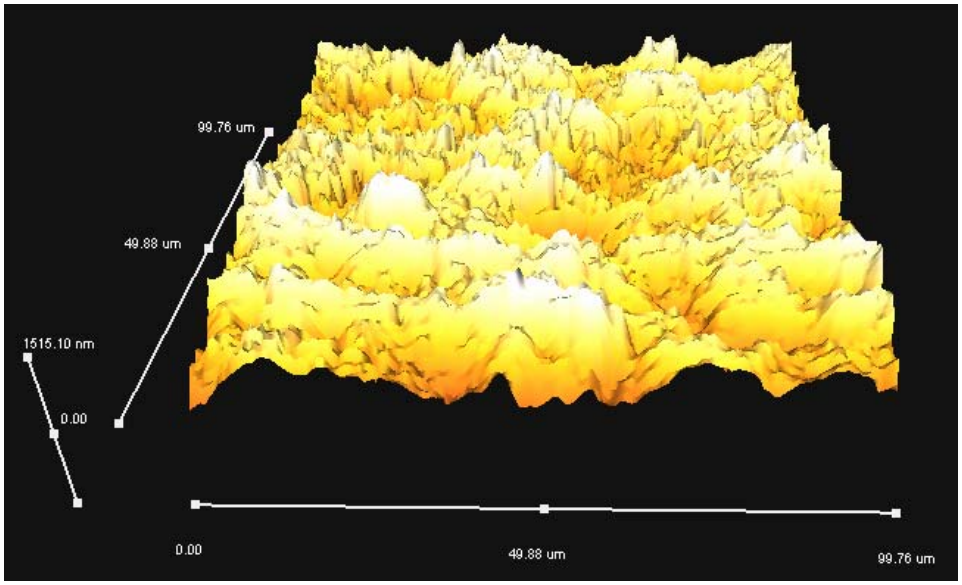

Figure 4.1 AFM measurement of gold pad surface

Based on our measurement, the total resistance of an NCA/NCF joint is 1.5×10^{-4} Ω. As one can see, the constriction resistance only composed a negligible amount of an NCA/NCF joint resistance. Therefore, our micromechanical model showed that the tunnel resistance is the main source for the joint resistance. Now the electrical resistance of an NCA/NCF joint can be written as Equation 4-9:

$$R_{jo\,\mathrm{int}} = (\xi / \pi a^2) / n_s \tag{4-9}$$

From Equation 4-9, one can obtain the tunnel resistivity (ξ) as 1.40×10^{-9} Ω•cm^2 for our experiment. In order to increase the performance of NCA/NCF material, one needs to decrease the tunnel resistivity. From Equation 4-7 one can tell that the tunnel resistivity is dependent on the film thickness, electron-injection barrier, and dielectric constant of the intermediate layer material. The thickness of the film is dependent on the applied processing pressure and it cannot be increased further due to process requirement. The parameters one can control are electron-injection barrier and dielectric constant.

4.3.3 Tunnel resistivity

Before investigation of the effect of electron-injection barrier and dielectric constant, the NCA/NCF film thickness between the two gold pad surfaces needs to be estimated experimentally, which can be fitted from Equation 4-7. It is already known that the tunnel resistivity (ξ) is equal to 1.40×10^{-9} Ω•cm^2, and the dielectric constant of base epoxy resin is about 3.5. The electron-injection barrier of electron from gold to intermediate film is difficult to measure. Based on the literature the work function of gold is 5.20 eV [134], while the electron affinity (EA) of the epoxy polymer (difference between lowest unoccupied molecular orbital and vacuum level) can be roughly taken as 2.5 eV. Then the 2.7 eV difference between the work function and EA gives the electron-injection barrier. By substituting these values into Equation 4-7 one can obtain the film thickness as 5.3 Å. Since this film thickness is just an estimate, the effect of electron-injection barrier and dielectric constant will be investigated at different film thicknesses from 4.3 to 6.3 Å.

Figure 4.2 shows the effect of film dielectric constant on tunnel resistivity at different film thickness. The electron-injection barrier is 2.7 eV. As one can tell tunnel resistivity remain almost unchanged when the dielectric constant is changed from 2.5 to 5.

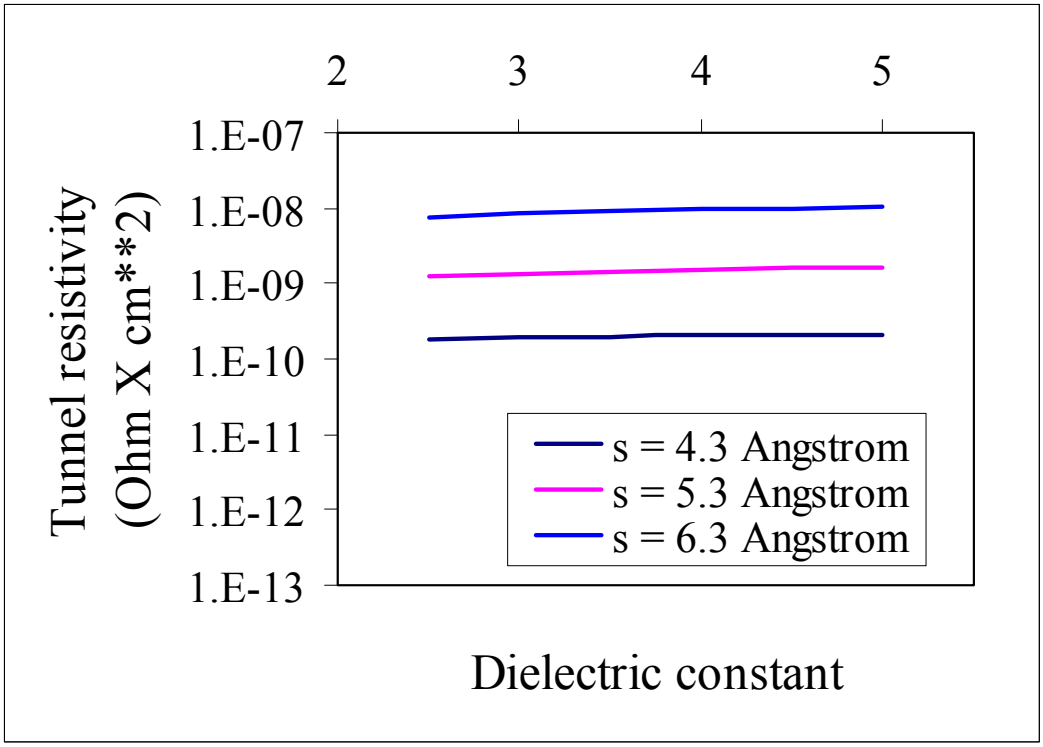

Figure 4.2 Effect of dielectric constant on tunnel resistivity (electron-injection barrier = 2.7 eV)

However, the effect of electron-injection barrier is much more significant. As one can see from Figure 4.3, the tunnel resistivity decreased with the decreasing of electron-injection barrier. For all film thickness, the tunnel resistivity was reduced by two magnitudes when the electron-injection barrier was changed from 1.5 eV to 3.5 eV. Therefore, we think there is not much one can do in order to improve the electrical

performance by modifying the dielectric property of resin system. More researches should be conducted to reduce the tunnel resistivity by decreasing the electron-injection barrier.

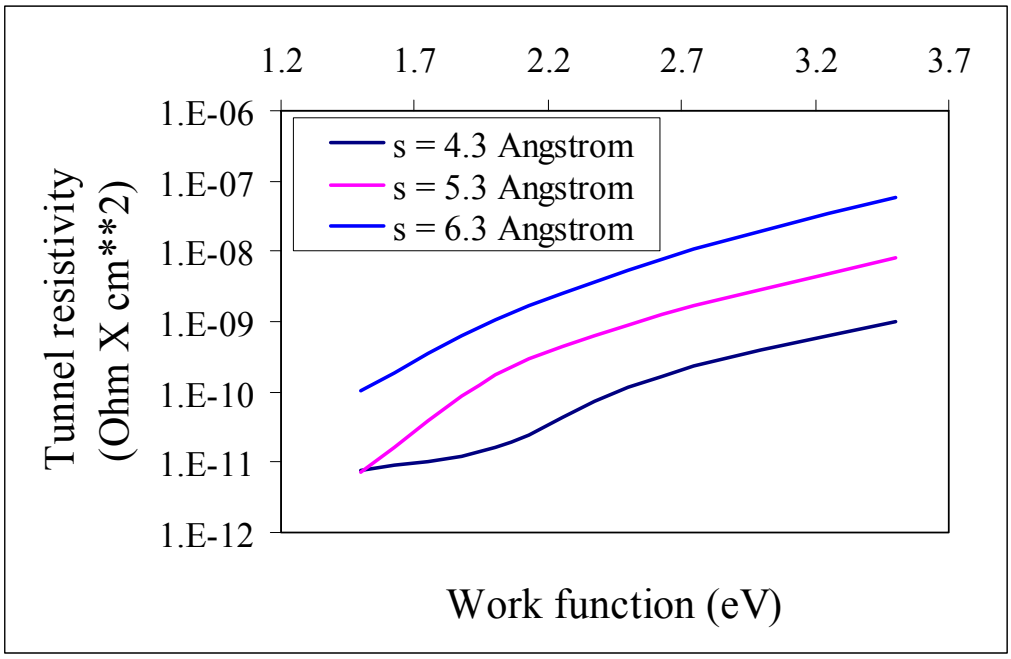

Figure 4.3 Effect of electron-injection barrier on tunnel resistivity (dielectric constant = 3.5)

4.3.4 Prediction of the effect of π-conjugated Self Assembled Molecules on the joint resistance of NCF

In semiconductors, self-assembled molecular wires have seen importance in tuning the metal work function (Φ) and electrical conduction of metal-molecule contact. In particular, conjugated molecules which have a smaller gaps between the highest occupied molecular orbital (HOMO) and the lowest unoccupied molecular orbital (LUMO) and possess delocalized π-electrons can contribute to conduction. Heimel et. al

[128] demonstrated that biphenyldithiol (BPD) can reduce the work function of gold by 1.02 eV. As such, the work function will be reduced to 4.2 eV. Film thickness and dielectric constant are still 3.2 Å and 3.5, by assuming that the physical properties of intermediate layer do not change with the addition of BPD. If those values are substituted in Equation 4-7, the tunnel resistivity can be obtained as 2.06×10^{-10} Ω•cm^2. Assuming the size and number of micro-contacts do not change with the incorporation of BPD, we could substitute the value of tunnel resistivity into Equation 4-9 and get the contact resistance of the joint as 0.5×10^{-4} Ω, as compared to the value of 1.5×10^{-4} Ω without BPD.

4.4 Experimental verification of effects of π-conjugated Self Assembled Molecules on the electrical performance of NCA/NCF

4.4.1 Effects of π-conjugated thiol molecules on the electrical conduction between Au electrodes

To study the effects of molecular wires on the electrical conduction between electrodes, the Au-finished test vehicle was treated with BDT and BPD solutions and heat treated at 150^{o}C for 40 minutes. The contact resistance (R=U/I) was *in-situ* measured as a function of applied pressure and shown in Figure 4.4. For all the joints, a relatively low contact resistance could be achieved at pressures higher than 100 MPa. The untreated joints showed a contact resistance of 3×10^{-3} Ω, while BDT and BPD treated joints showed an obviously lower contact resistance of 2×10^{-3} Ω and 1×10^{-3} Ω, respectively.

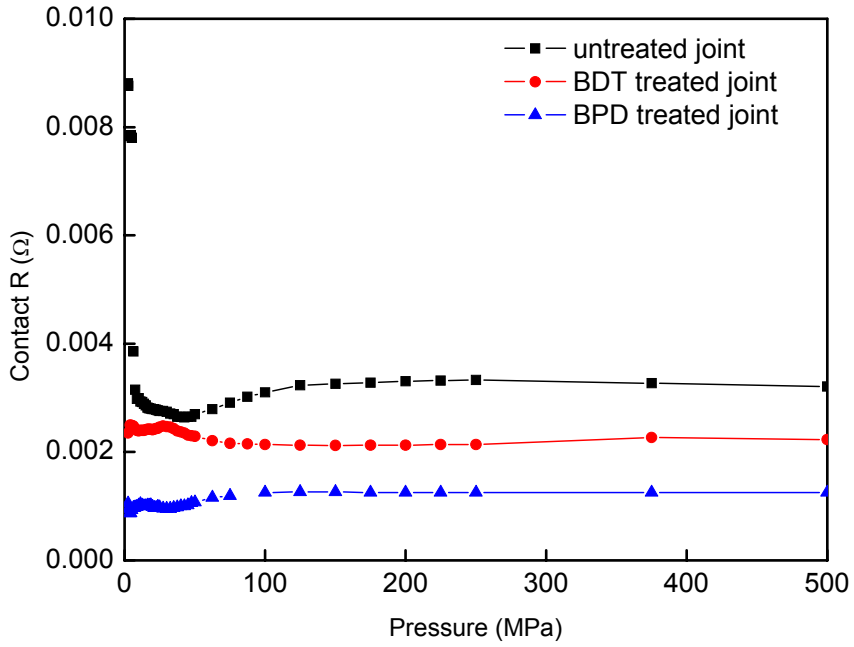

Figure 4.4 Contact resistances between gold electrodes as a function of applied pressure

4.4.2 Effects of π-conjugated thiol molecules on the electrical conduction of NCF joints

To study the effects of conjugated molecular wires on the electrical conduction of NCF, the current-voltage (I-V) relationship and correspondingly current-resistance (I-R) relationship of NCF joints with π-conjugated thiol molecules are compared in Figure 4.5. The untreated NCF joints showed a contact resistance of 0.15 $\times 10^{-3}$ Ω and current carrying capability (maximum current below which the I-V relationship remains linear) of 2.7 A. After incorporating conjugated molecular wires, the joint resistance of NCF could be reduced to 0.1 $\times 10^{-3}$ Ω and 0.05 $\times 10^{-3}$ Ω with BDT and BPD, respectively. Similar to the data without adhesives shown in Figure 4.4, BDT incorporated NCF decreased the joint resistance by 1/3 and BPD incorporated NCF decreased the joint resistance by 2/3.

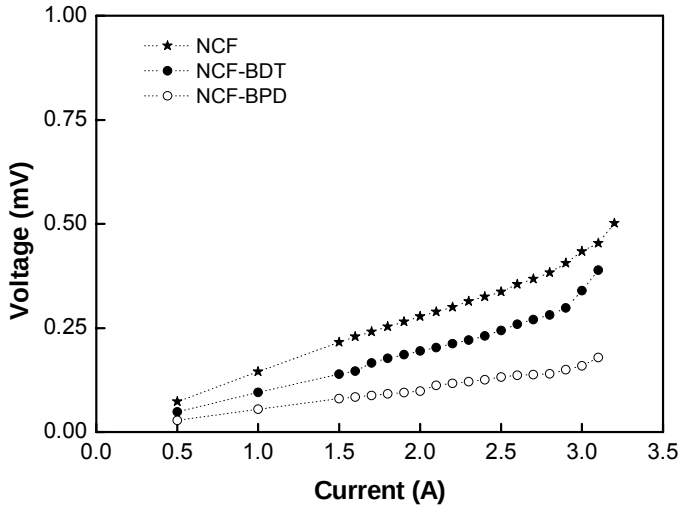

(a)

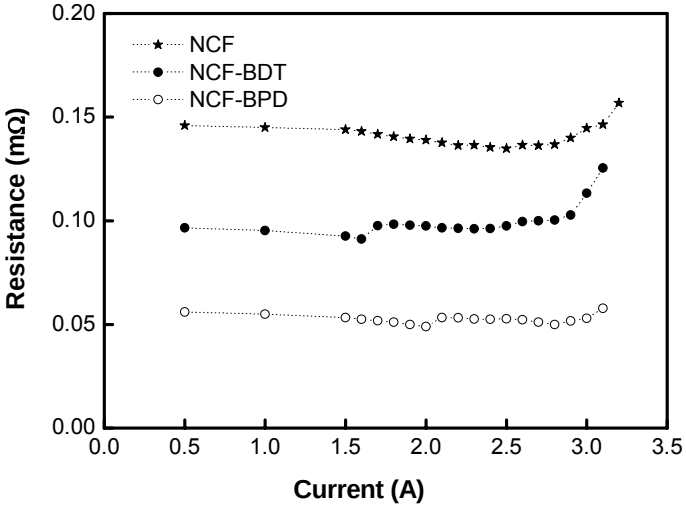

(b)

Figure 4.5 Electrical properties of NCF joints with molecular wires. (a) I-V relationship of NCF joints and (b) corresponding I-R relationship of NCF joints.

4.4.3 Surface Characterization of π-conjugated thiol molecules on Au

In order to understand the interaction between and Au, contact angle measurement and XPS characterizations were conducted. Figure 4.6a shows the contact angle values of DI H_2O droplets on Au surfaces as a function of treatment time. For both BDT and BPD treatment surfaces, the contact angle decreased after treatment, indicating the adsorption of molecular wires on the Au surfaces. It has been reported that thiolate tends to self-assemble on the Au surface forming chemical bonding. For conjugated dithiol BDT and BPD, the exposed hydrophilic terminal thiol group (-SH) of the molecular wires contributed to the lower contact angles. The stability of the interface between Au surface and the SH-terminated molecular wires after heat treatment is crucial to the performance of NCF, because the processing temperature can be as high as 150^{o}C, at which many self-assembled molecular wires could de-bond or degrade. Figure 4.6b shows the contact angle of DI water on Au surfaces after baking the treated surfaces at 150^{o}C for 40 minutes. For the BDT, although an obviously lower contact angle has been observed after treatment, the contact angle value tended to return to the initial value after baking at 150^{o}C. For BPD, on the other hand, a slightly lower contact angle could be remained after baking. The different behaviors should be attributed to different thermal stability of the molecular wires. Unlike BDT which suffers thermal degradation at 150^{o}C, the S-Au bond for BPD was more thermally stable. The higher thermal stability of BPD could be due to the higher aromaticity (more aromatic rings) and thus the increased van der Waals (VDW) interactions for the longer chain of the compound.

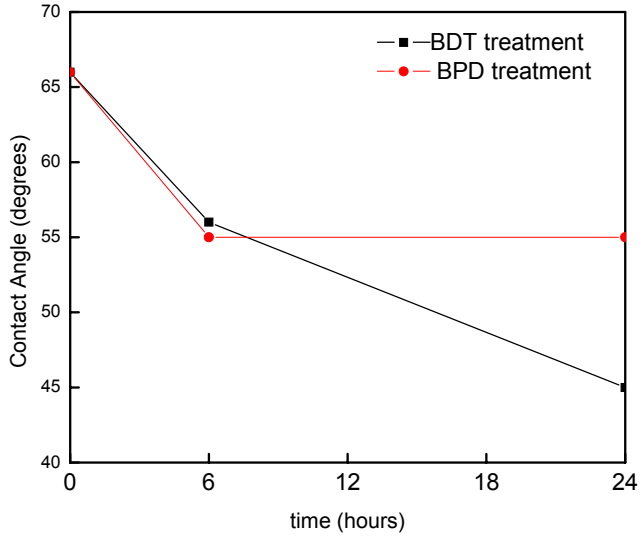

(a)

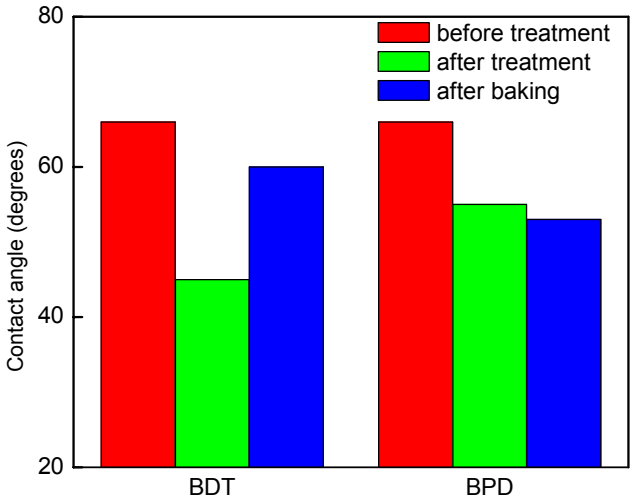

(b)

Figure 4.6 Contact angle of DI H_2O on Au surfaces treated with conjugated –SH molecular wires. (a) contact angle values as a function of treatment time and (b) contact angle values after treatment and baking at 150^{o}C for 40 minutes.

X-ray photoelectron spectroscopy (XPS) studies exhibit a more distinct result for the interaction of Au electodes with the –SH terminated molecular wires. Table 4.2 summarizes the XPS spectra analysis of different Au surfaces. For untreated gold, only the elements of gold (Au), carbon (C) and oxygen (O) were detected. For BDT and BPD treated Au surfaces, in addition to Au, C and O, sulfur (S) could also be detected in the amount of 0.5% and 1.9%, respectively. The relatively amount of C also increased from 63% to 75% and 78% (high resolution XPS spectra of C_{1s} are shown in Figure 4.7). The occurrence of S and increase of C clearly indicated the adsorption of BDT and BPD on Au surfaces. After baking the surfaces at 150^{o}C for 40 minutes, there was no obvious change on untreated Au surface. However, significant changes have been observed for BDT treated surface. The annealed BDT/Au surface showed similar spectra as untreated Au surface from the disappearance of S and reduction of C peaks, suggesting a desorption/debonding of BDT on Au and subsequently the evaporation of debonded BDT. For BPD treated surface, however, the adsorption became more apparent due to the higher concentration of S on Au surfaces (5.2%). Thiol adsorption on gold is considered as a combination of two steps, a diffusion-controlled Langmuir adsorption and a surface crystallization process. The Langmuir adsorption process strongly depends on thiol concentration, while the kinetics of crystallization is related to chain disorder and thus depends on temperature. When increasing the temperature, in addition to possibility of thermal degradation of S-Au bond as in BDT, the behavior of molecular wires on Au could also be controlled by two aspects. Thermodynamically, the increased entropy led to less ordered structure. Simultaneously, enhanced crystallization during annealing could

induce more distinct sulfur peak which should be the controlling factor for the more ordered structure observed on BPD/Au surface after baking.

Table 4.2 XPS Elemental Composition (at %) of Au/wafer surfaces

Samples	Au 4f	C1s	O1s	S2p
untreated Au	22.5%	63%	14.5%	
BDT/Au	15%	75%	9%	0.5%
BPD/Au	11.7%	77.8%	8.6%	1.9%
untreated Au-after baking	22.9%	60.6%	16.6%	
BDT/Au-after baking	20%	66%	14%	
BPD/Au-after baking	10.7%	75.7%	8.4%	5.2%

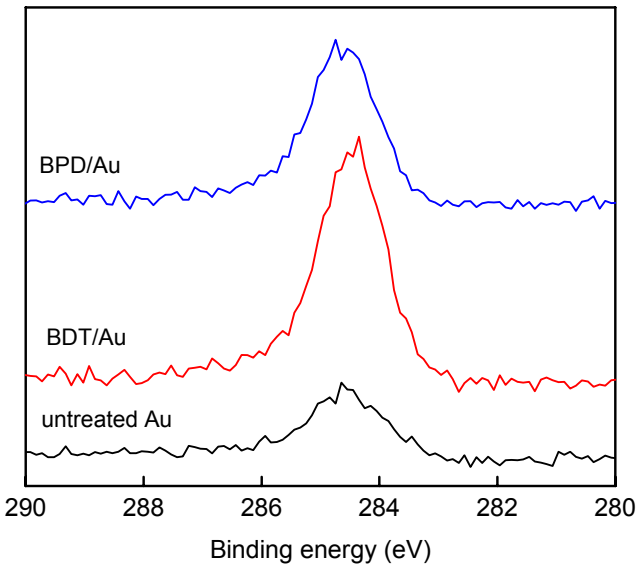

(a)

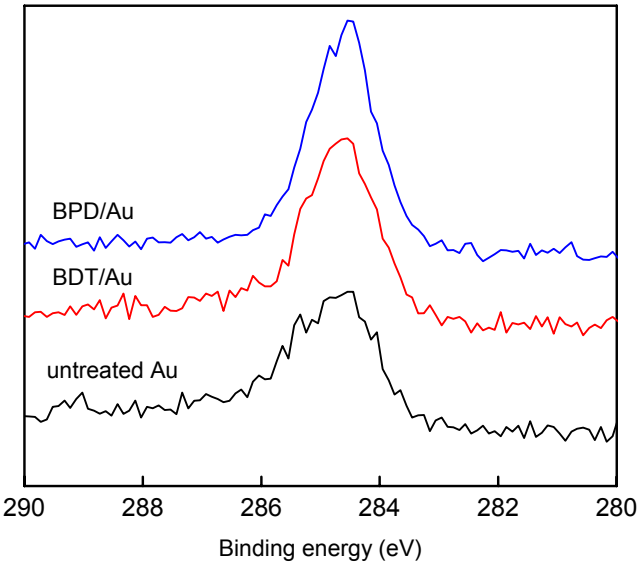

(b)

Figure 4.7 High resolution XPS spectra of C1s on Au surfaces (a) after treatment and (b) after baking at 150^{o}C for 40 minutes.

4.5 Conclusions

A micromechanical model was developed to study the electrical conductance of NCA/NCF assembly. Analytical expressions were obtained for both constriction and tunnel resistance. Modeling results showed that the constriction resistance was negligible compared to tunnel resistance.

Tunnel resistance is dependent on the material properties (dielectric constant and electron-injection barrier) and the processing pressure. Model results demonstrated that electron-injection barrier played a much more important role in controlling the tunnel resistivity, compared to the effect of dielectric constant.

To verify the model and reduce the joint resistance, two types of conjugated molecular wires, BDT and BPD, were introduced at the interface of NCF joints. The molecular wires could adsorb on the gold electrodes and improve the interface properties. Formation of electrical junction with molecular wires between Au electrodes could tune the effective work function (Φ) of Au electrodes. The lower work function reduced the tunnel resistivity and thus improving the electrical conduction significantly. The joint resistance of NCF with BDT and BPD was reduced by 1/3 and 2/3, respectively. The more distinct improvement with BPD was due to the higher thermal stability of BPD than BDT. The preliminary work pointed a potential way of enhancing the electrical performance of NCA/NCF. More systematic research needs to be conducted in future, in order to identify the best π-conjugated self assembled molecules and fine tune the processing conditions to achieve better electrical conductance and higher current carrying capabilities. Improvement of electrical performance of NCF will enable the application of NCF in fine pitch and high performance interconnects in microelectronics.

CHAPTER 5
PERSPECTIVES OF ECO-FRIENDLY CURING AGENT FOR ECAS- FUNDAMENTAL UNDERSTANDING OF THE CURING MECHANISM OF AMINO ACID-EPOXY CROSSLINKING SYSTEM

5.1 Introduction

Due to their chemical inertness, excellent adhesion strength and low cost, the epoxy type resins have been widely used in electronic industry, such as flip-chip underfill, low dielectric constant (k) components, semiconductor encapsulation films and represent a primary matrix resin for the adhesives. Various types of curing agents, such as nitrogen (amines), oxygen (anhydrides) and sulfur (mercaptans) containing compounds, have been used for cross-linking [135, 136]. The choice of a particular curing agent depends on the processing requirements (e.g., viscosity, pot life, application method, curing temperature, reactivity, mixing ratio) and the end-use requirements (e.g., thermal and chemical resistance, shear strength, toughness) of the cured adhesives. The curing agents along with the epoxy resin determine the type of chemical bonds and the degree of crosslinking that will occur.

Although these curing agents have been used for several decades, these systems do have some environmental problems and have been especially noted in recent years. One problem is from the halogen-containing epoxy resins which are particularly useful for printed circuit board applications. These epoxy systems are synthesized from the reaction of diglycidyl ether of bisphenol A (DGEBA) with tetrabromobisphenol A. They usually generate dense smoke and toxic decomposition products during combustion [137-138]. Halogen-free epoxy resins cured with phosphorus-containing compounds exhibit

good flame retardancy and are promising solutions to this problem [139-148]. Another environmental problem of epoxy resins is that all the curing agents are toxic before cure [135, 136, 149-152]. The aliphatic amines, cycloaliphatic amines, and anhydrides curing agents may cause irritation or damage to the skin, eyes, and lungs. Certain aliphatic and cycloaliphatic amines are skin sensitizers and may absorb through the skin and cause damage to organs such as the liver and interfere with the blood's ability to carry oxygen. In addition, organic acid anhydrides (OAAs) are low molecular weight chemicals used in the industry for manufacturing of plastics. Especially, anhydride type curing agents are the most popular curing agent in electronic materials, such as the flip-chip underfills and adhesives, due to its low viscosity, low internal stress, and thermal stability. Exposure to these chemicals may lead to symptoms from the eyes and the respiratory tract in the form of conjunctivitis, rhinitis, and asthma. In many works, production of specific IgE (Immunoglobulin Erythema) antibodies is induced, suggesting that a type-1 allergy mediated mechanism is involved. The OAAs act as haptens and the binding to endogenous proteins is likely an important part of the pathophysiological mechanism [152]. Solid anhydride curing agents may cause sensitization in workers exposed to the curing agent dust. Even for cured epoxy resins that seem safe, toxicity can not be totally avoided because of the possibility of incomplete consumption of curing agents and subsequently the hazards introduced by the residue curing agents. Therefore, the development of environmentally friendly epoxy systems is of great importance for designing green and biocompatible materials in many applications [153-155].

In this chapter, biochemical building blocks, amino acids are used as non toxic and environmentally benign curing agents. Their reaction mechanism and curing kinetics are investigated.

Amino acids are organic molecules possessing carboxylic and amino groups, both of which may react and crosslink with the epoxy group. As shown in Figure 5.1, at the center of the amino acid is an asymmetric carbon atom. Its four different partners are an amino group, a carboxyl group, a hydrogen atom, and a variable group symbolized by R. Amino acids are biochemical building blocks and can form short chemical chains called polypeptides or peptides, which in turn form proteins. Over 500 amino acids have been found in nature, while the diversity arises from the intrinsic properties of only 20 commonly occurring amino acids. Amino acids are usually classified by properties of the side chain: acidic, basic, hydrophilic (polar), and hydrophobic (nonpolar). Some representative examples of amino acids are shown in Figure 5.2.

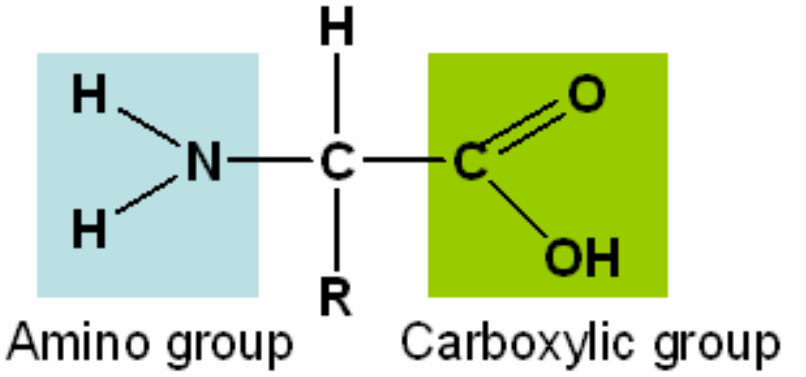

Figure 5.1 Chemical structure of amino acid.

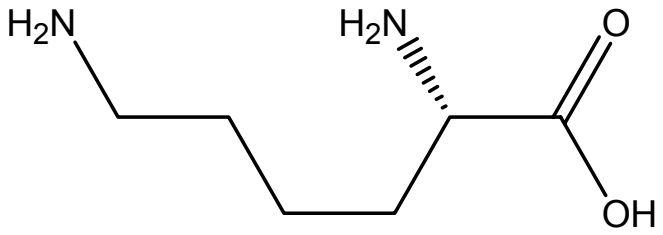

lysine (polar, basic)

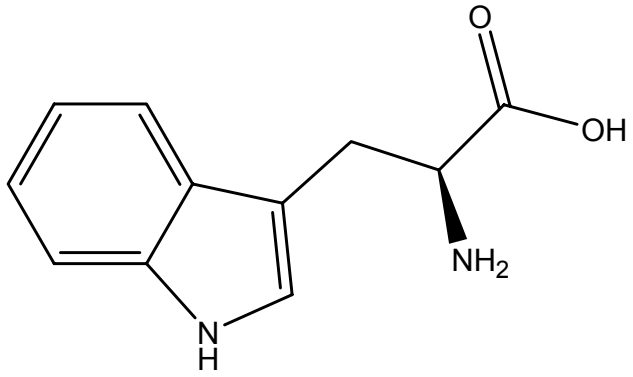

tryptophan (nonpolar, neutral)

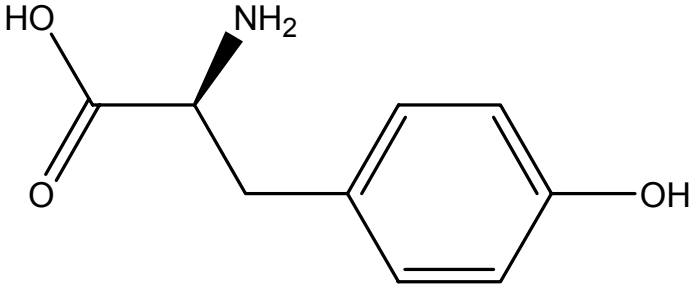

tyrosine (polar, neutral)

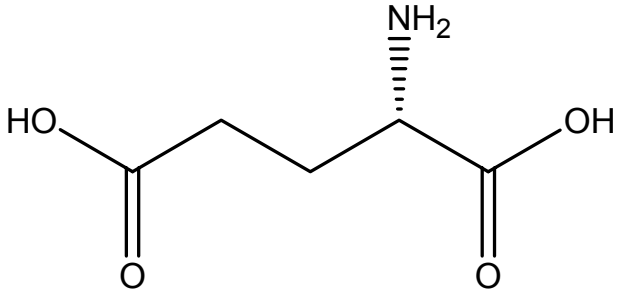

Glutamic acid (polar, acidic)

Figure 5.2 Examples of different types of amino acids

5.2 Experimental

5.2.1 Materials

Diglycidyl ether of bisphenol-A (DGEBA) EPON 828 with an epoxy equivalent weight (EEW) of 187 g/equiv was kindly supplied by Shell Chemicals. L-tryptophan with 99% purity was purchased from Aldrich Chemical Company, Inc. A typical curing agent, methylhexahydrophthalic anhydride (HMPA) was used for comparison. The catalyst, 1-cyanoethyl-2-ethyl-4-methylimidazole (2E4MZCN), was supplied by Shikoku Chemicals Corporation (Japan). The chemical structures of these materials are shown in Figure 5.3. Tryptophan was grounded into fine powders before use, while all the other chemicals were used as received. The samples with different ratios of DGEBA and tryptophan were mixed well before characterizations.

5.2.2 Characterizations

The curing profile was determined using a modulated differential scanning calorimeter (MDSC, TA Instruments, model 2970). A mixture ~10 mg of epoxy and tryptophan with different ratios was sealed in a hermetic aluminum pan and dynamic DSC scans were made on the samples at a heating rate of 5°C/minute from 25°C to 300°C under nitrogen. After the dynamic scan, the sample was cooled to room temperature and then re-scanned at the same heating rate from 25°C to 200°C for glass transition temperature (Tg) measurement. The isothermal DSC scans were made on the samples at various temperatures and the curing conditions of DGEBA and tryptophan were determined from the DSC results.

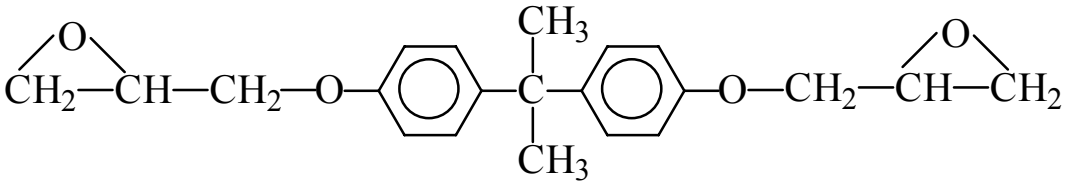

(a) DGEBA

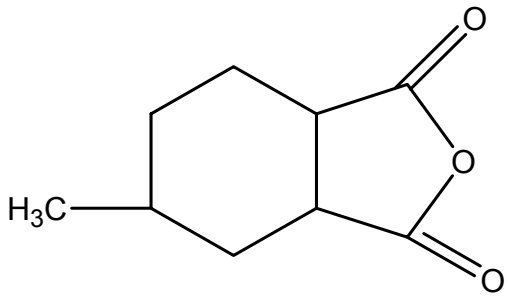

(b) HMPA

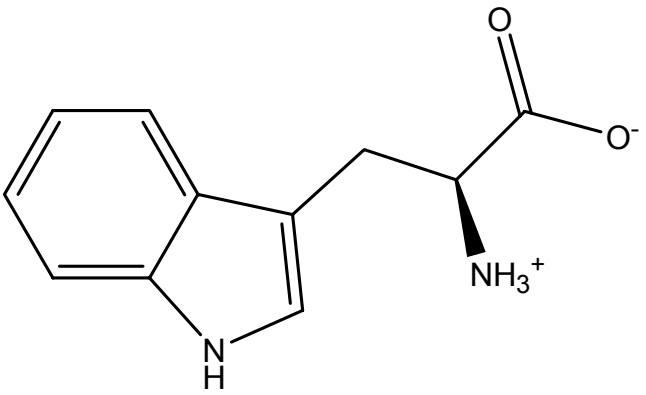

(c) Tryptophan

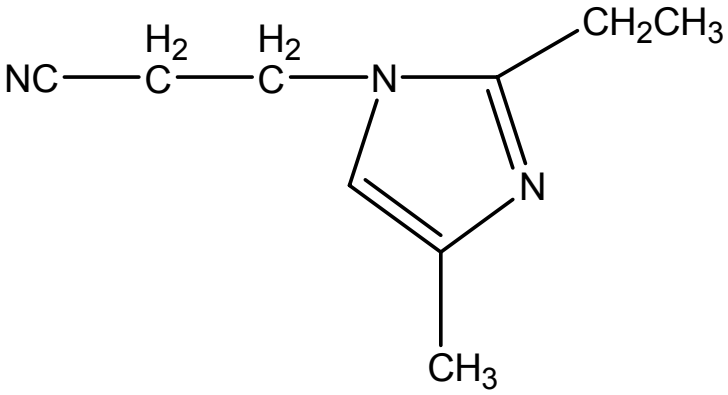

(d) 2E4MZCN

Figure 5.3 Chemical structures of the materials used

To study the curing mechanism, the DGEBA/tryptophan mixture was sandwiched between the two KBr plates and *in-situ* measured by Fourier Transfer Infrared (FT-IR) spectroscopy. The FTIR spectra of DGEBA/tryptophan mixture at different temperatures and time were collected.

Thermal stability of the epoxy resins were examined using thermogravimetry analyzer (TGA, TA Instruments, model 2050). The temperature was raised from 25°C to 600°C at a heating rate of 10°C/minute in nitrogen.

5.3 Results and Discussion

5.3.1 Curing capability investigation of DGEBA with tryptophan

Figure 5.4 shows the heat flow of the DGEBA/tryptophan mixture with a molar ratio of 3:1. An obvious exothermic peak was observed at 216^{o}C with a reaction heat of 200 J/g. The glass transition temperature (Tg) obtained from second dynamic DSC run was 80^{o}C. The obvious exothermic peak and the corresponding Tg suggested the feasibility of using tryptophan as a novel curing agent for DGEBA.

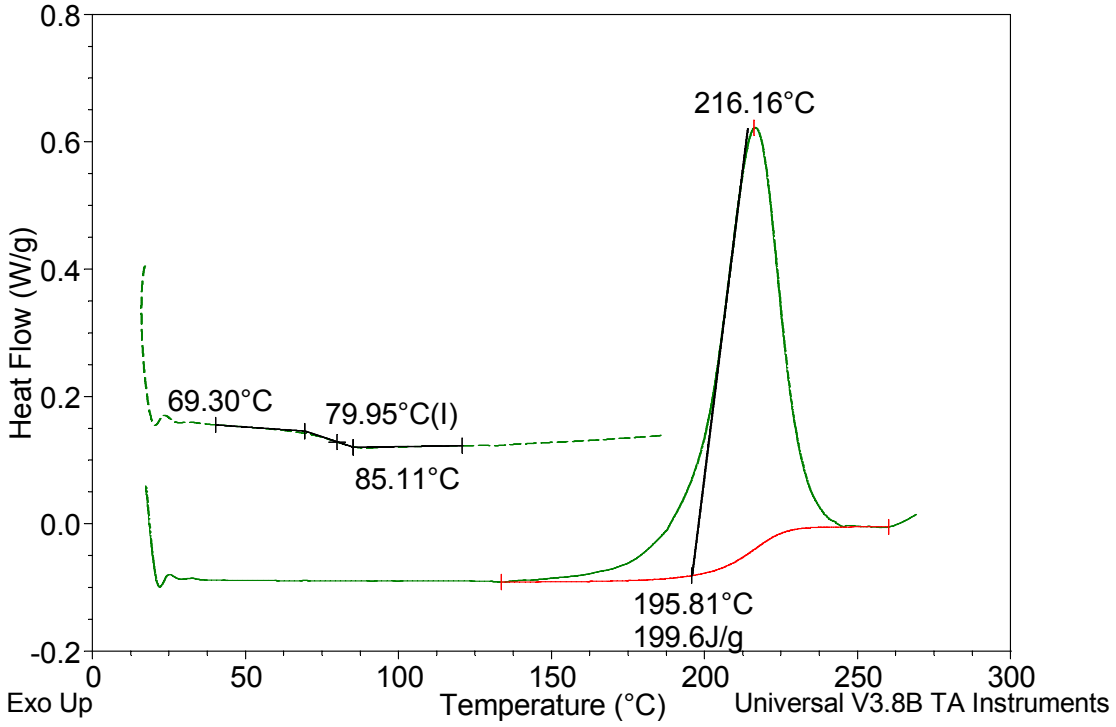

Figure 5.4 Dynamic DSC of DGEBA/tryptophan (3:1 ratio)

Isothermal DSC peaks at different temperatures are shown in Figure 5.5. At 150^{o}C, no obvious reaction was observed after 90 minutes. Increasing temperature to 175^{o}C triggered the curing reaction. The reaction lasted for about 60 minutes at 175^{o}C and the total reaction heat measured from the area of the reaction peak was 156 J/g. When the isothermal temperature was further increased to 200^{o}C, the reaction proceeded faster and more complete. A total reaction heat of 277 J/g was observed after holding at 200^{o}C for 45 minutes. The higher reaction heat at 200^{o}C than that observed from dynamic DSC scan (Figure 5.4) should be attributed to the more reaction with longer reaction time.

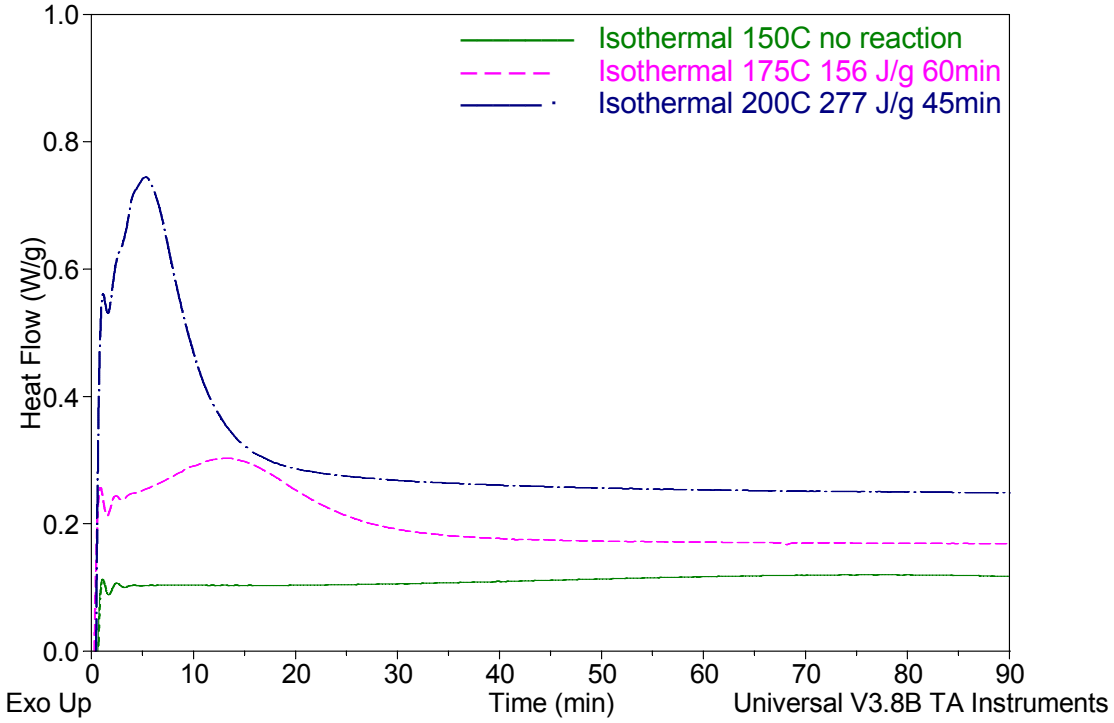

Figure 5.5 Isothermal DSC for DGEBA/tryptophan mixture (3:1 ratio)

The glass transition temperatures (Tgs) of cured samples were measured and compared in Figure 5.6. The DGEBA/tryptophan mixture (3:1 molar ratio) heat treated at 150^{o}C for 2 hours didn't show very obvious glass transition temperature. On the other hand, samples cured at 175^{o}C and 200^{o}C for 2 hours exhibited obvious Tgs at ~87^{o}C, which suggested the crosslinked structure of using tryptophan as curing agent for DGEBA.

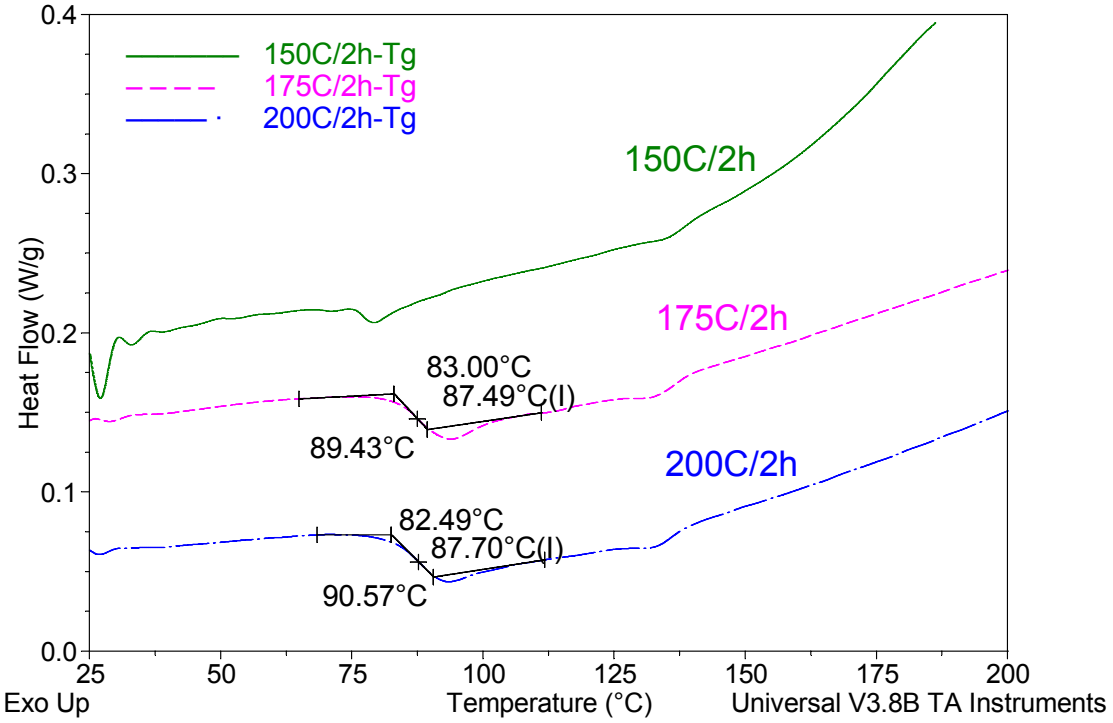

Figure 5.6 Tgs of DGEBA/tryptophan mixtures (3:1) after cured at different temperatures for 2 h.

5.3.2 Effect of catalyst on the curing reaction of DGEBA with tryptophan

Compared to the typical anhydride-cured DGEBA which can be cured at 150°C with a high reaction heat of 348 J/g (Figure 5.7a), the high reaction temperature and low reaction heat suggested a low reactivity of DGEBA/tryptophan crosslinking and correspondingly the incomplete reaction. This lower reactivity should be due to the electrostatic interaction between zwitterions [$^{+}H_3N$-CH(-R)-COO^{-}] in tryptophan, which has much lower reactivity than the free primary amine and carboxylate anions.

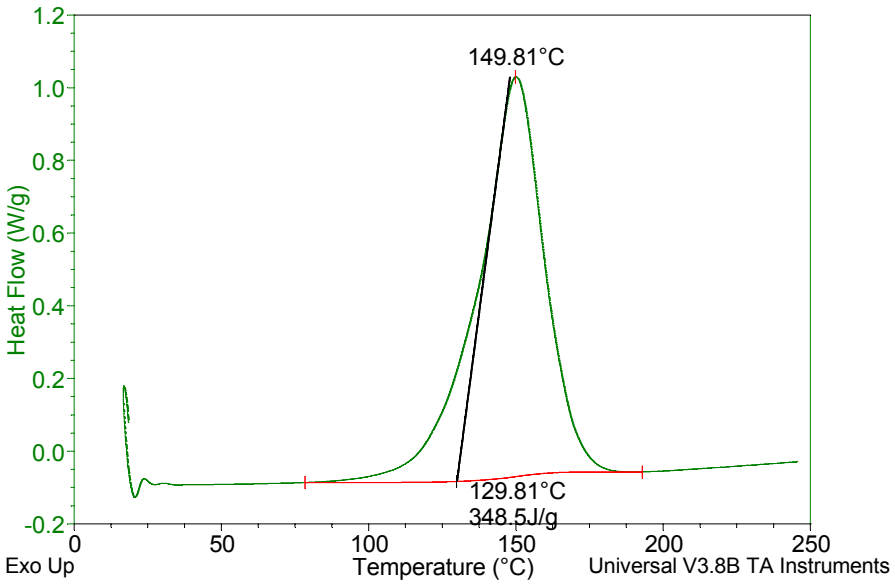

(a)

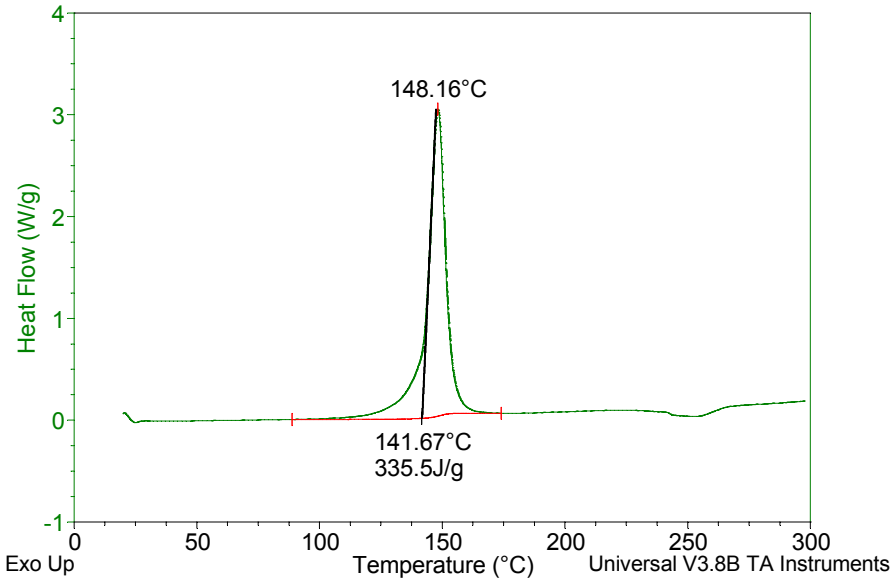

(b)

Figure 5.7 Dynamic DSC of (a) typical DGEBA/HMPA (1:1) with catalyst; (b) DGEBA/tryptophan (3:1) with catalyst; (c) cured DGEBA/tryptophan (3:1) with catalyst

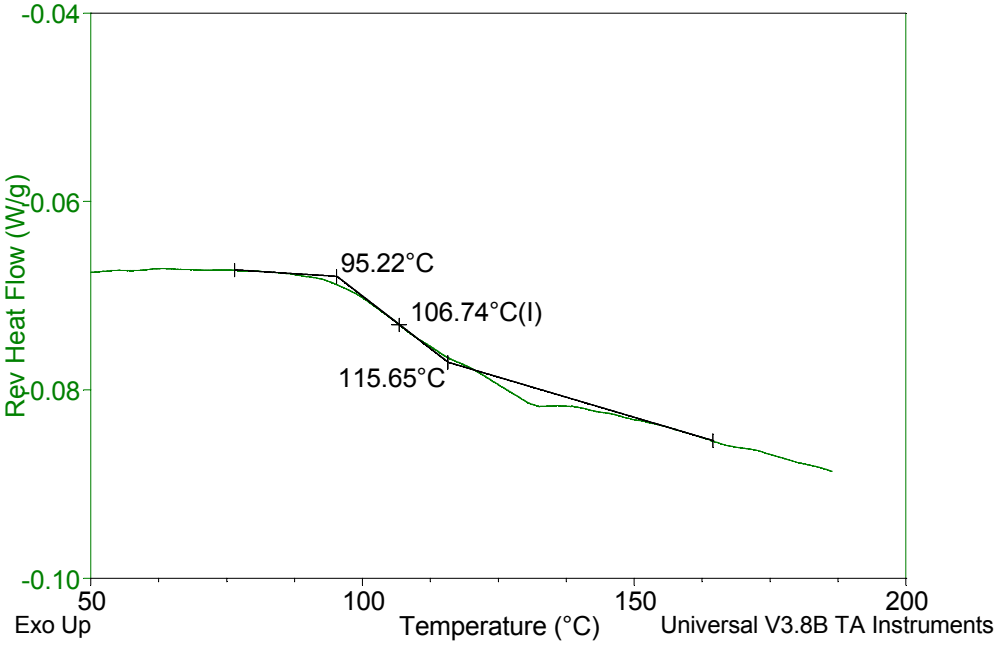

(c)

Figure 5.7 continued.

To enhance the reactivity and induce a more complete reaction, 1 wt% of an imidazole-type catalyst (2E4MZCN) was added in the DGEBA/tryptophan mixture and the curing profile was collected by DSC. As shown in Figure 5.7b, with addition of catalyst, a sharp reaction peak could be obtained at a much lower reaction temperature of 148^{o}C, and the total reaction heat increased dramatically to 335 J/g. In addition, the glass transition temperature obtained from second dynamic DSC run was 107^{o}C (Figure 5.7c), significantly higher than the samples without catalyst. The reaction heat is similar to a typical anhydride cured DGEBA, indicating a complete reaction with the application of catalyst. To verify the crosslinking reaction of DGEBA/tryptophan with catalyst, the

solubility of cured samples was tested in 2-butanone, ethanol, 4-methyl-pentanone, respectively. There was no obvious weight change before and after solvent treatment at room temperature and 100^{o}C. The insolubility of samples in the common epoxy solvents confirmed the crosslinking reaction.

Isothermal DSC of DGEBA/tryptophan mixture (3:1) with catalyst was also conducted. As can be seen from Figure 5.8, samples at 110^{o}C showed obvious reaction latency. There was no exothermic reaction until after holding at the temperature for over 20 minutes, when a broad and relatively small reaction peak was observed. The reaction lasted for over 50 minutes and the total reaction heat was 300 J/g. At 130^{o}C, a relatively faster reaction could be achieved within 10 minutes. The reaction completed after 30 minutes with a total reaction heat of 320 J/g. Although the reaction heat was much higher than that observed for DGEBA/tryptophan mixture without catalyst, the lower value compared to the dynamic DSC in Figure 5.7b suggested an incomplete reaction. With increasing isothermal temperature to 150^{o}C, however, a very fast and complete reaction was observed. The total reaction heat was 350 J/g and the reaction can be completed within 10 minutes from isothermal DSC.

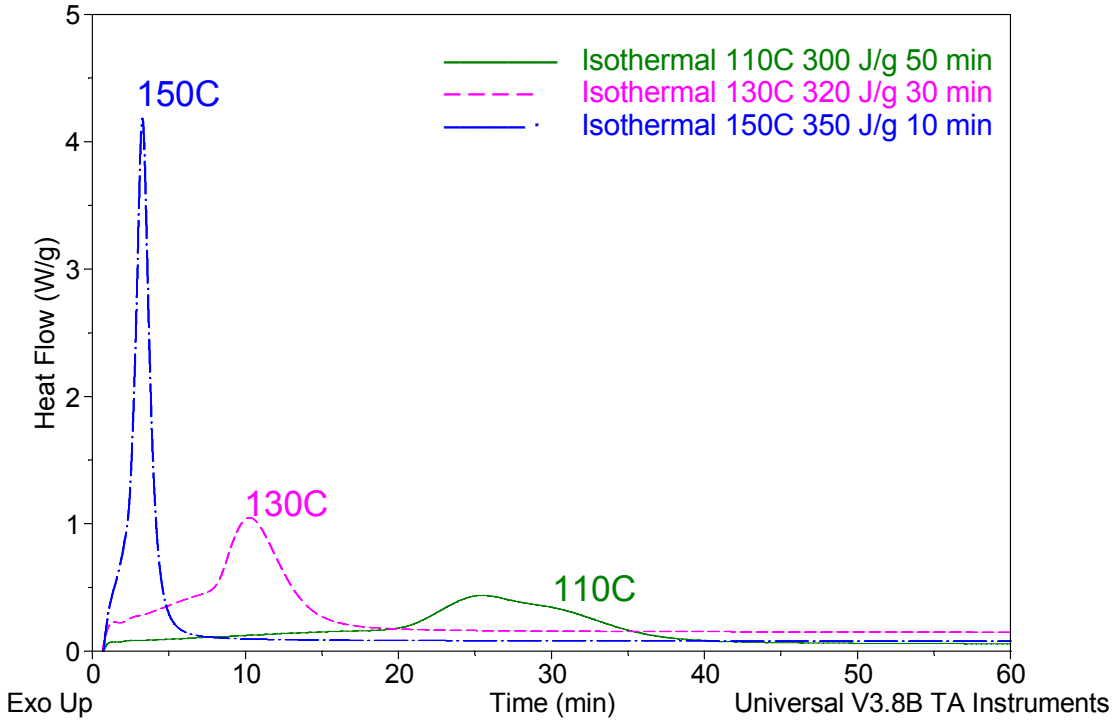

Figure 5.8 Isothermal DSC for DGEBA/tryptophan mixture (3:1) with catalyst at different temperatures

5.3.3 Effect of molar ratio on the curing reaction of DGEBA/tryptophan

To study the appropriate amount and reaction mechanism of using tryptophan as curing agent for DGEBA, dynamic DSC of various molar ratios (2:1, 3:1 and 4:1) of DGEBA/tryptophan were compared. Without catalyst, all the reactions showed high reaction temperature and low reaction heat (Figure 5.9). DGEBA/tryptophan 4:1 has the lowest reaction heat of 128 J/g, indicating many epoxides have not been able to participate in the reaction because of the excess of DGEBA. DGEBA/tryptophan 3:1 showed the highest reaction heat of 200 J/g, while further increasing the tryptophan

amount to 2:1 ratio didn't increase the reaction heat, which indicated no further reaction could be conducted for the mixture.

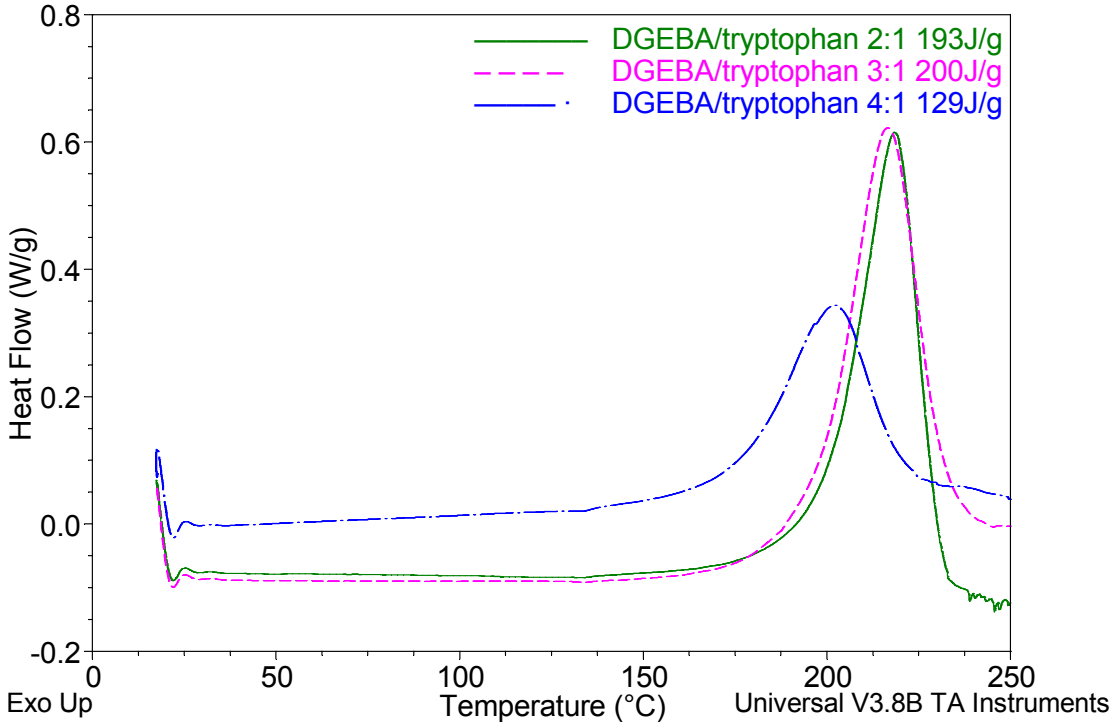

Figure 5.9 Dynamic DSC of DGEBA/tryptophan of various molar ratios without catalyst

With addition of 1 wt% catalyst, all formulations showed a significantly lower reaction temperature and higher reaction heat (Figure 5.10). The DGEBA/tryptophan 3:1 showed the lowest reaction temperature and very narrow peak, while the 2:1 and 4:1 ratios showed slightly higher peak temperatures and broader peaks.

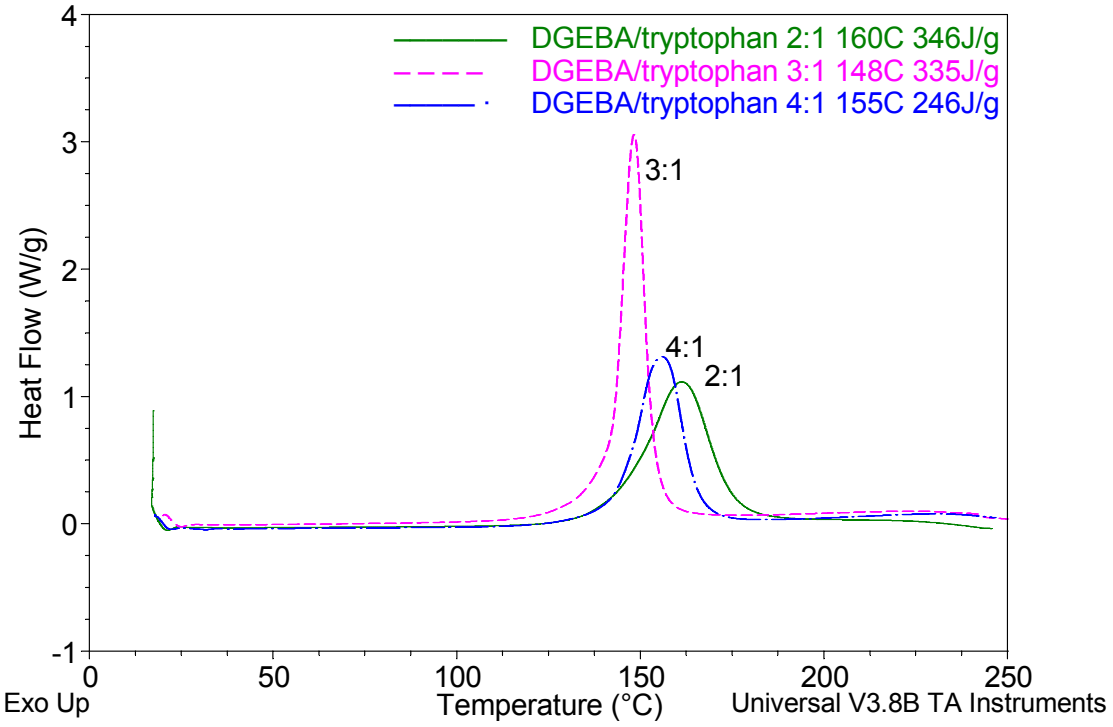

Figure 5.10 Dynamic DSC of DGEBA/tryptophan of various molar ratios with 1wt% catalyst

The total reaction heat and the glass transition temperatures of cured samples are compared in Table 5.1. The reaction heat of DGEBA/tryptophan 2:1 and 3:1 was very much similar to that of HMPA-cured DGEBA. However, DGEBA/tryptophan 4:1 can only achieve approximately 75% of the reaction heat as the other two formulations, which suggested only 75% of epoxides have been reacted in the 4:1 ratio. Therefore, one part of trytophan can at most effectively react with 3 epoxide groups. The glass transition temperature of DGEBA/tryptophan 2:1 showed the lowest value (93^{o}C), due to the lower crosslinking density and the residue small molecules (tryptophan) after reaction. On the

other hand, both DGEBA/tryptophan 3:1 and 4:1 showed relatively high Tgs of 107°C and 105°C respectively, which is attributed to a higher crosslinking density. Although there are extra epoxides after reaction in 4:1 ratio, the crosslinked network is considered to be formed. Therefore, when using tryptophan as curing agent for DGEBA, a molar ratio of DGEBA/tryptophan 3:1 with 1wt% imidazole type catalyst is preferred.

Table 5.1 Curing properties of DGEBA with tryptophan at various ratios

Formulations	**DGEBA/ HMPA**	**DGEBA/ tryptophan (2:1)**	**DGEBA/ tryptophan (3:1)**	**DGEBA/ tryptophan (4:1)**
Peak temperature (°C)	150	160	148	155
Total reaction heat (J/g)	320	346	335	246
Tg of cured samples (°C)	127	93	107	105

5.3.4 *In-situ* FTIR of DGEBA/tryptophan (3:1) with catalyst

To understand the reaction mechanism of DGEBA/tryptophan with catalyst, FTIR spectra of DGEBA/tryptophan (3:1) were *in-situ* collected during curing and are illustrated in Figure 5.11. Figure 5.11a shows the spectra of DGEBA/tryptophan mixtures at different temperatures. As can be seen from the spectra, no obvious peak change occurred from room temperature to 140°C, while after reaching 150°C, an obviously varied spectrum was observed. The dramatically reduced peak strength for epoxide group at ~915cm^{-1} and amino acid characteristic peak at ~2100cm^{-1} suggested a ring opening

reaction between them. The observed reaction latency of the novel epoxy-curing system at relatively lower temperatures is in accordance with the DSC results from Figure 5.7b and Figure 5.8. The reaction latency offers the system an advantage of longer shelf life for storing and handling.

FTIR spectra at room temperature and 150^{o}C for 20 min, 30 min and 90 min were compared at both high wavenumbers (Figure 5.11b) and low wavenumbers (Figure 5.11c). At room temperature, a strong and sharp peak was observed at ~3400cm^{-1}, which corresponds to the N-H stretching in indole group of tryptophan. Broad peaks between 3200-2700 cm^{-1} is the characteristic of NH_3^+ in the zwitterions [$^{+}H_3N$-CH(-R)-COO^{-}] of tryptophan. After heating at 150^{o}C for 20 min, a broad peak ranging between 3200 and 3650 cm^{-1} was observed. The absorption in this range could be a combination of several stretch modes, including N-H in indole, primary amine (R-NH_2) and secondary amine (R-NH) groups formed from zwitterions as well as the O-H group. The primary aliphatic amine could be formed from the zwitterions [$^{+}H_3N$-CH(-R)-COO^{-}] after the initiation by imidazole, and the secondary aliphatic amine was formed from the ring opening of epoxide with the primary amine. This ring opening reaction could also form a hydroxy group which has a characteristic broad peak at around 3500 cm^{-1}. Increasing the reaction time to 30 min changed the peak to a broad one at ~3550-3500 cm^{-1} and a narrow one at ~3400 cm^{-1}. The broad peak should be from the H-bonded O-H group while the peak at ~ 3400cm^{-1} could be assigned to N-H stretching band from indole and small amount of unreacted secondary amine. The absorption change at high frequency range suggested the formation of primary amine from zwitterions with the initiation of imidazole and epoxy

ring opening reaction by primary amine and followed by further ring opening by formed secondary amine.

At low wavenumbers, more IR peaks were observed and the peak change was more significant. At room temperature, there were obvious IR bands between 1700 and 1300 cm^{-1} that corresponded to different modes associated with the zwitterions [$^{+}H_3N$-CH(-R)-COO^{-}] in amino acid, such as NH_3^{+} asymmetric deformation mode at 1665 cm^{-1}, COO^{-} symmetric stretching mode at 1415 cm^{-1}, and CH deformation mode at 1360 cm^{-1} [156, 157]. Other peaks between 1600 and 1450 cm-1 should be from other stretching modes of zwitterions and the indole group in tryptophan. After heating up at 150^{o}C for 10-20 minutes, an obvious ester carbonyl stretch was observed at ~1740 cm^{-1}, indicating the reaction of carboxylic anion with epoxy. Meanwhile, the intensity of some amino acid zwitterions peaks reduced, in particular the NH_3^{+} asymmetric deformation, COO^{-} symmetric stretching and CH deformation modes.

Although obvious peak changes have been detected after heating at 150^{o}C for 30 minutes, further increasing the curing time till 90 minutes didn't introduce more reaction, which can be seen from the similarity between the two spectra at 150^{o}C for 30 minutes and 90 minutes.

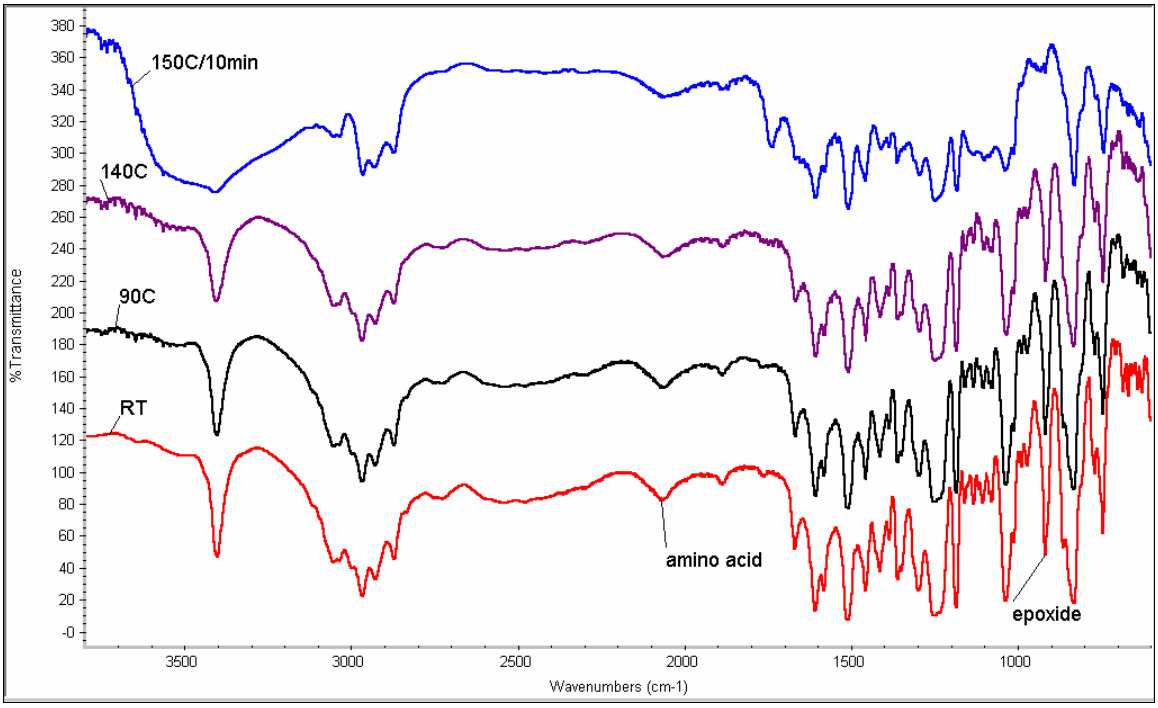

(a)

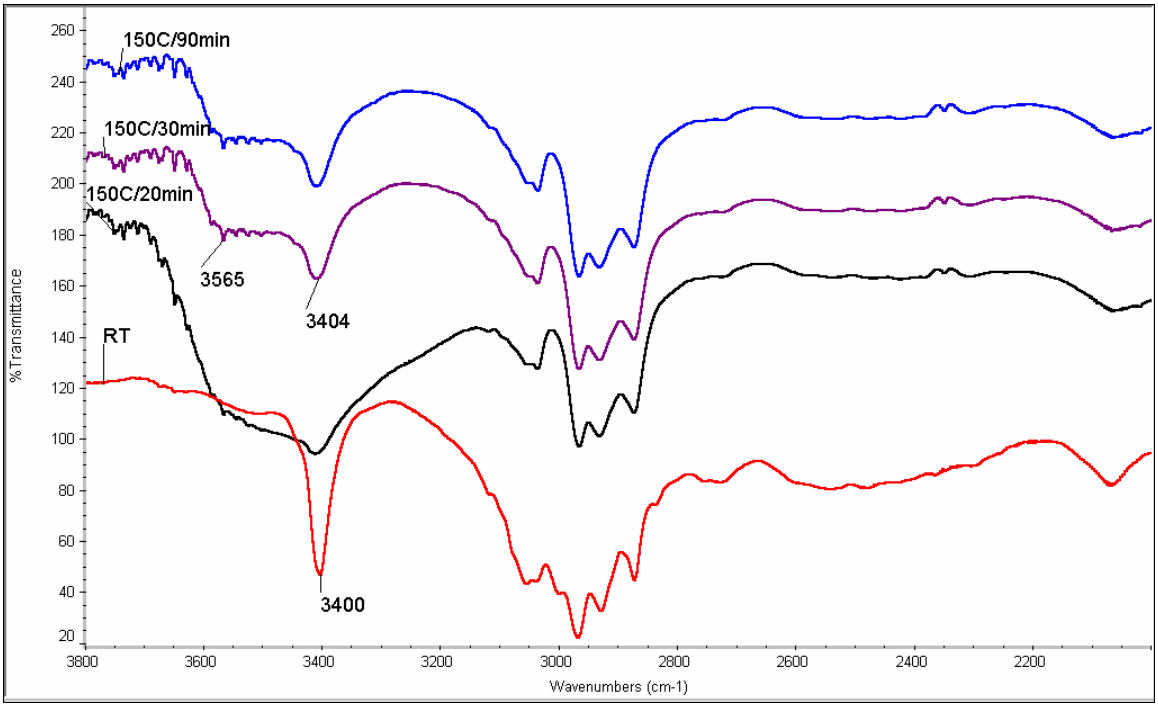

(b)

Figure 5.11 FTIR spectra of DGEBA/tryptophan mixture (3:1) with catalyst. (a) General spectra at various temperatures; (b) spectra at high wavenumbers with curing; and (c) spectra at low wavenumbers with curing.

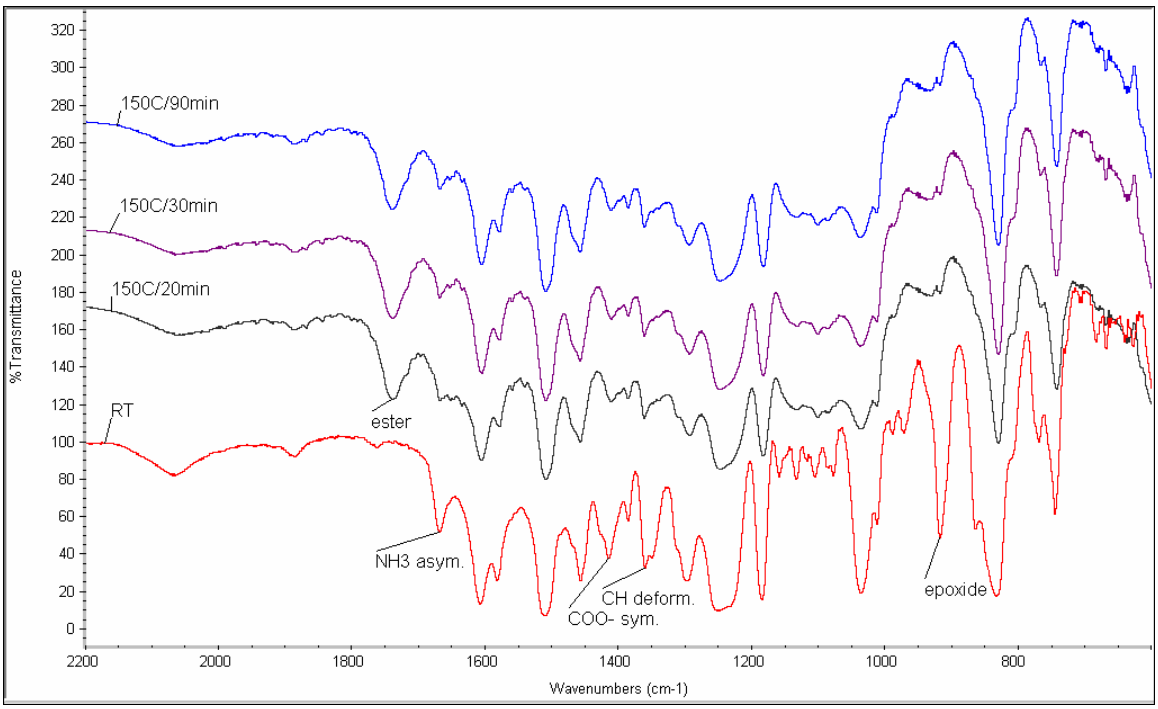

(c)

Figure 5.11 continued.

5.3.5 Curing mechanism of imidazole-initiated epoxy-amino acid reaction

Combined the thermochemical results from DSC and the structural results from FT-IR spectra, imidazole-initiated chain reaction mechanism of curing reaction of DGEBA/tryptophan can be proposed in Figure 5.12. Activation of zwitterions by catalyst imidazole initiated the reaction, and the ionized epoxide could extract a hydrogen from NH_3^+ in zwitterions and form a primary amine (Figure 5.12 a). The formed primary amine (amino carboxylate anion), even with small amount, could significantly increase the reactivity of COO^- in amino acid which triggered the esterification of carboxylate anion with epoxy and subsequently extraction of hydrogen from another NH_3^+. These two

reactions can be repeated in a chain mode and result in the formation of primary amine (Figure 5.12 b). The resulting primary amine from the chain reaction can undergo a nucleophilic attack on an epoxy ring (Figure 5.12 c) and the formed secondary amine could further react with another epoxy giving tertiary amine (Figure 5.12 d). Meantime, the formed hydroxyl (-OH) group from the epoxy ring during the reactions can auto-catalyze those reactions. With continuation of these reactions, the highly crosslinked structure could be formed with a relatively short period of time (30 min). Although the nitrogen atom in indole also has a lone pair of electrons, the lone pair is mostly likely delocalized and contributes to the aromatic system. Therefore, it has a much lower reactivity as compared to aliphatic amine groups and thus is less likely to contribute to the crosslinking reaction with DGEBA. The reaction mechanism in Scheme 1 also explains the optimized molar ratio of 1:3 of tryptophan to epoxide groups. Furthermore, this catalyst-initiated chain reaction mechanism is suitable for all zwitterionic amino acid curing reaction. Therefore, all amino acids, even without additional reactive functional group, have potential to be used as curing agent for epoxy resin system.

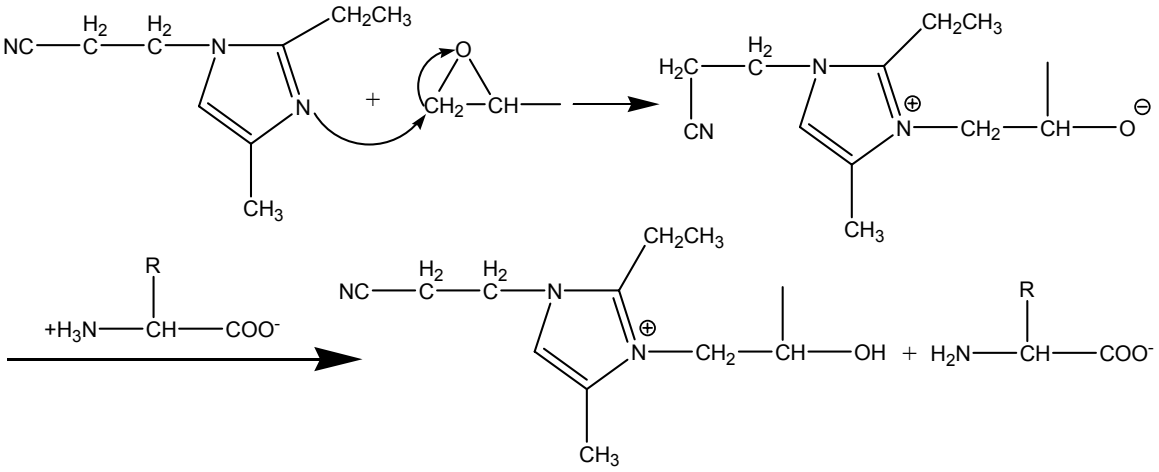

(a) Initiation and activation of amino acid zwitterions [$^{+}H_3N$-CH(-R)-COO^{-}]

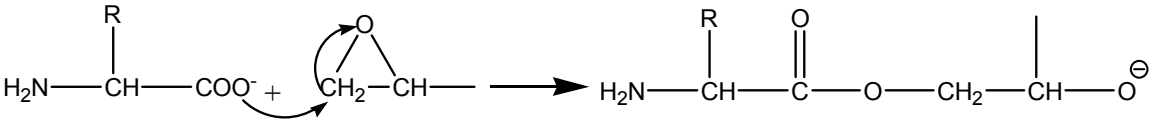

i)

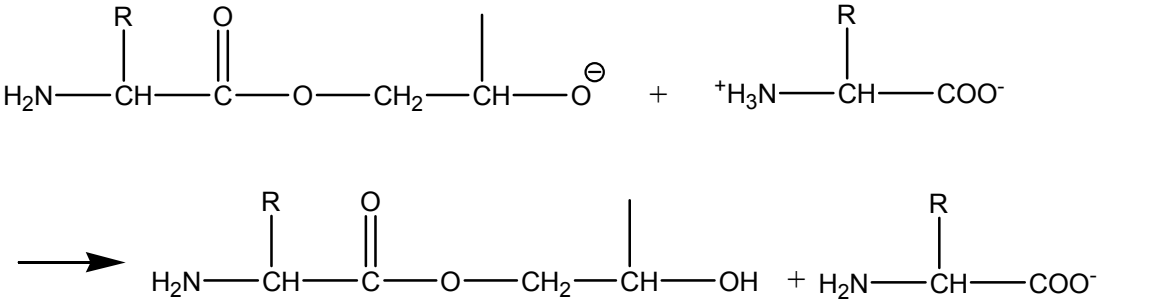

ii)

(b) Chain reaction (i→ii→i→ii…) between carboxylate anion and epoxy

Figure 5.12 Reaction mechanism of tryptophan cured epoxy, where R=

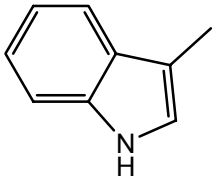

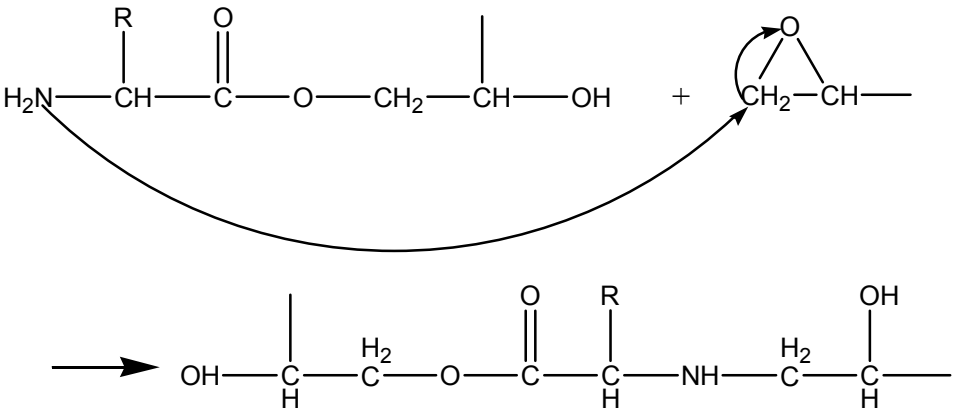

(c) Nucleophilic substitution of primary amine on epoxy

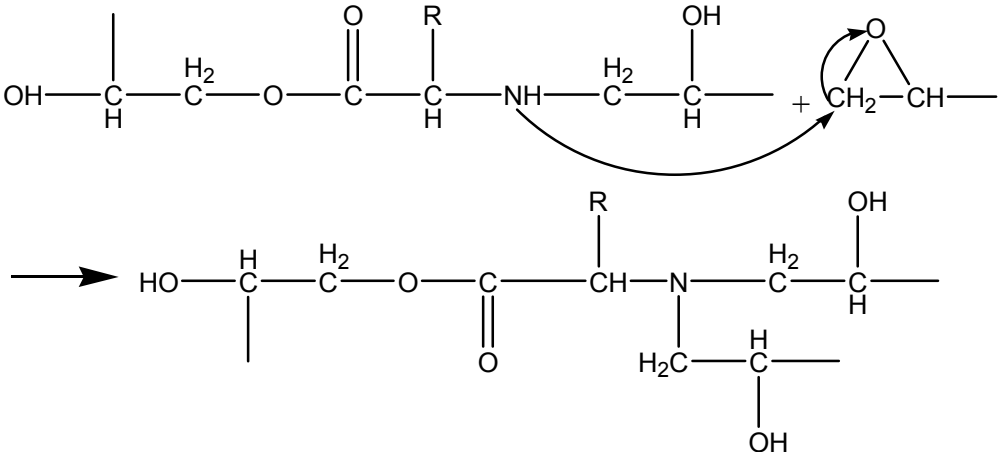

(d) Further nucleophilic substitution of secondary amine on epoxy

Figure 5.12 continued

5.3.6 Thermal stability of cured DGEBA with tryptophan

The thermal stability of tryptophan cured DGEBA with catalyst was studied by measuring the weight change of cured samples with TGA. Figure 5.13 shows the weight-

loss and derivative curves of cured samples with temperature. The weight loss of cured DGEBA/tryptophan started at ~ 284°C [temperature of 5% weight loss ($T_{5\%}$)] with the peak temperature of weight loss at 335°C, which was similar to a typical anhydride or amine cured epoxy.

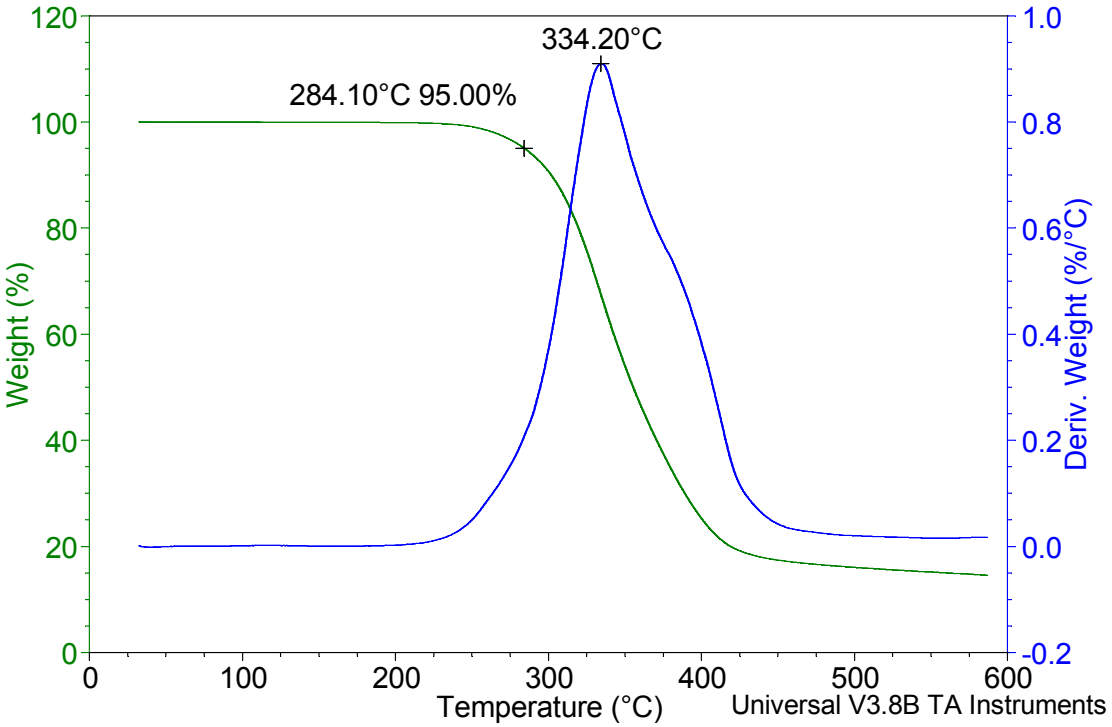

Figure 5.13 TGA curves of tryptophan-cured DGEBA

5.4 Conclusions

Novel eco-friendly curing agent – tryptophan is used in the crosslinking of diglycidyl ether of bisphenol-A (DGEBA) epoxy resin. Without catalyst, the crosslinking reaction can only be conducted at high temperatures (200^{o}C), while addition of small amount of 1-cyanoethyl-2-ethyl-4-methylimidazole (2E4MZCN) catalyst enabled a much lower reaction temperature (150^{o}C) and higher crosslinking density. With the initiation of imidazole, nucleophilic primary amine and carboxylate anions in zwitterions could readily participate in the ring opening reaction of epoxy. The secondary amine formed could further participate in the ring opening and form the crosslinked network. The crosslinked structure exhibits a reasonably high glass transition temperature (Tg) and thermal stability. A catalyst-initiated chain reaction mechanism was proposed for the curing reaction of epoxy with zwitterions amino acid. The mechanism is suitable for all zwitterions amino acid curing reaction, and therefore suggests that all amino acids, even without additional reactive functional group such as acid or base amino acids, can be used as curing agent for epoxy resin. The application of the new class of eco-friendly epoxy curing agents provides an important step toward next-generation green electronics.

CHAPTER 6
CONCLUSIONS AND SUGGESTED WORK

6.1 Conclusions

Tin-lead solder alloys are widely used in the electronic industry. They serve as interconnects that provide the conductive path required to achieve connection from one circuit element to another. There are increasing concerns with the use of tin-lead alloy solders in recognition of hazards of using lead. Electrically conductive adhesives (ECAs) have been considered as one of the most promising alternatives of tin-lead solder. ECAs consist of a polymeric resin (such as, an epoxy, a silicone, or a polyimide) that provides physical and mechanical properties such as adhesion, mechanical strength, impact strength, and a metal filler (such as, silver, gold, nickel or copper) that conducts electricity. ECAs offer numerous advantages over conventional solder technology, such as environmental friendliness, mild processing conditions (enabling the use of heat-sensitive and low-cost components and substrates), fewer processing steps (reducing processing cost), low stress on the substrates, and fine pitch interconnect capability (enabling the miniaturization of electronic devices). Therefore, conductive adhesives have been used in LCD (liquid crystal display) and smart card applications as an interconnect material and in flip-chip assembly, CSP (chip scale package) and BGA (ball grid array) applications in replacement of solder. However, no currently commercialized ECAs can replace tin-lead metal solders in all applications due to the limited interfacial properties. In order to develop high performance conductive adhesives in various lead-free components, fundamental understanding and modification of the interfacial properties of different types of conductive adhesives, such as isotropically conductive

adhesives (ICA), anisotropically conductive adhesives/films (ACA/ACF) and nonconductive adhesives/films (NCA/NCF), are of great importance.

ICA contains a high loading of conductive fillers (typically 1-10 μm sized Ag flakes fillers) above the percolation threshold and has been used in electronic packaging industry primarily as die attach adhesives. Recently, ICAs have also been proposed as an alternative to tin/lead solders in surface mount technology (SMT) applications. However, the relatively lower electrical conductivity and unstable contact resistance on non-noble metal surfaces under elevated temperature and humidity has restricted the application of ICA. The lower electrical conductivity of ICA is mainly from the polymer matrix and also the surfactant on silver flakes. The polymer matrix provides the mechanical strength and adhesion of ICA and cannot be removed. In order to improve the electrical conductivity of ICA, various types of short-chain dicarboxylic acids are introduced to *in-situ* replace or remove the surfactant (long chain fatty acid) on silver flakes. Due to the strong affinity of carboxylic acids to silver, the short-chain dicarboxylic acids could attach on silver flakes during the mixing and curing process of ICA and partially remove/replace the insulative surfactant layer. As such, it could improve the silver-silver interactions and facilitate the electrons tunnelling between silver flakes, therefore improving the electrical conductivity of ICAs.

Another critical issue of ICAs is the unstable contact resistance on non-noble metal finishes (such as Cu, Sn/Pb, Sn, Al, etc.) under elevated temperature and humidity environment (i.e. 85^{o}C/85%RH) due to galvanic corrosion. In addition to oxygen scavengers and sacrificial materials, corrosion inhibitors were used as a novel approach to stabilize the contact resistance on non-noble metal surfaces due to the relatively high

efficiency and low cost. Organic corrosion inhibitors are chemicals that adsorb on metal surfaces, and act as a barrier layer between the metal and the environment by forming a film over the metal surfaces. Efficient corrosion inhibitors can reduce the corrosion rate by virtue of interacting with metal surface and, therefore, reducing its corrosion tendency. Various types of corrosion inhibitor with either $-NH_2$ or –COOH groups were used to stabilize the contact resistance of ICA on Sn surfaces. The surface characterization of these corrosion inhibitors on Sn showed that these organic compounds could strongly attach on the Sn surface and form an efficient passivation layer. The thin passivation layer acted as a barrier between the Sn surface and environment by preventing diffusion of oxygen and moisture into the Sn pad surface. Therefore, ICA/Sn interface was effectively protected from corrosion during the elevated temperature and humidity environment, leading to a significantly improved reliability of ICA.

With the trend for high density microelectronics device, ACA/ACF has drawn more and more attention in particular for the fine-pitch capability. Actually, ACFs are already widely used for high-density interconnection between liquid-crystal display (LCD) panels and tape carrier packages (TCPs) to replace the traditional soldering or rubber connectors. In LCD applications, traditional soldering may not be as effective as ACFs in interconnecting materials between indium tin oxide (ITO) electrodes and TCP. Recently, ACFs have also been used as an alternative to soldering for interconnecting TCP input lead bonding to printed-circuit boards (PCBs). However, ACA/ACF joints tend to have lower electrical conductivity and poor current carrying capability because there is only mechanical/physical contact of the joints and no metallurgical contact of interconnects. To ensure low contact resistance and high current density, interface

between conductive fillers and electrode should be improved. One of the approaches to minimize the resistance at the interface was to study the nano-silver sintering behavior at the processing temperature of ACA/ACF and incorporate the sintered nano particles into the ACA/ACF formulations. For the nano-silver particles, due to the high surface area and surface energy, the particles could be sintered at a much lower temperature than the typical melting temperature of bulk silver particles. With sintering, the nano-silver particles could fuse with each other through their surfaces and decrease the number of interfaces between particles. Therefore, the joint resistance was significantly reduced with improved current carrying capability.

Another approach to improve the interfacial properties of ACAs was the introduction of self-assembled monolayer (SAM) on the interface between the metal particles and between the ECA/metal bond pads. An important consideration when examining the advantages of organic monolayers pertains to the affinity and thermal stability of organic compounds to specific metal surfaces. By investigating the affinity and thermal stability of SAMs with various functional groups and chain structures, different types of SAMs were used in ACA and ACF formulations with different metal fillers. The electrical property of ACAs with micron-sized Au/polymer filler improved obviously for low curing temperature curable formulation with treated conductive fillers and treated bond pad. However, the improvement was not obvious for high curing temperature ACAs. With the introduction of SAM-treated nano Ag fillers and metal bond pads in the nano-Ag ACAs, on the other hand, the electrical conductivity and current carrying capability of ACAs were enhanced significantly even at relatively high curing temperature. The improved interfacial properties of nano Ag ACA with SAM through the

metal-polymer and metal-metal filler interactions also contributed to the increased thermal conductivities of the ACAs.

In the Ag-filled conductive adhesives, silver migration under bias is always a major concern which can result in an electrical short circuit. In order to control the silver migration, the nano-silver particles were protected with different types of organic monolayers. Formation of surface complex between the carboxylate anion and surface silver ion reduces the solubility and diffusitivity significantly of migration components and therefore contributes to effective migration control. The control of silver migration enables the application of the silver composites in fine pitch and high performance electronic device interconnects.

In addition to ICA and ACA, recently NCA/NCF is considered as a low-cost option for flip chip assemblies and fine pitch interconnections. For NCA/NCF joints, contacts between the bottom and top surfaces lead to the electrical conduction. NCA/NCF requires no conductive fillers, but needs a relatively high pressure for bonding between the IC chip and the substrate coupled with heat. During bonding, the heat and pressure are applied and the direct physical contacts between the two surfaces of the IC bump and the substrate bond pad can be achieved. The electrical contact resistance of an NCA/NCF joint is controlled by the processing pressure, surface roughness and NCA/NCF material properties. A micromechanical model was developed to study the electrical conductance of NCA/NCF assembly. Analytical expressions were obtained for both constriction and tunnel resistance. Modeling results showed that the constriction resistance was negligible compared to tunnel resistance. Tunnel resistance is dependent on the material properties (dielectric constant and electron-injection barrier) and the

processing pressure. Model results also demonstrated that electron-injection barrier played a much more important role in controlling the tunnel resistivity, compared to the effect of dielectric constant.

To verify the model and reduce the joint resistance, conjugated molecular wires were introduced at the interface of NCF joints. The molecular wires could adsorb on the gold electrodes and improve the interface properties. Formation of electrical junction with molecular wires between Au electrodes could tune the effective work function (Φ) of Au electrodes. The lower work function reduced the tunnel resistivity and thus improving the electrical conduction significantly. Improvement of electrical performance of NCF will enable the application of NCF in fine pitch and high performance interconnects in microelectronics.

6.2 Suggested work

The previous study on the electrically conductive adhesives focused on the fundamental understanding of the materials, processing and applications and the improvement of the electrical and thermal properties for high performance lead-free interconnect applications. In order to achieve the enhanced interfacial properties, organic surface modifiers/molecular wires and nano-conductive fillers were the major approaches. However, as the filler size decreases into the nano region, the dispersion, rheological, mechanical and thermal mechanical properties of the composites change significantly. The nano particles are usually not uniformly dispersed in the polymer matrix and tend to be agglomerated, which limits the fine pitch capability of the composite in spite of the small particle used. The nano particles also can affect the

rheology and increase the viscosity of the composite which is important for the processability of ECAs. Therefore, there is a need to fundamentally understand the interaction between nano conductive fillers and polymer matrix in various types of ECAs. In addition, fundamental understanding of electrical and thermal properties of the organic modifiers/molecular wires as electrical junctions is of great importance as well. The following work is suggested to develop a high performance, high reliability, low cost and environmentally friendly conductive adhesive for high power lead-free electronics.

6.2.1 *In-situ* formation of the nano particles in the polymer matrix

An alternative approach to prepare the nano-composite is the *in-situ* formation of nano-conductive particles in the polymer matrix by decomposition or chemical reduction of a metallic precursor dissolved into the polymer. By controlling the materials (such as polymer matrix, reducing agents, solvents, type and mount of capping agents, etc.) and processing conditions (such as processing temperature, time, pressure, etc.), the particles with desired size and distribution should be obtained with more uniform dispersion and less agglomeration. The *in-situ* formed nano-conductive adhesives can be used for ultra-fine pitch interconnect applications.

6.2.2 Systematic investigation of various conjugated self-assembled monolayer (SAM) on metal surfaces

This thesis utilized several types of SAM compounds such as aliphatic and aromatic thiols and carboxylic acids to enhance the electrical properties of ECAs. In order to achieve better electrical conductance and higher current carrying capabilities for various ECA systems and metal bond pad, it is necessary to systematically investigate different types of π-conjugated self-assembled molecules to identify the best SAMs and

fine tune the processing conditions. It is also necessary to study the adherence, alignment configurations and thermal behaviors of the π-conjugated self-assembled molecules on different metal surfaces and particles with different sizes and shapes. Effects of different the π-conjugated self-assembled molecules on the interfacial properties, electrical junctions and energy-level of electrodes need to be further clarified.

6.2.3 Development of High performance, low cost, oxide free Cu-filled ECAs

Currently, the most widely used conductive fillers for ECAs are noble metals, such as Au or Ag. However, the high cost of these noble metals has significantly increased the cost of ECA, compared to solder materials. In order to develop the low cost ECAs, copper can be a promising candidate for conductive filler due to its low resistivity, low cost and improved electromigration performance. However, copper particles are easily oxidized and cause this metal to lose its conductivity. It is challenging but necessary to remove the copper oxide and prevent the copper oxidation during processing, curing and reliability conditions for the development of low-cost and high performance Cu-based ECAs. Two approaches could be considered for surface treatment on copper fillers in ECAs. One is inorganic material coating by electro or electroless deposition with silver, gold and nickel/gold and solder materials (Sn, InSn, etc), and the other one is organic material coating with azole, thiol compound, silane coupling agent or organosilicic compound etc. Typically, Cu fillers already possess oxides, so the procedure should include the elimination of oxide followed by the effective coating.

6.2.4 Wafer level lead-free interconnect and packaging

Wafer level packaging (WLP) has become more and more popular because it can increase the silicon efficiency, reduce the packaging size and achieve “true” chip scale

packaging. For the ACF assembly process, the ACF could also potentially be applied on the wafer level before dicing as shown in Figure 6.1. This will eliminate the dispensing step in the component level and thus makes the ACF interconnect compatible with standard thermo-compression assembly process.

Figure 6.1 Wafer level ACF process compared to the conventional ACF process

The WLACF provides a lead-free and fine-pitch-capable interconnect, as well as a wafer level package to protect the wafer during test and burn-in. The cost of packaging can be dramatically reduced because it avoids the solder bumping process, combines interconnect and encapsulation, and enables wafer level test and burn-in. After the chip assembly, the ACF layer also acts as an underfill to redistribute the thermo-mechanical stress generated from the CTE mismatch between the chip and the substrate. Wafer level

ACF could combine the concepts of conductive adhesives and the underfill, providing the electrical conductivity and the mechanical enhancement at the same time. Through the thermo-mechanical modeling and the tailoring of polymer chemistry and filler technology, optimized material properties for enhanced reliability can be achieved in the case of low k dies, thinned dies, large and small dies, respectively.

APPENDIX A

AUTHOR'S AWARDS, PATENTS, AND PUBLICAITONS

A.1 Awards

[1] Best Session Paper Award, "Formation of Self-assembled Monolayer (SAM) on Metal Surfaces for High Performance Anisotropically Conductive Adhesives", IEEE 9th International Symposium on Advanced Packaging Materials: Process, Properties, and Interfaces, Nano Materials Session (2004)

[2] Best Session Paper Award, "A Novel Technique for Lead-Free Soldering Using Variable Frequency Microwave (VFM)" IEEE 9th International Symposium on Advanced Packaging Materials: Process, Properties, and Interfaces, in Lead- free Alloy Session (2004).

[3] NaST (Nanoscience and Technology) Scholarship, 2004-2006, Georgia Institute of Technology

[4] Best paper award, "Novel Nanotechnology for Environmentally Friendly Interconnect Materials in Microelectronic Packaging Applications", 2006 IEEE International Symposium on Electronics and the Environment.

[5] Best Paper Award in Symposium V (Advanced Electronics Packaging), 2006 MRS (Materials Research Society) Fall Meeting

[6] Graduate Student Silver Award, 2006 MRS (Materials Research Society) Fall Meeting

[7] Chinese Government Award for Outstanding Self-Financed Students Abroad, 2006

[8] Advanced Publication Award, School of Materials Science and Engineering, Georgia Institute of Technology (2006)

[9] Initiation Publication Award, School of Materials Science and Engineering, Georgia Institute of Technology (2006)

[10] Advanced Publication Award, School of Materials Science and Engineering, Georgia Institute of Technology (2007)

[11] Finalist for the 15th Motorola-IEEE/CMPT Fellowship at 57th Electronic Component & Technology Conference, 2007

A.2 Patents

[1] Y. Li, K. Moon, C.P. Wong, "Innovative Corrosion Inhibitors for ECAs on Leadfree Surfaces." U.S. Patent pending, GTRC Invention No. 3281. (2004), filed on 10/18/2005, serial number 11/252,371.

[2] Y. Li, K. Moon, C.P. Wong, "Aldehydes for High Performance ECAs", U.S. Patent pending, GTRC Invention No. 3240 (2004), filed on 10/14/2005, serial number 11/251,240

[3] Y. Li, M. J. Yim, K. Moon, and C. P. Wong, "Introduction of Self Assembled Monolayer in Electrically Conductive Adhesive Joints to Enhance Electrical Current Carrying Capability and Electrical Stability", U.S. Patent pending, GTRC Invention No. 3975 (2006)

[4] Y. Li, and C. P. Wong, "Metal migration control in conductive adhesives by incorporation of organic monolayers for fine pitch, high reliability, high voltage and lead-free interconnects", U.S. Patent pending, GTRC Invention No. 3642 (2005) Provisional patent filed on May 30, 2006.

[5] Y. Li, Z. Zhang, K. Moon, C.P. Wong, "Ultra-Fine Pitch Wafer Level ACF (Anisotropic Conductive Film) Interconnect by in-situ formation of nano fillers with High Current Carrying Capability" U.S. Patent pending, GTRC Invention No. 3330., provisional patent filed on March 7, 2006.

A.3 Book Chapters

[1] Y. Li and C.P. Wong, "Electrical Conductive Adhesives for Electronics Packaging Interconnects-A Lead-Free Alternative" The World of Electronic Packaging and System Integration, Edit. By Bernd Michel, ddp goldenbogen 2004, Dresden, Germany publisher, 66-76.

[2] Y. Li and C. P. Wong, Chapter 11 "Anisotropic Conductive Film (ACF) for Advanced Microelectronic Interconnects" in Dielectric Films for Advanced Microelectronics, Edit by K. Maex, M. R. Baklanov, M. Green, 2007, John Wiley & Sons. Ltd. p. 453-475.

[3] Y. Li and C. P. Wong, Chapter 22 "Recent Advances of Conductive Adhesives: A Lead-free Alternative in Electronic Packaging" in Physics and Mechanics of Polymers for Electronic and Photonics, Edit by E. Suhir, C. P. Wong and Y.C. Lee, 2007, Springer, p. 611-627.

A.4 Journal Publications

[1] S. Pothukuchi, Y. Li, C. P. Wong, "Development of a novel polymer-metal nanocomposite obtained through the route of in situ reduction for integral capacitor application", J. Appl. Polym. Sci., 93-4 (2004) 1531-1538

[2] K. Moon, H. Dong, R. Maric, S. Pothukuchi, A. Hunt, Y. Li, C. P. Wong, "Thermal Behavior of Silver Nanoparticles for Low-temperature Interconnect Application", J. Electron. Mater, 34-2 (2005) 132-139.

[3] Y. Li, K. Moon and C. P. Wong, "Adherence of Self-Assembled Monolayers on Gold and their Effects for High Performance Anisotropic Conductive Adhesives", J. Electron. Mater, 34-3 (2005) 266-271.

[4] Y. Li, K. Moon and C. P. Wong, "Electronics without Lead", Science, 308 (2005) 1419-1420.

[5] K. Moon, Y. Li, J. Xu, and C.P. Wong, "Lead-Free Interconnect Technique by Using Variable Frequency Microwave (VFM)", J. Electron. Mater. 34-7 (2005) 1081-1088.

[6] H. Chiang, C. Chung, L. Chen, Y. Li, C. P. Wong and S. Fu, "Processing and Shape Effects on Silver Paste Electrically Conductive Adhesives (ECAs)", J. Adhes. Sci. Technol., 19 (7), (2005) 565-578.

[7] Y. Li, K. Moon, and C. P. Wong, "Monolayer Protected Silver Nano-particle Based Anisotropic Conductive Adhesives (ACA): Electrical and Thermal Properties Enhancement", J. Electron. Mater., 34-12 (2005) 1573-1578.

[8] Y. Li, K. Moon, and C. P. Wong, "Reliability Improvement of Conductive Adhesives on Tin (Sn) Surfaces", J. Adhes. Sci. Technol.,19-16 (2005) pp. 1427-1444.

[9] Y. Li, K. Moon and C. P. Wong, "Electrical Property Improvement of Electrically Conductive Adhesives through in- situ Replacement by Short-Chain Difunctional Acids", IEEE Trans. Compon. Packaging Technol., 29-1 (2006) 173-178.

[10] Y. Li, K. Moon, and C. P. Wong, "Enhancement of Electrical Properties of Anisotropically Conductive Adhesive (ACA) Joints via Low Temperature Sintering", J. Appl. Polym. Sci., 99-4 (2006) 1665-1673.

[11] Y. Li, F. Xiao, K. Moon and C. P. Wong, "A novel curing agent for lead-free electronics: amino acid", J. Polym. Sci. Pol. Chem, 44 (2006) 1020-1027.

[12] Y. Li and C. P. Wong, "Recent advances of conductive adhesives as a lead-free alternative in electronic packaging: materials, processing, reliability and applications", Mat. Sci. Eng. R., 51 (2006) 1-35.

[13] H.J. Jiang, K. Moon, Y. Li, C. P. Wong, "Surface Functionalized Silver Nanoparticles for Ultrahigh Conductive Polymer Composites", Chem. Mat., 18-13 (2006) 2969-2973.

[14] Y. Li and C. P. Wong, "High performance anisotropic conductive adhesives for lead-free interconnects", Solder. Surf. Mt. Technol.,18-2 (2006) 33-39.

[15] Y. Li, and C. P. Wong, "Monolayer-Protection for Eletrochemical Migration Control in Silver Nano composite", Appl. Phys. Lett., 89 (2006) 112112.

[16] Y. Li, K. Moon, A. Whitman, and C. P. Wong, "Enhancement of Electrical Properties of Electrically Conductive Adhesives (ECAs) by Using Novel Aldehydes", IEEE Trans. Compon. Packaging Technol., 29-4 (2006) 758-763.

[17] Y. Li, F. Xiao, and C. P. Wong, "Novel Environmentally Friendly crosslinking system of epoxy using amino acid- Tryptophan-cured Diglycidyl ether of bisphenol-A epoxy", J.Polym. Sci. Pol. Chem,, 45 (2007) 181-190.

[18] H. Dong, Y. Li, M. J. Yim, K. Moon, and C. P. Wong, "Investigation of electrical contact resistance for nonconductive film functionalized with π-conjugated self-assembled molecules", Appl. Phys. Lett.,90 (2007) 092102.

[19] Y. Li, M. J. Yim, and C. P. Wong, "High Performance Nonconductive Film with π-Conjugated Self-Assembled Molecular Wires for Fine Pitch Interconnect Applications", J. Electron. Mater., 36-5 (2007) 549-554.

[20] C. Lao, Y. Li, C. P. Wong, Z. L. Wang, "Enhancing the Electrical and Optoelectronic Performance of Nanobelt Devices by Molecular Surface Functionalization", Nano Letters, 7-5 (2007) 1323-1328.

[21] M. J. Yim, Y. Li, K. Moon, and C. P. Wong, "Oxidation Prevention and Electrical Properties Enhancement of Copper-filled Isotropically Conductive Adhesives", J. Electron. Mater. 36-10 (2007) 1341-1347.

[22] Y. Li, M. J. Yim, K. Moon, and C. P. Wong, "Novel Nano-scale Conductive Films with Enhanced Electrical Performance and Reliability for High Performance Fine Pitch Interconnect", IEEE Trans. Adv. Packaging., submitted (2007).

REFERENCES

[1] R. R. Tummala, E. J. Rymaszewski, and A. G. Klopfenstein, Microelectronics Packaging Handbook. Part II, Second ed. Norwell: Kluwer Academic Publishers, 1997.

[2] J. H. Lau, Chip on Board Technologies for Multichip Modulues. New York: Van Nostrand Reinhold, 1994.

[3] R. R. Tummala and V. Madisetti, "System on Chip or System on Package," IEEE Design and Test of Computer, vol. 4, pp. 48, 1999.

[4] P. T. Vianco, in: K. J. Puttlitz, K. A. Stalter (Eds), Handbook of Lead-free solder Technology for Microelectronic Assemblies, Marcel Dekker, Inc, New York, U.S.A, 2004, pp.167-210.

[5] M. Abet and G. Selvaduray, Materials Science & Engineering, 27 (2000) 95-141.

[6] RoHS Regulations (UK) Government guidance notes, August 2005.

[7] J. Cannis, Green IC packaging, Advanced Packaging 8 (2001) 33-38.

[8] C.M.L. Wu, D.Q. Yu, C.M.T. Law, L. Wang, Mater. Sci. Eng. R 44 (2004) 1–44.

[9] J. S. Hwang, (Ed.) Environment-Friendly Electronics: Lead-free Technology, Electrochemical Publications Ltd., Port Erin, UK, 2001; Chapter 1.

[10] J. Lau, C. P. Wong, N. C. Lee, S. W. R. Lee, in Electronics Manufacturing: with Lead-Free, Halogen-Free, and Conductive-Adhesive Materials; McGraw Hill, New York, NY, 2002.

[11] J. Liu, (Ed.) Conductive adhesives for Electronics Packaging (Electrochemical Publications Ltd.Isle of Man, British Isles, 1999).

[12] A. Z. Miric and A. Grusd, Soldering and Surface Mount Technology, 10 (1998) 19-25.

[13] C. Andersson, Z. Lai, J. Liu, H. Jiang, Y. Yu, Materials Science & Engineering, A: Structural Materials: Properties, Microstructure and Processing A 394 (1-2) (2005) 20-27.

[14] K. J. Puttlitz, K. A. Stalter (Eds), Handbook of Lead-free solder Technology for Microelectronic Assemblies, Marcel Dekker, Inc, New York, U.S.A, 2004, pp.211-300.

[15] K. Chen and K. Linz, IEEE Proceedings of the 4th International Symposium on Electronic Materials and Packaging, Dec. 406, 2002, pp. 49-54.

[16] C. T. Murray, R. L. Rudman, M. B. Sabade, A. V. Pocius, Mater. Res. Bull., 28 (2003) 449-454.

[17] E.P. Wood and K.L. Nimmo, J. Electron. Mater. 23 (8) (1994) 709-714.

[18] Environmental Protection Agency, National Air Quality and Emission Trend Report, 1989, EPA-450/4-91-003, Research Triangle Park, NC, 1991.

[19] J. Liu, Materials Technology, 10 (11/12) (1995) 247-252.

[20] H. Kristiansen, J. Liu, IEEE Transactions on Components, Packaging, and Manufacturing Technology, Part A, 21 (2) (1998) 208-214.

[21] K. Gilleo, in: J. S. Hwang (Ed), Environment-Friendly Electronics: Lead-free Technology, Electrochemical Publications Ltd., Port Erin, UK, 2001, Chapter 24.

[22] G. Nguyen, J. Williams, F. Gibson, and T. Winster, Proceedings of International Electronic Packaging Conference, 1993, pp. 479-486.

[23] M.A. Gaynes, R.H. Lewis, R.F. Saraf and J.M. Roldan, IEEE Transactions on Components, Packaging, and Manufacturing Technology, Part B, 18-2 (1995) 299-304.

[24] L. Li, J. E. Morris, J. Liu, Z. Lai, L. Ljungkrona, C. Li, Proceedings of the 45th IEEE Electronic Components and Technology Conference, May 21-24, 1995 pp. 114 - 120.

[25] D. Cavasin, K.Brice-Heams, and A.Arab, in Proc. 53rd Electronic Components and Technology Conf. , 2003, pp.1404~1407

[26] R. Kisiel, J. of Electronic Packag., 124, 367 (2002)

[27] H. de Vries, J. van Delft, and K. Slob, IEEE Trans. on Comp. and Packag. Technol. 28 (2005) 499.

[28] M. A. Lutz, R. L. Cole, Hybrid Circuits, 23 (1990) 27-30.

[29] J. M. Pujol, C. Prudhomme, M. E. Quenneson, R. Cassat, Journal of Adhesion, 27 (1989) 213-229.

[30] V. Krishnamurthy, K. Paik, D. Lester, International Society for Hybrids and Microelectronics Society (ISHM), '92 Proceedings, 1992, pp. 719-724.

[31] J. Ivan, J. Gonzales, M. G. Mena, Proceedings of the 47th IEEE Electronic Components and Technology Conference, May 18-21, 1997, pp. 525-535.

[32] J. Liu, Z. Lai, H. Kristiansen, C. Khoo, in Proc. 3rd Int'l Conf. on Adh. Join. & Coat. Tech. in Electr. Manuf., Binghamton, NY, 1998, pp.1-17.

[33] J. Liu, Circuit World, 19 (1993) 4.

[34] J. Liu, Soldering & Surface Mount Tech., 13 (2001) 39.

[35] K. Gilleo, Soldering & Surface Mount Tech., 19 (1995) 12.

[36] S. Lim, P. Siang, T. A. Min, C. Lee, Proceedings of the 54th Electronic Components and Technology Conference, June 1-4, 2004, pp. 450-454.

[37] J. Liu, J. E. Morris, American Society of Mechanical Engineers 27th Workshop on Polymeric Materials for Microelectronics and Photonics Applications: Mechanics, Physics, Reliability, Processing, 1999, 259-281.

[38] I. Watanabe et al., In Proc. Asia Display/IDW, 2001, pp. 553~556.

[39] H. Nishida, K. Sakamoto, and H. Ogawa, IBM J. Research and Development, 42 (1998) 517.

[40] D. J. Williams et al., Soldering & Surface Mount Tech., 4 (1993).

[41] J. Liu, A. Tolvgard, J. Malmodin, and Z. Lai, IEEE Trans. Comp. Packag., Manufact. Technol., 22, (1999) 186.

[42] P. Clot, J. F. Zeberli, J. M. Chenuz, F. Ferrando, and D. Styblo, in Proc. Electronics Manufac. Technol. Symp., 24th IEEE/CPMT, 1999, pp. 36.

[43] R. Joshi, Microelec. Journal, 29 (1998) 343.

[44] I. Watanabe, K. Takemura, N. Shiozawa, and T. Ohta, in Flip Chip Technologies, edited by John H. Lau, McGraw Hill, 1996, Chapter 9,.

[45] M.J. Yim, J.S.Hwang, and K.W.Paik, Int'l J. Adhesion and Adhesives, 26, (2006) 304.

[46] J. Pajonk, Proceedings of IEEE/CPMT/SEMI the 29th International Electronics Manufacturing Technology Symposium, July 14-16, 2004, pp.165-170.

[47] F. Ferrando, J. Zeberli, P. Clot, and J. Chenuz, Proceedings of the 4th IEEE International Conference on Adhesive Joining and Coating Technology in Electronics Manufacturing, June 18-21, 2000, pp. 205-211.

[48] S. Ito, M. Mizutani, H. Noro, M. Kuwamura, and A. Prabhu, Proceedings of the 48th IEEE Electronic Components and Technology Conference, May 25028, 1998, pp.1047-1051.

[49] J. Caers, X. Zhao, E. Wong, C. Ong, Z. X. Wu, and R. Ranjan, Proceedings of the 53rd IEEE Electronic Components and Technology Conference, May 2-30, 2003, pp. 1176-1180.

[50] R. D. Pendse, K-M Kim and S. Tam, Proceedings of the 52nd IEEE Electronic Components and Technology Conference, May 28-31, 2002, pp. 100-104.

[51] H. Yu, S. G. Mhaisalkar, E. H. Wong, J. Mater. Res., 20 (2005) 1324-1329.

[52] L. K. The, E. Anto, C. C. Wong, S. G. Mhaisalkar, E. H. Wong, P. S. Teo, Z. Chen. Thin Solid Films, 462 (2004) 446-453.

[53] M-J Yim, J-S Hwang, W. Kwon, K. W. Jang, K-W Paik, IEEE Transactions on Electronics Packaging Manufacturing, 26-2 (2003) 150-155.

[54] "Assembly and Packaging," Semiconductors, 2004.

[55] D. Lu, Q.K. Tong, and C.P. Wong, IEEE Transactions on Components, Packaging, and Manufacturing Technology, Part C, 22 (1999) 223-227.

[56] C. Gallagher, G. Matijasevic, and J.F. Maguire, Proceedings of 47th IEEE Electronic Components and Technology Conference, May 18-21, 1997, pp.554-560.

[57] J.W. Roman and T.W. Eagar, Proceedings of the International Society for Hybrids and Microelectronics Society (San Francisco, CA), Oct. 1992, p.52.

[58] L. Smith-Vargo, Electronic Packaging & Production, August 1986, pp. 48-49.

[59] E.M. Jost and K. McNeilly, Proceedings of International Society for Hybrids and Microelectronics Society 1987, pp. 548-553.

[60] S. M. Pandiri, Adhesives Age, Oct. 1987, pp. 31-35.

[61] D. Lu, Q.K. Tong, and C.P. Wong, IEEE Transactions on Components, Packaging and Manufacturing Technology, Part A, 22-3 (1999) 365-371.

[62] H. Botter, Proc. of the 2nd International Conference on Adhesive Joining & Coating Technology in Electronics Manufacturing, Stockholm, Sweden, 30-37 (1996).

[63] C.P. Wong, D. Lu, S. Vona, and Q.K. Tong, Proc. of the 1st IEEE International Symposium on Polymeric Electronics Packaging, Norrkoping, Sweden, 1997, pp. 80-85.

[64] M. Zwolinski, J. Hickman, H. Rubon, and Y. Zaks, Proc. of the 2nd International Conference on Adhesive Joining & Coating Technology in Electronics Manufacturing, Stockholm, Sweden, 1996, pp. 333-340.

[65] D. Lu, Q.K. Tong, and C.P. Wong, IEEE Transactions on Components, Packaging, and Manufacturing Technology, Part C, 1999, Vol. 22, No. 3 (1999) 228-232.

[66] K. Persson, A. Nylund, J. Liu and I. Olefjord, Proceedings of the 7th European Conference on Applications of Surface and Interface Analysis, Gothenburg, June 1997.

[67] H. Leidheiser, Jr., J. Coatings Technol., 53 (1981) 29.

[68] P.A. Reardon, Corrosion ’86, Paper no. 175, The National Association of Corrosion Engineers (NACE), Houston, TX, 1986.

[69] M.G. Noack, Corrosion’89, Paper no. 436, The National Association of Corrosion Engineers (NACE), Houston, TX, 1989.

[70] P.A. Reardon and W.E. Bernahl, Corrosion’87, Paper no. 438, The National Association of Corrosion Engineers (NACE), Houston, TX, 1987.

[71] S. Romaine, Proceedings of the American Power Conference, (Chicago, IL), April 1986, pp. 1066-1073.

[72] H. Li, K. Moon, and C.P. Wong, Journal of Electronic Materials, 33 (2004) 106-113.

[73] H. Takezawa, T. Mitani, T. Kitae, H. Sogo, S. Kobayashi and Y. Bessho, Proceedings of 8th IEEE International Symposium on Advanced Packaging Materials: Processes, Properties and Interfaces, Atlanta, GA, March 3-6, 2002, pp. 39-143.

[74] K. Moon, S. Liong, H. Li, C.P. Wong, Journal of Electronic Materials, 33-2 (2004) 1381-1388.

[75] C. Cheng, G. Fredrickson, Y. Xiao, Q. K. Tong and D. Lu, US Patent No. 6,344,157 (2002).

[76] G. Trabanelli and V. Carassiti, in: G. Fontana and R. W. Staehle (Eds), Advanced Corrosion Science and Technology, M.. Plenum Press, New York, NY, 1970, Vol. 1, pp. 147–229

[77] G. Trabanelli, in: F. Mansfeld (Ed.), Corrosion Mechanisms, Marcel Dekker, New York, 1987, pp. 119–164.

[78] O. L. Riggs, Jr., in: C. C. Nathan (Ed.), Theoretical Aspects of Corrosion Inhibitors and Inhibition, The National Association of Corrosion Engineers (NACE), Houston, TX (1973) pp. 2–27.

[79] L. J. Matienzo, F. D. Egitto and P. E. Logan, J. Mater. Sci. 38 (2003) 4831–4842.

[80] L. Allen, R.A. Bayles, W.W. Gile and W.A. Jesser, "Small Particle Melting of Pure Metals", Thin Solid Film, 144 (1986) 297.

[81] K. Moon, H. Dong, R. Maric, S. Pothukuchi, A. Hunt, Y. Li, C. P. Wong, J. Electronic Materials, 34 (2005) 132-139.

[82] Y. Matsuba, Erekutoronikusu Jisso Gakkaishi. , 6 (2) (2003) 130-135.

[83] M. Y. Efremov, F. Schiettekatte, M. Zhang, E. A. Olson, A. T. Kwan, R. S. Berry, L. H. Allen, Physical Review Letters, 85 (2000) 3560-3563.

[84] A. Ulman, Chem. Rev. 96 (1996) 1533-1554.

[85] J. Christopher Love, L. A. Estroff, J. K. Kriebel, R. G. Nuzzo, and G. M. Whitesides, Chem. Rev. 105 (2005) 1103-1169.

[86] G. E. Poirier, E. D. Pylant, Science 272 (1996) 1145.

[87] R. G. Nuzzo, D. L Allara, J. Am. Chem. Soc. 105 (1983) 4481.

[88] M. D. Porter, T. B. Bright, D. L. Allara, C. E. D. Chidsey, J.Am. Chem. Soc. 109, (1987) 3559.

[89] L. H. Dubois, R. G. Nuzzo, Annu. Rev. Phys. Chem. 43 (1992) 437.

[90] C. D. Bain, J. Evall, G. M.Whitesides, J. Am. Chem. Soc. 111 (1989) 7155.

[91] C. D. Bain, G. M. Whitesides, Science 240 (1988) 62.

[92] P. E. Laibinis, G. M. Whitesides, D. L. Allara, Y. T. Tao, A. N. Parikh, R. G. Nuzzo, J. Am. Chem. Soc. 113 (1991) 7152.

[93] L. H. Dubois, B. R. Zegarski, R. G. Nuzzo, J. Chem. Phys. 98 (1993) 678.

[94] F. Schreiber, Prog. Surf. Sci. 65 (2000) 151.

[95] G. E. Poirier, Chem. Rev. 97 (1997) 1117.

[96] Y.T. Tai, J. Am. Chem. Soc. 115 (1993) 4350-4358.

[97] N. E. Schlotter, M. D. Porter, T. B. Bright, D. L. Allara, Chem. Phys. Lett. 132 (1986) 93.

[98] Y. T. Tao, M. T. Lee, S. C. Chang, J. Am. Chem. Soc., 115 (1993) 9547.

[99] M. G. Samant, C. A. Brown, J. G, Gordon II, Langmuir, 9 (1993) 1082-1085.

[100] S. W. Joo, S. W. Han, H. S. Han and K. Kim, J. Raman Spectrosc. 31 (2000) 145-150.

[101] M. Moskovits and J. S. Suh, J. Am. Chem. Soc., 107 (1985) 6826-6829.

[102] K. Bandyopadhyay, V. Patil, K. Vijayamohanan, and M. Sastry, Langmuir, 13 (1997) 5244-5248.

[103] G. Davies and J. Sandstrom, Circuits Mfg., Oct. 1976. pp. 56-62.

[104] G. Harsanyi and G. Ripka, Electrocomp. Science And Tech., 11 (1985) 281-290.

[105] G. D. Giacomo, in: J. McHardy and F. Ludwig (Eds), Electrochemistry of semiconductors and electronics: Processes and Devices, Noyes Publications Park Ridge, N.J., U.S.A. 1992, Chapter 6, pp. 255-295.

[106] R. Manepalli, F. Stepniak, S. A. Bidstrup-Allen, P. A. Kohl, IEEE Transactions on Advanced Packaging, 22 (1999) 4-8.

[107] G. D. Giacomo, Reliability of Electronic Packages and Semiconductor Devices, McGraw-Hill, New York, NY, U.S.A 1997, Chapter 9.

[108] R. Wassink, Hybrid Circ. no. 13, May 1987, pp. 9-13.

[109] Shirai, Y.; Komagata, M.; Suzuki, K., 1st International IEEE Conference on Polymers and Adhesives in Microelectronics and Photonics, 21-24 Oct. 2001, pp.79 – 83.

[110] A. Der Marderosian, Ratheon Co. Equipment Division, Equipment Development Laboratories, pp. 134-141.

[111] H. Schonhorn, L. H. Sharpe, Prevention of surface mass migration by a polymeric surface coating. US Patent 4377619 (1983).

[112] V. Brusic, G. S. Frankel, J. Roldan, R. Saraf, Journal of the Electrochemical Society, 142 (1995) 2591-2594.

[113] P-I Wang, T-M Lu, S. P. Murarka, R. Ghoshal, US Patent No. 20050236711 (2005).

[114] J. H. Cho, J. A. Lim, J. T. Han, H. W. Jang, J-L Lee, K. Cho, Appl. Phys. Lett. 86 (2005) 171906.

[115] G. Parthasarathy, P. E. Burrows, V. Khalfin, V. G. Kozllov, S. R. Forrest, Appl. Phys. Lett. 72 (1996) 2138.

[116] Y. Hirose, A. Kahn, V. Aristov, P. Soukiassian, Appl. Phys. Lett. 68 (1996) 217.

[117] P. G. Piva, G. A. Dilabio, J. L. Pitters, J. Zikovsky, M. Rezeq, S. Dogel, W. A. Hofer, R. A. Wolkow, Nature 435 (2005) 658.

[118] B. de Boer, A. Hadipour, M. M. Mandoc, T. van Woudenbergh, P. W. M. Blom, Adv. Mater. 17 (2005) 621-625.

[119] M. J. Yim, W. Ryu, Y. D. Jeon, J. Lee, S. Ahn, J. Kim and K. W. Paik, IEEE Transactions on Component and Packaging Technology, 22(4) (1999) 575-581.

[120] R. Holm, In Electrical Contacts, 1967, New York: Springer

[121] M. Chin, K.A. Iyer, and S.J. Hu, IEEE Trans. Compon. Packaging Technol. 27 (2) (2004) 317-326.

[122] L. Kogut, and K. Komvopoulos, J. Appl. Phys. 95 (2) (2004) 576-585.

[123] T. Dadosh, Y. Gordin, R. Krahne, I. Khivrich, D. Mahalu, V. Frydman, J. Sperling, A. Yacoby, I. Bar-Joseph, Nature 436 (2005) 677-680.

[124] C. Joachim, J. K. Gimzewski, A. Aviram, Nature 408 (2000) 541-548.

[125] Q. Sun, A. Selloni, G. Scoles, J. Phys. Chem. B 110 (2006) 3493-3498.

[126] Y-H Kim, S. S. Jang, W. A. Goddard III, J. Chem. Phys. 122 (2005) 244703.

[127] N. Koch, A. Kahn, J. Ghijsen, J-J. Pireaux, J. Schwartz, R. L. Johnson, A. Elschner, Appl. Phys. Lett. 82 (2003) 70-72.

[128] G. Heimel, L. Romaner, J-L Brédas, E. Zojer, Phys. Rev. Lett. 96 (2006) 196806.

[129] B. de Boer, M. M. Frank, Y. J. Chabal, W. Jiang, E. Garfunkel, Z. Bao, Langmuir 20 (2004) 1539-1542.

[130] J. B. Williamson, J. Pullen, R. T. Hunt, D. Leonard, "The shape of solid surfaces", Surface Mechanics, ASME, Ney York, 1969, pp. 24.

[131] M.G. Cooper, B.B. Mikic, M.M. Yovanovich, Thermal contact conductance, Int. J. Heat Mass Trans. 12 (1969) 279.

[132] R. Holm, "Electric contacts, theory and application", Springer-Verlag, New York, 1967, pp. 123.

[133] B. Kshirsagar, P. Misra, N. Jampana, and M. V. Krishna Murthy, Thermal Contact Conductance Across Gold-Coated OFHC Copper Contacts in Different Media, Journal of Heat Transfer, 127 (2005) 657.

[134] G. Heimel, L. Romaner, J.-L. Bredas, and E. Zojer, Physical Review Letter, 96 (2006) 196806.

[135] Chemistry and Technology of Epoxy Resins; Ellis, B., Ed.; Blackie Academic & Professional, 1993.

[136] E. M. Petrie, (Ed.) Epoxy adhesive formulations McGraw Hill, New York, NY, 2006.

[137] D. Derouet, F. Morvan, J. C. Bross, J Appl Polym Sci, 62 (1996) 1885.

[138] G. Camino, L. Costa, G. Martinasso, Polym Degrad Stab, 23 (1989) 359.

[139] M. J. Alcón, G. Ribera, M. Galià, V. Cádiz, J. Polym Sci Part A: Polym Chem, 43 (2005) 3510.

[140] C. H. Lin, S. X.Cai, T. S.Leu, T. Y. Hwang, H. H. Lee, J Polym Sci Part A: Polym Chem, 44 (2006) 3454-3468.

[141] L. A. Mercado, G. Robera, M. Galià, V. Cádiz, J Polym Sci Part A: Polym Chem, 44 (2006) 1676-1685.

[142] Y-L Liu, G-P Chang, C-S Wu, Y-S. Chiu, J Polym Sci Part A: Polym Chem, 43 (2005) 5787.

[143] S. X. Cai, C.H. Lin, J Polym Sci Part A: Polym Chem, 43 (2005) 2862

[144] M. A. Espinosa, M. Galià, V. Càdiz, J Polym Sci Part A: Polym Chem, 42 (2004) 3516.

[145] Y. L. Liu, C. S. Wu, Y. S. Chiu, W. H. Ho, J Polym Sci Part A: Polym Chem, 41 (2003) 2354.

[146] J. Ding, H. Liang, W. Shi, X. Shen, J Appl Polym Sci, 97 (2005) 1776.

[147] S. Levchik, A. Piotrowski, E. Weil, Q. Yao, Polym Degrad Stab, 88 (2005) 57.

[148] J-Y Shieh, C-S. Wang, Polymer, 42 (2001) 7617.

[149] S. Ohshima, T. Shibata,; N. Sasaki, H. Okuda, H. Nishizawa, M. Ohsawa, M. Matsumoto, E. Nakayama, Sangyo. Igaku, 26(3) (1984) 197.

[150] T. Fishback, C.McMillin, M. Farona, Biomed Mater Eng., 2 (2) (1992) 83.

[151] P. Bastian, Med J. Aust, 141 (8) (1984) 533.

[152] M. Kristiansson, Protein adducts of hexahydrophthalic anhydride- chemical structures and biomarkers, Ph.D. thesis, University Hospital, Lund, Sweden 2004.

[153] H. Yeganeh, M. M. Lakouraj, S. Jamshidi, J Polym Sci Part A: Polym Chem, 43 (2005) 2985-2996.

[154] C. Mas, A. Mantecón, A. Serra, X. Ramis,J. M. Salla, J Polym Sci Part A: Polym Chem, 43 (2005) 2337-2347.

[155] Y. L. Liu, G. P. Chang, C. S. Wu, Y. S. Chiu, J Polym Sci Part A: Polym Chem, 43 (2005) 5787-5798.

[156] R. J. Koegel, J. P. Greenstein, M. Winitz, S. M. Bumbaum, R. A. McCallum, J. Am. Chem. Soc., 77 (1955) 5708.

[157] K. Fukushima, T. Onishi, T. Shimanouchi, S. Mizushima, Spectrochim. Acta, 15 (1959) 236.